IOWA STATE UNIVERSITY
Digital Repository

1996

Development and application of spread-spectrum ultrasonic evaluation technique

Jahangir Khan Kayani
Iowa State University

Follow this and additional works at: https://lib.dr.iastate.edu/rtd

Part of the Electrical and Electronics Commons

www.manaraa.com

INFORMATION TO USERS

Development and application of spread-spectrum ultrasonic evaluation technique

by

Jahangir Khan Kayani

A Dissertation Submitted to the

Graduate Faculty in Partial Fulfillment of the

Requirements for the Degree of

DOCTOR OF PHILOSOPHY

Department: Electrical and Computer Engineering
Major: Electrical Engineering
(Communications and Signal Processing)

Approved:

In Charge of Major Work

For the Major Department

For the Graduate College

Iowa State University
Ames, Iowa
1996

UMI Number: 9924786

UMI
300 North Zeeb Road
Ann Arbor, MI 48103

TABLE OF CONTENTS

LIST OF FIGURES

LIST OF TABLES

ACKNOWLEDGEMENTS

CHAPTER 1 INTRODUCTION

1.1 Introduction to Ultrasonic NDE

Nondestructive evaluation (NDE) is an interdisciplinary field which refers to the process by which various properties of a test object are examined without breaking it. Out of the various methods of nondestructive evaluation, the ultrasonic method is by far the most popular for determining the hidden flaws and characteristics of the test specimen [1]. This is mainly because,

   (a) ultrasound can be generated and detected relatively inexpensively,

   (b) ultrasonic signals have better penetration capabilities, and

   (c) the ultrasonic return signal has sufficient information carrying capacity.

In 1942, Firestone, an American, pioneered the use of pulsed ultrasonic energy for the testing of materials by disclosing the Reflectoscope. About the same time, Sproule, an Englishman, developed a similar pulse-echo instrument [2]. From these early beginnings, ultrasonic NDE has developed into a very sophisticated engineering discipline. The classical perception of ultrasonic NDE is that it involves the detection and characterization of flaws. Modern ultrasonic NDE, however, also includes the measurement of material microstructure and associated factors that govern mechanical properties and dynamic response. It goes beyond flaw detection and defect characterization. Ultrasonic NDE can assess and verify material moduli, strength, toughness and a host of other mechanical properties and morphological conditions. It provides a nondestructive approach to characterizing initial states of engineering solids and their degradation or modification on exposure to service environments [3]. In the medical profession ultrasonic NDE is increasingly used for the in-vivo and in-vitro analysis of human tissues for diagnostic purposes [4].

1.2 Problem Statement

In order to realize the full potentials of ultrasonic NDE in meeting the challenges and new demands of the engineering world, there is an evergrowing interest in exploring advanced signal acquisition, processing, and analysis methods. It is important to view ultrasonic NDE from various other perspectives and not just the extension of the Reflectoscope idea. The present research is an effort in that direction.

The problem of ultrasonic NDE is viewed as the acoustic-impulse-response estimation and characterization problem. It is compared with the analogous problem from the field of radio communications, namely, radio-detection-and-ranging (radar). Based on the well-known, spread-spectrum principles of communications field, a new, improved approach to the acoustic-impulse-response estimation is being investigated.

This new approach to ultrasonic NDE, called Spread-Spectrum Ultrasonic Evaluation (SSUE), produces an acoustic-impulse-response estimate that has a very large dynamic range and high signal-to-noise-ratio. The measured acoustic-impulse-response is, therefore, much more sensitive to very small changes in the acoustic characteristics of the test specimen; when compared with the conventional techniques.

1.3 Significance of Work

SSUE employs a non-traditional approach to ultrasonic NDE that makes it more robust and powerful. One significant feature of SSUE technique is that it overcomes the maximum average power limitation of the existing techniques. Conventional pulsed ultrasonic NDE systems are peak power limited by the transducer breakdown voltage and the average power is limited by the narrow pulse duration which is important to maintain good resolution. In certain NDE applications, there are factors other than the transducer peak power limitation which limit the amplitude of the transmitted signal. In the case of medical ultrasound devices, for example, the peak power limit arises from the risk of causing tissue damage. Also, the application of ultrasonic NDE in an explosive

environment restricts the peak signal power level to within certain safe limits. For such kinds of applications, SSUE has a direct solution to increasing the average power while maintaining the resolution.

The resolution of an ultrasonic signature is directly related to the operating frequencies of the NDE system. Higher frequencies provide better resolution but, unfortunately, they often experience greater attenuation, thus lowering the SNR. Here again the SSUE can help in improving the SNR to workable limits.

Ultrasonic instrumentation in a field or industrial environment is subject to all kinds of acoustic and electromagnetic interferences. This causes a degradation of instrument sensitivity and reliability. SSUE, by virtue of its robust operating principal, is capable of interference rejection to a much larger extent.

The SSUE technique assures that numerous wave interactions occur in the entire volume of the test object. Hence, the received signal undergoes multiple interactions with many material properties, making this technique very sensitive to changes in the material characteristics. Most of the ultrasonic NDE is based upon a linear model for the interaction of ultrasound with the material. This assumption can only be valid if the acoustic signal amplitudes do not exceed the elastic limit of the material. This means that the linearity assumption might be violated when attempting to increase the SNR by increasing the signal amplitude. Since the SSUE technique works with low signal amplitudes, this also justifies the significance of SSUE.

1.4 Dissertation Objectives

The acoustic-impulse-response estimation approach to ultrasonic NDE will be formulated and the choice of spread-spectrum technique of impulse-response estimation will be justified. The development and optimization of a prototype SSUE system is presented. The optimized SSUE system employs a carefully tailored, pseudorandom excitation waveform, and, correlation processing at the receiver. A comprehensive analysis of the various alternatives for the optimum waveform and the correlation receiver

design is the central research focus of this work. The optimized system is implemented in the hardware and its performance compared with the theoretically predicted results. The effectiveness of the SSUE technique is verified through a number of different experiments representing various practical NDE situations.

To summarize, the dissertation objectives can be enumerated as,

(a)   Comparing the SSUE approach of acoustic impulse response estimation with established well-known approaches.

(b)   Developing a practical SSUE system optimized for self-noise and various other factors.

(c)   Investigating the fundamental and technological limitations of the SSUE technique.

(d)   Demonstrate the effectiveness of the SSUE technique in various ultrasonic NDE applications.

1.5 Dissertation Organization

The technology background for the development of the SSUE technique, including a comprehensive literature survey, is presented in chapter 2. Chapter 3 describes the theoretical formulation of the SSUE technique and its comparison with various other competing techniques. It also discusses the fundamental constraints of a practical SSUE system. The concepts of optimum and sub-optimum SSUE designs are defined in chapter 4, followed by various approaches to an improved system design. The simulations of the developed approaches to SSUE system design and their performance evaluations are presented in chapter 5. Chapter 6 presents the lab-grade instrument development details and the evaluation of the system performance and limitations under various practical situations. An efficient method of correlator implementation is also discussed in chapter 6 along with the comparison of its performance with various other, existing methods. Various signal processing tools used for the evaluation of the measured ultrasonic correlation signature are discussed in chapter 7. The effectiveness of the SSUE technique

under various practical NDE applications is demonstrated in chapter 8. Finally, chapter 9 presents a summary of the research effort towards the development of this new approach to ultrasonic NDE and discusses the future direction of this work.

1.6 Summary of Major New Contributions

(a) The SSUE approach of acoustic-impulse-response estimation is compared with the other well known methods (Section 3.2 & 3.3). It is shown that the SSUE technique performs equivalent to the averaging technique for uniform random noise. However, for the case of narrowband interference, it performs better than the averaging technique (Figure 3.5).

(b) The problem of self-noise associated with the ultrasonic correlation systems is analyzed and two general strategies for the self-noise suppression are developed. The first is based on the design of appropriate pseudorandom excitation waveforms (Section 4.4), while the other is based on the design of an appropriate self-noise suppression filter (Section 4.5).

(c) It is proved that a bandpass waveform based on polyphase sequences does not exhibit perfect periodic autocorrelation properties (Section 4.4.3), even though the PACF of the sequence is perfect.

(d) Analysis of various noise sources and the non-ideal effects in a practical SSUE instrument was performed and the fundamental and technological limitations of the system were established (Section 6.5).

(e) A new design for the DSP based correlator is developed that is much more efficient compared to the earlier correlator implementations (Section 6.6).

(f) A signature discrimination technique, based on the statistical pattern recognition methods, was developed (Section 7.3).

(g) The application of the SSUE technique for geophysical exploration is considered which can eliminate the self-noise problem of the existing chirp-signal method (Section 8.5).

CHAPTER 2   TECHNOLOGY REVIEW

This chapter reviews the fundamental concepts of ultrasonic nondestructive evaluation. This is followed by a survey of current ultrasonic NDE and NDT techniques, their capabilities and their limitations. The new problems and challenges faced by the NDE community and various newly emerging techniques in ultrasonic inspection and testing are discussed. Also, the science of ultrasonic NDE is compared with geophysics and radio communications and the fundamental similarities and differences are highlighted. The application of spread-spectrum techniques from radio communication, to address the problem of ultrasonic NDE, is discussed. Finally, the literature survey related to the current research work is presented.

2.1 Fundamentals of Ultrasonic NDE

Ultrasonic waves are vibrational waves having a frequency higher than the hearing range of the normal human ear, which is typically considered to be 20,000 cycles per second (Hz). The upper end of the range is not very well defined; however, most practical ultrasonic NDE is accomplished with frequencies from 200 KHz to 20 MHz [2]. Ultrasonic waves can be injected into an object and are thus used in materials and structures for flaw detection and material property determination. Ultrasonic inspection is accomplished by having electronically controlled ultrasound pulses introduced into the material. The ultrasonic energy then propagates within the material, finally reaching a detector. Material condition is diagnosed from the characteristics of the received ultrasonic energy.

2.1.1 Propagation of Ultrasound

Practical ultrasonic wave propagation requires the presence of a medium such as a fluid or a solid. The wave propagates as a result of the vibration or periodic displacement of successive elements of the medium. The propagation speed, C, is related to the excitation frequency, f, by,

$$C = f \cdot \lambda \qquad (2.1)$$

where λ represents the ultrasound wavelength. The major types of ultrasonic waves are, longitudinal , transverse (shear), and surface. Most of the wave types are named according to the relationship of particles motion relative to the direction of propagation of ultrasonic wave. For longitudinal waves, the propagation and particle motion directions are the same. Since compressional and dilatational forces are involved, these are also called compression or pressure waves. These waves can propagate in solids, liquids and gases and are the most utilized wave mode for NDE applications. Shear waves, on the other hand, have particle motion transverse to the direction of propagation, that is, in a plane perpendicular to the direction of propagation. Shear wave inspection is generally restricted to solids only, since the propagation of shear wave can only occur in highly viscous fluids. Although many types of surface waves exist, a Rayleigh wave is the one most frequently used in nondestructive testing. These waves have an elliptical particle motion in the vertical plane and normally travel undispersed on smooth surfaces. Wave propagation properties are directly related to the elastic properties of the medium and the relative size of the object. Velocities of the various wave types are determined by the modulus, density, and Poisson's ratio for the particular material in which they are propagating. When an ultrasound wave strikes the interface between two media having different wave speeds, it is bent or refracted in the same manner as light refracts when passing from one material to another having different optical properties. The diffraction phenomenon of an ultrasonic wave is also similar to the diffraction of a light wave. Ultrasonic diffraction can be caused by small pores, inclusions, or the edge of cracks in metals.

2.1.2 Coupling of Ultrasound to Test Object

Ultrasonic waves are attenuated very rapidly in air, especially the higher test frequencies. Additionally, differences in the acoustic impedance of air and of solid material cause most of the ultrasonic energy to be reflected at the surface of the solid rather than propagate in it. Consequently, a liquid couplant or direct transducer contact is required to couple the ultrasonic energy into solid materials. Liquid couplants may be in a tank where the test object is immersed, or a stream of water can be used to provide a sound path to test large objects and structures. When direct coupling is used, some oil, grease, or other viscous material is placed between the transducer and test object. For some applications, adhesive or pressure coupling is practical.

The most important aspects of coupling acoustical energy into a medium are the uniformity and repeatability of the energy transfer and the percentage of the incident energy that is transferred. These are dependent on the mechanical factors, such as surface roughness and the material factors, such as relative acoustic impedances of the two mediums.

The increased sensitivity of an ultrasonic NDE technique, such as the SSUE technique, makes it even more vulnerable to variations in the measurements because of various coupling effects, such as, transducer alignment, surface roughness, couplant thickness, etc.. There can be three solutions to this problem, that are used either independently or in some combination, depending upon the specific application. They are:

(a) use of very precise, high quality fixtures to ensure a high degree of repeatability of transducer registration and applied pressure,

(b) permanent mounting of transducers or embedding the transducer as an integral part of the test specimen itself,

(c) use of advanced signal processing techniques to desensitize the measurements from the coupling variations.

2.1.3 Attenuation of Ultrasonic Waves

Like all other forms of energy, ultrasonic waves attenuate as they propagate through a medium. Excessive attenuation in some materials can severely limit the use of ultrasound as a flaw detection method. This can be especially troublesome when searching for small flaws. Positive aspects of ultrasonic attenuation include the nondestructive determination of certain material properties such as grain structure and intergranular stress.

Major categories of attenuation mechanisms include scattering, absorption and geometric factors. Scattering in metallic materials can be attributed to very small discontinuities, such as precipitates, and larger areas, such as, grain boundaries. Dislocation along with magnetic and thermoelastic damping are major types of absorption mechanisms. Geometric factors include diffraction, beam spreading, and coupling losses. Typical attenuation coefficients [2] may range from less than 1 dB/cm for certain kind of steel to approximately 10 dB/cm for stainless steel and to over 30 dB/cm for polymers.

2.1.4 Generation and Detection of Ultrasound

Although numerous methods can be used to generate ultrasonic waves, piezoelectric transducers are the most common type. The piezoelectric effect occurs when an electric charge develops on the faces of a piezoelectric element that is mechanically deformed. Conversely, an electric signal or voltage applied across the faces will cause deformation. Thus, deformation of a crystal at high frequencies generates ultrasonic vibration that propagate as waves in the material when a suitable couplant is placed between the crystal and the material to be inspected.

Piezoelectric transducers come in many types, sizes, and shapes. Two basic types are immersion and contact. Since shear waves do not propagate in a fluid, longitudinal probes are required for exciting both longitudinal and shear waves in a solid inspected by the immersion method. Contact transducers may be normal-beam or angle beam type.

Transducers can be selected to generate an ultrasonic beam at a specific angle in a specific type of material, as governed by Snell's law [2].

2.1.5 Ultrasonic NDE Model

Figure 2.1 shows a typical model of ultrasonic NDE. The instrumentation block represents the excitation of the test object with ultrasound and the detection of the scattered/reflected/attenuated ultrasound. This leads to the measurement of an appropriate acoustic signature that represents the characteristics of the test object. Depending upon the specific NDE requirement, various acoustic parameters like, velocity, attenuation, absorption and scattering are estimated from the measured acoustic signature. Finally, the measured values of these acoustic parameters are used for the characterization / classification of the test object. This final step can be based on the theoretical modeling of the acoustic signal propagation through the test object. In certain NDE situations, however, the interaction of the acoustic signal with the test material is very complicated and a realistic propagation model is hard to develop. For these situations, the characterization/classification process is based on the empirical correlations.
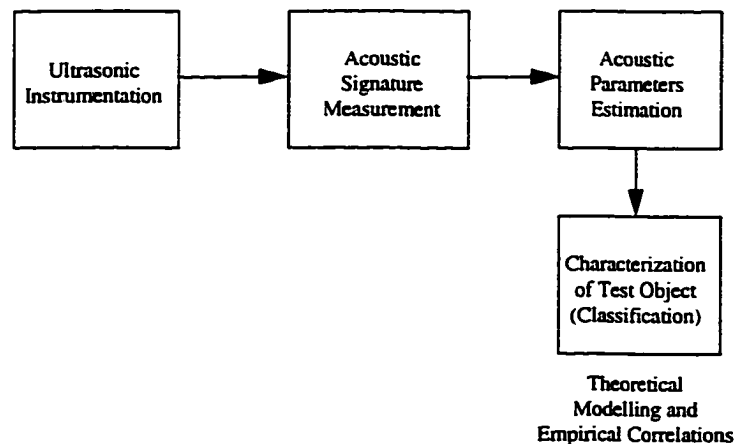
Figure 2.1: Ultrasonic NDE model.

2.2 Current Ultrasonic NDE Techniques

Although there exists a wide range of different ultrasonic NDE techniques, each is designed for a certain kind of NDE requirement. These can be broadly grouped into the following categories.

2.2.1 Pulse-Echo Technique

Pulse-echo describes the technique where a pulsed ultrasonic beam, generated by an ultrasonic transducer, is transmitted into the material to be tested. The ultrasonic energy propagates into the test material and is reflected back from the discontinuities in the material and the boundary surfaces. The reflected ultrasound is picked up by a receiving ultrasonic transducer and converted to an electrical signal. Typically, a single transducer acts both as the transmitting and the receiving transducer much as a radar system uses only one antenna (Figure 2.2).
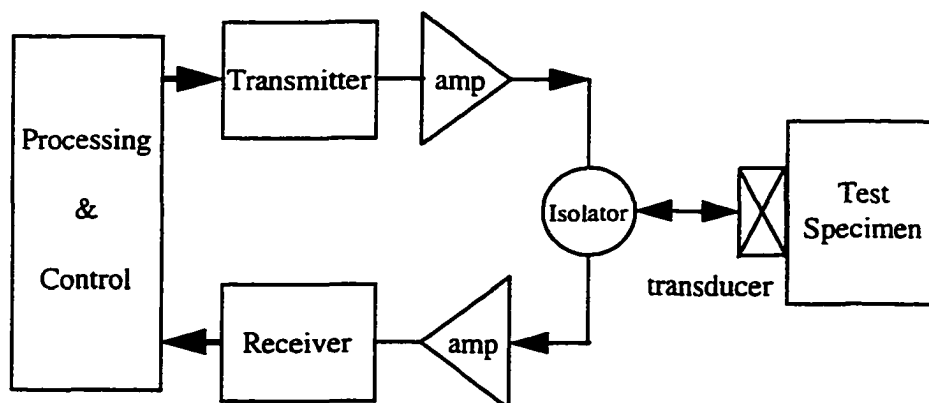
Figure 2.2: Pulse-echo ultrasonic NDE technique.

2.2.2 Through-Transmission Technique

The through transmission technique is used in several cases, particularly for highly attenuative materials where a pulse-echo trip causes a significant loss in signal strength. In this case two separate transducers are required for signal transmission and reception. This technique requires access to the two opposing surfaces of the test object. Flaws are indicated by the loss or reduction of energy through the material (Figure 2.3).
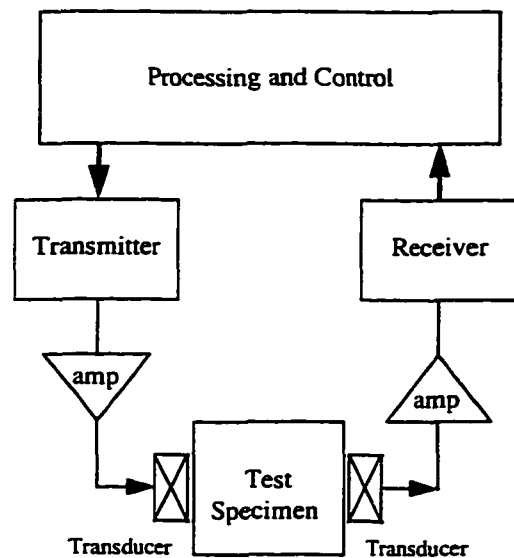
Figure 2.3: Through-transmission NDE technique.

2.2.3 Pitch-Catch Technique

This technique is actually a generalization of the pulse-echo and through transmission technique. It involves separate transmit and receive transducers like the through-transmission method, however, the transducers are located at an angle between zero and 180 degrees. The angle is chosen such that there is little or no signal received unless there are flaws in the material (Figure 2.4).
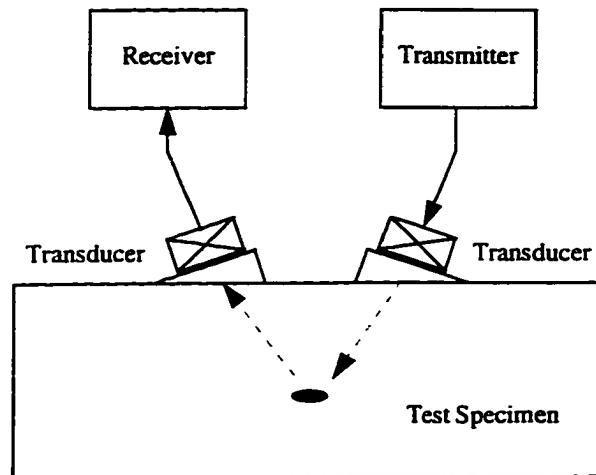
Figure 2.4: Pitch-catch ultrasonic NDE technique.

2.2.4 Pulse Averaging Technique

This technique can be used in conjunction with any one of the three pulsed excitation techniques mentioned above. It is applied in situations where the desired signal is very weak compared to the unwanted random noise. It is based upon the fact that the random noise in the received signal is uncorrelated from one acquisition to another and hence the averaging of multiple acquisitions tend to suppress the random noise component. However, this technique does not suppress the so-called "grain noise" which dominates many metals measurements.

2.2.5 Ultrasonic Spectroscopy

Ultrasonic spectroscopy is the study of ultrasonic waves resolved into their Fourier frequency components. Since many material properties manifest themselves as amplitude or phase changes in the ultrasonic waves used to interrogate a specimen, ultrasonic
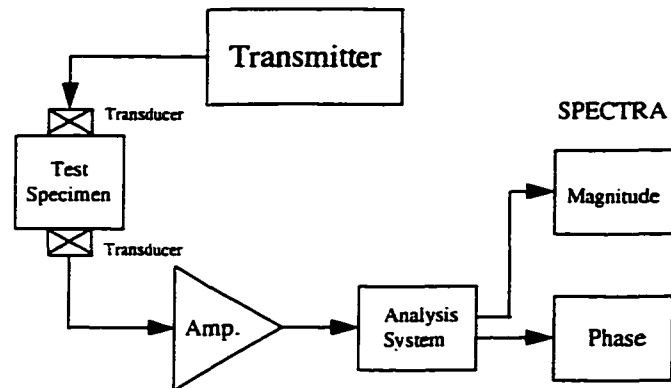
Figure 2.5: Generalized ultrasonic spectroscopy system.

spectroscopy has proven quite valuable. In addition to the use of ultrasonic spectroscopy for defect characterization and material property assessment, it has also proven useful for monitoring corrosion and the measurement of frequency dependent attenuation [5] and velocity (Figure 2.5). However, mode conversion in a specimen limits the usefulness

2.3 New Applications and Newly Emerging Techniques of Ultrasonic NDE

Although historically, nondestructive techniques have been used almost exclusively for the detection of macroscopic defects in structures after they have been in service for some time, it has become increasingly evident that it is both practical and cost effective to expand the role of nondestructive evaluation to include all aspects of materials production and application. Currently, efforts are directed at developing and perfecting nondestructive evaluation techniques which are capable of monitoring and controlling the materials production process; the materials stability during transport storage and fabrication; and the amount and the rate of degradation during the materials in-service life [6]. Ultrasonic techniques afford very useful and versatile nondestructive methods for evaluating the microstructure , associated mechanical properties, and macroscopic flaws in solid materials.

Realization of these potentials of ultrasonic NDE demand the advancement in the areas of signature acquisition, processing, and analysis methods, with emphasis on automated, digital techniques. As a result of this driving force, a number of new techniques of ultrasonic NDE have emerged in recent years. Although these techniques are still restricted to lab investigations, their effectiveness for certain NDE applications has been well established. Some of the newly emerging techniques of ultrasonic NDE are, (a) acousto-ultrasonics, (b) split-spectrum processing, and (c) correlation techniques.

2.3.1 Acousto-Ultrasonic Technique

Composite materials fail in a manner different from other materials such as metals. Whereas metals fail due to the initiation and propagation of cracks, advanced composite materials fail due to an overall degradation of various physical properties [7]. Consequently, the NDE of such materials involves assessing the combined effects of the material's damaged condition rather than identifying and sizing single critical imperfections. The acousto-ultrasonic NDE technique [8, 9, 10, 11, 12] addresses this requirement.

The term acousto-ultrasonics, as the name indicates, denotes an NDE technique that combines some aspects of acoustic emission methodology with ultrasonic simulation of stress waves. The acousto-ultrasonics approach uses analysis of simulated stress waves for detecting and mapping variations in mechanical properties. A short ultrasonic pulse of suitable center frequency is selected to simulate the stress wave and is transmitted into the material. Unlike most NDE techniques, acousto-ultrasonics is less concerned with flaw detection than with the assessment of the collective effects of various flaws and material anomalies. Acousto-ultrasonics is an extremely powerful technique because the induced stress waves interact with the entire volume of material through which they travel. As a result, propagation of stress waves is related to the total damage state of the material that lies in their path.

2.3.2 Split-Spectrum Processing Technique

A limitation of ultrasonic nondestructive evaluation of materials with coarse structure is the poor signal-to-noise ratio caused by backscattering noise. Split-spectrum processing is a frequency diversity technique used to enhance the signal-to-noise ratio of ultrasonic signals in such situations [13, 14, 15]. The SNR of a received ultrasonic signal can be affected by two kinds of noise contents, (a) incoherent random noise such as instrumentation noise, which can be suppressed by temporal averaging or correlation techniques, and (b) coherent noise or clutter produced by the interference of the wavelets scattered by the randomly packed grain structure of the material. Due to the physical nature of the origin of clutter, the coherent noise is time-invariant and hence is not removed by temporal averaging or correlation techniques. It can be reduced by either spatial averaging or frequency diversity techniques such as split-spectrum processing.

In split-spectrum processing, a wideband signal is transmitted and the received signal spectrum is partitioned into different frequency bands using spectral windows [16] to obtain a set of decorrelated signals. Once the decorrelation of grain echos has been achieved through the split-spectrum processing, noise suppression algorithms [17] can be applied to the resulting data to enhance the flaw signal. Therefore, split-spectrum processing eliminates the need for complex modulation techniques or multiple transmitters to achieve frequency diverse signals at the receiver.

2.3.3 Correlation Technique

It is well-accepted that the traditional ultrasonic NDE systems are peak power limited much like radar systems. Also, there is an evergrowing demand for greater measurement sensitivity and detectability for improved defect characterization. A common technique often employed by ultrasonic systems is temporal averaging [18]. However, there is a practical limit to which the improvement can be made. Another technique that is gaining popularity in ultrasonic applications is the random signal

correlation technique [19]. It can be shown that, in theory, the correlation technique gives the same degree of improvement as temporal averaging [20]. However, the correlation technique provides certain practical advantages.

Ultrasonic correlation systems [21] are based on the use of coded excitation waveforms of longer duration and the correlation processing of the received signal. Coded excitation accompanied by the received signal correlation permits order of magnitude improvement of SNR at modest peak signal amplitudes compared to conventional pulsed techniques [22, 23].

The SSUE technique bears some resemblances and some differences with the above described ultrasonic NDE techniques. These are summarized as follows:

(a)   The SSUE technique is similar to the ultrasonic correlation technique as both employ pseudorandom excitation waveforms and correlation processing at the receiver.

(b)   The conventional correlation technique is self-noise limited, whereas the SSUE technique does not have self-noise limitation. This difference comes from the fact that SSUE employs periodic transmission of an optimized excitation waveform, as opposed to a pulsed transmission of a coded waveform.

(c)   The improvement in signal-to-random-noise ratio of the SSUE technique, the conventional correlation technique, and the averaging technique, are equivalent, as long as the noise is uniformly distributed over the entire spectral width.

(d)   The SSUE technique is similar to the acousto-ultrasonic technique since both are aimed at assessing the integrated state of the material's damaged condition rather than identifying and sizing single critical imperfections.

(e)   The SSUE technique is different than the acousto-ultrasonic technique as the first uses a continuous pseudorandom excitation waveform, while the later uses a pulsed excitation waveform.

(f)   The SSUE technique is totally different than the split-spectrum processing technique, since the first is aimed at the suppression of random uncorrelated noise, while the later is aimed at the suppression of correlated grain noise.

2.4 Comparison of NDE with Geophysics and Communications

The problem of ultrasonic nondestructive evaluation bears striking basic similarities with the seismic exploration problem of geophysics and the radar problem of communications field. There are four basic elements common to each problem.

(a) use of an excitation/interrogation signal of some form

(b) measurement of echo/scattered signal

(c) quasi-stationary unknown channel

(d) processing of measured signal to extract useful information

The purpose of the seismic exploration [24] is to determine the nature of different layers of earth beneath its surface. This is mainly done to search for oil and gas reservoirs. In this process dynamite or some other type of impulsive energy source is used to excite a "seismic wavelet" inside the earth. The wavelet is partially reflected back from various layers of earth and is recorded with "geophones". The essential features of a seismic exploration system are,

(a) an active source of energy at the surface of earth, such as dynamite, air gun, or a chirp signal generator,

(b) propagation of acoustic (vibrational) waves outward from the source into the earth,

(c) reflection of vibrational waves from the interfaces between geologic layers in the earth's crust,

(d) detection of the reflected waves at the surface of earth.

The original purpose for which radar systems were developed was to detect the presence of friendly and enemy aircraft flying at very long range and high altitudes. With the advancement in radar technology, it became possible to characterize the detected targets and also the atmospheric channel through which the radar signal propagates. Radar target characterization typically involves, the location of the target in space about the radar, the time rate of change of the target's location in space, and in some cases, the identification of the target as being a particular one of a number of classes of targets [25].

A conventional radar transmits a very short time-duration pulse of radio frequency energy into the air as an electromagnetic wave. The transmitted signal propagates into the channel obeying the laws of electromagnetic wave propagation and is scattered by the presence of any conducting structure like an aircraft. A portion of the scattered signal travels back towards the radar antenna and is picked up by the receiver. The radar receiver discriminates against the ever-present noise from various sources and a very weak echo signal that represents the presence of a valid target. The accuracy of the data available from a radar is limited by the thermal noise introduced by the radar receiver, echos from targets of no interest (known as clutter), and externally generated interference. In order to combat against the unwanted noise and clutter, present day radars often employ some form of pulse compression. By using pulse compression methods it is possible to extract a considerably weak echo signal out of orders-of-magnitude stronger random noise and in the presence of intentional interference or jamming.

2.5 Application of Spread-Spectrum Techniques

Spread-spectrum techniques were primarily developed for the military applications of signal hiding, interference suppression, and anti-jamming [26]. For a long time its application was restricted to military communications and radars. It was only recently that these techniques became well known in the private sector and gradually their potential is being realized by researchers in various fields of science.

Because of the striking similarities, geophysics people adopted these techniques with remarkable success [27]. In the ultrasonic NDE area, these concepts can also be applied but the adaptation has been slow. In ultrasonic NDE, the use of pulse compression techniques has been studied by many people but they have not become widely known or used, probably for two reasons,

(a)   lack of theoretical appreciation, and

(b)   self-noise limitation of these techniques.

The SSUE system bears a very close resemblance to a spread-spectrum

communication system. In fact, the governing principles of SSUE are derived from the spread-spectrum concepts in the communications field. However, there are quite a few important differences between the two systems. It is very important to clearly understand the similarities and the differences between the two systems, so that the techniques and the concepts from one field can be successfully adopted to the other field. Some important similarities and differences between the two systems are highlighted below:

(a)   A typical communication system is based on data transmission and spread-spectrum techniques are used to make the system robust under adverse/hostile operating conditions. SSUE is dissimilar in this respect as there is no data transmission involved.

(b)   A radar system employs spread-spectrum techniques to increase the time-bandwidth product, thereby maximizing resolution and SNR at the same time. SSUE system also uses spread-spectrum techniques for the same purpose.

(c)   A radar system has to deal with doppler frequency shift as the targets of interest are in motion with respect to the transmitter/receiver. The typical SSUE application involves signal returns from a stationary test object, so the doppler shift is not a problem.

(d)   A radar transmitter is limited mainly by its peak power. The SSUE transmitter, i.e., an ultrasonic transducer, is also limited by its peak power handling capacity.

(e)   Typically, a radar transmitter uses a saturation amplifier at its final amplification stage. Therefore, an amplitude modulated signal can not be effectively used. SSUE has a linear power amplifier, so it can handle AM signals without any problem.

(f)   In most communication systems the carrier frequency, f_o, is much larger than the system bandwidth, B, so it is easy to filter out the harmonics. Thus the mathematical analysis of the system often assumes, ($f_o \gg$ B). In SSUE, typically, ($f_o = B/2$), so the narrow bandwidth assumption is not valid.

(g)   In both SSUE and a monostatic radar system, the transmitter and receiver are co-located. Hence, synchronization error and carrier frequency & phase estimation

errors can be eliminated / minimized by using a common local oscillator and synchronization clock. However, the stability of carrier and the sync clock are very crucial for the optimum system performance.

(h)   SSUE estimates the impulse response of the channel/ medium/ test object, and requires a large dynamic range. A radar system also does the same and has similar requirements.

2.6 Literature Survey

Since the development of spread-spectrum ultrasonic evaluation technique is based upon the concepts and research derived from the diverse fields of radio communication, geophysics and ultrasonics, the literature survey performed for this work is grouped into the following three categories,

        (a) Communication and radar systems

        (b) Geophysical exploration systems

        (c) Ultrasonic correlation systems

2.6.1 Communication and Radar Systems

There are two major applications of spread-spectrum techniques in radio communication area. In data communication systems, spread-spectrum techniques are employed, predominantly, for the purpose of channel sharing [28], narrow-band interference rejection and signal hiding [29]. In radar systems, spread-spectrum techniques are used for anti-jamming, interference rejection and improving the target detection capability (MDS, minimum discernable signal) [30].

Three kinds of techniques are used to increase the detection capability of a radar. These are, swept frequency chirp signal, pseudorandom sequences, and polyphase pulse compression waveforms [31]. The swept frequency chirp was the easiest for analog circuit implementation, so it was more popular prior to the era of digital signal processing.

The analog implementation of the frequency chirp technique was carried out by the use of dispersive delay lines as a pulse expander-compressor [32]. The advancement in digital signal processing facilitated the use of various pseudorandom binary sequences of which the maximal-length sequences are the most frequently used [33]. These sequences did not have very good autocorrelation sidelobe characteristics and also were very sensitive to doppler frequency shifts [34]. This led to the development of a new class of sequences called Polyphase sequences. In 1965, Golomb and Scholtz [35] proposed a class of generalized polyphase Barker sequences that have good periodic and aperiodic autocorrelation properties [36]. Well known polyphase sequences are Golomb sequences, Frank sequences, P1, P2, P3 and P4 sequences [37]. It has been shown that all these sequences have better correlation properties than the pseudorandom binary sequences. Also, they exhibit better doppler tolerance [38, 39, 40].

In addition to the above techniques, the use of amplitude modulated sequences, like Huffman sequences, has also been considered for radar applications [41]. Huffman sequences exhibit very good correlation properties, however, the Huffman waveform consists of sequence elements that vary both in amplitude and the phase, which is typically not suited for radar applications.

2.6.2 Geophysical Exploration Systems

Although a number of nonexplosive energy sources are used in the seismic exploration, the source employed in a majority of all work on land is dynamite [42]. Until about 1955, this was the only source that provided sufficient energy to yield satisfactory reflection seismograms. However, the introduction of magnetic tape recording and computers in the 1950s made it possible to build up usable signals from low-energy nonexplosive sources by adding synchronized returns from many individual impacts [43]. This is an equivalent of averaging technique of ultrasonic NDE discussed earlier in section 2.2.2. The various types of nondynamite sources offered operational and economic advantages over dynamite in many types of exploration areas, and as a result their use has

risen steadily since their introduction [44, 45, 46].

The nonexplosive sources allow an almost unlimited number of effectively simultaneous impulses to introduce energy into the earth's crust, without the cost of drilling and without the hazards involved with dynamite. These alternative sources involve mechanical impact upon the land surface or shaking the surface with a mechanical vibrator. A typical weight dropping source is a "Thumper" and a typical vibratory source is "Vibroseis". In the Thumper, the weight is carried by a crane on a special truck. When released, the weight drops down 3 meters. It is hoisted from the ground immediately after the impact so that it can be dropped again. The seismic waves resulting from each drop are picked up by the detectors and recorded for subsequent processing by the computer.

In Vibroseis, the source is oscillatory rather than impulsive and continues from 7 to 21 seconds, depending upon the purpose. The frequency of the signal slowly changes over the duration of signal, so the signal is of swept-frequency type or chirp-signal, commonly used in radars. The return signals recorded in the field cannot be interpreted directly, as is generally possible for return signals produced by impulsive sources. As a result, Vibroseis data must be computer processed by cross-correlation of the received signal with the swept frequency source signal. A typical Vibroseis source is made up of a 2 ton mass with a hydraulic vibrator controlled by a preprogrammed swept-frequency signal.

2.6.3 Ultrasonic Correlation Systems

The use of random signal correlation techniques for ultrasonic NDE applications was first envisioned in early 70's by a group of researchers at the School of Electrical Engineering, Purdue University [47, 48, 49]. The basic approach in those systems, however, was of transmitting an expanded pulse and performing pulse compression at the receiver. The first concept was presented by [50] where the system was based on purely random noise. The random noise was generated by a radio frequency noise generator. A

major problem in that system was of signal storage and delay generation. The delay line used first was a tube of water of variable length. The integrator was also of analog type [51]. The next generation correlation systems used a digital delay line, but here again signal storage was a problem [52].

The concept of random signal correlation system is theoretically very attractive but there are a number of practical limitations. A more practical alternative is the use of pseudo-random signals instead of purely random ones. The use of deterministic pseudo-random sequences instead of a purely random waveform was first reported by Elias in 1980 [53]. They used a pseudorandom signal generator which can simultaneously generate the transmitted waveform and a delayed version of the transmitted waveform required for the correlation operation at the receiver. The problem was self-noise and base-band signal.

The self-noise problem was theoretically solved by the use of Golay codes. There were two problems here. The practical results were not as good and secondly, the procedure was quite complicated [54, 55, 56].

There has also been quite an interest in the use of FM chirp signals for pulse-compression in ultrasonic NDE systems [57, 58, 59]. An extension of this idea is the use of a pseudo-chirp waveform [60]. The self-noise problem exists in those systems as well and various filtering techniques are developed for self-noise suppression.

CHAPTER 3   THEORETICAL DEVELOPMENT

This chapter establishes the basic theoretical framework in which the spread-spectrum ultrasonic evaluation (SSUE) technique is developed and analyzed. The acoustic impulse response approach to the problem of ultrasonic NDE is formulated and the concepts of correlation and convolution are used to describe the governing principals of various correlation techniques for impulse response estimation. Finally, the conceptual model of the SSUE technique is presented along with the associated theoretical formulation.

3.1 Acoustic Impulse Response Approach to Ultrasonic NDE

With the exception of a few specialized cases, all ultrasonic NDE techniques are based on the acquisition of a signature function, obtained by introducing an acoustic signal of some sort into the test object. Hence, these techniques can be modeled as an input output system (Figure 3.1), and the signature function is equivalent to the modeled system impulse response. A generalized ultrasonic NDE system model contains provisions for,

   (a)   generating ultrasound and coupling it to the test object,

   (b)   receiving a portion of the ultrasound which has interacted with the object under study,

   (c)   analyzing the received signal, and

   (d)   interpretation of results.

In the generalized system model of Figure 3.1, an electrical waveform generated by the transmitter is applied to the transmitting transducer. Conversion of the electrical energy into the mechanical energy occurs within the transducer, producing an ultrasonic waveform. As the wave propagates through the material being studied, interactions of the
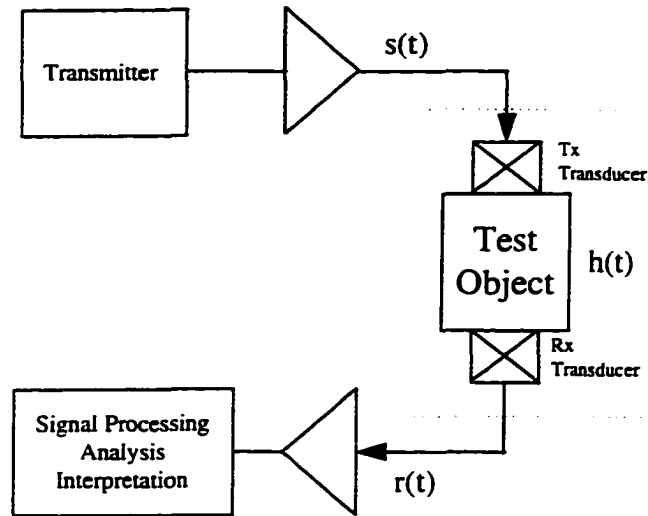
Figure 3.1: Generalized ultrasonic NDE system model.

ultrasonic energy with the material alter the amplitude, phase and direction of the wave. A receiving transducer intercepts a portion of the ultrasonic energy and conversion occurs from mechanical to electrical energy. Because the electrical signal is usually very weak, an amplifier is used to increase the signal strength to useable limits. The purpose of the analysis system, that follows the amplifier, is to extract various kinds of information out of the received signal and to characterize the test object on the basis of extracted information.

Since, in nondestructive evaluation applications, it is not desirable that the ultrasonic waves alter the material through which they pass, it is necessary to work with very low amplitude waves, which, in most cases, can be considered to obey the linear elasticity theory [6]. Also, the ultrasonic transducer is a linear device in which voltage is directly related to the pressure and current to displacement. As long as the material is excited in its elastic region, the linearity principal holds. Thus a small-signal linear model can be developed for most ultrasonic nondestructive testing applications and the generalized theory of linear-time-invariant (LTI) systems can be applied.

3.1.1 LTI System model

The impulse response model of an LTI system is shown in Figure 3.2. The output of the system, y(t), is the convolution of the system input, x(t), and the system impulse response, h(t), given as,

$$y(t) = \int_{-\infty}^{\infty} h(v)x(t-v)dv \qquad (3.1)$$

and represented by the convolution notation as,

$$y(t) = x(t) * h(t) \qquad (3.2)$$

LTI system

input   output

x(t) ——▶ h(t) ——▶ y(t)
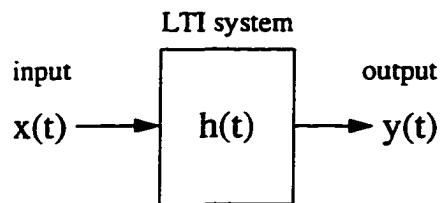
Figure 3.2: Impulse response model of an LTI system.

For an LTI system, its impulse response completely describes the system characteristics. Not only does this means that, given an arbitrary input the corresponding output can be determined, but a wealth of information regarding the physical nature of the system is also contained in the output. A summary discussion on the concept of impulse response for an LTI system is provided in Appendix B. An important conclusion is that, for physically realizable systems, the associated impulse response has the following characteristics:

(a)   h(t) is a real function

(b)   h(t) is causal

(c)   h(t) is of finite duration

(d)   h(t) has finite energy

Thus the infinite integral of equation (3.1) modifies to,

$$y(t) = \int_0^{T_o} h(v)x(t-v)dv \qquad (3.3)$$

where T_o is the time span of the impulse response function, h(t).

3.2 Acoustic Impulse Response Estimation Methods

After establishing a linear time-invariant system model of ultrasonic NDE, it is possible to apply linear system theory to determine the impulse response of this model. Even though the true impulse response is physically nonrealizable, it is possible to make a reasonable estimate of the true impulse response and there exists more than one methods of doing so. A detailed discussion and comparison of various methods of impulse response estimation is provided as Appendix C. The focus here is on correlation techniques for impulse response estimation. These techniques can be further classified according to Figure 3.3. There are two main features common to all types of correlation techniques. These are:

    (a)   use of an excitation signal with a large time-bandwidth product, and

    (b)   use of a correlation filter at the receiver.

The operating principal of each correlation technique is governed by a particular definition of the correlation function. A detailed discussion on various definitions of the correlation function is provided as Appendix A. The important results from the appendix are reproduced here.

Statistical definition of correlation function: Let the waveforms x(t) and y(t) represent two independent and jointly ergodic processes. Their crosscorrelation function is defined as,
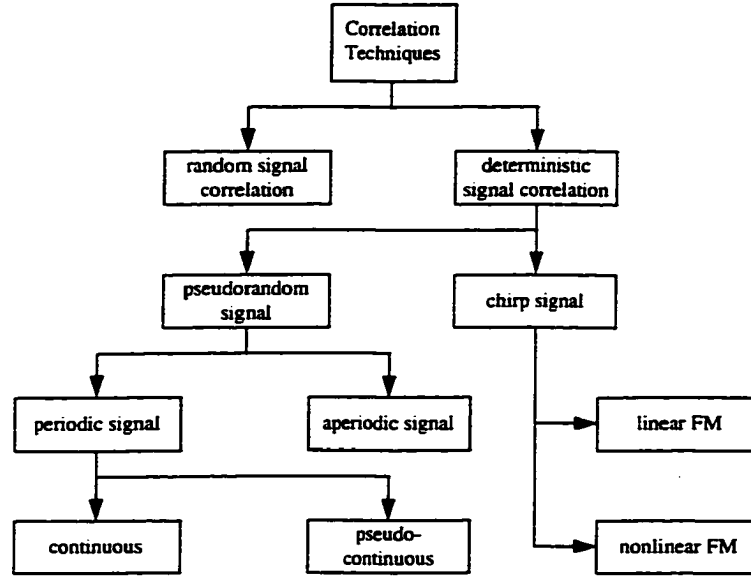
Figure 3.3: Classification of correlation techniques.

$$\phi_{xy}(\tau)=\lim_{T\to\infty}\frac{1}{T}\int_0^T x(t)y^*(t-\tau)dt \qquad (3.4)$$

Mathematical definition of correlation function: A deterministic waveform can either be time-limited or periodic. For time-limited waveforms, the correlation process is called linear correlation. Hence the linear crosscorrelation function (LCCF) of two waveforms, x(t) and y(t), both timelimited to ($0 < t < T_0$), is defined as,

$$\phi_{xy}(\tau)=\frac{1}{T_0}\int_\tau^{T_0} x(t)y^*(t-\tau)dt, \quad 0\le t\le T_0 \qquad (3.5)$$

Another situation can be when one of the two waveforms, say x(t), is periodic with period T_p, while the other, y(t), is timelimited to ($0 < t < T_0$), such that, ($T_p > T_0$). The crosscorrelation function of such waveforms will also be periodic with period, T_p. It is therefore called a periodic crosscorrelation function (PCCF), and is given by,

$$\phi_{xy}(\tau) = \frac{1}{T_p} \int_0^{T_p} y(t)\, x^*(t-\tau)\, dt \qquad\qquad (3.6)$$

3.2.1 Random and Pseudorandom Signal Correlation Methods

A generalized correlation system model is shown in Figure 3.4. The output of the correlator, as derived in Appendix C, is given as,

$$\phi_{sr}(\tau) = \phi_{ss}(\tau) * h(\tau) \qquad\qquad (3.7)$$

The random signal correlation method is based on the statistical definition of correlation function. It employs a random excitation waveform, and the correlator approximates the true crosscorrelation function as defined in equation (3.4), by integrating over a sufficiently large time interval.

In addition to the obvious disadvantage of having a non-ideal correlator, there are two practical problems associated with this method, especially in the digital system implementation. These are:

(a)   generation and storage of a truly random excitation signal,

(b)   generation of arbitrary delay in the reference signal required for crosscorrelation.
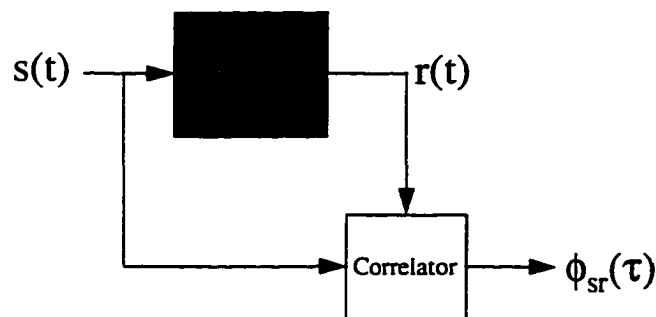
Figure 3.4: Generalized correlation system model.

The pseudorandom signal correlation method is based on the mathematical definition of correlation function. It employs a pseudorandom excitation waveform, which can either be an expanded pulse, for a coded-pulse correlation system, or a continuous periodic waveform, for a periodic correlation system. The correlator in both the cases evaluates the exact correlation function as represented by equations (3.5) & (3.6).

3.2.2 Self-Noise in Correlation Systems

In all types of correlation systems, it is desired to employ an excitation waveform that possesses perfect autocorrelation properties. A perfect autocorrelation function in the present context implies zero correlation sidelobes. Thus, the ideal autocorrelation function of an excitation waveform, s(t), can be written as,

$$\phi_{ss}(\tau)=0 \quad for \quad \tau>T_c \tag{3.8}$$

where T_c represents the symbol duration or the "chip interval", and is inversely related to the bandwidth of the excitation waveform.

If the excitation waveform does not meet this condition, it results into what is called the self-noise of the system. Self-noise is an undesirable characteristics of correlation systems as it can bring unreal artifacts in the measured impulse response. Self-noise can result into masking of weaker signal components of the true impulse response.

In case of random signal correlation systems, the self-noise is a result of non-ideal correlator implementation and it can only be minimized by increasing the integration interval of the correlator, which means, at the cost of increased processing resources. Thus, in practice such systems provide much lesser advantage than their pseudorandom counterparts.

In the pseudorandom category, the coded-pulse systems employ a linear correlator and hence, the linear autocorrelation characteristics of the excitation waveform is of

importance. There has been extensive research in the field of communications [35, 36, 37] to design waveforms with smaller and smaller autocorrelation sidelobes. The autocorrelation characteristics of a pseudorandom waveform directly depends on the autocorrelation properties of the corresponding pseudorandom sequence. A variety of sequences have been developed for this purpose. Some well known sequences in this context are, Barker sequences, maximal-length sequences, polyphase sequences, complementary sequences, and Golomb sequences. However, there is a fundamental lower limit beyond which sidelobe suppression is not possible, and out of all the different sequences mentioned above, only the Barker sequences meet this limit [35].

In case of periodic signal correlation systems, the periodic correlation characteristics of the excitation waveform and the associated sequence determine the self-noise level. There is no fundamental limit to sidelobe suppression, and in theory, the sidelobes can be completely eliminated. This issue is further discussed in the next chapter.

3.3 Correlation versus Impulse Response Averaging

The output of a correlation system is proportional to the impulse response of the composite test system, analogous to the output of a pulsed system (see Appendix C for detail). However, the correlation system provides an improvement in the output signal-to-noise ratio (SNR). Another technique frequently used for SNR improvement is impulse response averaging. In certain respects correlation processing and impulse response averaging are very similar. There are however, certain practical benefits which makes the correlation technique superior. The following discussion indicates the strengths of correlation technique over impulse response averaging.

The averaging technique is based on the ensemble-average concept of a random signal, while, the correlation technique implies the time-average concept. It is well known [61] that, if the random process can be considered ergodic, the two types of averages are equivalent and hence, in theory, correlation and averaging techniques are equivalent. The

difference comes in the practical implementation. In order to perform an ensemble-averaging of L realizations of the measurement, one has to transmit L periodic pulses, and receive L periods of the pulse-echo waveform. On the other hand, the correlation technique can provide the equivalent averaging effect with only a single period of the pseudorandom waveform.

There is yet another argument which shows the robustness and the superiority of correlation method over the averaging technique. So far, in our analysis we assumed that the noise spectrum is uniformly distributed over the spectrum of the interrogation signal. In the absence of any specific knowledge about the unwanted system noise characteristics, this is considered a reasonable assumption. It generally represents the worst case and provides the lower bound on the system performance.

While the assumption of uniform distribution of the frequency spectrum of noise is true in many situations, it is rarely true in certain other situations, especially in broadband systems. Particularly, in ultrasonic NDE, acoustic noise has a non-uniform spectrum, various kinds of electrical interferences are in fact highly narrowbanded. This fact was practically observed during the instrument development and laboratory experimentation part of the current research work. The operation of ultrasonic NDE instrument in a field environment is even more susceptible to various kinds of interferences. Under these conditions, correlation method performs superior than the averaging method.

3.5.1 Mathematical Analysis

Let the impulsive excitation system be represented in discrete time by,

$$y(n) = x(n) * h(n) + u(n) \qquad (3.9)$$

where $x(n)$ is a pulsed excitation signal. The width of the pulse is T_c and the pulse repetition interval is LT_c. Here, $h(n)$ represents the impulse response of the composite system, and $y(n)$ is the measured system output which consists of a signal component,

and an interference component, u(n). Assuming a perfectly coherent system, the multiple realizations of the received signal will have the same signal component but different interference components. Hence they can be represented as,

$$y_k(n) = x(n) * h(n) + u_k(n) \tag{3.10}$$

The result of impulse averaging can be represented by,

$$z(n) = \sum_{k=1}^{L} y_k(n) = \sum_{k=1}^{L} x(n) * h(n) + \sum_{k=1}^{L} u_k(n) \tag{3.11}$$

$$z(n) = L[x(n) * h(n)] + \sum_{k=1}^{L} u_k(n) \tag{3.12}$$

$$z(n) = L[x(n) * h(n)] + w_a(n) \tag{3.13}$$

where $w_a(n)$ represents the interference component of the averaged signal, $z(n)$.

The received signal in a pseudorandom correlation system can be written as,

$$r(n) = s(n) * h(n) + u(n) \tag{3.14}$$

and the correlator output is given by,

$$\phi_{sr}(\tau) = \phi_{ss}(\tau) * h(\tau) + \sum_{n=1}^{L} s(n) u(n - \tau) \tag{3.15}$$

$$\phi_{sr}(\tau) = \phi_{ss}(\tau) * h(\tau) + w_c(\tau) \tag{3.16}$$

where $w_c(\tau)$ represents the interference component of the correlator output. If the excitation signals s(n) and x(n) have equal amplitudes and the period of s(n) is L times the duration of x(n), it can be shown that,

$$\phi_{ss}(\tau) * h(\tau) = L[x(\tau) * h(\tau)] \qquad (3.17)$$

Hence the energy of the signal components of equations (3.16) and (3.13) is equal and the performance comparison reduces to the comparison of the interference components, $w_a(n)$ and $w_c(\tau)$, which are given as,

$$w_a(n) = \sum_{k=1}^{L} u_k(n) \qquad (3.18)$$

$$w_c(\tau) = \sum_{n=1}^{L} s(n-\tau) u(n) \qquad (3.19)$$

As a worst case scenario, the interfering signal can be considered as a single frequency component having an amplitude A, and the averaging operation will result into the coherent averaging of the interfering signal, leading to,

$$w_a(n) = LA \cos(\omega_0 n) \qquad (3.20)$$

Thus the interference signal power will be $(LA)^2/2$. The expression of equation (3.19) for the case of single frequency interference component can be written as,

$$w_c(\tau) = A \sum_{n=1}^{L} s(n-\tau) \cos(\omega n) \qquad (3.21)$$

Considering that s(n) is a discrete-time binary pseudorandom waveform, with elements +1 and -1, the product $s(n-\tau)\cos(\omega n)$ in equation (3.21) represents a BPSK modulation of the interfering signal. This process makes the interfering signal uncorrelated from one sample to another. Hence, the summation in equation (3.21) represents averaging of independent samples (non-coherent averaging), and the power of $w_c(\tau)$ will be $LA^2/2$. This represents the reduction of interference power by a factor of L, compared to the averaging case.

Figure 3.5 gives the graphical representation of the SNR improvement by correlation versus averaging methods under different conditions of interference. It is assumed that the average power of the interfering signal remains constant. The spectral power distribution of interference signal varies from one extreme of uniform distribution to the other extreme of a single frequency component.

3.4 Spread-Spectrum Ultrasonic Evaluation Technique

Spread-spectrum ultrasonic evaluation (SSUE) is a new technique of ultrasonic nondestructive evaluation that is being investigated at the Iowa State University [62, 63, 64]. This technique is based upon the impulse response approach to ultrasonic NDE. It estimates the acoustic-impulse-response of the test object through the method of periodic pseudorandom signal correlation. The basic method of generation of pseudorandom excitation waveform and the correlation processing of the received signal is adopted from the Direct-Sequence Spread-Spectrum technique of communications field, hence the name spread-spectrum ultrasonic evaluation (SSUE) is given to this technique.
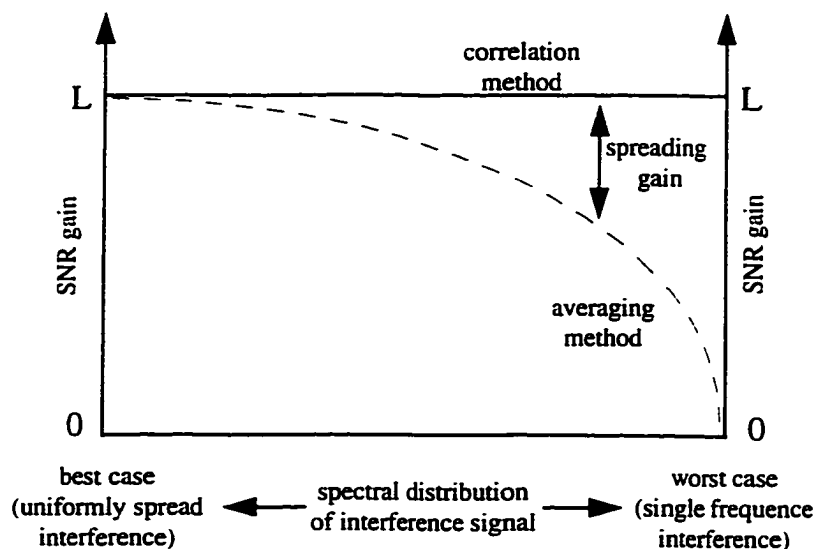
Figure 3.5: Performance comparison of correlation and averaging technique.

The block diagram of the SSUE system is given in Figure 3.6. The spread-spectrum transmitter generates a pseudorandom excitation waveform, s(t). This is introduced into the test object as an ultrasonic signal using a suitable transmit transducer. The scattered ultrasound is picked up by the receiving transducer and converted into an electrical signal, r(t). Function h(t) represents the impulse response of the composite system which includes, the test object, transmit and receive transducers and their associated electronics. The spread-spectrum correlation receiver computes the cross-correlation between the received waveform, r(t) and the transmitted waveform, s(t). Since the ultrasonic transducers typically have a bandpass characteristics, the excitation waveform, s(t), is generated by the modulation of a carrier signal of frequency, f_o, with a pseudorandom sequence.

The output of the correlator under ideal conditions can be written as,

$$\phi_{sr}(\tau)=h(\tau) \tag{3.22}$$

The correlator output, $\phi_{sr}(\tau)$, is referred as the ultrasonic correlation signature as it
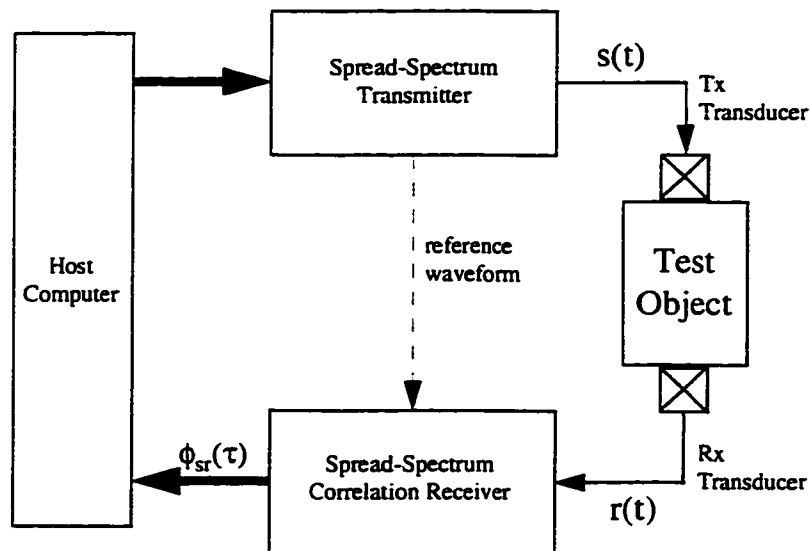
Figure 3.6: SSUE system block diagram.

represents the characteristic signature of the test object. A host computer controls the transmitter and the receiver. It is also used as the signal processing platform for the analysis of the measured ultrasonic correlation signature.

3.5 Practical Considerations for SSUE Technique

A practical SSUE system has to deal with the following undesirable system characteristics,

(a)   Input signal, s(t), is not perfect

(b)   Various kinds of noise is present

A perfect input signal for SSUE is one whose PACF is given by equation (3.8). The received signal, r(t), under the above conditions is given by,

$$r(t) = h(t) * s(t) + n(t) \tag{3.23}$$

and the output of the correlator can be written as,

$$\phi_{sr}(\tau) = h(\tau) * \phi_{ss}(\tau) + N_r(\tau) \tag{3.24}$$

where $N_r(\tau)$ represents the random noise component of the ultrasonic correlation signature and is a result of the additive random noise component of the received signal r(t). It is given by,

$$N_r(\tau) = \int_{t=t_o}^{(t_o+T)} s(t+\tau)\, n(t)\, dt \; . \tag{3.25}$$

The first term in equation (3.24) represents the convolution of the input signal PACF with the composite system impulse response. It can be considered as consisting of two additive components, such that,

$$\phi_{sr}(\tau) = h(\tau) + N_s(\tau) + N_r(\tau) \tag{3.26}$$

Here $N_s(\tau)$ represents the self- noise component of the ultrasonic correlation signature. Self noise is a result of the autocorrelation sidelobes of the input signal. It is correlated with the input signal, s(t), and the system impulse response, h(t). Magnitude of self noise depends on, (a) the level of PACF sidelobes with respect to the mainlobe of the input signal, s(t), and, (b) the nature of the system impulse response, h(t). If h(t) contains a strong component like backwall reflection, the magnitude of $N_s(\tau)$ can be large enough to mask a weaker component of h(t).

Various sources of random noise are, (a) electrical noise, (b) acoustic noise, and, (c) quantization noise. All noise components can be assumed to be uncorrelated with each other as well as with h(t) and s(t). Magnitude of $N_r(\tau)$ depends on the period of the input signal, i.e., the extent of pulse compression.

Since $N_s(\tau)$ and $N_r(\tau)$ are independent and uncorrelated with respect to each other, the total noise magnitude will be dominated by the stronger of the two components. It is useful to define two types of signal to noise ratios,

SNR_s Signal to self noise ratio

SNR_r Signal to random noise ratio

Under certain experimental conditions, SNR_s will be much lesser than SNR_r. In such a situation, the overall SNR can only be improved by increasing the pulse compression. In other conditions, the accuracy in the estimation of h(t) will be limited by the SNR_s .

The above analysis opens three directions for further investigation, in order to achieve a better estimate of h(t). These are,

(a) design of excitation waveform with better autocorrelation properties

(b) design of improved correlation receiver in order to suppress self-noise

(c) efficient correlator design, both in terms of time and computer resources

The first two deal with the system design strategy. These are investigated in the following chapter. While, the third is a system implementation issue, and is, therefore, discussed at a later stage under Chapter 6.

CHAPTER 4   OPTIMUM SSUE SYSTEM DESIGN

This chapter investigates various designs of the SSUE system and compares their performance. First the optimality criteria is defined followed by the analysis of an optimum SSUE system. Two types of system design approaches are considered. One is the optimum system design approach and the other is a sub-optimum system design approach. Finally, system optimization under the bandwidth constraint is considered.

4.1 Mathematical Definitions and Preliminaries

1. Pseudorandom Sequence: A set of numbers, real or complex, possessing certain randomness properties. A two-valued pseudorandom sequence is based on two elements A and B, where A and B can be real or complex constants of any value. A binary pseudorandom sequence is a special case, where $A = +1$ and $B = -1$. A complex sequence $\{z_n\}$ can be represented by its real and imaginary components or alternately by its magnitude and phase components, such that,

$$z_n = a_n + jb_n = r_n e^{j\theta_n} \tag{4.1}$$

2. PACF of a Pseudorandom Sequence: The periodic autocorrelation function of a complex pseudorandom sequence, $\{z_n\}$, is defined as,

$$P_{zz}(k) = \sum_{n=1}^{L} z_n z^*_{n+k} \tag{4.2}$$

where $k = 0, 1, 2, \ldots , (L-1)$, and L is the length of the sequence.

3. **Perfect Pseudorandom Sequence:** A given pseudorandom sequence is considered perfect if it possesses ideal PACF properties, defined as,

$$P_{zz}(k=0)=\sum_{n=1}^{L} z_n z^*_n = M \tag{4.3}$$

$$P_{zz}(k \neq 0)=\sum_{n=1}^{L} z_n z^*_{n+k} = 0 \tag{4.4}$$

where M is a real constant. For binary sequences, M = L.

4. **Baseband Pseudorandom Waveform:** This is a baseband periodic waveform, c(t), based on the pseudorandom sequence, $\{z_n\}$, and given by,

$$c(t)=\sum_{n=1}^{L} z_n p(t-nT_c) \tag{4.5}$$

where, p(t) is a unit amplitude pulse of duration T_c starting at time zero. The period of the waveform, T, is given by,

$$T=L \cdot T_c \tag{4.6}$$

An alternate representation of c(t) is,

$$c(t)=\sum_{n=1}^{L} a_n p(t-nT_c) + j\sum_{n=1}^{L} b_n p(t-nT_c)$$

$$=a(t)+jb(t) \tag{4.7}$$

where, a(t) and b(t) are respectively the inphase and quadrature waveform components.

5. **Bandpass Pseudorandom Waveform:** Also called pseudorandom excitation waveform, this is a periodic bandpass waveform, s(t), based on the pseudorandom sequence, $\{z_n\}$, and

given by,

$$s(t) = a(t)\cos(\omega_o t) - b(t)\sin(\omega_o t) \tag{4.8}$$

where, a(t) and b(t) are respectively the inphase and quadrature components of the baseband pseudorandom waveform, c(t), and $\omega_o = 2\pi f_o$ is the center frequency or carrier frequency of the bandpass waveform.

6. PACF of a Pseudorandom Waveform: The periodic autocorrelation function of a pseudorandom waveform, s(t), is defined, in continuous time, as,

$$\phi_{ss}(\tau) = \int_{t=0}^{T} s(t-\tau)s(t)dt \tag{4.9}$$

and in discrete time as,

$$\phi_{ss}(\tau) = \sum_{n=1}^{N} s(n-\tau)s(n) \tag{4.10}$$

7. Perfect Pseudorandom Waveform: A given pseudorandom waveform is considered perfect if it possesses ideal PACF properties, defined as,

$$\phi_{ss}(\tau) = 0 \quad for \quad T > \tau > T_c \tag{4.11}$$

8. PCCF of two Pseudorandom Waveforms: The periodic crosscorrelation function of two waveforms is defined, in continuous time, as,

$$\phi_{sr}(\tau) = \int_{t=0}^{T} s(t-\tau)r(t)dt \qquad (4.12)$$

and in discrete time as,

$$\phi_{sr}(\tau) = \sum_{n=1}^{N} s(n-\tau)r(n) \qquad (4.13)$$

9. Ideal System Impulse Response: This is the impulse response of composite ultrasonic NDE system that includes the test object, the transmit and receive transducers and associated amplifiers. The ideal impulse response, h(t), can be represented by,

$$h(t) = h_0(t) * h_s(t) \qquad (4.14)$$

where, $h_o(t)$ represents the impulse response of the test object, and

$h_s(t)$ represent the impulse response of the transducers, etc.

10. Bandlimited System Impulse Response: The bandlimited SSUE system impulse response is represented by $\bar{h}(t)$ and is given by,

$$\bar{h}(t) = \bar{h}_0(t) * \bar{h}_s(t) \qquad (4.15)$$

where $\bar{h}_o(t)$ and $\bar{h}_s(t)$ are the bandlimited versions of $h_o(t)$ and $h_s(t)$ respectively.

11. Signal-to-random-noise ratio: The signal-to-random-noise ratio (SNR_r) of the measured correlation signature represents the ratio of peak signal power and the average uncorrelated random noise power. It is defined as,

$$SNR_r = \text{Peak Signal Power} / \text{Average Noise Power}$$

If the correlation signature has a peak amplitude of A units, then the above definition is equivalent to,

$$SNR_r = A^2 / Var(n)$$
(4.16)

A general definition of signal-to-noise ratio (SNR) always implies the randomness of noise. The categoric mention of the random-noise here is only for the purpose of distinction from the later described signal-to-self-noise ratio (SNR_s).

12. Signal-to-self-noise ratio: The signal-to-self-noise ratio (SNR_s) of the measured correlation signature represents the ratio of peak signal power and the peak self-noise power. It is defined as,

SNR_s = Peak Signal Power / Peak Self-Noise Power

For a pseudorandom waveform based on a maximal length sequence of length, L, the signal-to-self-noise ratio expressed in dB is given by,

$$SNR_s = 20 \log_{10}(1/L)$$
(4.17)

13. Dynamic Range: Dynamic range of a signal or a waveform is defined as the ratio of amplitudes of the strongest signal component to the weakest signal component of interest. In ultrasonic NDE systems, it is generally desired to have a large dynamic range so that very weak reflections from a flaw can be detected in the presence of strong boundary reflections.

14. Sensitivity: Sensitivity is a qualitative term used to describe or compare the performance of a system in detecting very small changes in its measurements. It is directly related to the SNR of the system. Thus if a measurement system has large SNR, it is capable of detecting small changes in the measured parameters and is, therefore, more sensitive.

4.2 Ideal versus Practical SSUE

As we move from a mathematically ideal concept of SSUE technique towards a practical SSUE instrument, various non-ideal effects have to be taken into consideration. For the purpose of analysis, this transition from the ideal to a practical SSUE system is discussed through the following steps.

(a) Ideal SSUE system: The ideal SSUE system is considered to have zero self-noise and no bandwidth limitation, thus the correlator output can be written as,

$$\phi_{sr}(\tau)=h(\tau)+N_r(\tau) \tag{4.18}$$

The system performance in this case is only limited by the signal to random noise ratio as defined earlier.

(b) Bandwidth constrained SSUE system: This represents an SSUE system with zero self noise, but having a finite system bandwidth B. The correlator output for such a system can be represented as,

$$\phi_{sr}(\tau)=\tilde{h}(\tau)+\tilde{N}_r(\tau) \tag{4.19}$$

where $\tilde{h}(\tau)$ represents a bandlimited version of the true impulse response, $h(\tau)$, and $\tilde{N}_r(\tau)$ represents the bandlimited version of the additive whit noise, $N_r(\tau)$. The system performance in this case is limited by the signal to random noise ratio and the loss of resolution of h(t) due to the bandlimiting effect.

(c) Self-Noise constrained SSUE system: This represents an SSUE system that has a non-zero self-noise but has no bandwidth limitation. The correlator output in this case is represented by three additive terms as,

$$\phi_{sr}(\tau)=h(\tau)+N_r(\tau)+N_s(\tau) \qquad (4.20)$$

where $N_s(\tau)$ represents the self-noise component of the measured correlation signature. The system performance in this case can be limited by either the signal to random noise ratio or the signal to self noise ratio depending upon specific application conditions.

(d) Bandwidth and Self-Noise constrained SSUE system: This represents an SSUE system that has a non-zero self-noise and also has a finite system bandwidth. The correlator output in this case is represented by three additive terms as,

$$\phi_{sr}(\tau)=\tilde{h}(\tau)+\tilde{N}_r(\tau)+\tilde{N}_s(\tau) \qquad (4.21)$$

where $\tilde{N}_s(t)$ represents the bandlimited version of the self-noise component, $N_s(t)$. The system performance in this case is limited by all the three factors, the signal to random noise ratio, signal to self noise ratio and the loss of resolution.

The effect of finite bandwidth is the loss of resolution of h(t). Also, the high frequency (characteristics) features of the true impulse response would be missing in the measured correlation signature. This can be a setback in applications where high resolution is important or where high frequency characteristics are crucial to the nature of the problem. However, in certain other applications, it may not be a big disadvantage. An appropriate waveform design can ensure that we gain the maximum benefit of loss of average noise power as a result of bandlimiting, while minimizing the loss in signal power and its resolution. This aspect of the optimum waveform design will be discussed in section 4.6.

The second non-ideal effect is due to the non-perfect PACF of the excitation waveform. As discussed earlier in section 3.7, this can be a serious limitation in various NDE situations, especially when an object of smaller dimensions is inspected. A major part of the present research effort was devoted to studying various methods of eliminating the self-noise. It was found that there can be two broad approaches to suppress the self-

noise. One approach searches for various pseudorandom waveforms that have perfect PACF properties, while the other searches for an appropriate self-noise suppression filter for the given excitation waveform. The first approach results into what is called an optimum SSUE design and is discussed under section 4.4, while the second approach corresponds to the sub-optimum SSUE design and is presented under section 4.5. Before that, however, the optimality criteria for the system design needs to be defined.

4.3 Optimality Criteria for a Practical SSUE System

The SNR gain of SSUE system is first defined and evaluated. Various system optimization factors are then presented followed by a discussion on the optimization strategies pursed for SSUE system design.

4.3.1 SNR Gain of SSUE

This is the gain in signal-to-random-noise ratio of SSUE correlation signature compared to the signal-to-noise ratio of a pulsed excitation system, under the condition that the excitation waveform is peak-amplitude limited. For a pulsed excitation system, the received signal, y(k), is given as,

$$y(k) = x(k) * h(k) + n(k) \qquad (4.22)$$

where, x(k) is the input pulse of amplitude A, h(k) is the impulse function, and n(k) is the random noise with a standard deviation of σ_n. For the purpose of SNR analysis, the impulse response, h(t), can be assumed to be a delta function. Hence,

$$y(k) = x(k) + n(k) \qquad (4.23)$$

The SNR of this received signal is defined as,

$$SNR_p = (\frac{A}{\sigma_n})^2 \qquad (4.24)$$

For the SSUE system, the received signal is given by,

$$r(k) = s(k) * h(k) + n(k) \qquad (4.25)$$

where, s(k) is the pseudorandom excitation waveform having an amplitude A, h(k) is the system impulse function, and n(k) is the additive random noise with a standard deviation of σ_n. The output of the correlation filter can be written as,

$$\phi_{sr}(\tau) = \phi_{ss}(\tau) * h(\tau) + N_r(\tau) \qquad (4.26)$$

Once again assuming $h(\tau) = \delta(\tau)$, we get,

$$\phi_{sr}(\tau) = \phi_{ss}(\tau) + N_r(\tau) \qquad (4.27)$$

where,

$$\phi_{ss}(\tau) = \sum_{k=1}^{L} s(k)s(k+\tau) \qquad (4.28)$$

and,

$$N_r(\tau) = \sum_{k=1}^{L} n(k)s(k+\tau) \qquad (4.29)$$

The SNR for the correlator output is given by,

$$SNR_c = \frac{(\phi_{ss}(\tau=0))^2}{Var(N_r(\tau))} \qquad (4.30)$$

$$SNR_C = \frac{\left(\sum_{k=1}^{L} s(k)^2\right)^2}{\sigma_n^2 \sum_{k=1}^{L} s(k)^2}$$ (4.31)

The pseudorandom excitation waveform can be represented as the product of a pseudorandom sequence, z(k), with a pulse x(k) having amplitude A, such that,

$$s(k)=z(k).x(k)$$ (4.32)

$$SNR_C = \frac{A^2}{\sigma_n^2} \sum_{k=1}^{L} z(k)^2$$ (4.33)

Comparing equation (4.33) with (4.24), the SNR gain, G, is given by,

$$G=\sum_{k=1}^{L} z(k)^2$$ (4.34)

If z(k) represents a binary sequence with elements +1 and -1, the above equation reduces to,

$$G=L$$ (4.35)

where L is the length of pseudorandom binary sequence, z(k).

4.3.2 System Optimization Factors

There are four basic factors to be optimized in the design process of an SSUE system. These are:

    (a) SNR Gain   (b) Signal-to-self noise ratio

    (c) Energy efficiency   (d) Resolution

The definitions of SNR gain factor and the signal-to-self-noise ratio for SSUE system has already been presented. The energy efficiency, η, is defined as,

$$\eta = \frac{average\ transmit\ power}{peak\ transmit\ power} \tag{4.36}$$

The optimality in resolution is independent of the other three optimization criterion. It is, therefore, discussed separately under section 4.6 of this chapter. Thus, the general approach is to first optimize the system with respect to the first three optimization factors and then to consider the optimization in resolution. Two types of system optimization strategies were pursed,

(a) Optimum SSUE design

(b) Sub-optimum SSUE design

Sometimes, from the system implementation point of view, a sub-optimum design performs better or equally well with respect to the optimum designs and this was the spirit in pursing both the above strategies. The implementation losses for the optimum designs lower the overall performance compared to the suboptimum case. Also economic constraints might favor the suboptimum design.

4.4 Optimum SSUE Design

Optimum SSUE design implies optimum transmitter and optimum receiver (Figure 4.1). An optimum transmitter is one that generates a periodic excitation waveform that has perfect PACF properties. An optimum receiver is one that provides the maximum theoretical SNR gain factor.

4.4.1 Optimum Transmitter

The SSUE transmitter consists of a waveform generator and a modulator (Figure 4.2). The waveform generator generates the continuous-time baseband waveform, c(t),
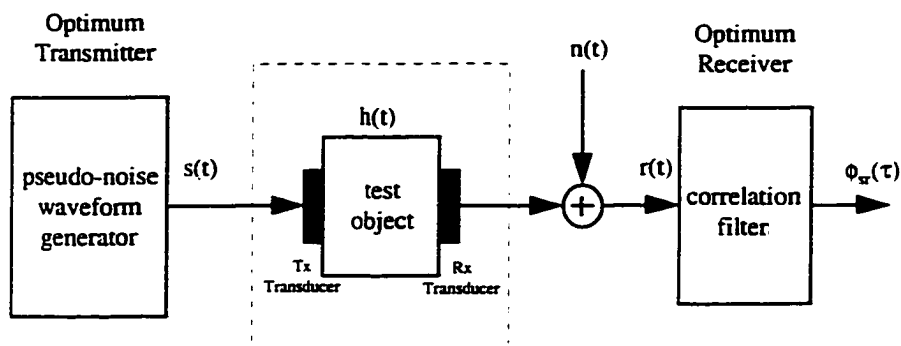
Figure 4.1: Optimum SSUE model.

based on the pseudorandom sequence, z(n), and the pulse function, p(t). For the present discussion, p(t) is assumed to be a rectangular pulse function, however, it is explained later that this is not the best choice of a pulse function for SSUE application. The modulator translates the baseband waveform, c(t), to a suitable center frequency f_0, depending upon the specific application and the choice of transducers. The PACF of the final (bandpass) waveform, s(t), depends on the PACF properties of the baseband
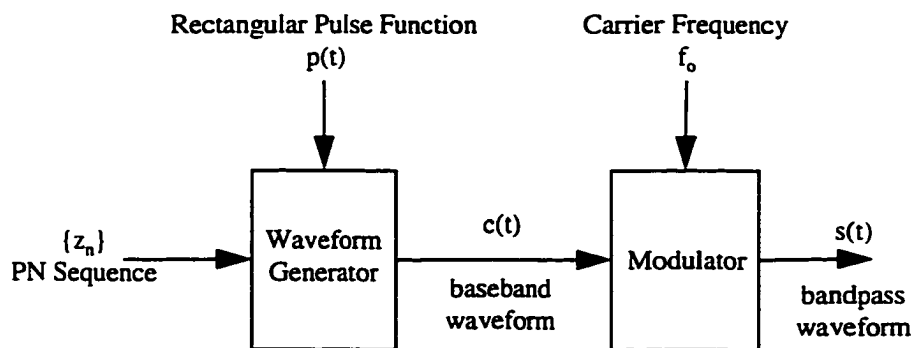
Figure 4.2: SSUE transmitter block diagram.

waveform, c(t), and in turn on the properties of the pseudorandom sequence, z(n).

In order to generate a perfect excitation waveform, s(t), we need to begin with a perfect pseudorandom sequence, z(n), ensure that the corresponding baseband waveform, c(t), is perfect and that the modulator preserves the perfect PACF characteristics of the waveform as it translates from baseband to a center frequency f_0.

4.4.2 General Problem Formulation

The perfect excitation waveform design problem is broken down into the following steps. Each step is mathematically analyzed and a set of necessary conditions are developed which lead to the design of a perfect excitation waveform.

(a)   Evaluation of PACF of a sequence

(b)   Evaluation of PACF of baseband waveform

(c)   Evaluation of PACF of bandpass waveform

PACF of a Pseudorandom Sequence: Let $\{z_n\}$ be a complex PN sequence of length L, such that,

$$z_n = (a_n + jb_n)$$

(4.37)

The PACF of the sequence is defined as,

$$P_{zz}(d) = \sum_{n=1}^{L} z_n z^*_{n+d}$$

(4.38)

$$P_{zz}(d) = \sum_{n=1}^{L} (a_n + jb_n)(a_{n+d} - jb_{n+d})$$

(4.39)

$$P_{zz}(d) = \sum_{n=1}^{L} (a_n a_{n+d} + b_n b_{n+d}) + j\sum_{n=1}^{L} (a_{n+d} b_n - a_n b_{n+d})$$

(4.40)

where, $d = 1, 2, 3, \ldots$ (L-1). The PACF is considered perfect if,

$$P_{zz}(d) = \sum_{n=1}^{L} z_n z^*_{n+d} = L, \text{ for } d=0 \ (\text{mod } L) \tag{4.41}$$

$$P_{zz}(d) = \sum_{n=1}^{L} z_n z^*_{n+d} = 0, \text{ for } d \neq 0 \ (\text{mod } L) \tag{4.42}$$

This implies that, for perfect PACF,

$$\sum_{n=1}^{L} (a_n b_{n+d} - a_{n+d} b_n) = 0, \text{ for all } d \tag{4.43}$$

$$\sum_{n=1}^{L} a_n a_{n+d} + b_n b_{n+d} = 0 \text{ for } d \neq 0 \tag{4.44}$$

PACF of Baseband Pseudorandom Waveform: Let c(t) be a periodic waveform of period T, based on the sequence $\{ z_n \}$ and given by,

$$c(t) = \sum_{n=1}^{L} z_n p(t - nT_c) \tag{4.45}$$

where, p(t) is a unit amplitude pulse of duration T_c starting at time zero. Also,

$$T = L \cdot T_c \tag{4.46}$$

The periodic autocorrelation function (PACF) of the baseband waveform is defined as,

$$\phi_{cc}(\tau) = \int_{t=0}^{T} c(t) c^*(t+\tau) dt, \ 0 \leq \tau \leq T \tag{4.47}$$

The integral over the waveform period, T, can be written as the sum of sub-integrals over one chip duration. Therefore,

$$\phi_{cc}(\tau) = \sum_{n=1}^{L} \int_{(n-1)T_c}^{nT_c} c(t) c^*(t+\tau) dt, \quad 0 \le \tau \le T \tag{4.48}$$

Each sub-integral of equation (4.48) can be further split into two parts, such that, the product $[c(t).c^*(t+\tau)]$ is constant over each integration interval (Figure 4.3). Also, the correlation lag, τ, can be written as,

$$\tau = dT_c + \Delta\tau, \quad \Delta\tau < T_c \tag{4.49}$$

$$\phi_{cc}(\tau) = \sum_{n=1}^{L} [\int_{(n-1)T_c}^{nT_c - \Delta\tau} z_n z_{n+d} dt + \int_{nT_c - \Delta\tau}^{nT_c} z_n z_{n+d+1} dt] \tag{4.50}$$

$$\phi_{cc}(\tau) = \sum_{n=1}^{L} [z_n z_{n+d}(T_c - \Delta\tau) + z_n z_{n+d+1}\Delta\tau] \tag{4.51}$$

$$\phi_{cc}(\tau) = \Delta\tau \sum_{n=1}^{L} z_n z_{n+d+1} + (T_c - \Delta\tau) \sum_{n=1}^{L} z_n z_{n+d} \tag{4.52}$$

$$\tau = \Delta\tau + dT_c$$
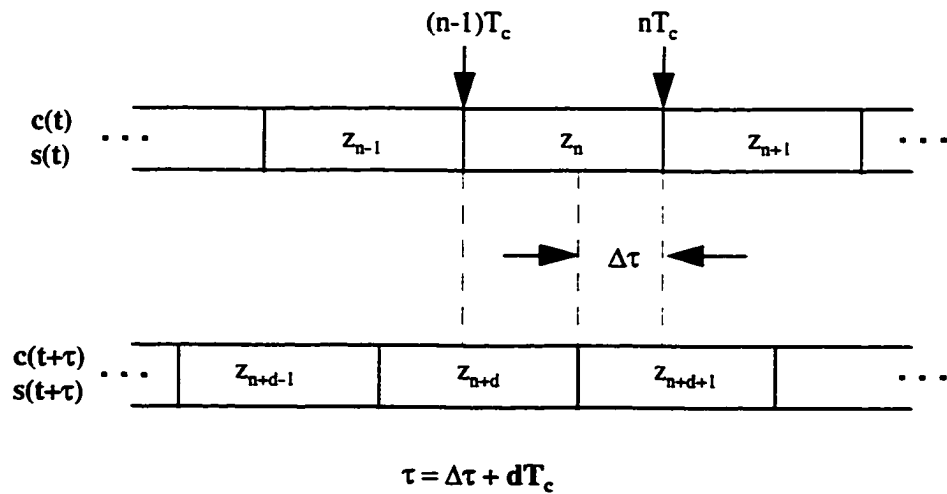
Figure 4.3: Graphical representation of correlation.

Equation (4.52) is now in the form where the PACF properties of the sequence can be applied. If the sequence has perfect PACF as defined by equations (4.41) & (4.42), then, when $(\tau < T_c), d=0, \tau = \Delta\tau$ and equation (4.52) reduces down to,

$$\phi_{cc}(\tau) = L(T_c - \tau), \; for \; \tau \leq T_c \qquad (4.53)$$

when $(\tau > T_c), d \neq 0$ and equation (4.52) reduces down to,

$$\phi_{cc}(\tau) = 0, \; for \; \tau > T_c \qquad (4.54)$$

Equations (4.53) and (4.54) define the perfect PACF of a baseband PN waveform. The above results lead to the conclusion that, for any complex pseudorandom sequence with perfect PACF, the resulting baseband waveform will also have a perfect PACF.

PACF of Bandpass Pseudorandom Waveform: Let $s(t)$ be a periodic bandpass waveform with period T, based on the complex sequence $\{z_n\}$, and given by,

$$s(t) = a(t)\cos(\omega_0 t) - b(t)\sin(\omega_0 t) \qquad (4.55)$$

where, $\omega_0 = 2\pi f_0$ is the carrier frequency. Also, we assume that the period of the carrier frequency, T_0, is an integral multiple of the chip interval, T_c. The periodic autocorrelation function (PACF) of the bandpass waveform is given as,

$$\phi_{ss}(\tau) = \int_{t=0}^{T} s(t)s(t+\tau)dt \qquad (4.56)$$

The product s(t)s(t+τ) can be written as,

$$s(t)s(t+\tau)=a(t)a(t+\tau)\cos(\omega_0 t)\cos(\omega_0 t+\omega_0\tau)$$
$$+ b(t)b(t+\tau)\sin(\omega_0 t)\sin(\omega_0 t+\omega_0\tau)$$
$$- a(t)b(t+\tau)\cos(\omega_0 t)\sin(\omega_0 t+\omega_0\tau)$$
$$- a(t+\tau)b(t)\sin(\omega_0 t)\cos(\omega_0 t+\omega_0\tau)$$

$$(4.57)$$

and after applying some trigonometric identities as,

$$2s(t)s(t+\tau)= a(t)a(t+\tau)[\cos(\omega_0\tau)+ \cos(2\omega_0 t+\omega_0\tau)]$$
$$+ b(t)b(t+\tau)[\cos(\omega_0\tau)- \cos(2\omega_0 t+\omega_0\tau)]$$
$$- a(t)b(t+\tau)[\sin(\omega_0\tau)+ \sin(2\omega_0 t+\omega_0\tau)]$$
$$+ a(t+\tau)b(t)[\sin(\omega_0\tau)- \sin(2\omega_0 t+\omega_0\tau)]$$

$$(4.58)$$

Hence, the PACF function, $\phi_{ss}(\tau)$, will consist of the following four integral terms,

$$2\phi_{ss}(\tau)= \int_{t=0}^{T} [a(t)a(t+\tau)+b(t)b(t+\tau)]\cos(\omega_0\tau)dt$$
$$+ \int_{t=0}^{T} [a(t)a(t+\tau)-b(t)b(t+\tau)]\cos(2\omega_0 t+\omega_0\tau)dt$$
$$- \int_{t=0}^{T} [a(t)b(t+\tau)+b(t)a(t+\tau)]\sin(2\omega_0 t+\omega_0\tau)dt$$
$$+ \int_{t=0}^{T} [b(t)a(t+\tau)-a(t)b(t+\tau)]\sin(\omega_0\tau)dt$$

$$(4.59)$$

The last integral term of equation (4.59) above goes to zero and the expression for $\phi_{ss}(\tau)$ simplifies to,

$$2\phi_{ss}(\tau) = \cos(\omega_0\tau)\int_{t=0}^{T} [a(t)a(t+\tau)+b(t)b(t+\tau)]dt$$

$$(4.60)$$

$$+ \cos(\omega_o \tau) \int_{t=0}^{T} [a(t)a(t+\tau) - b(t)b(t+\tau)]\cos(2\omega_o t)dt \qquad (4.61)$$

$$- \sin(\omega_o \tau) \int_{t=0}^{T} [a(t)a(t+\tau) - b(t)b(t+\tau)]\sin(2\omega_o t)dt \qquad (4.62)$$

$$- \cos(\omega_o \tau) \int_{t=0}^{T} [a(t)b(t+\tau) + b(t)a(t+\tau)]\sin(2\omega_o t)dt \qquad (4.63)$$

$$- \sin(\omega_o \tau) \int_{t=0}^{T} [a(t)b(t+\tau) + b(t)a(t+\tau)]\cos(2\omega_o t)dt \qquad (4.64)$$

In order to evaluate the integral terms of equations (4.61) through (4.64), the integration interval is once again split into sub-intervals such that the PN sequence $[z_n = a_n + jb_n]$ is constant over the sub-intervals, leaving behind only the cosine and sine expressions. In conjunction with Figure 4.3, this can be represented as,

$$\int_{t=0}^{T} (--)dt = \sum_{n=0}^{(L-1)} [\int_{t=nT_c}^{nT_c+\Delta\tau} (--)dt + \int_{nT_c+\Delta\tau}^{(n+1)T_c} (--)dt] \qquad (4.65)$$

Next we need to evaluate the integrals containing cosine and sine expressions over the two sub-intervals. This leads to the following four results.

$$\int_{t=nT_c}^{nT_c+\Delta\tau} \cos(2\omega_o t)dt = \frac{\sin(2\omega_o nT_c + 2\omega_o \Delta\tau) - \sin(2\omega_o nT_c)}{2\omega_o}$$
$$= \frac{\sin(2\omega_0 \Delta\tau)}{2\omega_o}$$

(4.66)

$$\int_{t=nT_c}^{nT_c+\Delta\tau} \sin(2\omega_o t)dt = \frac{\cos(2\omega_o nT_c) - \cos(2\omega_o nT_c + 2\omega_o \Delta\tau)}{2\omega_o}$$
$$= \frac{[1-\cos(2\omega_0 \Delta\tau)]}{2\omega_o}$$

(4.67)

$$\int_{nT_c+\Delta\tau}^{(n+1)T_c} \cos(2\omega_o t)dt = \frac{\sin[2\omega_o(n+1)T_c] - \sin(2\omega_o nT_c + 2\omega_o \Delta\tau)}{2\omega_o}$$
$$= - \frac{\sin(2\omega_0 \Delta\tau)}{2\omega_o}$$

(4.68)

$$\int_{nT_c+\Delta\tau}^{(n+1)T_c} \sin(2\omega_o t)dt = \frac{\cos(2\omega_o nT_c + 2\omega_o \Delta\tau) - \cos[2\omega_o(n+1)T_c]}{2\omega_o}$$
$$= - \frac{[1-\cos(2\omega_0 \Delta\tau)]}{2\omega_o}$$

(4.69)

Applying the results from equations (4.66) through (4.69) in conjunction with equation (4.65) reduces the four integrals of equations (4.61) to (4.64) as,

$$\frac{\cos(\omega_o \tau)\sin(2\omega_o \Delta\tau)}{2\omega_o} \sum_{n=1}^{L} (a_n a_{n+d} - b_n b_{n+d}) - (a_n a_{n+d+1} - b_n b_{n+d+1})$$

(4.70)

$$\frac{\sin(\omega_o\tau)[1-\cos(2\omega_o\Delta\tau)]}{2\omega_o}\sum_{n=1}^{L}(a_n a_{n+d+1}-b_n b_{n+d+1})-(a_n a_{n+d}-b_n b_{n+d}) \qquad (4.71)$$

$$\frac{\cos(\omega_o\tau)[1-\cos(2\omega_o\Delta\tau)]}{2\omega_o}\sum_{n=1}^{L}(a_n b_{n+d+1}+b_n a_{n+d+1})-(a_n b_{n+d}+b_n a_{n+d}) \qquad (4.72)$$

$$\frac{\sin(\omega_o\tau)\sin(2\omega_o\Delta\tau)}{2\omega_o}\sum_{n=1}^{L}(a_n b_{n+d+1}+b_n a_{n+d+1})-(a_n b_{n+d}+b_n a_{n+d}) \qquad (4.73)$$

For a bandpass pseudorandom waveform to be perfect, it is to be proved that the expressions of equations (4.70) to (4.73) reduce to zero. Hence the final expression for $\phi_{ss}(\tau)$ can be written as,

$$\phi_{ss}(\tau) = \cos(\omega_0\tau)\int_{t=0}^{T}[a(t)a(t+\tau)+b(t)b(t+\tau)]dt$$

$$= \phi_{cc}(\tau)\cos(\omega_o\tau) \qquad (4.74)$$

where, $\phi_{cc}(\tau)$ represents the PACF of the baseband waveform.

4.4.3 Perfect Waveform Design Approaches

After developing a generalized approach for the synthesis and evaluation of the pseudorandom excitation waveform, and specifying a set of conditions that has to be met in order to get a perfect waveform design, this section presents four different waveform design approaches. Each approach is evaluated according to the generalized formulation of section 4.4.2 and tested for the set of conditions. Computer simulations for each of these approaches are discussed in the following chapter.

<u>Approach 1: Amplitude Modulated Pseudorandom Waveform:</u> This approach is based upon the transformation of a binary maximal-length sequence to a two-valued sequence, such that the resulting sequence exhibits perfect PACF properties. A binary sequence based on the two elements +1 and -1 can be considered as a complex sequence with constant magnitude and having phase angles 0 and 180 degrees. The new sequence described here has non-uniform magnitude and thus results into an amplitude-modulated waveform. This was the reason for calling the resulting waveform as an amplitude modulated pseudorandom waveform.

Let $\{a_n\}$ be a periodic maximal-length sequence with period L, and consisting of two elements +1 and -1. Based on the characteristics of maximal-length sequences, we can write the following,

$$\sum_{n=1}^{L} a_n = \sum_{n=1}^{L} a_{n+d} = +1 \qquad (4.75)$$

$$\sum_{n=1}^{L} a_n a_{n+d} = \sum_{n=1}^{L} a_n a_{n+d+1} = -1, \quad for\ d \neq 0 \qquad (4.76)$$

$$\sum_{n=1}^{L} a_n a_{n+d} = L, \quad for\ d = 0 \qquad (4.77)$$

The PACF of the sequence is given by,

$$P_{aa}(d) = \sum_{n=1}^{L} a_n a_{n+d} \qquad (4.78)$$

Now if we consider a maximal-length sequence with a dc offset, i.e., $\{z_n\} = \{a_n + A\}$, the PACF of this sequence is given by,

$$P_{zz}(d) = \sum_{n=1}^{L} z_n z_{n+d} \qquad (4.79)$$

$$P_{zz}(d) = \sum_{n=1}^{L} [a_n a_{n+d} + A a_n + A a_{n+d} + A^2] \qquad (4.80)$$

Using the identities of maximal-length sequence we get,

$$P_{zz}(d=0) = [L + 2A + LA^2] \qquad (4.81)$$

for the correlation sidelobes and,

$$P_{zz}(d \neq 0) = [-1 + 2A + LA^2] \qquad (4.82)$$

for the correlation peak. Setting equation (4.82) equal to zero and solving for the unknown constant A, we get,

$$[LA^2 + 2A - 1] = 0 \qquad (4.83)$$

$$A = \frac{(-1 \pm \sqrt{L+1})}{L} \qquad (4.84)$$

Hence, if A is chosen according to the above relation, then the sequence $\{z_n\}$ will be based upon two elements $'A + 1'$ & $'A - 1'$, and the PACF of the sequence will be perfect. This means that,

$$P_{zz}(d \neq 0) = \sum_{n=1}^{L} z_n z_{n+d} = 0 \qquad (4.85)$$

$$P_{zz}(d=0) = \sum_{n=1}^{L} z_n z_n = [L+1] \qquad (4.86)$$

In order to test for the perfect bandpass waveform, s(t), based on the above sequence, the following four expressions needs to be evaluated,

$$\frac{\cos(\omega_o\tau)\sin(2\omega_o\Delta\tau)}{2\omega_o}\sum_{n=1}^{L}(a_na_{n+d}-b_nb_{n+d})-(a_na_{n+d+1}-b_nb_{n+d+1}) \tag{4.87}$$

$$\frac{\sin(\omega_o\tau)[1-\cos(2\omega_o\Delta\tau)]}{2\omega_o}\sum_{n=1}^{L}(a_na_{n+d+1}-b_nb_{n+d+1})-(a_na_{n+d}-b_nb_{n+d}) \tag{4.88}$$

$$\frac{\sin(\omega_o\tau)\sin(2\omega_o\Delta\tau)}{2\omega_o}\sum_{n=1}^{L}(a_nb_{n+d+1}+b_na_{n+d+1})-(a_nb_{n+d}+b_na_{n+d}) \tag{4.89}$$

$$\frac{\cos(\omega_o\tau)[1-\cos(2\omega_o\Delta\tau)]}{2\omega_o}\sum_{n=1}^{L}(a_nb_{n+d+1}+b_na_{n+d+1})-(a_nb_{n+d}+b_na_{n+d}) \tag{4.90}$$

Since the sequence under consideration is a real sequence, i.e., ($b_n = 0$), equations (4.89) and (4.90) reduce to zero and equations (4.87) and (4.88) can be rewritten as,

$$\frac{\cos(\omega_o\tau)\sin(2\omega_o\Delta\tau)}{2\omega_o}\sum_{n=1}^{L}(a_na_{n+d}-a_na_{n+d+1}) \tag{4.91}$$

$$\frac{\sin(\omega_o\tau)[1-\cos(2\omega_o\Delta\tau)]}{2\omega_o}\sum_{n=1}^{L}(a_na_{n+d+1}-a_na_{n+d}) \tag{4.92}$$

Applying the identity of equation (4.76) reduces equations (4.91) and (4.92) also to zero. Hence the bandpass waveform meets the necessary conditions for a perfect waveform.

Energy Efficiency: The waveform generated through the above method will consist of two amplitude levels, (A+1) and (A-1). Each period of the waveform can be thought to consist of L segments of constant amplitude where each segment represents one

sequence symbol. Also, a sequence of length L will have (L+1)/2 symbols of amplitude (A+1) and (L-1)/2 symbols of amplitude (A-1). Hence, the energy efficiency achievable with this waveform is given by,

$$\eta = \frac{(L+1)(A+1)^2 + (L-1)(A-1)^2}{2(A+1)^2 L} \tag{4.93}$$

For a 10th order sequence with L=1023, the constant A takes the value of (0.0303) and the energy efficiency comes out to 0.943 or 94%.

Approach-2: Offset-Phase Modulated Pseudorandom Waveform: This approach is based upon the transformation of a binary maximal-length sequence to a complex two-valued sequence, such that the resulting sequence exhibits perfect PACF properties. A binary sequence based on the two elements +1 and -1 can be considered as a complex sequence with phase angles 0 and 180 degrees. The new complex sequence described here has the phase angles 0 and θ, where θ is slightly offset from 180 degrees and that was the reason of naming it as an offset-phase sequence.

If we consider a new sequence $\{z_n\}$, by making the following transformation on the earlier described maximal-length sequence $\{x_n\}$,

$$z_n = 1, \qquad \text{when} \quad x_n = +1,$$

$$z_n = e^{i\theta}, \qquad \text{when} \quad x_n = -1,$$

the PACF of the resulting complex sequence is given by,

$$P_{zz}(d) = \sum_{n=1}^{L} z_n \cdot z^*_{n+d} \tag{4.94}$$

Based on the properties of maximal-length sequences, we can write,

$$\sum_{n=1}^{L} z_n \cdot z^*_{n+d} = \sum_{n=1}^{L} z_n \cdot z^*_{n+d+1}, \text{ for } d \neq 0 \tag{4.95}$$

The product $z_n z_{n+d}$ in the above equation can have only two values, 1 and $e^{i\theta}$. Hence

the equation reduces to,

$$P_{zz}(d \neq 0) = \alpha.1 + \beta.e^{i\theta}$$

(4.96)

where α and β are constants. For maximal-length sequences it can also be shown that,

$$P_{zz}(d \neq 0) = \frac{(L-1)}{2} + \frac{(L+1)e^{i\theta}}{2}$$

(4.97)

In order to set the magnitude of $P_{zz}(d \neq 0)$ equal to zero, we get the constraint equation as,

$$(L-1) + (L+1).\cos(\theta) = 0$$

(4.98)

which gives the value of the phase angle as,

$$\theta = \cos^{-1}(-\frac{L-1}{L+1})$$

(4.99)

Hence, if θ is chosen according to the above relation, then the sequence $\{z_n\}$ will be based upon two elements '+1' & $e^{i\theta}$, and the PACF of the sequence will be perfect. This means that,

$$P_{zz}(d \neq 0) = \sum_{n=1}^{L} z_n z^*_{n+d} = 0$$

(4.100)

$$P_{zz}(d = 0) = \sum_{n=1}^{L} z_n z^*_n = L$$

(4.101)

In order to test for the perfect bandpass waveform, s(t), based on the above sequence, the following four expressions needs to be evaluated,

$$\frac{\cos(\omega_o \tau)\sin(2\omega_o \Delta \tau)}{2\omega_o}\sum_{n=1}^{L}(a_n a_{n+d}-b_n b_{n+d})-(a_n a_{n+d+1}-b_n b_{n+d+1})\qquad(4.102)$$

$$\frac{\sin(\omega_o \tau)[1-\cos(2\omega_o \Delta \tau)]}{2\omega_o}\sum_{n=1}^{L}(a_n a_{n+d}+b_n b_{n+d})-(a_n a_{n+d+1}+b_n b_{n+d+1})\qquad(4.103)$$

$$\frac{\sin(\omega_o \tau)\sin(2\omega_o \Delta \tau)}{2\omega_o}\sum_{n=1}^{L}(a_n b_{n+d+1}+b_n a_{n+d+1})-(a_n b_{n+d}+b_n a_{n+d})\qquad(4.104)$$

$$\frac{\cos(\omega_o \tau)[1-\cos(2\omega_o \Delta \tau)]}{2\omega_o}\sum_{n=1}^{L}(a_n b_{n+d}+b_n a_{n+d})-(a_n b_{n+d+1}+b_n a_{n+d+1})\qquad(4.105)$$

To do that equation (4.95) is rewritten in terms of its real and imaginary parts as,

$$\sum_{n=1}^{L}(a_n a_{n+d}+b_n b_{n+d})=\sum_{n=1}^{L}(a_n a_{n+d+1}+b_n b_{n+d+1})\ ,\ for\ d\neq0\qquad(4.106)$$

$$\sum_{n=1}^{L}(b_n a_{n+d}-a_n b_{n+d})=\sum_{n=1}^{L}(b_n a_{n+d+1}+a_n b_{n+d+1})\ ,\ for\ d\neq0\qquad(4.107)$$

These results when applied to equations (4.102) through (4.105) prove that the bandpass waveform, s(t), meets all the conditions of a perfect waveform.

Energy Efficiency: The waveform generated through the above method will have constant amplitude, and therefore, it will have 100% energy efficiency.

Approach 3: Polyphase Sequence based Excitation Waveform: Another class of pseudorandom sequences called polyphase sequences was investigated for possible application to SSUE technique. As the name indicates, polyphase sequences are complex

sequences based on more than two sequence elements, each element representing a different phase angle. Some well known classes of polyphase sequences are Golomb sequences, Frank sequences, P1, P2, P3 and P4 sequences [35]. Two important properties of polyphase sequences that made them attractive for the SSUE consideration were,

(a) perfect PACF properties

(b) better bandpass performance

Various classes of polyphase sequence were investigated for possible application to the SSUE technique. In the following the analysis of only one class, the polyphase P3 sequences is presented. First, the method of sequence generation is described, followed by the waveform generation and testing of various necessary conditions. The simulation work related to the polyphase sequences is presented under section 5.2.

Polyphase P3 Sequences: Any complex sequence, $\{z_n\}$, of length L, can be represented as,

$$z_n = r_n e^{(j\theta_n)} \tag{4.108}$$

For polyphase sequences, the sequence magnitude, r_n, is unity and the sequence element, z_n, is determined by the corresponding phase angle, θ_n. Hence,

$$z_n = e^{j\theta_n} \tag{4.109}$$

For polyphase P3 sequences, the phase angles are given by the formula,

$$\theta_n = \frac{\pi(n-1)^2}{L} \tag{4.110}$$

The periodic autocorrelation function (PACF) of P3 sequence can be written as,

$$P_{zz}(d) = \sum_{n=1}^{L} e^{j\theta_n} e^{-j\theta_{n+d}}$$ (4.111)

or alternately as,

$$P_{zz}(d) = \sum_{n=1}^{L} \exp[\frac{j\pi}{L}((n-1)^2 - (n-1+d)^2)]$$ (4.112)

$$P_{zz}(d) = \sum_{n=1}^{L} \exp[\frac{j\pi}{L}(2d - 2nd - d^2)]$$ (4.113)

$$P_{zz}(d) = e^{\frac{j\pi(2d-d^2)}{L}} \sum_{n=1}^{L} e^{\frac{-j2\pi nd}{L}}$$ (4.114)

The right hand side of the above equation reduces to zero for all nonzero lag values. Thus,

$$P_{zz}(d \neq 0) = 0$$ (4.115)

Thus the sequence exhibits perfect PACF properties, given by,

$$\sum_{n=1}^{L} (a_n b_{n+d} - a_{n+d} b_n) = 0, \text{for all } d$$ (4.117)

$$\sum_{n=1}^{L} a_n a_{n+d} + b_n b_{n+d} = 0 \text{ for } d \neq 0$$ (4.116)

In order to test for the perfect bandpass waveform, s(t), based on the above polyphase sequence, the following four expressions needs to be evaluated,

$$\frac{\cos(\omega_o\tau)\sin(2\omega_o\Delta\tau)}{2\omega_o}\sum_{n=1}^{L}(a_na_{n+d}-b_nb_{n+d})-(a_na_{n+d+1}-b_nb_{n+d+1}) \qquad (4.118)$$

$$\frac{\sin(\omega_o\tau)[1-\cos(2\omega_o\Delta\tau)]}{2\omega_o}\sum_{n=1}^{L}(a_na_{n+d+1}-b_nb_{n+d+1})-(a_na_{n+d}-b_nb_{n+d}) \qquad (4.119)$$

$$\frac{\sin(\omega_o\tau)\sin(2\omega_o\Delta\tau)}{2\omega_o}\sum_{n=1}^{L}(a_nb_{n+d+1}+b_na_{n+d+1})-(a_nb_{n+d}+b_na_{n+d}) \qquad (4.120)$$

$$\frac{\cos(\omega_o\tau)[1-\cos(2\omega_o\Delta\tau)]}{2\omega_o}\sum_{n=1}^{L}(a_nb_{n+d+1}+b_na_{n+d+1})-(a_nb_{n+d}+b_na_{n+d}) \qquad (4.121)$$

It was found that, for the given polyphase sequence, equations (4.118) through (4.121) do not uniquely reduce to zero. These equations can be shown to be equal to zero only for lag values in integer multiples of the chip (symbol) interval. This fact was verified through the computer simulation analysis as discussed under chapter 5.

Hence it was concluded that even though the polyphase sequences possess perfect PACF properties, a bandpass waveform derived from the polyphase sequence does not exhibit perfect PACF properties. This conclusion came as a bit of surprise as these results were not reported in the earlier work on the polyphase sequences [36, 37, 38, 39, 40]. A possible explanation of this apparent contradiction is that, in most of the radar and communication system analysis, the carrier frequency is assumed much larger than the bandwidth of the signal. Thus, various terms involving second harmonic of the carrier frequency are neglected. Such an assumption is not valid in case of the SSUE technique.

Approach 4: Complementary Sequence based Waveform: An indirect approach to achieving a perfect PACF is through the use of what are called complementary sequences.

Complementary sequences comprise a sequence pair of equal length and having the property that the sum of the PACFs of the individual sequence results into a perfect function. This is equivalent to saying that the PACF sidelobes of one sequence completely cancel the PACF sidelobes of the other sequence. Complementary sequences can be either binary or polyphase. Complementary pairs of binary sequences were originally considered by Golay [65]. Polyphase complementary sequences were reported by Sivaswamy [66]. If a pair of binary complementary sequences, each of length $L/2$, is represented by $\{a1_n\}$ and $\{a2_n\}$, their corresponding PACF is respectively given as,

$$P_{a1a1}(k) = \sum_{n=1}^{L/2} a1_n \cdot a1_{n+k}$$

(4.122)

$$P_{a2a2}(k) = \sum_{n=1}^{L/2} a2_n \cdot a2^*_{n+k}$$

(4.123)

By definition, for a pair of binary complementary sequences we can write,

$$P_{a1a1}(k) + P_{a2a2}(k) = L \ , \quad for \quad k=0$$

(4.124)

$$P_{a1a1}(k) + P_{a2a2}(k) = 0 \ , \quad for \quad k \neq 0$$

(4.125)

This implies that,

$$\sum_{n=1}^{L/2} (a1_n a1_{n+k} + a2_n a2_{n+k}) = 0 \ , \quad for \quad k \neq 0$$

(4.126)

The translation of sequence to a baseband waveform in this case implies a pair of waveforms corresponding to the complementary sequence pair $\{a1_n\},\{a2_n\}$, given as,

$$c1(t) = \sum_{n=1}^{L/2} a1_n p(t-nT_c)$$

(4.127)

$$c2(t)=\sum_{n=1}^{L/2} a2_n p(t-nT_c)$$

(4.128)

Based on the generalized analysis of section 4.4.2, the PACFs of the two waveforms can be written as,

$$\phi_{c1c1}(\tau)=\Delta\tau\sum_{n=1}^{L/2} a1_n a1_{n+d+1}+ (T_c-\Delta\tau)\sum_{n=1}^{L/2} a1_n a1_{n+d}$$

(4.129)

$$\phi_{c2c2}(\tau)=\Delta\tau\sum_{n=1}^{L/2} a2_n a2_{n+d+1}+ (T_c-\Delta\tau)\sum_{n=1}^{L/2} a2_n a2_{n+d}$$

(4.130)

For perfect cancellation of PACF sidelobes of c1(t) and c2(t), it is to be proved that,

$$\Delta\tau\sum_{n=1}^{L/2} a1_n a1_{n+d+1}+ a2_n a2_{n+d+1}+ (T_c-\Delta\tau)\sum_{n=1}^{L/2} a1_n a1_{n+d}+ a2_n a2_{n+d}= 0$$

(4.131)

This can be readily proved considering the identity of equation (4.126) for complementary sequences.

For a binary complementary sequence pair, the corresponding bandpass waveforms are given as,

$$s1(t)=c1(t)\cos(\omega_o t)$$

(4.132)

$$s2(t)=c2(t)\cos(\omega_o t)$$

(4.133)

For perfect cancellation of PACF sidelobes of s1(t) and s2(t), it is to be proved that,

$$\phi_{ss}(\tau)=\phi_{s1s1}(\tau)+\phi_{s2s2}(\tau)=0 \text{ , } for \text{ } \tau>T_c$$

(4.134)

Again making use of the argument and generalized results of section 4.4.2, the set of conditions to prove the above results are,

$$\frac{\cos(\omega_o\tau)\sin(2\omega_o\Delta\tau)}{2\omega_o}\sum_{n=1}^{L/2} a1_n a1_{n+d} - a1_n a1_{n+d+1} + a2_n a2_{n+d} - a2_n a2_{n+d+1} = 0 \quad (4.135)$$

$$\frac{\sin(\omega_o\tau)(1-\cos(2\omega_o\Delta\tau))}{2\omega_o}\sum_{n=1}^{L} a1_n a1_{n+d} - a1_n a1_{n+d+1} + a2_n a2_{n+d} - a2_n a2_{n+d+1} = 0 \quad (4.136)$$

Applying the identity of equation (4.126), the left hand side of equations (4.135) and (4.136) reduce to zero. Hence the given pair of bandpass waveforms meet the necessary conditions for producing zero self-noise.

<u>Energy Efficiency</u>: The complementary pair of waveforms generated through the above method will have constant amplitude. Hence, their energy efficiency will be 100%.

<u>Other Approaches</u>: In addition to the earlier described approaches for perfect waveform generation, two other possibilities considered were,

    (a)   use of chirp waveform

    (b)   use of Huffman sequences.

However, both the approaches were discarded because they did not meet at least one of the optimization criterion for SSUE waveform. The chirp waveform had unacceptably high signal-to-self-noise ratio, while the Huffman sequences had very low transmission efficiency, typically below 40%.

4.4.4 Optimum Receiver

In the SSUE system, the receiver performs two functions. One, to evaluate the crosscorrelation between the received waveform, and a reference waveform, in order to recover the system impulse function. Second, to suppress the random noise and provide maximum possible gain in the signal-to-random-noise ratio of the correlation signature. In

the following it is shown that a correlation filter that is matched to the transmit waveform performs these functions simultaneously and is, therefore, the optimum receiver.

Matched Filter as an Optimum Receiver: The SSUE received signal can be represented in matrix notation as,

$$\underline{r} = S\underline{h} + \underline{n} \tag{4.137}$$

where r is a column vector of length M, representing one period of the received signal, n is a column vector of the same length representing the random noise component of the received waveform. The impulse response of the composite system is represented by vector h. S is an MxM square matrix whose rows are based on the transmit vector s and each successive row is obtained by the circular shift of the elements of s. Hence, if s is given by,

$$\underline{s} = \begin{pmatrix} s_1 & s_2 & s_3 & \cdots & s_M \end{pmatrix} \tag{4.138}$$

The matrix S will be,

$$S = \begin{pmatrix} s_1 & s_2 & s_3 & \cdots & s_M \\ s_M & s_1 & s_2 & \cdots & s_{M-1} \\ s_{M-1} & s_M & s_1 & \cdots & s_{M-2} \\ \cdot\cdot & \cdot\cdot & \cdot\cdot & \cdots & \cdot\cdot \\ s_2 & s_3 & s_4 & \cdots & s_1 \end{pmatrix} \tag{4.139}$$

A correlation filter matched to the transmit waveform can be represented as,

$$\underline{\phi} = S^T \underline{r} = (S^T S)\underline{h} + S^T \underline{n} \tag{4.140}$$

Here, S^T. S represents the correlation matrix of vector s. If the transmit signal has perfect PACF, the correlation matrix S^T. S will be a diagonal Toeplitz matrix, and we get,

$$\underline{\phi} = k\underline{h} + S^T \underline{n} \tag{4.141}$$

where k is a scaling constant.

If the transmit signal, s, has a peak amplitude of A and the noise signal, n, has a variance of σ^2 , then the SNR of the received signal, r, will be A^2/σ^2. At the output of the correlator, as given by equation (4.141), the signal component will have a peak amplitude of MA, where M is the length of the signal vector s. Also, the noise component, S^T_n of the correlator output will have a variance of $M\sigma^2$. Hence the SNR at the correlator output will be $(MA)^2/\sigma^2$. This means that the SNR will improve by a factor of M, which corresponds to the maximum achievable SNR gain factor defined in section 4.3.3.

4.5 Sub-Optimum SSUE Design

In this case it is assumed that the transmitter is sub-optimum (Figure 4.4), i.e., the excitation waveform does not have a perfect PACF and hence self-noise exists. The problem then is how to design an optimum receiver in order to eliminate the self-noise while minimizing the reduction in SNR gain factor.
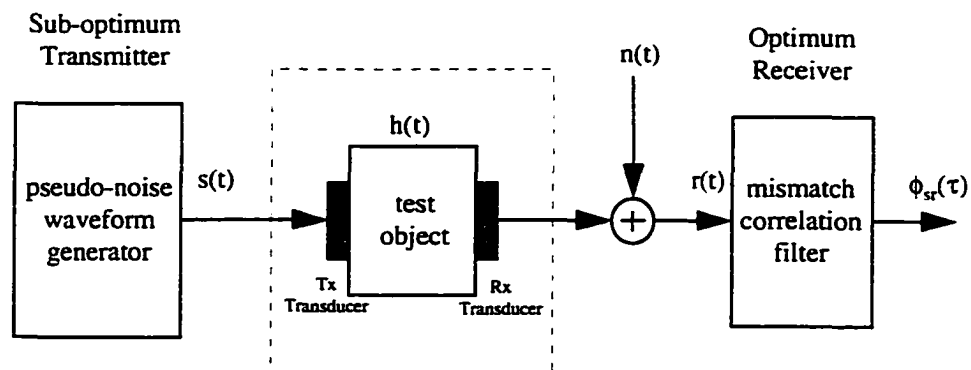
Figure 4.4: Sub-optimum SSUE model.

4.5.1 Deterministic Approach

This approach is based on the fact that even though the PACF of the excitation waveform is not perfect, it is deterministic. Thus the self-noise is deterministic, which, in principle, should be possible to separate out through the use of an appropriate filter at the receiver. Luckily the correlation sidelobes for a maximal-length sequence based waveform (m-sequence derived waveform) are mathematically trackable and hence the resulting self-noise can be estimated. The expression for the PACF of an m-sequence based waveform is given by,

$$\phi_{ss}(\tau)=[(\frac{N+1}{N})Tr(\tau)-\frac{1}{N}]\cos(\omega_0\tau)$$ (4.142)

where Tr(t) is a triangular pulse function defined in the time interval ($-T_c <$ t $< T_c$) as,

$$Tr(t)=1-mod[\frac{t}{T_c}] \ , for \ (-T_c < t < T_c)$$ (4.143)

Equation (4.142) can be rewritten as,

$$\phi_{ss}(\tau)=\frac{N+1}{N}Tr(\tau)\cos(\omega_0\tau) - \frac{1}{N}\cos(\omega_0\tau)$$ (4.144)

Recalling that the output of the correlator is given by,

$$\phi_{sr}(\tau)=\phi_{ss}(\tau)*h(\tau)$$ (4.145)

Hence,

$$\phi_{sr}(\tau)=\frac{N+1}{N}Tr(\tau)\cos(\omega_0\tau)*h(\tau) - \frac{1}{N}\cos(\omega_0\tau)*h(\tau)$$ (4.146)

The Fourier transform of equation (4.146) gives its frequency domain equivalent representation, which transforms the convolution operation in to a multiplication operation. Hence the frequency-domain version of equation (4.146) is given as,

$$\Phi_{sr}(\omega) = \frac{N+1}{2N}[Tr(\omega_0) + Tr(-\omega_0)]H(\omega) - \frac{H(\omega_0) + H(-\omega_0)}{2N} \tag{4.147}$$

where, $H(\omega)$ represents the Fourier transform of $h(\tau)$ and $Tr(\omega)$ represents the Fourier transform of $Tr(\tau)$. The self-noise term in the frequency-domain representation of equation (4.147) is a constant over the complete frequency range. The evaluation of the correlation signature function at ω_0 gives,

$$\Phi_{sr}(\omega_0) = \frac{N+1}{N}H(\omega_0) - \frac{H(\omega_0)}{N} \tag{4.148}$$

Hence the following algorithm can be applied for self-noise suppression.

(1)   Calculate the correlation signature using matched filter.

(2)   Calculate the FFT of the correlation signature.

(3)   Determine $H(\omega_0)$.

(4)   Correct the signature function in frequency domain.

(5)   Take inverse FFT to get back the signature in time-domain.

In a practical implementation of the above algorithm, the signature function will have an additive noise term, thus making the estimate of $H(\omega_0)$ inaccurate. In that case, the algorithm will introduce a systematic noise term in the correlation signature. Computer simulation of this method of self-noise suppression is presented in section 5.3.

4.5.2   Mismatched Filter Approach

This approach is based on the fact that a matched filter is an optimum receiver (according to the optimality criteria of section 4.3) only when the pseudorandom excitation waveform has perfect PACF. In the present case this condition is not true.

Therefore, an optimum filter to be developed for the present case can be called a mismatched filter (MMF).

The problem now is, given an imperfect pseudorandom waveform, design a mismatched filter that results into zero self-noise, without significantly reducing the SNR gain factor. This is equivalent to saying, given a pseudorandom waveform s(t), find another waveform (or function) u(t), such that their PCCF function is perfect. As was done earlier in case of optimum design strategy, this problem can be translated to the corresponding sequence level.

MMF design for an m-sequence: Let $\{a_n\}$ be a periodic maximal-length sequence with period L, and consisting of two elements +1 and -1. Based on the characteristics of maximal-length sequences, we can write the following,

$$\sum_{n=1}^{L} a_n = \sum_{n=1}^{L} a_{n+d} = +1 \tag{4.149}$$

$$\sum_{n=1}^{L} a_n a_{n+d} = -1, \text{ for } d \neq 0 \tag{4.150}$$

$$\sum_{n=1}^{L} a_n a_{n+d} = L \text{ , for } d = 0 \tag{4.151}$$

The periodic auto-correlation function (PACF) of the sequence is defined as,

$$P_{aa}(d) = \sum_{n=1}^{L} a_n a_{n+d} \tag{4.152}$$

If we consider another maximal-length sequence $\{y_n\}$, having a dc offset B, i.e., $\{y_n\} = \{a_n + B\}$, the periodic cross-correlation function (PCCF) of this sequence is given by,

$$P_{ay}(d=0) = [M+B] \tag{4.155}$$

$$P_{ay}(d) = \sum_{n=1}^{L} a_n y_{n+d} \tag{4.153}$$

$$P_{ay}(d) = \sum_{n=1}^{L} [a_n a_{n+d} + a_n B] \tag{4.154}$$

Using the identities of equations (4.150), (4.151) & (4.152) we get,

$$P_{ay}(d \neq 0) = [-1 + B] \tag{4.156}$$

Setting equation (4.156) equal to zero and solving for the unknown constant B, we get,

$$[B-1] = 0 \tag{4.157}$$

Hence, if B is chosen according to the above relation, then the sequence $\{y_n\}$ will be based upon two elements '+2' & '0', and the PCCF of the two sequences $\{a_n\}$ and $\{y_n\}$ will be perfect. This means that,

$$P_{ay}(d \neq 0) = \sum_{n=1}^{L} a_n y_{n+d} = 0 \tag{4.158}$$

$$P_{ay}(d=0) = [L+1] \tag{4.159}$$

SNR Gain Factor for a MMF: Let the BPSK transmit waveform based on a binary maximal-length sequence be represented in the vector notation as,

$$\underline{S} = [s_1 \ s_2 \ s_3 \ ... \ s_M] \tag{4.160}$$

The corresponding mismatch reference waveform based on a mismatch sequence as described above can be represented as,

$$\underline{y} = [y_1 \ y_2 \ y_3 \ ... \ y_M] \tag{4.161}$$

The expression for the SNR gain factor can be written as,

.

$$G=\frac{\left(\sum_{n=1}^{M} s_n y_n\right)^2}{\sum_{n=1}^{M} y_n^2} \qquad (4.162)$$

Considering the mismatch sequence generation method, if the transmit signal, s, has an amplitude A, the mismatch waveform vector, y, will have half the elements with amplitude 2A and rest of them will be zero. Thus the SNR gain becomes,

$$G=\frac{M}{2} \qquad (4.163)$$

This shows that the SNR gain factor reduces by 3 dB for the case of above described mismatch filter approach to self-noise elimination.

Generalized MMF Design: It was found that the maximal-length sequences are not ideally suited for the application of mismatch filter approach to self-noise elimination. The above mentioned 3 dB loss can be reduced if we choose a different sequence. In order to determine a mismatch sequence corresponding to any given sequence, a more general problem formulation is required and is presented as follows. Let a sequence, $\{c_n\}$ be represented as,

$$c=(c_0 \ c_1 \ c_2 \ ... \ c_{L-1})^T \qquad (4.164)$$

and the desired mismatch sequence as,

$$w=(w_0 \ w_1 \ w_2 \ ... \ w_{L-1})^T \qquad (4.165)$$

The PCCF of the two sequences is given as,

$$P_{cw}(d)=\sum_{n=1}^{L} w_n c_{n+d} \qquad (4.166)$$

For perfect PCCF,

$$P_{cy}(d \neq 0) = \sum_{n=1}^{L} c_n w_{n+d} = 0 \tag{4.167}$$

Equation (4.167) in matrix form can be written as,

$$C.w = g \tag{4.168}$$

where C is a cyclic Toeplitz matrix of the form,

$$C = \begin{pmatrix} c_1 & c_2 & c_3 & \cdots & c_M \\ c_M & c_1 & c_2 & \cdots & c_{M-1} \\ c_{M-1} & c_M & c_1 & \cdots & c_{M-2} \\ .. & .. & .. & \cdots & .. \\ c_2 & c_3 & c_4 & \cdots & c_1 \end{pmatrix} \tag{4.169}$$

and,

$$g = (1 \ 0 \ 0 \ 0 \ ..)^T \tag{4.170}$$

Equation (4.168) can be written as,

$$w = C^{-1}.g \tag{4.171}$$

Hence if C is a non-singular matrix, it is always possible to find w using the above equation. In reference [67] it is shown that for any length L, there exists at least one binary sequence c for which the MMF w can be calculated using the above procedure. Sequences with SNR loss as low as 0.2 dB are reported. However, it appears that, no systematic procedure exists to find the "best" sequence c and its corresponding MMF w, for a given length. There has been considerable work in this area as reported in [68, 69, 70]. For the present research work it was decided not to pursue this area further and to accept the 3 dB loss of the maximal-length sequence.

4.5.3 OOK Approach

This approach is a variation of the mismatch filter concept. If the transmit waveform and the mismatch reference waveform are interchanged, the transmit waveform can be considered as an equivalent of the on-off keying (OOK) technique of communication systems and that is why this approach is given the name of OOK approach. This approach is beneficial in applications where the system operation is average power limited. Thus if the maximum transmit signal amplitude in case of a BPSK waveform is A, the OOK approach can operate at a peak amplitude of $\sqrt{2}A$ to deliver the same average power.

4.6 Optimum Design of Bandwidth Constrained SSUE System

A practical SSUE system is always bandlimited, mainly because of the bandlimited response of the ultrasonic transmitting and receiving transducers. As indicated earlier, there are two consequences of this practical constraint. The loss of resolution of the measured signature function and the loss of high frequency features of the true impulse response. Unfortunately, there is not much that can be done in terms of recovering the high frequency characteristics of the system impulse response. A loss of resolution is also inevitable. The best that can be done is to minimize the degradation in resolution for a given system bandwidth. The system design criterion discussed in the previous section do not provide optimum resolution under the bandwidth constraint. This section discusses the optimum waveform designs for the bandwidth constrained SSUE system.

4.6.1 Ultrasonic Transducer's Frequency Characteristics

Ultrasonic transducers typically have a bandpass characteristics and the bandwidth of the passband varies according to the specific transducer design and intended

application. For the SSUE applications, transducers with large passband width are desirable. Most of the wideband transducers commercially available have a passband center frequency-to-bandwidth ratio of about two. Hence a transducer with the center frequency of 5 MHz covers a frequency range starting from almost DC to about 10 MHz (Figure 4.5).

4.6.2 Spectral Characteristics of SSUE excitation waveform

In the SSUE transmitter (Figure 4.2), the modulator translates the frequency spectrum of the baseband waveform, c(t), to the center frequency of the transducer spectrum. Hence, the main lobe of the excitation signal spectrum is aligned with the transducer passband. Also, the width of the spectral mainlobe is tailored to match to the width of the transducer passband (Figure 4.6). This is done by controlling the length of the signalling waveform p(t). However as the signal passes through the transducer, its spectral sidelobes gets filtered which correspond to the distortion of the waveform in the time domain and the broadening of the PACF mainlobe in the correlation domain.

With reference to Figure 4.2, the PN excitation waveform, s(t) can be written as,
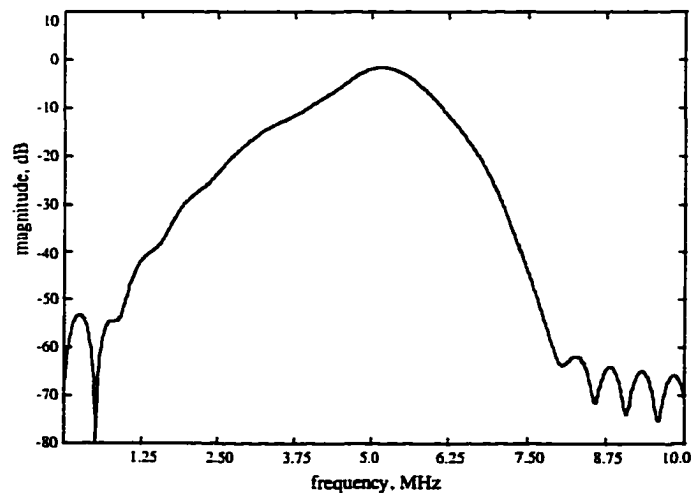
Figure 4.5: Typical frequency characteristics of a wideband ultrasonic transducer.
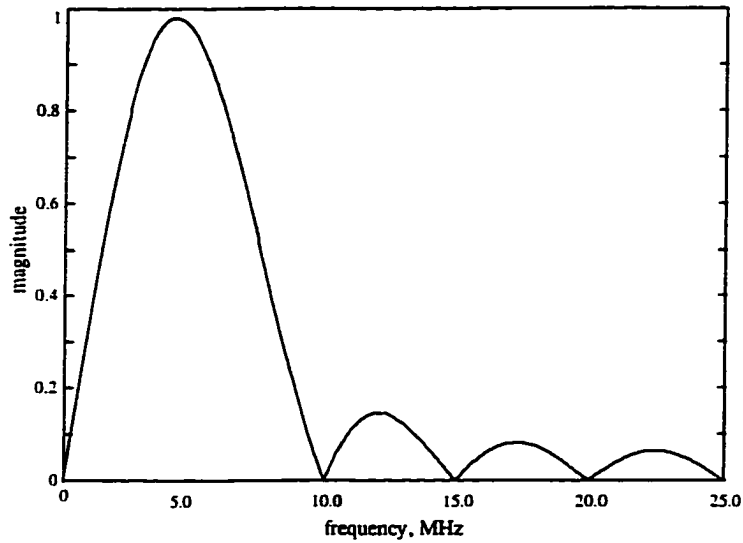
Figure 4.6: Spectrum of SSUE excitation waveform based on rectangular pulse function.

$$s(t)=c(t)\cos(2\pi f_0 t) \qquad (4.172)$$

where,

$$c(t)=z_n p(t-nT_c) \qquad (4.173)$$

If the power spectrum of the bandpass waveform, s(t), is represented by $S_s(f)$ and the power spectrum of the baseband waveform, c(t), is represented by $S_c(f)$, their inter-relation is given by,

$$S_s(f)=\frac{1}{2}[S_c(f+f_0)+S_c(f-f_0)] \qquad (4.174)$$

If the sequence $\{z_n\}$ is perfect, then $S_c(f)$ is given by,

$$S_c(f)=T_p\left(\frac{\sin(f T_p)}{f T_p}\right)^2 \qquad (4.175)$$

where T_p is the duration of the rectangular pulse function p(t). Thus, the spectrum of the

excitation waveform, s(t), will have a well known sync squared envelope with first spectral sidelobe level only -13 dB lower than the mainlobe.

4.6.3 Optimality Criteria

The relation between the PACF of the excitation waveform and the measured correlation signature is given by,

$$\phi_{sr}(\tau)=\phi_{ss}(\tau)*h(\tau)+N_r(\tau) \tag{4.176}$$

This indicates that the resolution of the measured correlation signature is directly related to its autocorrelation properties. In particular, the width of the autocorrelation mainlobe determines the overall signal resolution.

For bandlimited pseudo-random waveforms, the width of autocorrelation mainlobe is inversely proportional to the signal bandwidth. If the bandwidth is fixed then the autocorrelation mainlobes of different waveforms can be compared. Hence, the autocorrelation mainlobe width serves as the optimization criteria. It is desired to achieve a dynamic range of >80 dB, so that a very weak flaw signal in close vicinity of a strong (backwall) signal could be detected. Therefore, correlation mainlobe width at -80 dB level is chosen as the resolution measure of the SSUE system.

4.6.4 Waveform Design Approach

A rectangular pulse function has a relatively larger energy in its spectral sidelobes (Table 4.1). It, therefore, gets severely distorted while passing through the bandlimited system, and results into the broadening of the peaks in the measured correlation signature. A different pulse function that has most of its energy concentrated in its spectral mainlobe will undergo lesser distortion and the corresponding correlation signature will have better resolution. Thus, the optimum waveform is one that has minimum fraction of energy in the sidelobes compared to the mainlobe of its frequency spectrum.

This problem is analogous to the design of a timelimited function whose frequency spectrum is a window function having certain desirable properties [70]. Some popular functions in this category are Hanning function, Hamming function, and Blackman function. The following table compares the performance of some of the well-known pulse functions.

Table 4.1: Comparison of various candidate pulse functions.

Pulse Function	Highest Sidelobe Level	Sidelobe Falloff Rate
Recatagular	-13 dB	-6 dB
Hanning	-32 dB	-18 dB
Hamming	-43 dB	-6 dB
Blackman	-58 dB	-18 dB
Exact Blackman	-68 dB	-6 dB
Blackman-Harris	-72 dB	-6 dB

The exact comparison of these pulse functions should be done on the basis of their ratios of total energy to the spectral sidelobe energy. However, this figure was not readily available so the two related parameters, highest sidelobe level and the sidelobe falloff rate were used instead. The table indicates that the Blackman pulse functions are expected to give the best resolution. A detailed simulation analysis of these pulse functions and their effect on the resolution of the correlation signature is performed in Chapter 5 under section 5.4.

4.7 Summary and Comparison

The optimality criteria for a practical SSUE system is defined. There are four basic areas of optimization, (1) signal-to-random-noise ratio, (2) signal-to-self-noise ratio, (3) transmission efficiency, and (4) correlation signature resolution. The first three are interdependent, hence their optimization is considered first. Later, the optimization in resolution is carried out.

Two strategies of system optimization were pursed. First, the optimum system design strategy, in which both the transmitter and the receiver were optimum. Second, a sub-optimum system design strategy, where the transmitter was sub-optimum, but the receiver was optimized, taking into account the sub-optimality of the transmitter.

Under the optimum system design strategy, four different approaches were considered, these are,

    (a)   amplitude modulated waveform approach,

    (b)   offset-phase modulated waveform approach,

    (c)   polyphase sequence based waveform approach,

    (d)   complementary sequence based waveform approach.

It was shown that except for approach (d), all other approaches produce theoretically optimum results. Under the sub-optimum design strategy, three different approaches were considered, these are,

    (a)   deterministic approach,

    (b)   mismatch filter approach,

    (c)   on-off keyed waveform approach.

Even though these three approaches are not theoretically optimum, a common feature of all of them is zero self-noise.

Finally, for the optimization in resolution, the bandwidth constraint imposed by the ultrasonic transducers was considered and an improved waveform design, resulting in lesser out of band energy is presented.

4.7.1 Performance Comparison

Various system design approaches developed in this chapter can be compared on the basis of their energy efficiency and other characteristics as per Table 4.2.

Table 4.2: Comparison of different design approaches.

Waveform Design Approach	Energy Efficiency	Dynamic Range Limiting Factor	SNR Gain
Binary-phase modulation approach	100%	self-noise	L
Amplitude modulation approach	94%	random-noise	L
Offset-phase modulation approach	100%	random-noise	L
Complementary sequence approach	100%	random-noise	L
Mismatch filter based approach	100%	random-noise	L/2
On-off modulation approach	50%	random-noise	L/2

CHAPTER 5 SIMULATION ANALYSIS

This chapter presents the simulation work performed to verify the theoretical benefits of the SSUE approach over the conventional ultrasonic correlation system approach. Also, the simulation analysis of various approaches for SSUE system design developed in the previous chapter was carried out. Simulations were first performed at the baseband and then at the passband level. The effects of a bandlimited system and various waveform designs to enhance the resolution were also simulated. The simulation analysis was performed on IBM PC using the Matlab software environment. A 10th order maximal length sequence was chosen as a reference.

5.1 Self-noise Analysis of Conventional Correlation Systems

It was stated earlier under section 3.4 that the conventional ultrasonic correlation systems employ an expanded-pulse and their performance is based upon the linear autocorrelation properties of the pseudorandom excitation waveform. The linear autocorrelation sidelobes result into what is called the system self-noise. On the other hand, the performance of a periodic correlation system is governed by the periodic autocorrelation properties of its excitation waveform. This section presents the simulation study of self-noise effects of the two types of correlation systems.

5.1.1 Simulation details

The linear autocorrelation function (LACF) and the periodic autocorrelation (PACF) of a 10th order maximal-length sequence (ml-sequence) and the corresponding bandpass waveform are presented in Figures 5.1 through 5.4.
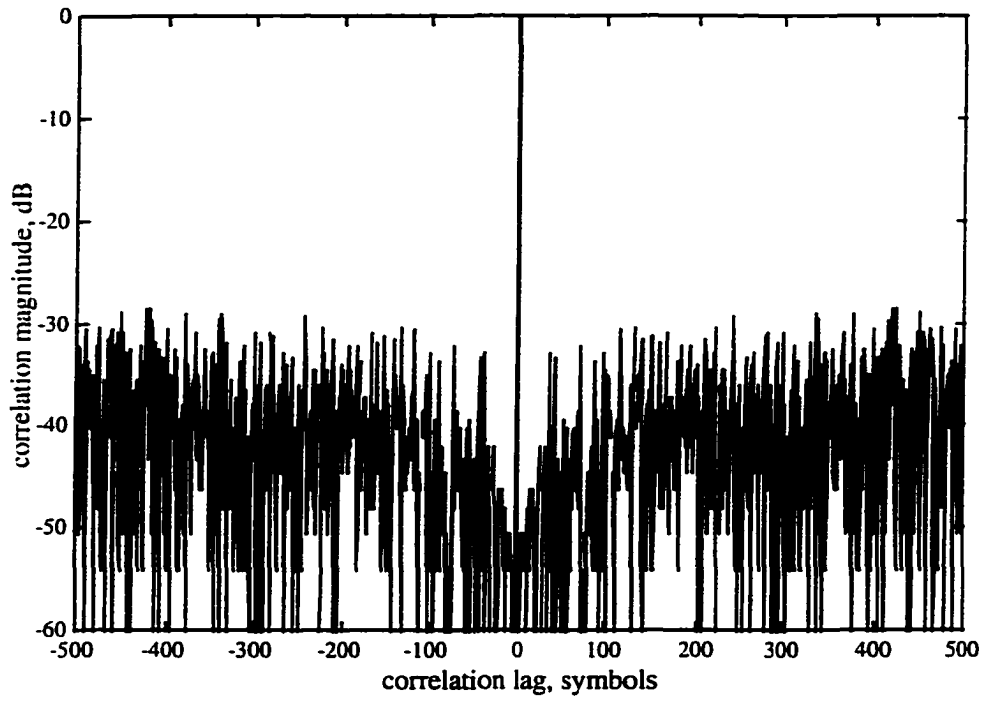
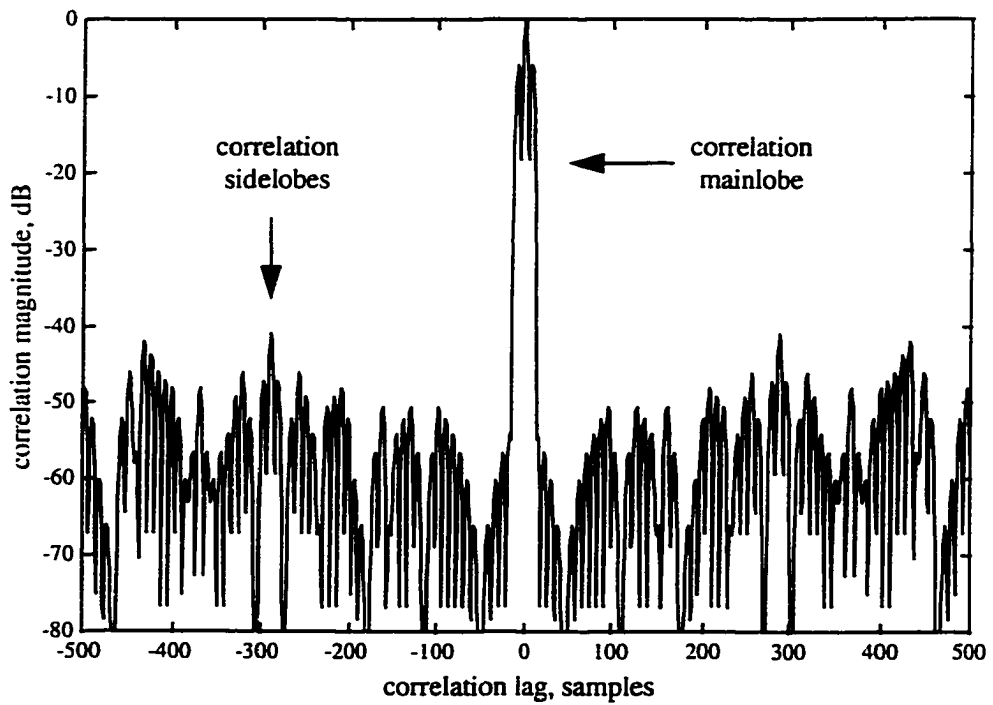Figure 5.1: LACF of a 10th order maximal-length sequence.

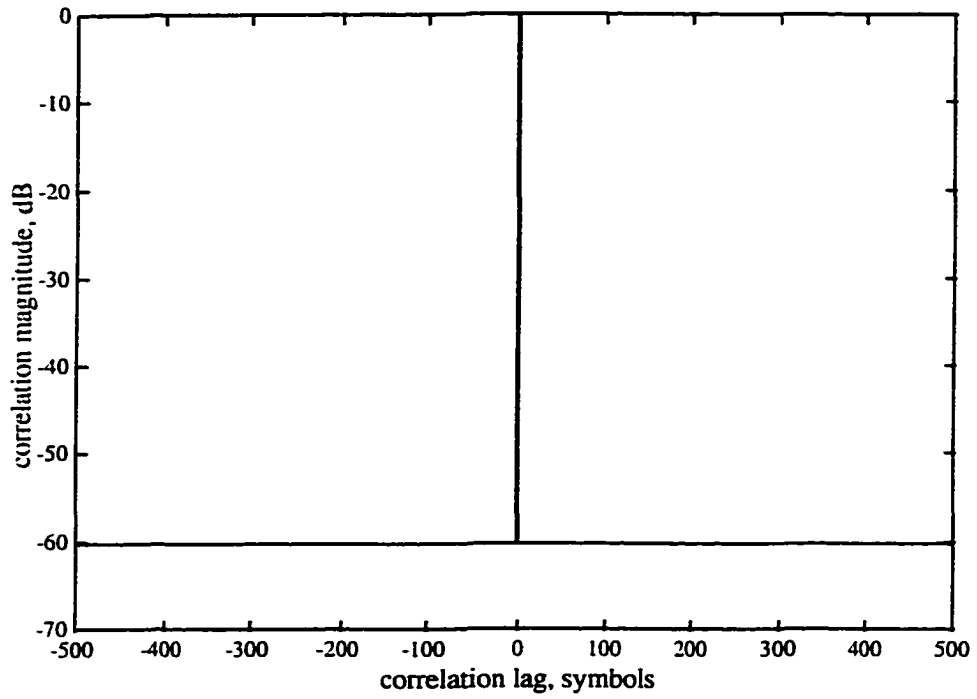Figure 5.2: LACF of ml-sequence based bandpass waveform.

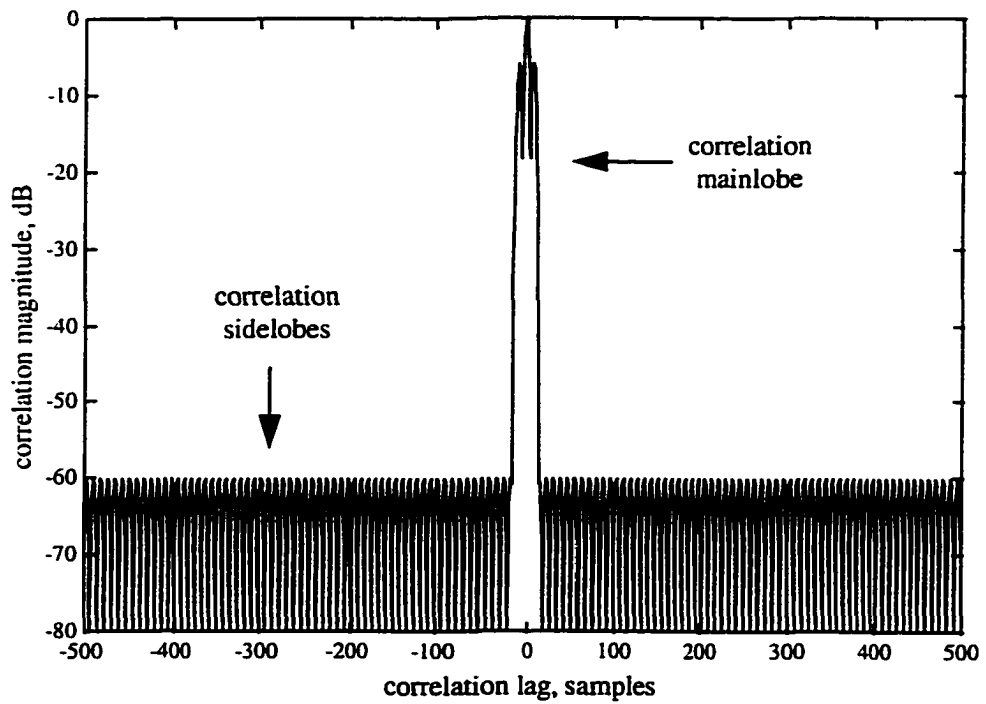Figure 5.3: PACF of a 10th order maximal-length sequence.

Figure 5.4: PACF of ml-sequence based bandpass waveform.

The bandpass waveforms generated for these simulations had one carrier cycle per chip (symbol) interval, and each chip consists of 16 samples. Two things can be observed through the comparison of Figures 5.1 through 5.4.

(a)   the non-zero lag autocorrelation values of the sequence result into the corresponding waveform autocorrelation sidelobes,

(b)   the LACF sidelobes are much larger than the PACF sidelobes.

In order to visualize the effect of the autocorrelation sidelobes in a correlation system, two simulation tests were performed. In test-1, an impulse response function with moderate dynamic range was selected. The impulse response model consists of five signal components, with each successive component 6 dB weaker (Figure 5.5). For test-2, an impulse response function with a large dynamic range was selected. The impulse response model in this case consists of four signal components, with each successive component 20 dB weaker (Figure 5.10). In both cases random Gaussian noise was gradually increased from zero to until the random noise level exceeds the self-noise level. For each noise level, impulse response estimates using the expanded-pulse correlation technique and the periodic correlation technique were calculated.

Simulation results corresponding to two cases are presented. One, when the random noise level is lower than the self-noise level. This condition is represented by $(SNR_r < SNR_s)$. Here, the system performance is determined by the self-noise level. Second, when the random noise level is higher than the self-noise level. This condition is represented by $(SNR_r > SNR_s)$. Here, the system performance is determined by the random-noise level. Figures 5.6 and 5.8 give the expanded-pulse correlation system measurements for the two cases of test-1, while Figures 5.7 and 5.9 give the periodic correlation system measurements for the two cases, again of test-1. Figure 5.10 represent the impulse response function used for test-2. The results of test-2 are shown in Figures 5.11 and 5.13 for the expanded-pulse correlation system, and in Figures 5.12 and 5.14 for the periodic correlation system.

Figure 5.5: Test-1 impulse response.
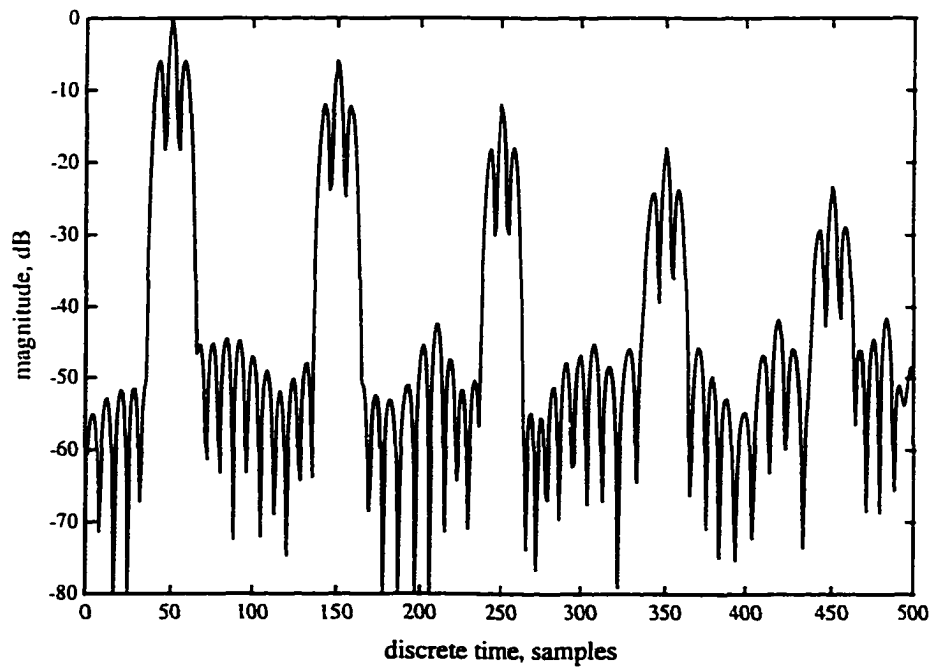
Figure 5.6: Expanded-pulse correlation system measurement (SNR$_r$ < SNR$_s$).
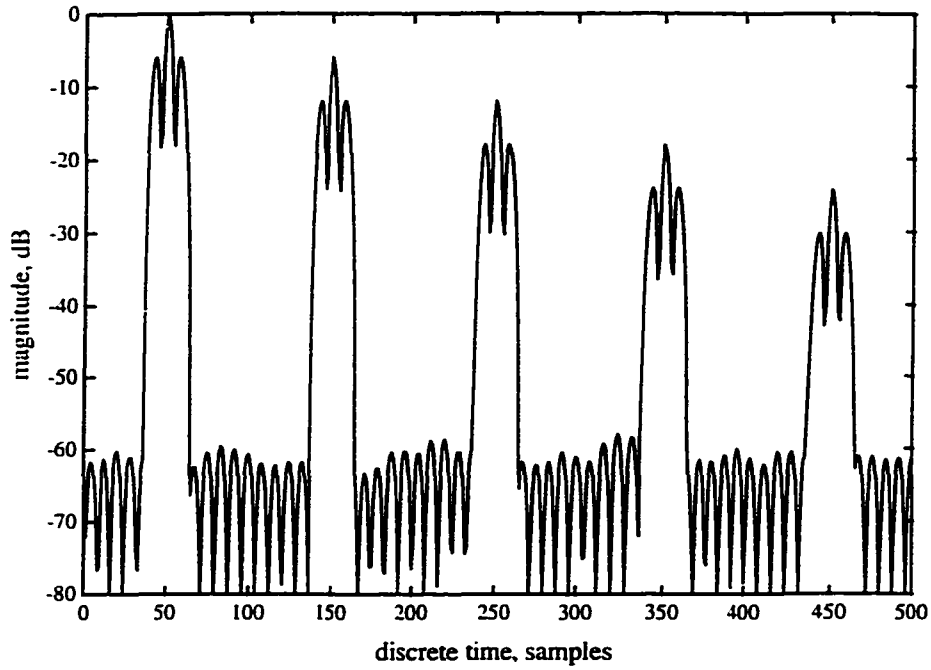
Figure 5.7: Periodic correlation system measurement ($SNR_r < SNR_s$).

Figure 5.8: Expanded-pulse correlation system measurement ($SNR_r > SNR_s$).
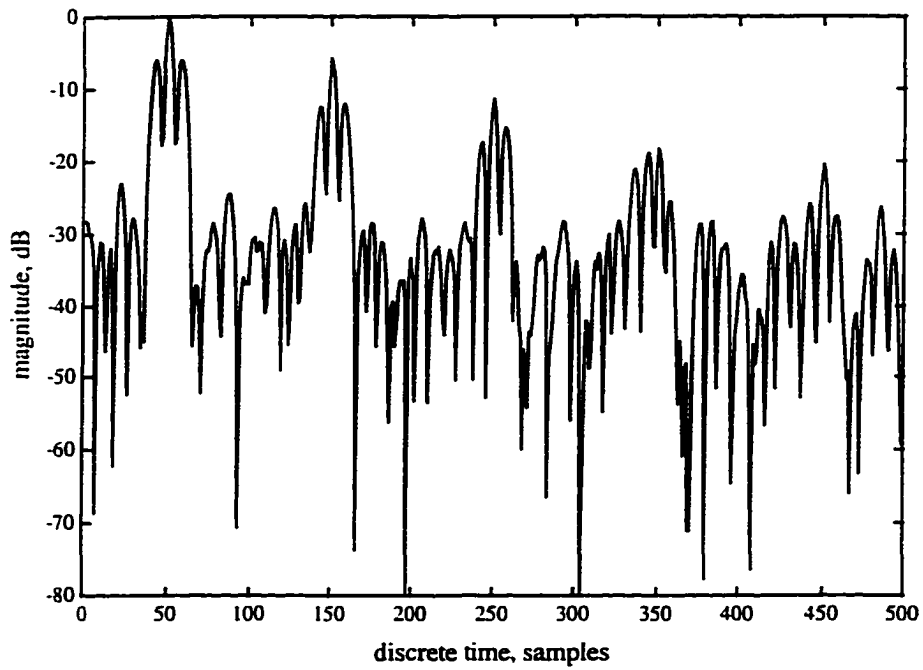
Figure 5.9: Periodic correlation system measurement ($SNR_r > SNR_s$).
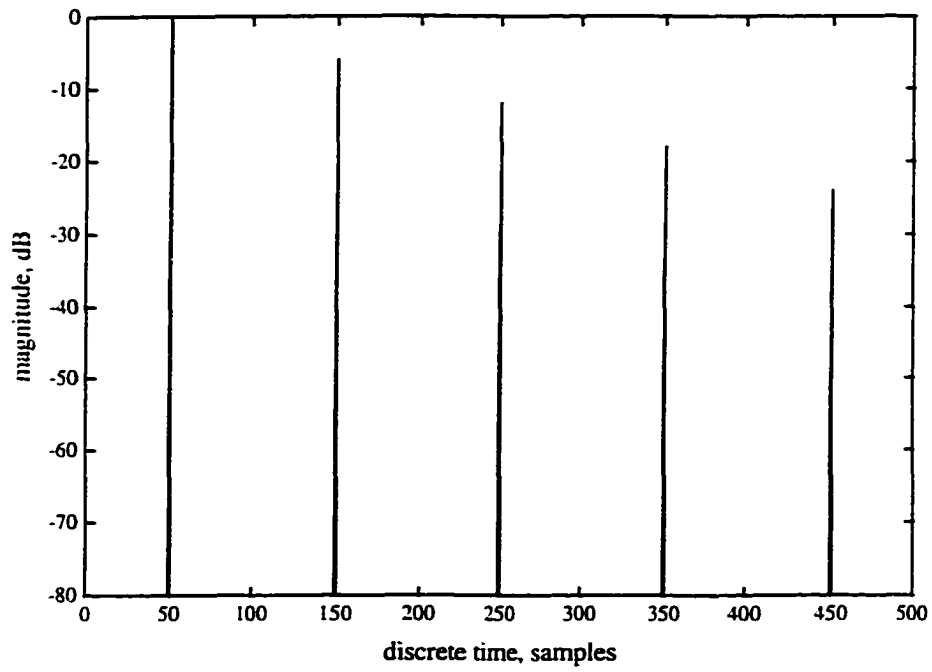

Figure 5.10: Test-2 impulse response.
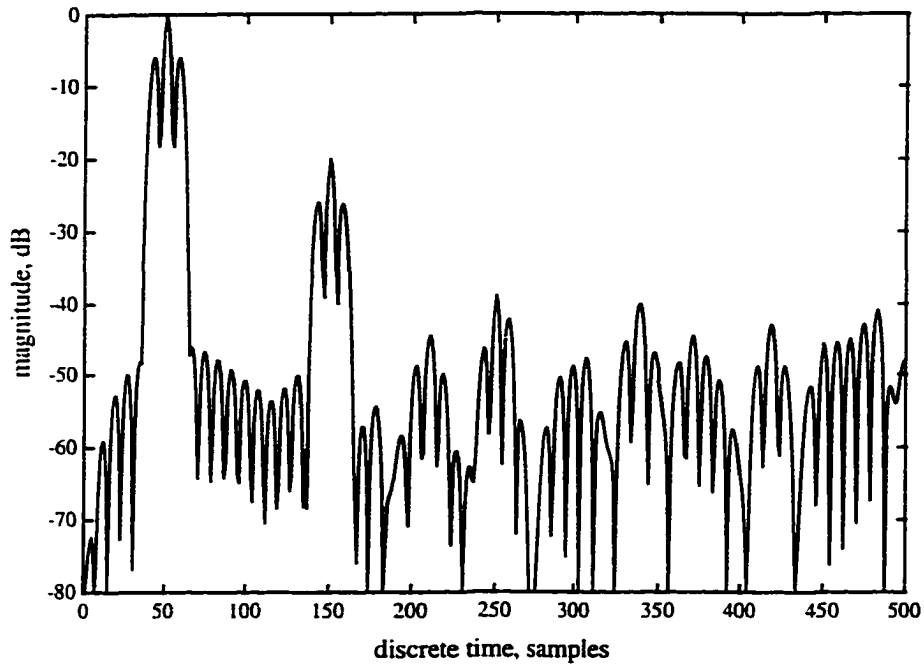
Figure 5.11: Expanded-pulse correlation system measurement (SNR$_r$ < SNR$_s$).

Figure 5.12: Periodic correlation system measurement (SNR$_r$ < SNR$_s$).
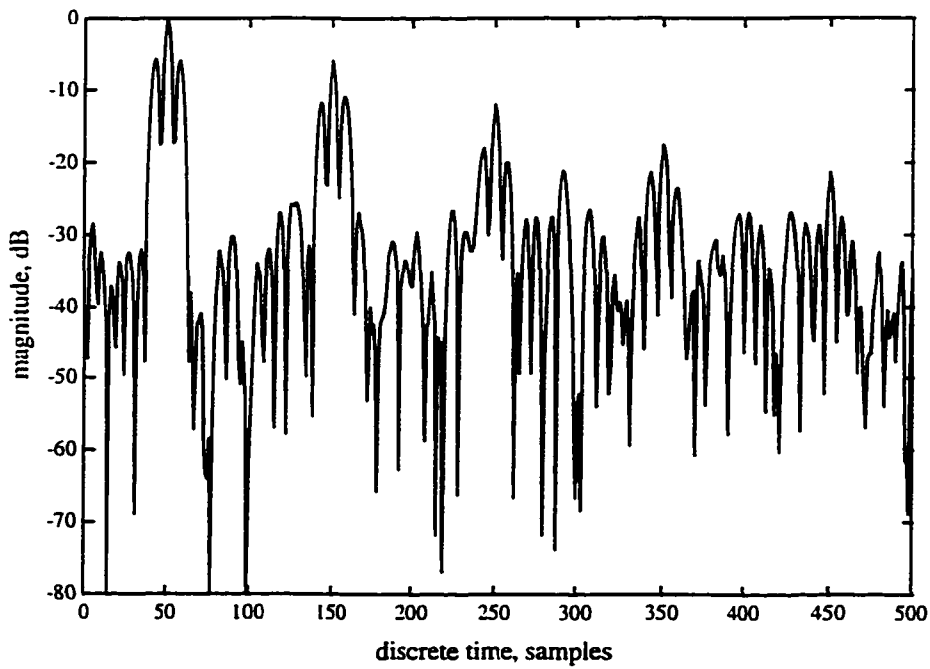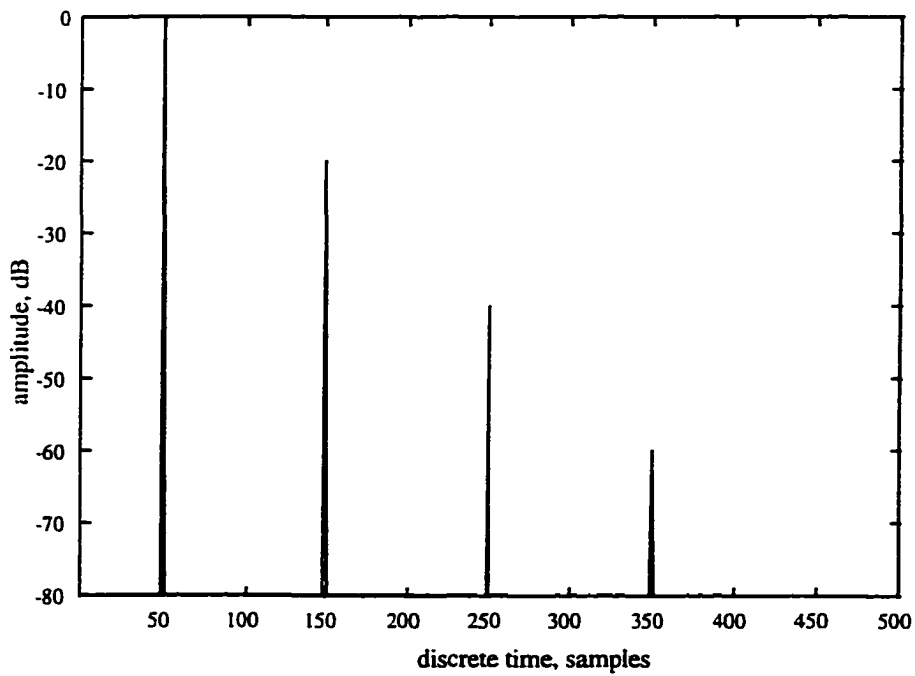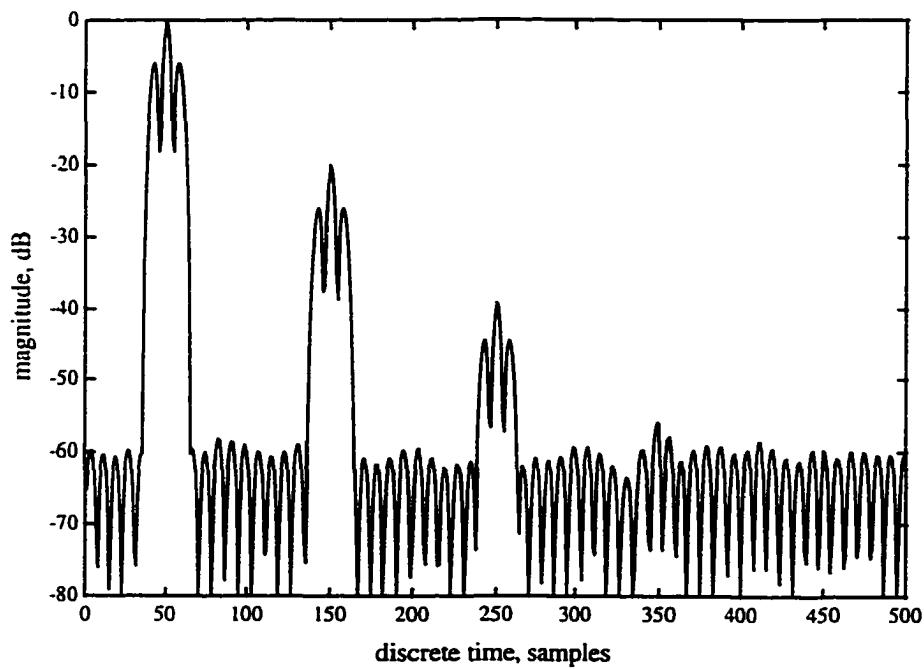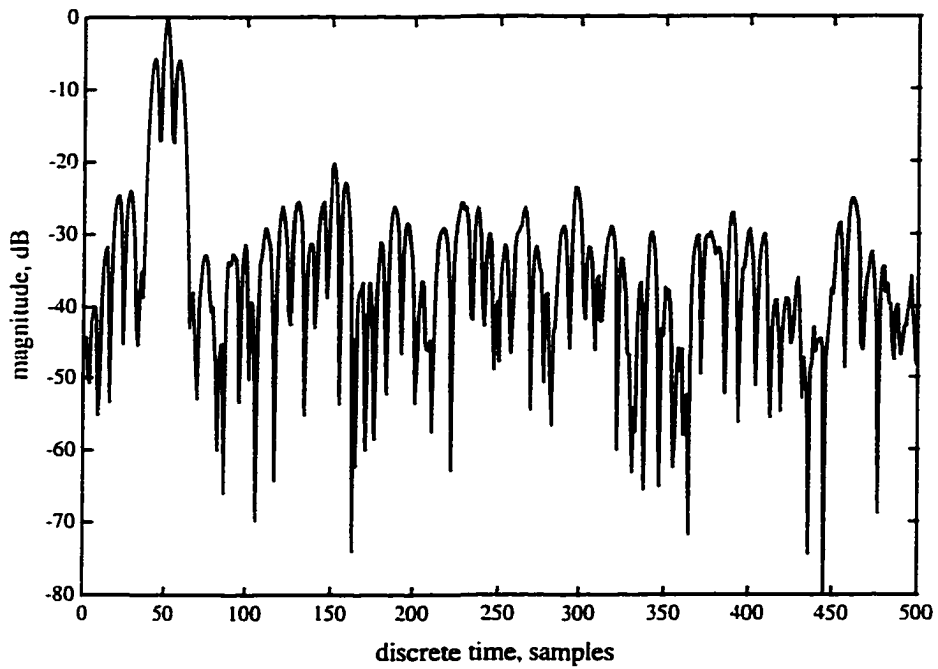
Figure 5.13: Expanded-pulse correlation system measurement (SNR$_r$ > SNR$_s$).
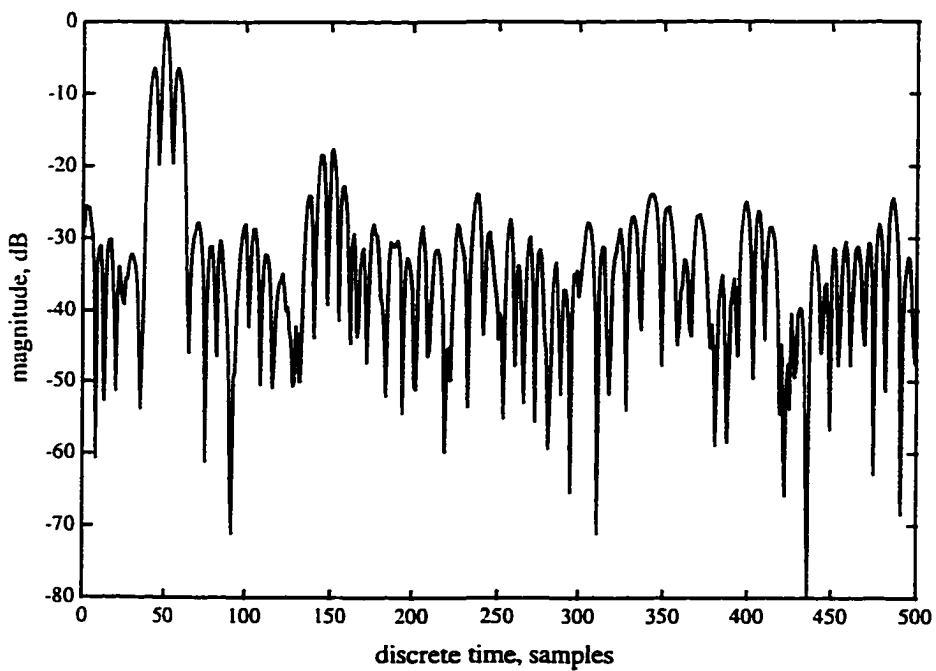

Figure 5.14: Periodic correlation system measurement (SNR$_r$ > SNR$_s$).

5.1.2 Discussion / Conclusion

Following observations are made based on the test results presented in Figures 5.6 through 5.9 and Figures 5.11 through 5.14.

(a) For low levels of random noise in test-1, the expanded-pulse correlation system successfully detected all the components of the impulse response. This was possible because the system self-noise level was around -40 dB whereas the weakest component of the impulse response was at -24 dB (Figure 5.6).

(b) For the same test conditions, the periodic correlation system produced better measurement. The system self-noise level in this case is around -60 dB (Figure 5.7).

(c) When the random noise level exceeds the self-noise level, the two systems give equivalent performance, which is determined by the signal-to-random-noise ratio (Figures 5.8 and 5.9).

(d) For low levels of random noise in test-2, the expanded-pulse correlation system could only detect the first two components of the impulse response. This was because the other components fell below the system self-noise level, which was around -40 dB (Figure 5.11).

(e) For the same test conditions, the periodic correlation system performed better. In this case, the system could clearly detect the first three components of the impulse response. The other weaker components fell below the self-noise level, which was around -60 dB (Figure 5.12).

(f) When the random noise level exceeds the self-noise level, the two systems give equivalent performance, which is determined by the signal-to-random-noise ratio (Figures 5.13 and 5.14).

Two conclusions can be drawn from the above observations:

(a) For applications with poor signal-to-random-noise ratios, self-noise does not limit the system performance and hence either type of correlation system is equally good (or bad).

(b) Periodic correlation systems perform better than the expanded-pulse correlation

systems where self-noise is the performance limiting factor.

It is to be noted that, Test-2 is a more realistic simulation of a practical ultrasonic NDE system. This is because the signal component from various object surfaces is usually orders of magnitude larger than the weak signal component representative of a flaw. Hence, in general, the periodic correlation technique is superior. Another conclusion that can be drawn from the test-2 result of Figure 5.13 is that, the self-noise level sets the fundamental limit on the achievable dynamic range, which is -60 dB in the present case. Hence, a further improvement in the dynamic range can only be possible by employing some method of self-noise suppression.

5.2 Optimum SSUE Simulation

In Chapter 4, various optimum SSUE system design approaches were developed. This section presents the simulation analysis of those approaches. The PACF of the sequence and the corresponding bandpass waveform is presented for the following waveform design approaches:

(a) Complementary sequence based waveform design, Figures 5.15 and 5.16.

(b) Polyphase sequence based waveform design, Figures 5.17 and 5.18.

(c) Amplitude modulated waveform design, Figures 5.19 and 5.20.

(d) Offset-phase modulated waveform design, Figures 5.21 and 5.22.

5.2.1 Discussion / Conclusion

The sequence PACF of all the four types of sequences was found perfect. However, it was observed that even though the Polyphase sequences had perfect PACF, the PACF of corresponding baseband waveform was not perfect. The performance of the other approaches was almost identical. Considering that the Complementary sequence approach is much more complicated to implement, we are left with the two optimum waveform design options of (c) and (d) above.
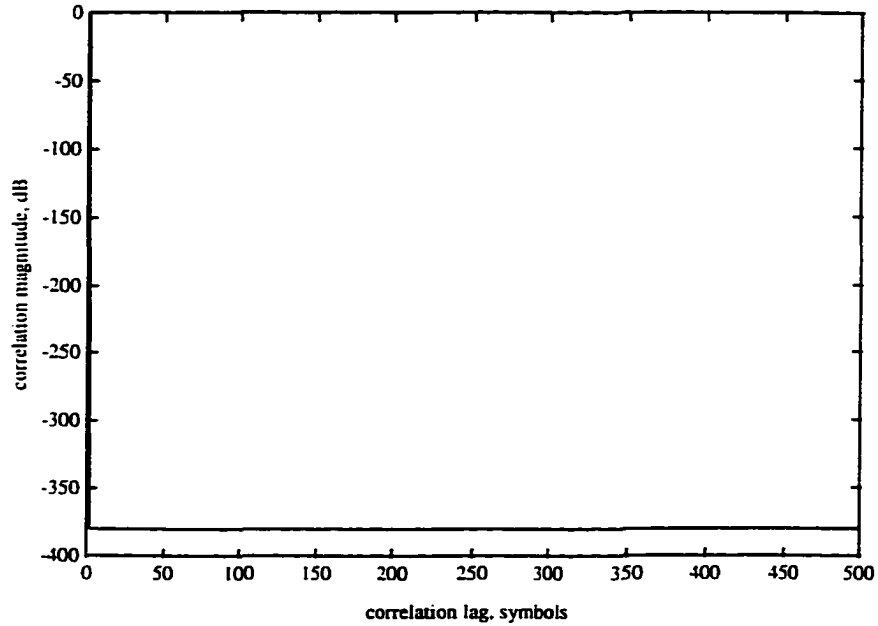
Figure 5.15: PACF of Complementary sequence.
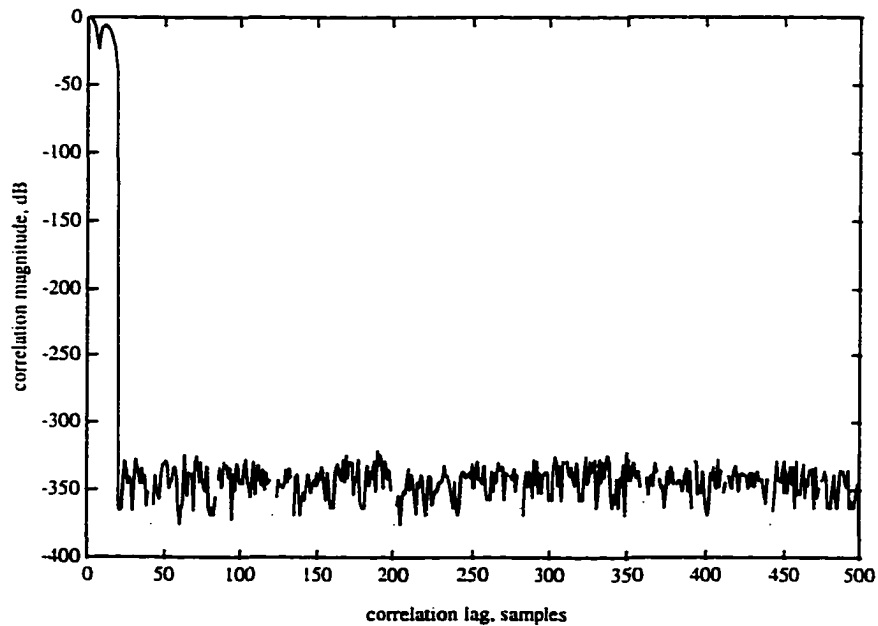

Figure 5.16: PACF of Complementary sequence based bandpass waveform.
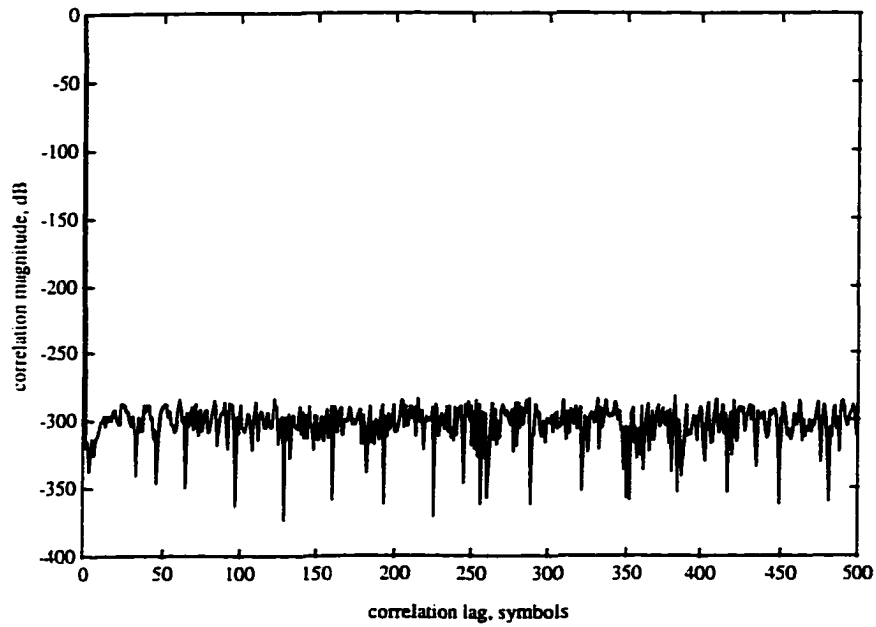
Figure 5.17: PACF of Polyphase sequence.
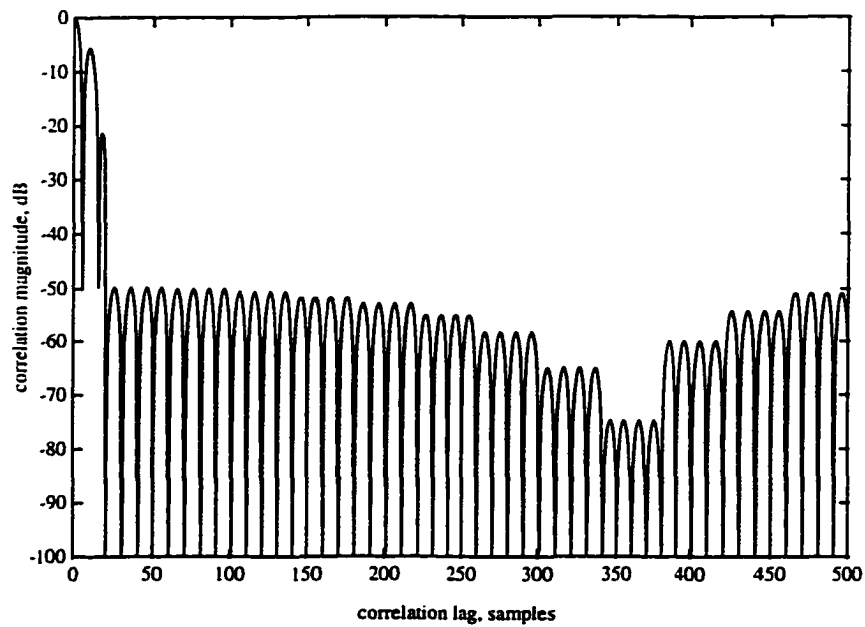
Figure 5.18: PACF of Polyphase sequence based bandpass waveform.
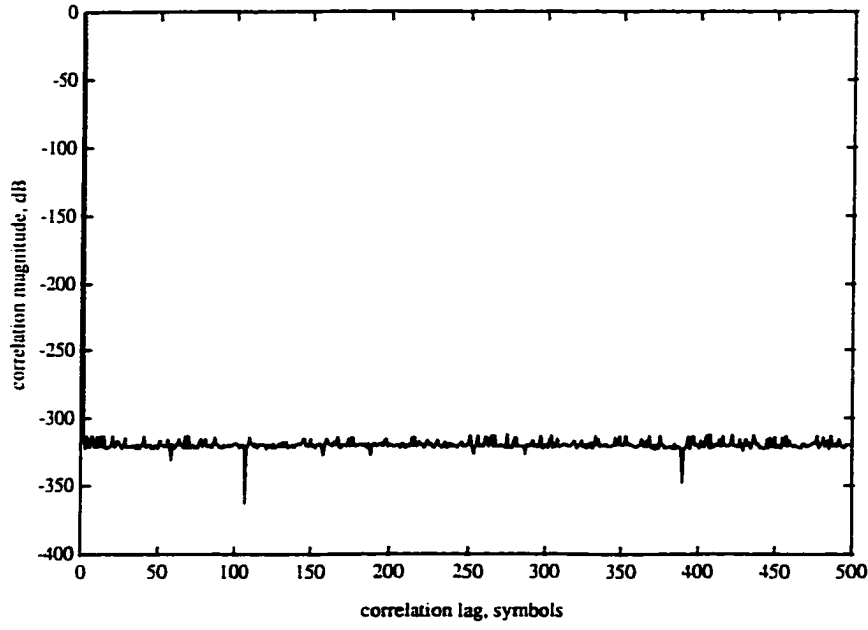
Figure 5.19: PACF of AM sequence.
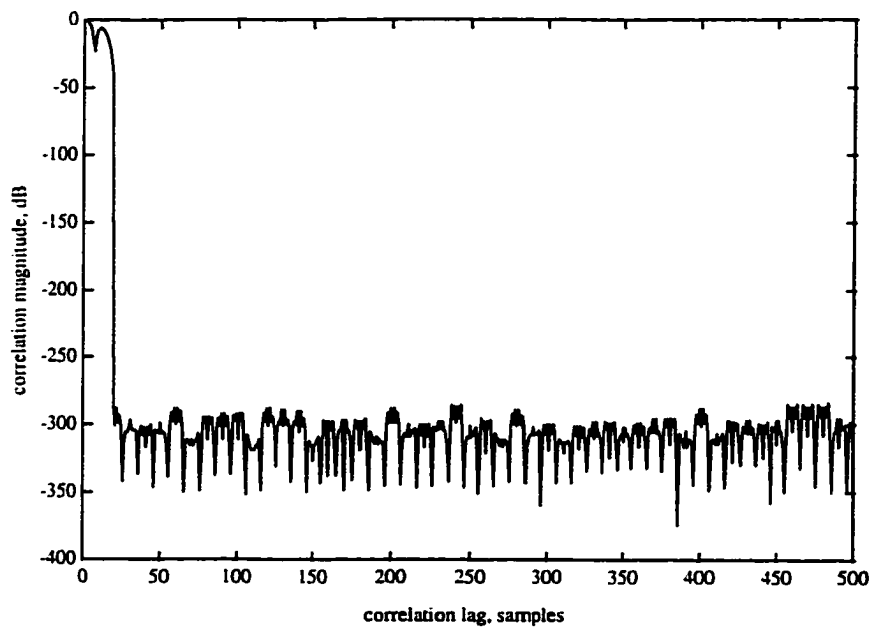
Figure 5.20: PACF of AM sequence based bandpass waveform.
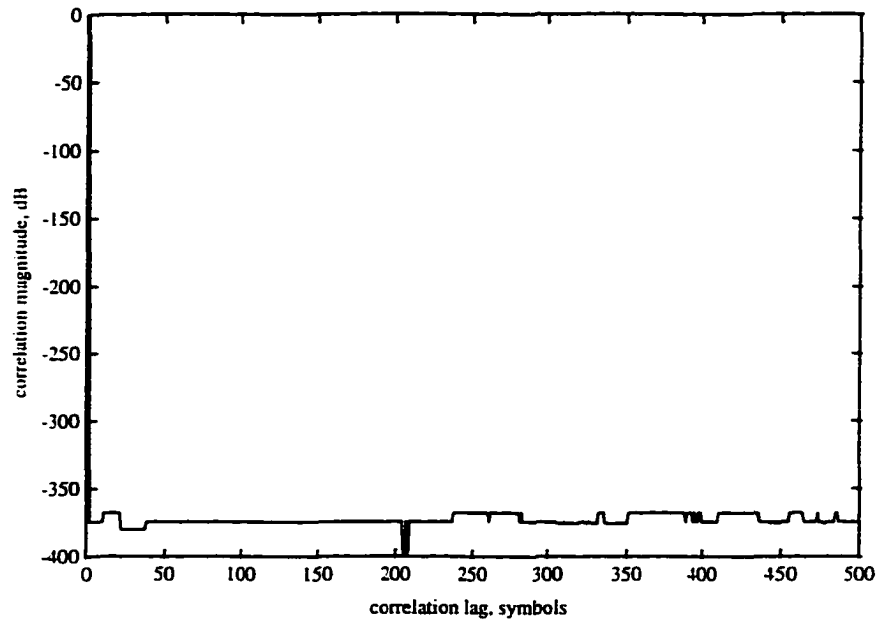
Figure 5.21: PACF of offset-phase sequence.
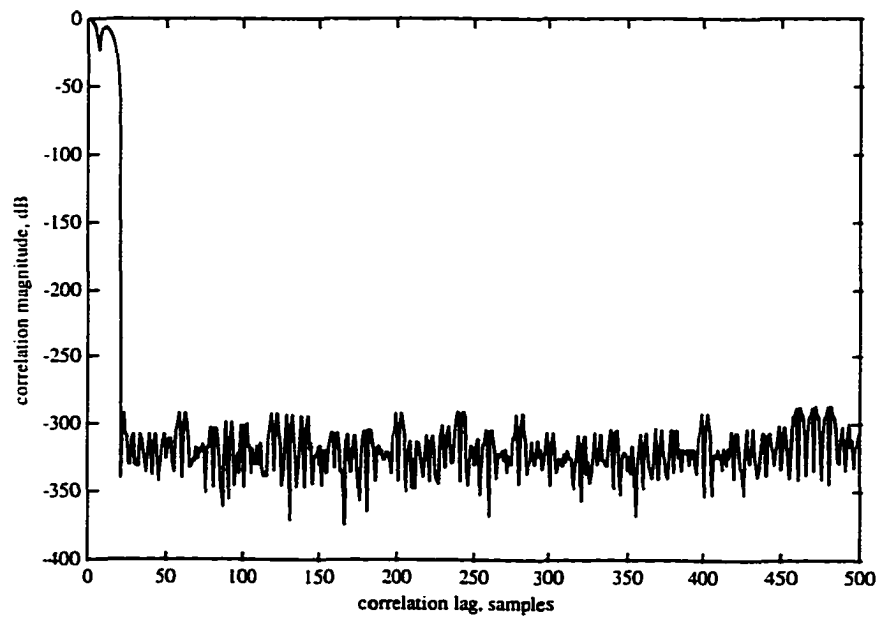
Figure 5.22: PACF of offset-phase sequence based bandpass waveform.

Next, the impulse response estimates corresponding to the amplitude modulated waveform approach (Figure 5.23) and the offset-phase modulated waveform approach (Figure 5.24) were evaluated assuming zero random noise, and it was verified that these two approaches completely eliminate the self-noise.

5.3 Sub-Optimum SSUE Simulation

In addition to the optimum SSUE system design approaches, a few sub-optimum approaches were also pursued in Chapter 4. This section presents the simulation analysis of two of those approaches.

5.3.1 Deterministic Approach

This approach is based on the estimation of self-noise component of the measured correlation signature and the subtraction of this component from the signature. The ultrasonic correlation signature is represented as,

$$\phi_{sr}(\tau)=\bar{h}(\tau)+N_s(\tau)+N_r(\tau) \tag{5.1}$$

So the goal is to make an estimate of $N_s(\tau)$. The test impulse response of Figure 5.10 was used to model this approach. The transmit waveform, s(t), was the BPSK signal based on a 10th order maximal-length sequence. The received signal, r(t), was simulated as,

$$r(t)=s(t)*h(t)+n(t) \tag{5.2}$$

where, n(t) represents the additive Gaussian noise. After determining the correlation signature, the self-noise component of the signature was estimated using the algorithm of section 4.5.1 and removed from the signature. It was found that under low noise conditions, the algorithm works well (Figure 5.25). However, as the additive noise level increases, accurate estimation of self-noise becomes difficult.
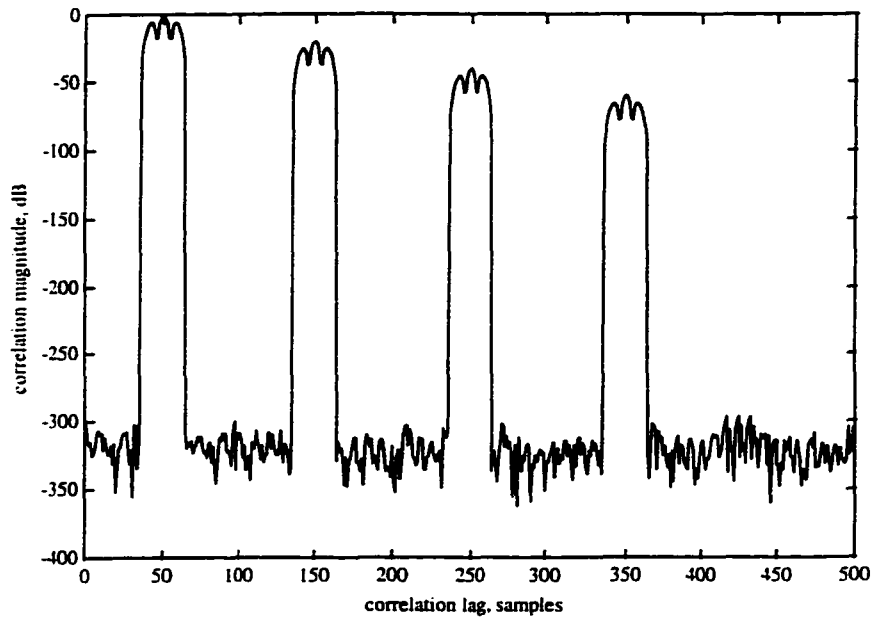
Figure 5.23: Impulse response estimate using amplitude modulated waveform.
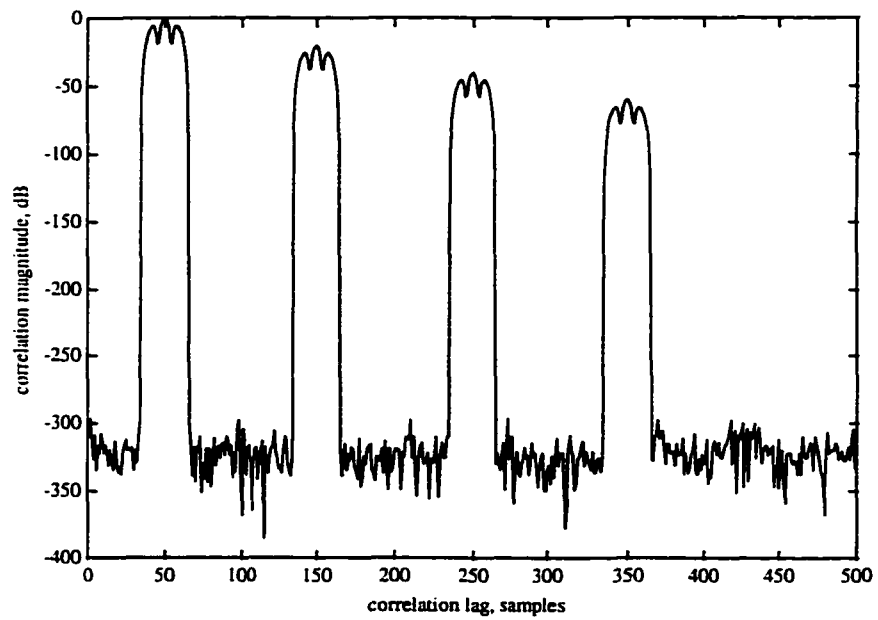
Figure 5.24: Impulse response estimate using offset-phase modulated waveform.
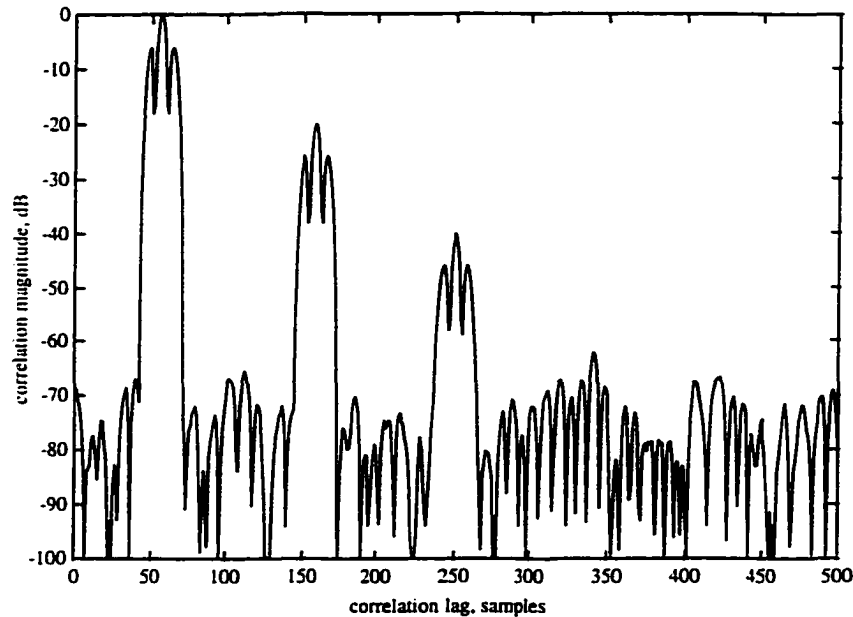
Figure 5.25: Impulse response estimate using the deterministic approach.

Another short-coming of this method is that it requires complete correlation signature for the estimation of self-noise and hence the partial evaluation of correlation signature (range gating of the signature) is not possible.

5.3.2 Mismatched Filter Approach

In this approach, the mismatch filter corresponding to the transmitted BPSK waveform, s(t), was developed. The PCCF of the transmitted signal, s(t), and the mismatch waveform is shown in Figure 5.26. The received signal, r(t), was generated as earlier and the crosscorrelation signature was calculated. The simulation results indicated complete suppression of self-noise (Figure 5.26), however, the random noise floor was about 6 dB higher than the equivalent cases of various optimum design approaches (Figure 5.27).
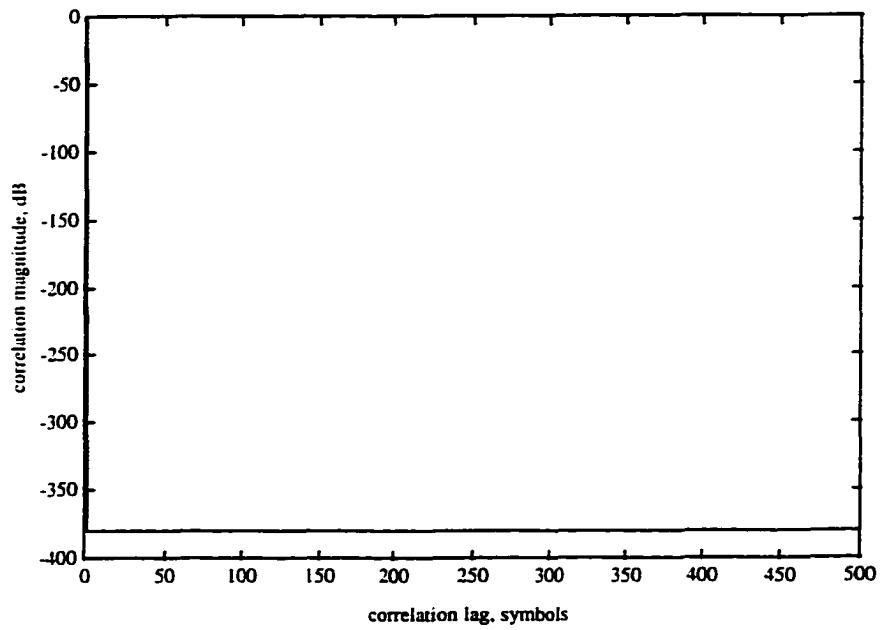
Figure 5.26: PCCF of transmit waveform and mismatch filter.
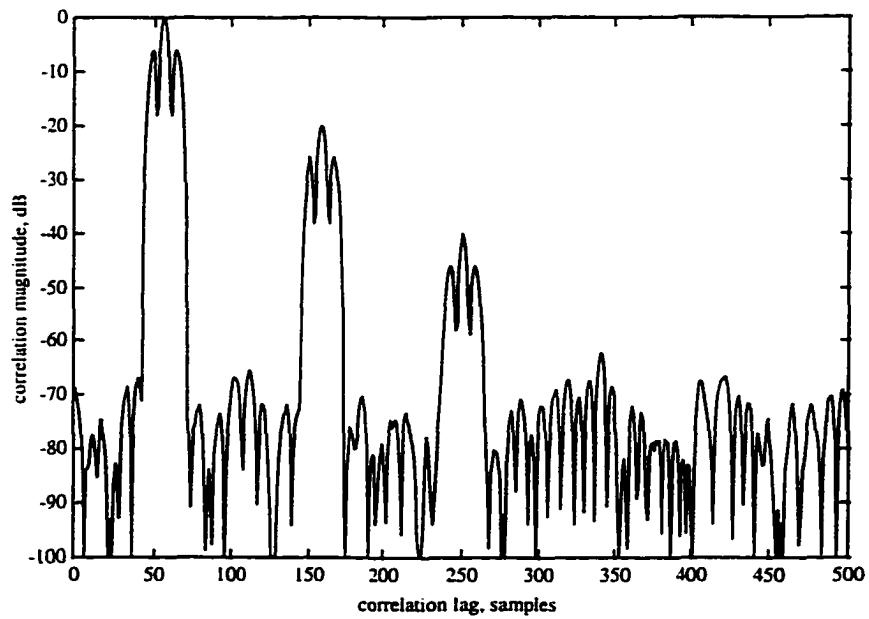
Figure 5.27: Impulse response estimate using the mismatch filter approach.

5.4 Optimization in Resolution

A practical SSUE system is always bandlimited, mainly because of the frequency selective response of the ultrasonic transducers. Hence, the spectral characteristics of the excitation waveform play an important role in achieving greater resolution in the measured ultrasonic correlation signature. Theoretical analysis dealing with the optimization of SSUE system with respect to signature resolution was carried out under section 4.6. This section presents the simulation results based on various pulse functions. The distortion of transmitted waveform due to the bandlimiting effect and the corresponding effect on the PACF function is compared.

5.4.1 Simulation Details

The effect of bandlimited channel on the correlation signature is first simulated. The undistorted baseband waveform, based on rectangular pulse function, is shown in Figure 5.28. There are 40 samples in each chip of the waveform, which means that, ideally, its PACF should have a mainlobe width of less than 80 samples. The PACF of this waveform is shown in Figure 5.29, and its mainlobe width at -80 dB level is about 80 samples. The distortion effect on the waveform due to bandlimiting is shown in Figure 5.30, and the PACF of the bandlimited waveform is given in Figure 5.31. The waveform exhibits ringing effect at the transition points due to the filtering of high frequency components. There is a drastic degradation of the PACF function. The PACF mainlobe width at -80 dB level is about 160 samples, twice that of the undistorted case. Next, various pulse function were considered for the generation of pseudorandom waveform. These are:

(a) Rectangular pulse function, given by,

$$p(k)=1 \qquad\qquad (5.3)$$

(b) Hanning pulse function, given by,
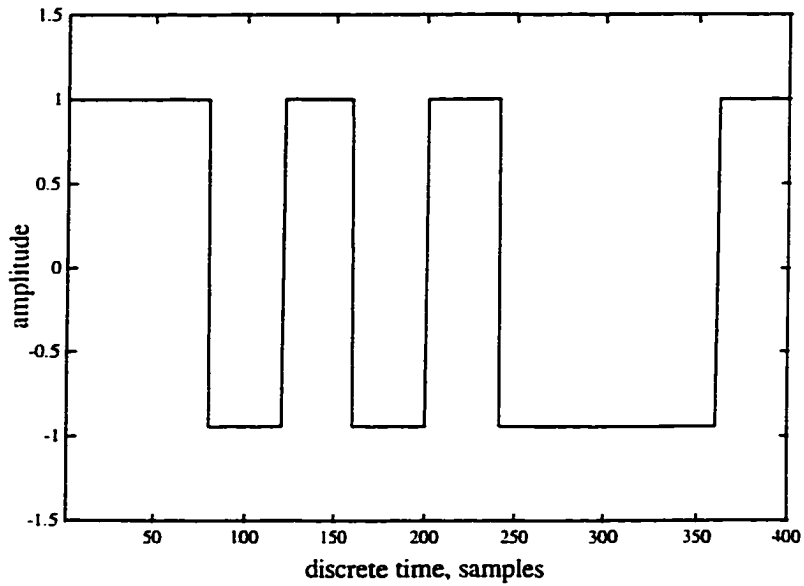
Figure 5.28: Baseband pseudorandom waveform based on rectangular pulse function.

mainlobe
width =
80 samples
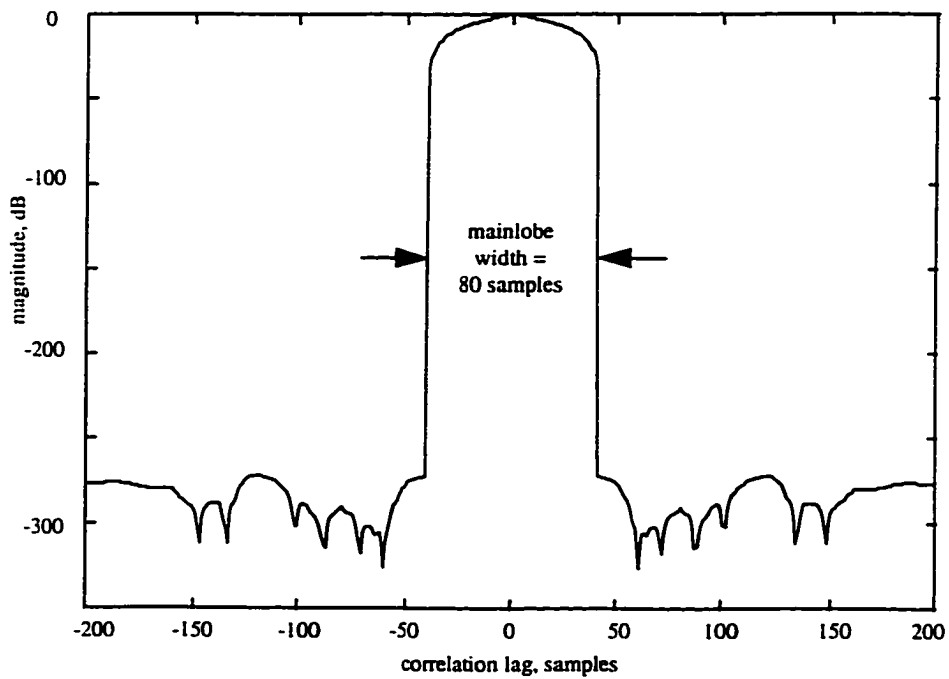
Figure 5.29: PACF mainlobe of waveform of Figure (5.28).
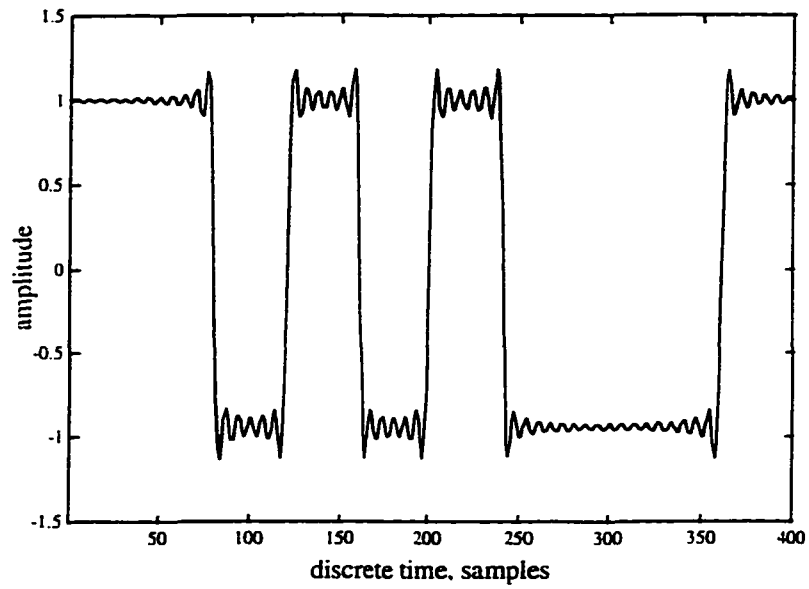
Figure 5.30: Bandlimited pseudorandom waveform based on rectangular pulse function.
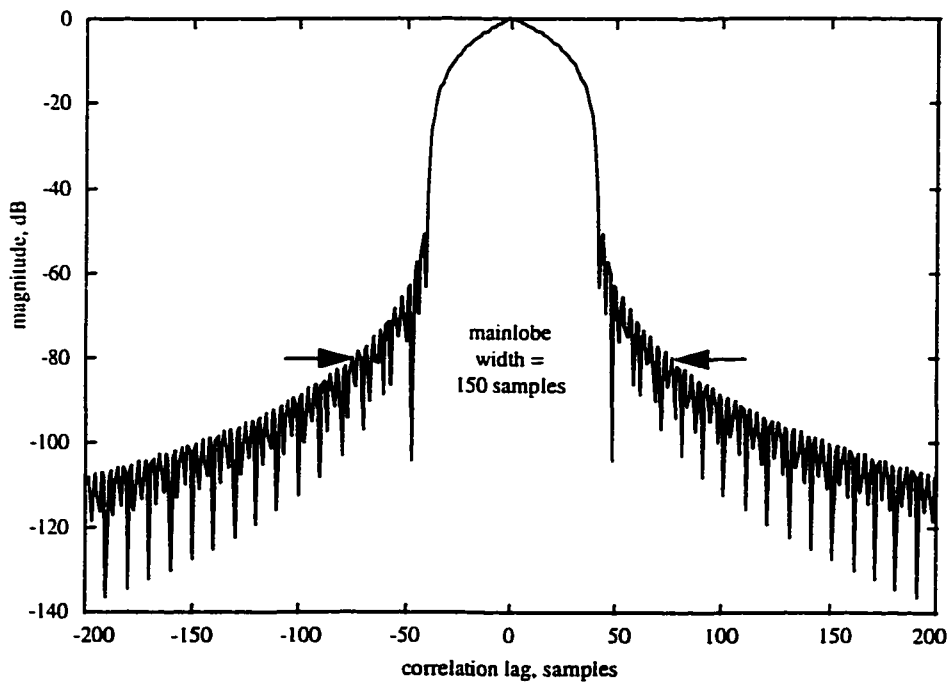
Figure 5.31: PACF mainlobe of bandlimited waveform of Figure (5.30).

$$p(k)=1-\cos(2\pi k/N) \tag{5.4}$$

(c) Hamming pulse function, given by,

$$p(k)=.54-.46\cos(2\pi k/N) \tag{5.5}$$

(d) Blackman pulse function, given by,

$$p(k)=.42-.5\cos(2\pi k/N)+.08\cos(4\pi k/N) \tag{5.6}$$

(e) Exact Blackman pulse function [71], given by,

$$p(k)=\frac{7938}{18608}-\frac{9240}{18608}\cos(\frac{2\pi k}{N})+\frac{1430}{18608}\cos(\frac{4\pi k}{N}) \tag{5.7}$$

(f) Blackman-Harris pulse function [71], given by,

$$p(k)=0.42323-0.49755\cos(\frac{2\pi k}{N})+0.07922\cos(\frac{4\pi k}{N}) \tag{5.8}$$

where, k = 0, 1, 2, ... (N-1) and N is the length of the pulse function in samples. The amplitude spectrum of these pulse functions is shown in Figures 5.32 through 5.37. Different pseudorandom waveforms based on the above pulse functions were generated and the degradation of PACF mainlobe due to bandlimiting was studied.

Finally, SSUE system simulations were carried out to demonstrate the improvement in the resolution of ultrasonic correlation signature through the use of different pulse functions. A test impulse response with two reflection components was chosen. The backwall reflection was at a lag of 60 samples, while the second reflection (corresponding to a small flaw) was at a lag of 40 samples. The second reflection component was chosen to be 80 dB weaker than the backwall component. The simulations were performed under zero random noise conditions. The correlation signatures corresponding to the six cases are presented in Figures 5.38 through 5.43. It can be seen that the flaw reflection is not visible at all in Figure 5.38, where as, the two
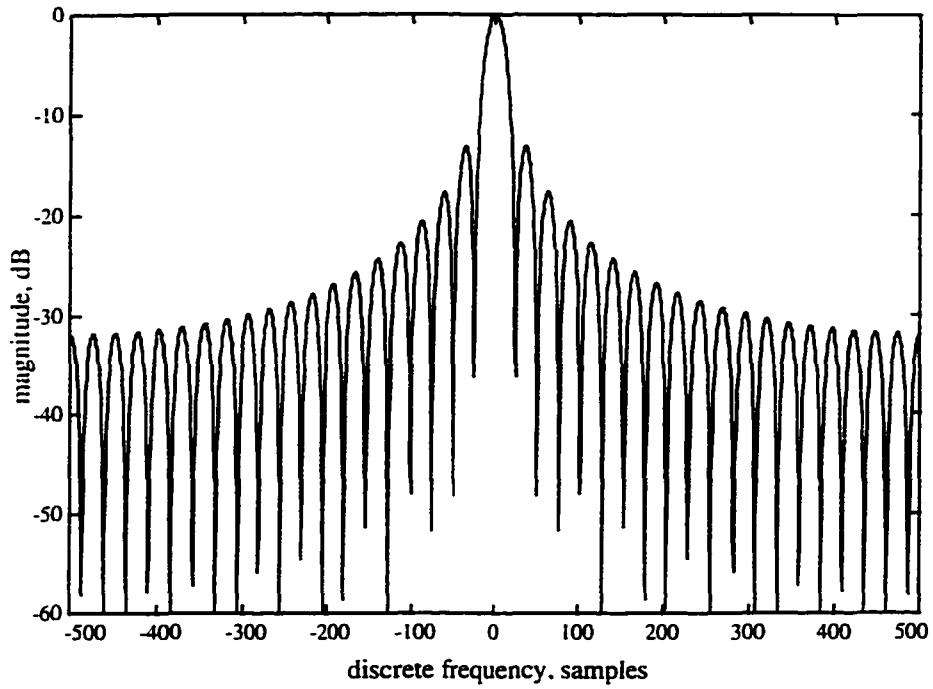
Figure 5.32: Magnitude spectrum of rectangular pulse function.
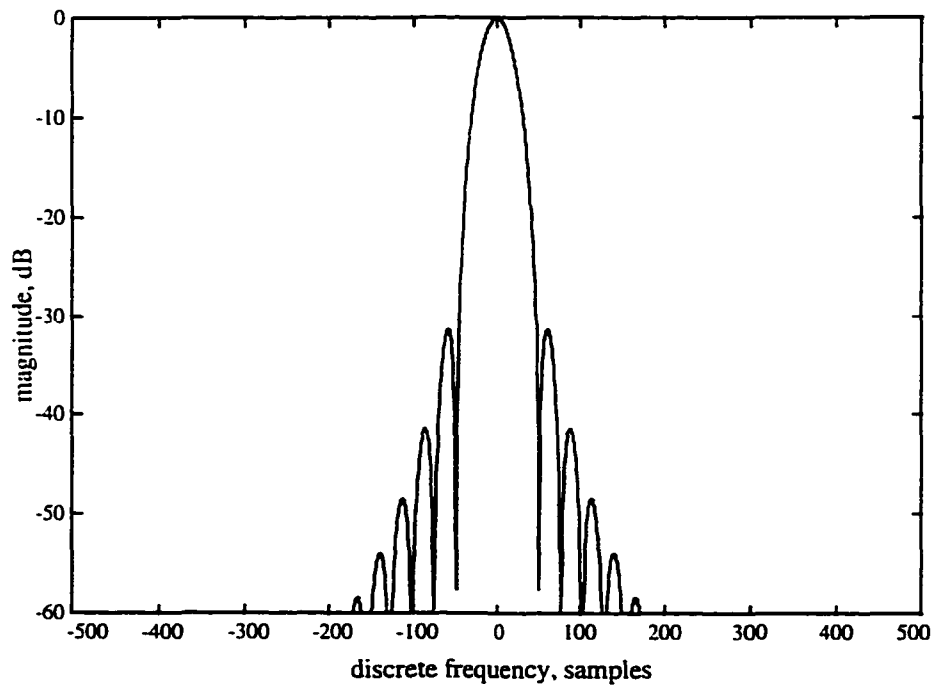
Figure 5.33: Magnitude spectrum of Hanning pulse function.
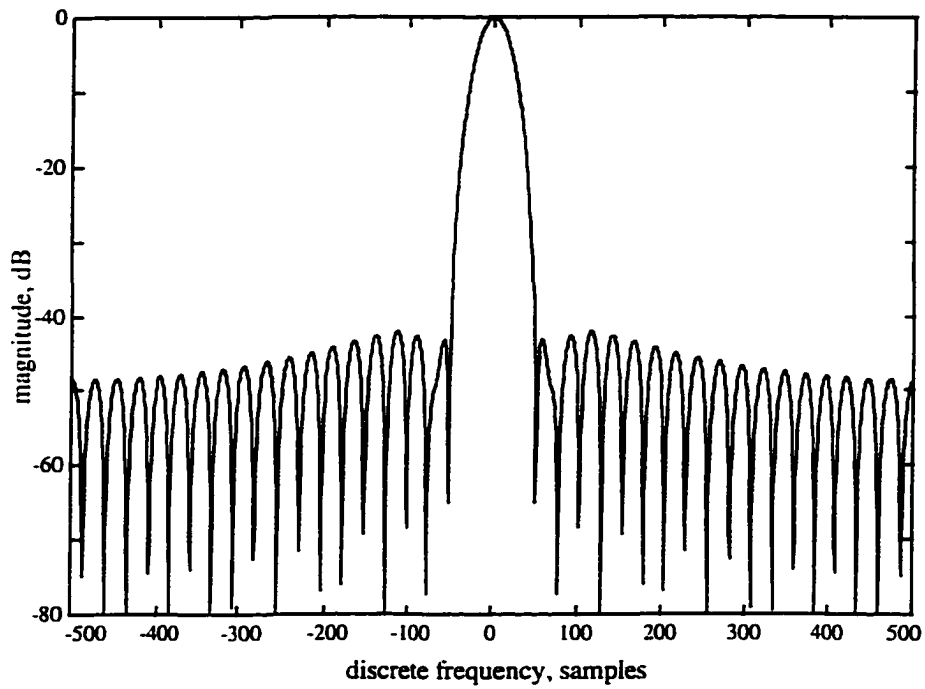
Figure 5.34: Magnitude spectrum of Hamming pulse function.
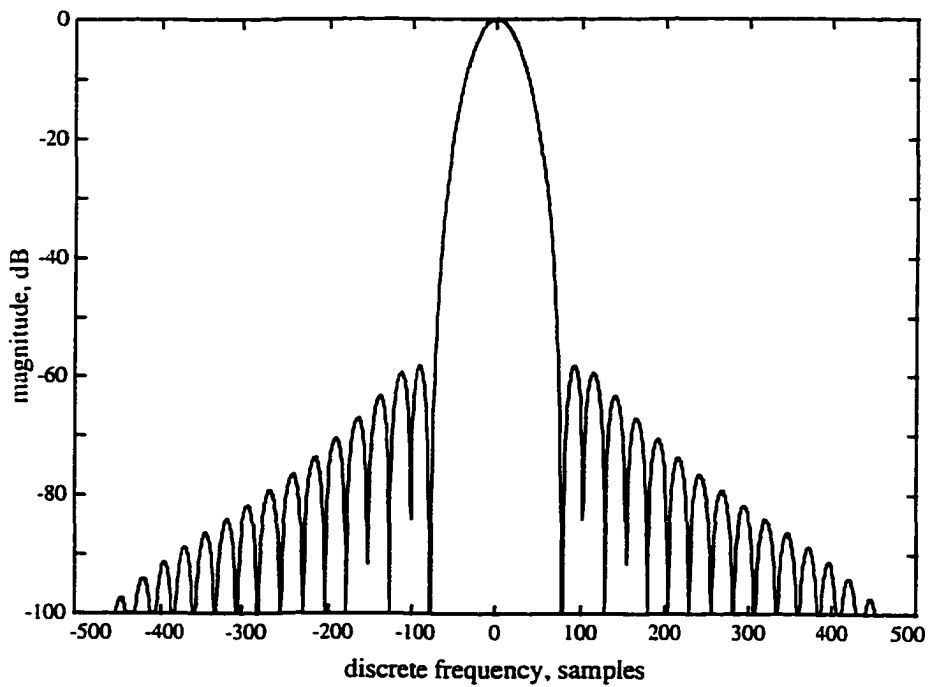
Figure 5.35: Magnitude spectrum of Blackman pulse function.
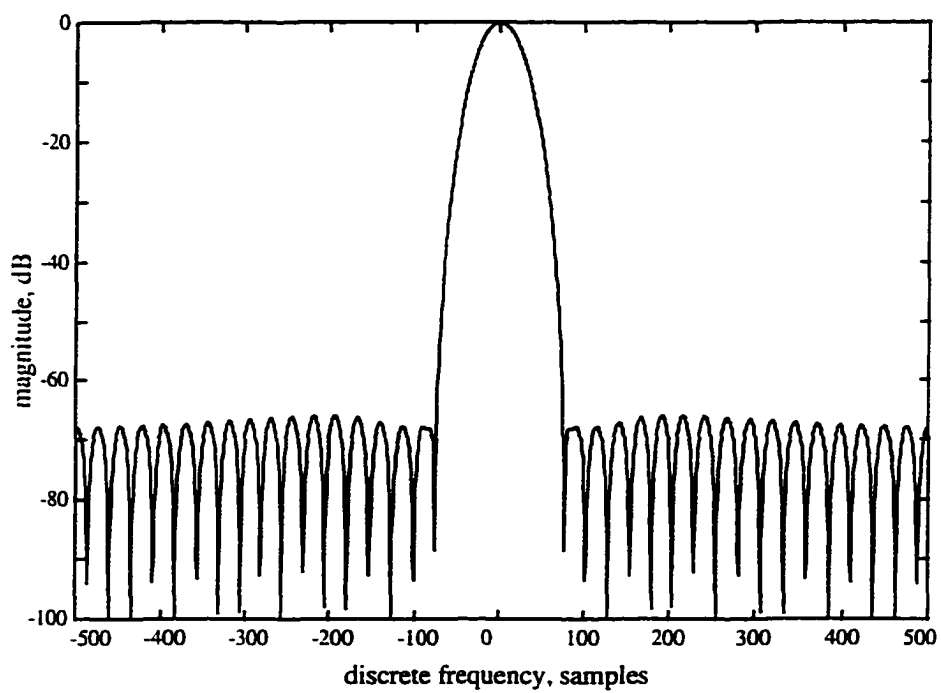
Figure 5.36: Magnitude spectrum of exact Blackman pulse function.
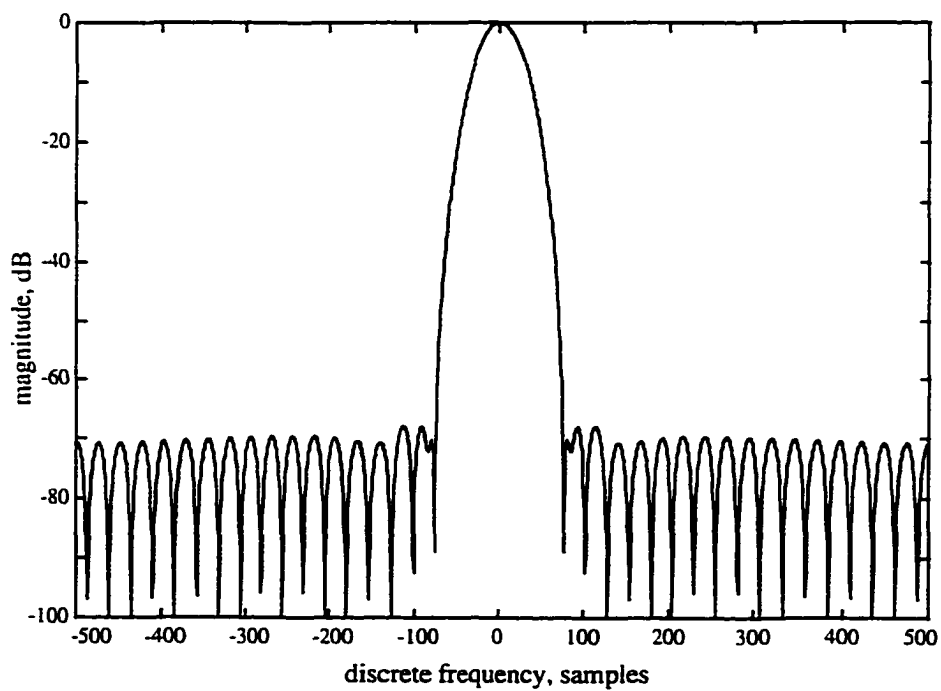
Figure 5.37: Magnitude spectrum of Blackman-Harris pulse function.
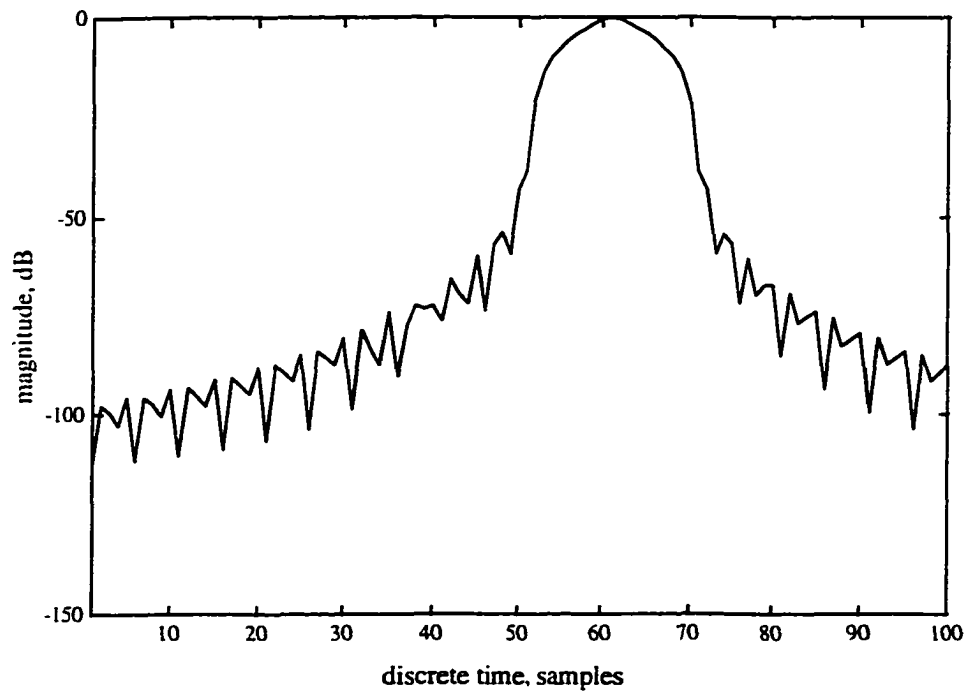
Figure 5.38: Correlation signature from rectangular pulse function.
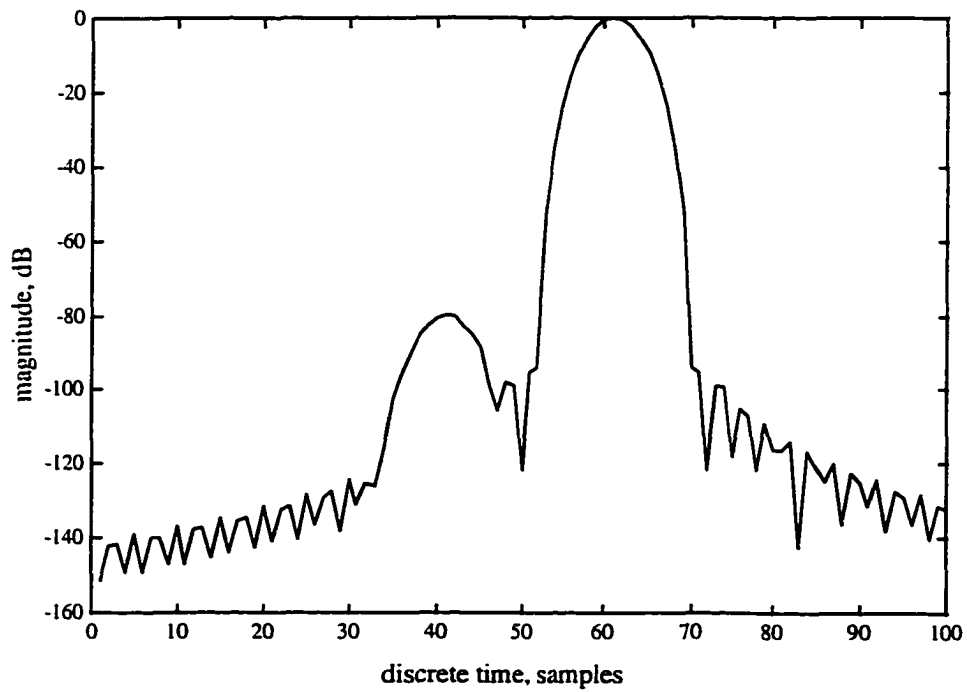
Figure 5.39: Correlation signature from Hanning pulse function.
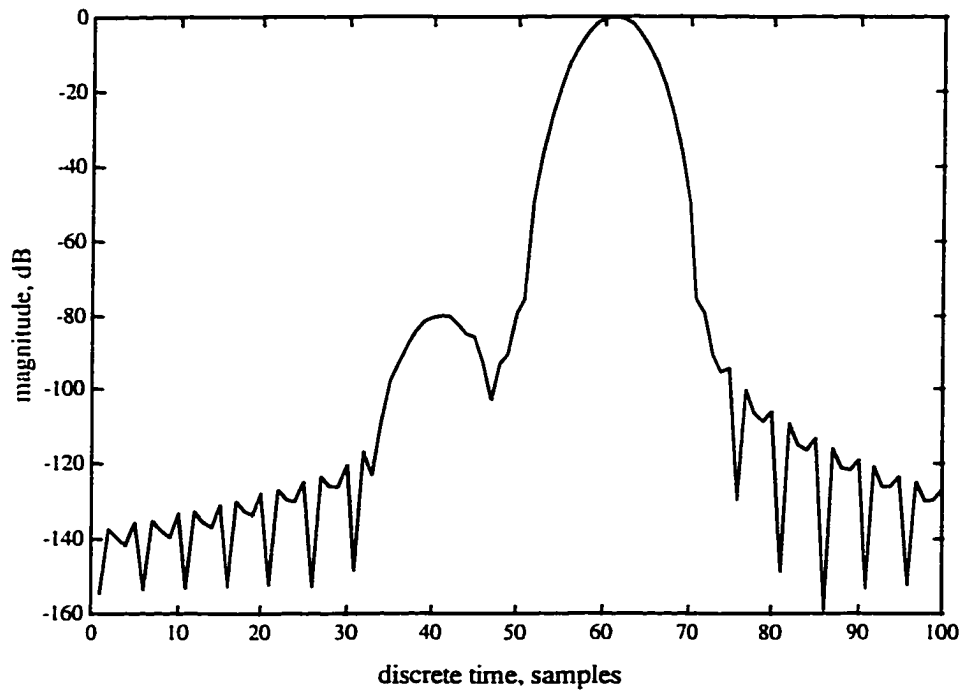
Figure 5.40: Correlation signature from Hamming pulse function.
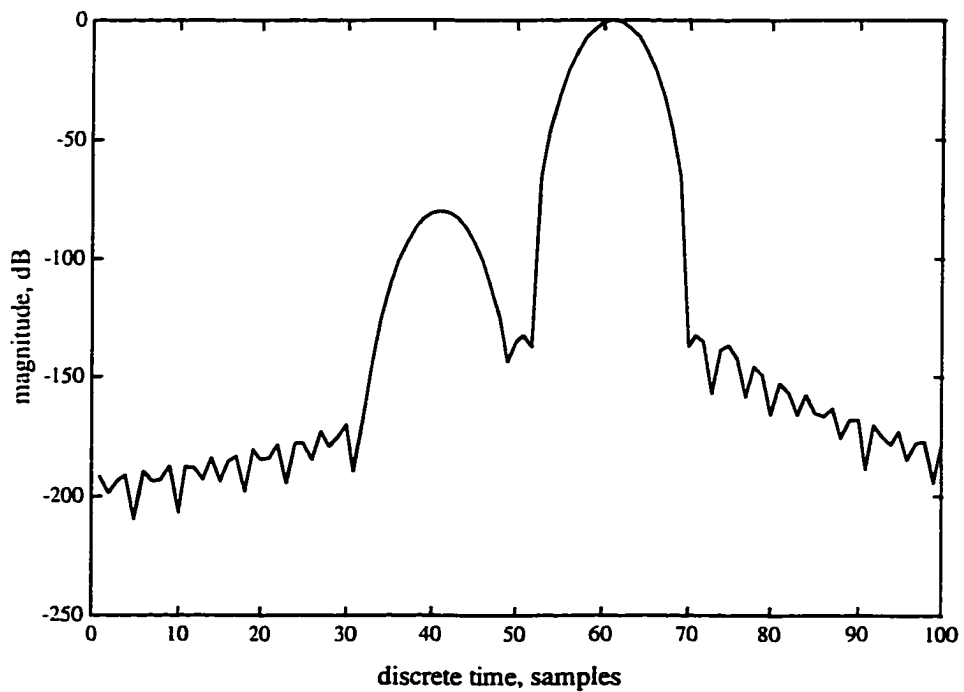
Figure 5.41: Correlation signature from Blackman pulse function.
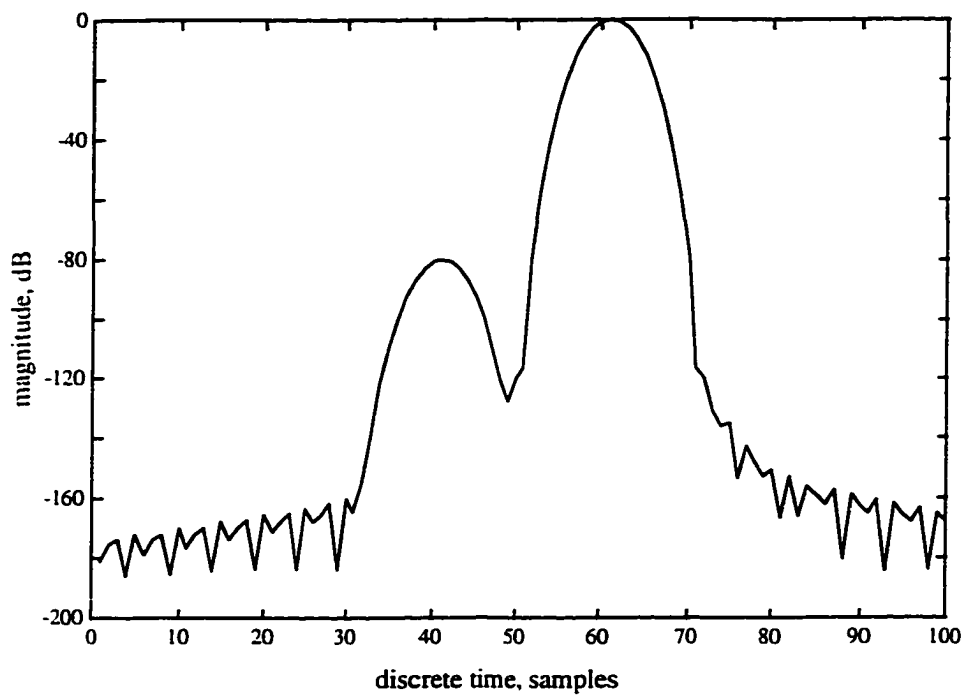
Figure 5.42: Correlation signature from exact Blackman pulse function.
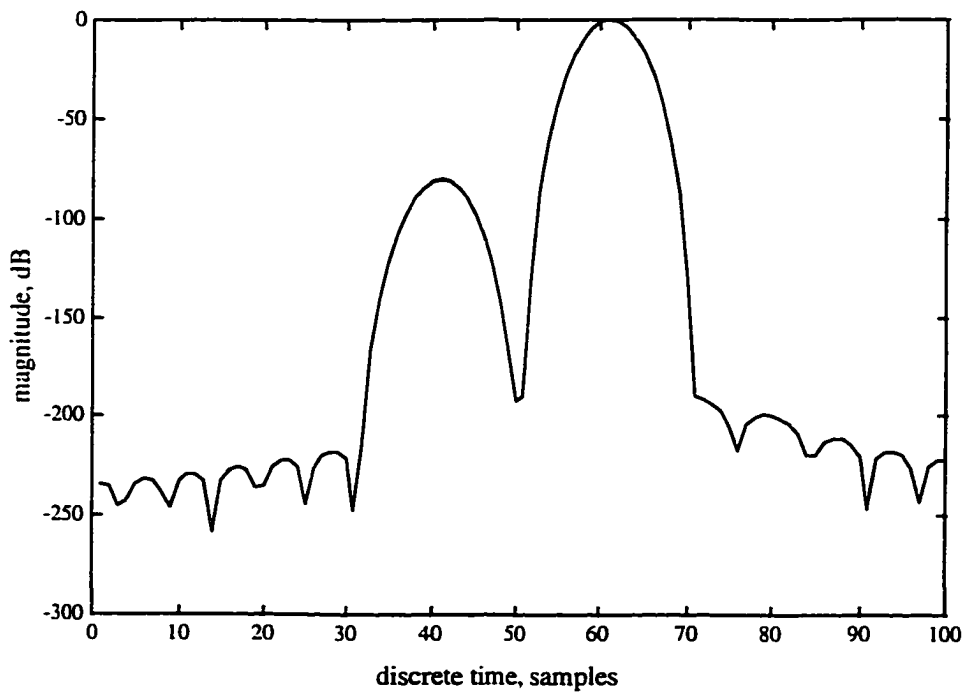
Figure 5.43: Correlation signature from Blackman-Harris pulse function.

components can be clearly distinguished in Figure 5.43. There were a few other pulse functions reported in the literature [71], that have even better spectral characteristics than the ones discussed here. However, they provided very little improvement in the correlation signature, and were more difficult to implement, so they were discarded.

5.5 Narrowband Interference Analysis

It was theoretically proved in section 3.5 that the SSUE technique performs equivalent to the averaging technique under the assumption of uniform white noise. However, when this assumption is not valid, i.e., when the additive noise is narrowband and hence correlated, the performance of SSUE technique is superior to the averaging method. This section presents the simulation details and the results to verify the theoretically derived results.

5.5.1 Modelling of Narrowband Noise

Four types of Gaussian bandlimited white noise waveforms, N1, N2, N3, and N4, were generated using the "RANDN" function of Matlab. The spectral bandwidths of these waveforms with respect to the SSUE system bandwidth, B, are,

bandwidth of waveform N1 = B

bandwidth of waveform N2 = B/8

bandwidth of waveform N3 = B/64

bandwidth of waveform N4 = B/512

A sample realization of the four types of waveforms and their corresponding autocorrelation functions are given in Figures 5.44 to 5.47. The relation between the noise bandwidth and its autocorrelation function is clearly observable. As the noise bandwidth becomes smaller the autocorrelation function dies down less rapidly with respect to the correlation lag.

(a) simulated noise waveform N1, (bandwidth=B)   (b) autocorrelation function of waveform N1
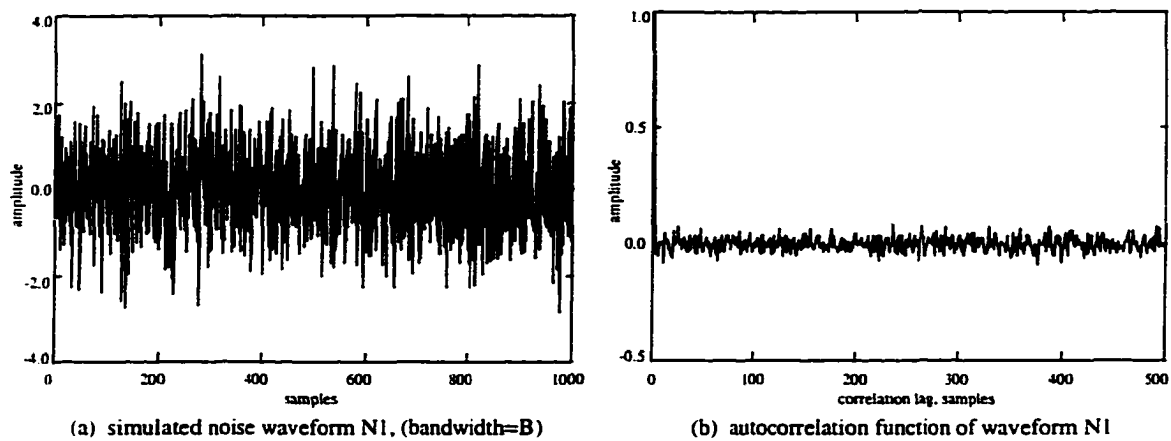
Figure 5.44: Noise waveform N1 and its autocorrelation function.

(a) simulated noise waveform N2, (bandwidth=B/8)   (b) autocorrelation function of waveform N2
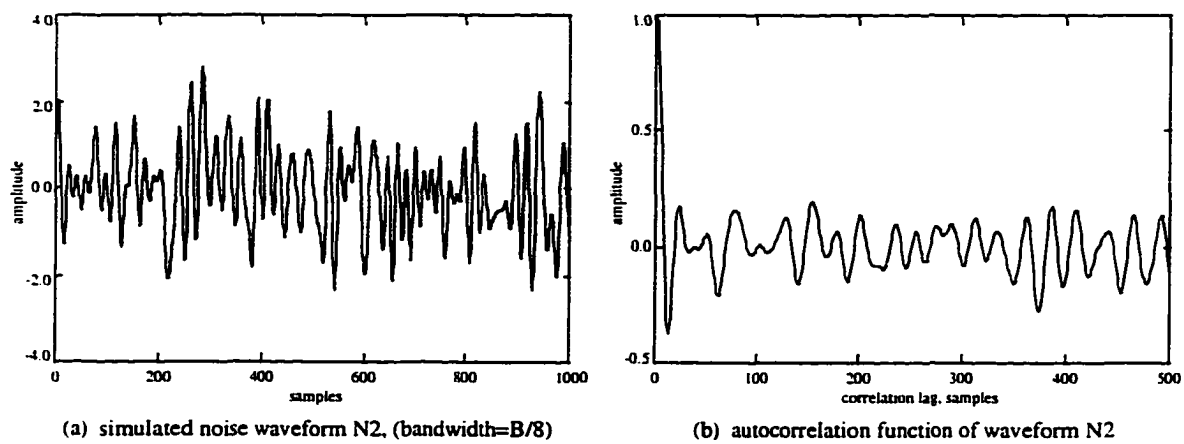
Figure 5.45: Noise waveform N2 and its autocorrelation function.

(a) simulated noise waveform N3, (bandwidth=B/64)

(b) autocorrelation function of waveform N3
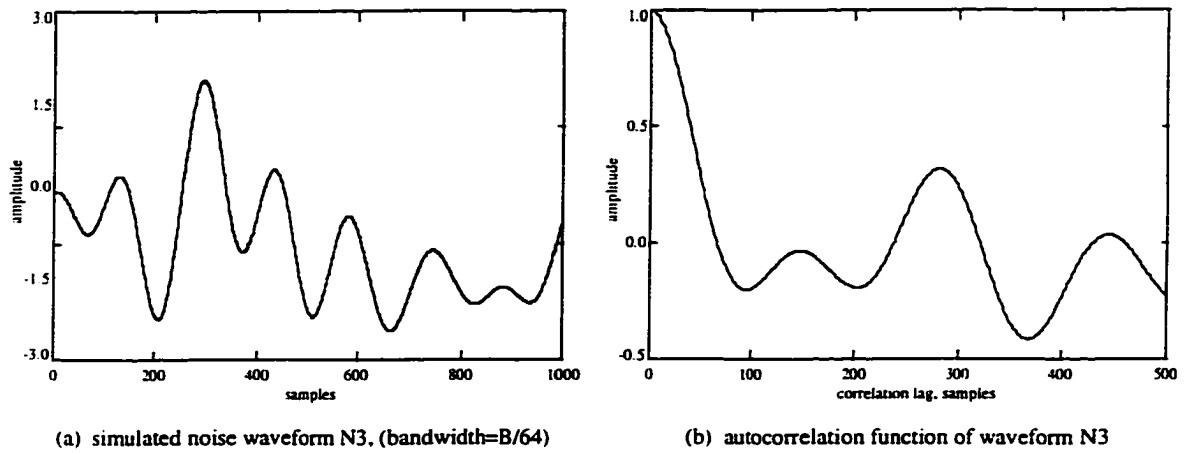
Figure 5.46: Noise waveform N3 and its autocorrelation function.

(a) simulated noise waveform N4, (bandwidth=B/512)

(b) autocorrelation function of waveform N4
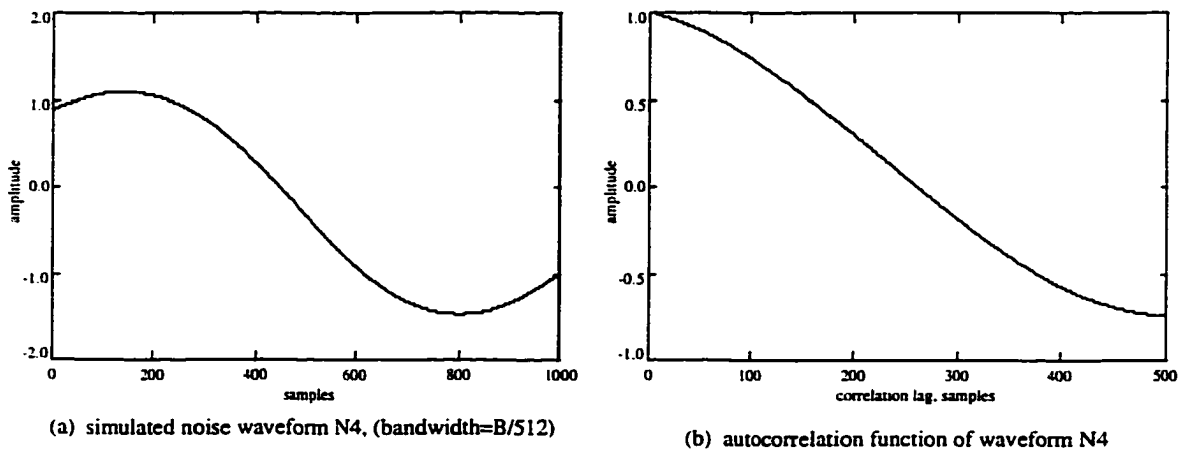
Figure 5.47: Noise waveform N4 and its autocorrelation function.

5.5.2 Effect of Bandlimited Noise on SSUE Signature

The effect of bandlimited white noise on the ultrasonic correlation signature of the SSUE technique was simulated. The ideal impulse response shown earlier in Figure x was used for these simulations also. The SSUE signature estimates corresponding to the noise waveforms N1, N2, N3, and N4 are given in Figures 5.48 to 5.51, respectively.

It can be seen that the noise floor level in all the three estimates remain almost constant at around -45 dB. The spectral characteristics of the random noise component of the correlation signature, however, retains the spectral characteristics of the bandlimited additive white noise.

5.5.3 Effect of Bandlimited Noise on Averaging Technique

The performance of averaging technique under various bandlimited noise conditions was also simulated. The theoretical analysis of section 3.5 predicts that the noise floor level in the averaged waveform should increase as the additive noise becomes more and more narrow-bandlimited. The simulation results corresponding to the noise waveforms N1, N2, N3, and N4 are given in Figures 5.52 to 5.55, respectively.

The results indicate that the variation in the noise floor level is not very apparent in the first three waveforms. However, it does shoot up drastically in the case of the noise waveform N4. A possible explanation of these results is that the correlation effect of the noise waveforms N2 and N3 die down significantly by the end of one acquisition frame. Since, in the coherent averaging process the corresponding samples of each frame are added, the correlation effect does not show up. If there are N samples per frame, it is the Nth autocorrelation lag value that will determine the correlation effect on the averaging process.
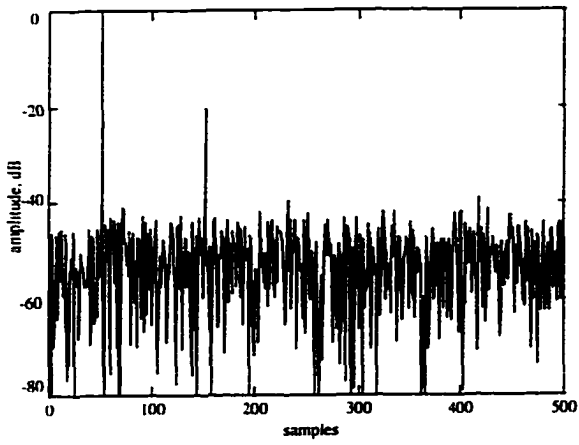
Figure 5.48: SSUE signature-1.
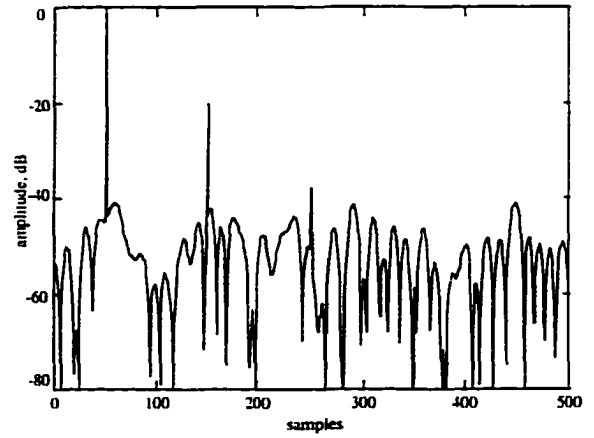
Figure 5.49: SSUE signature-2
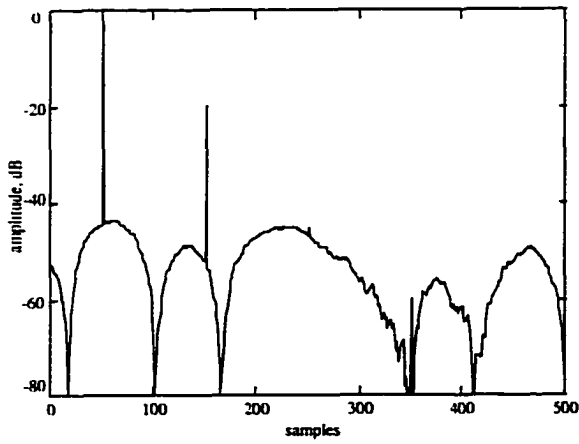
Figure 5.50: SSUE signature-3.
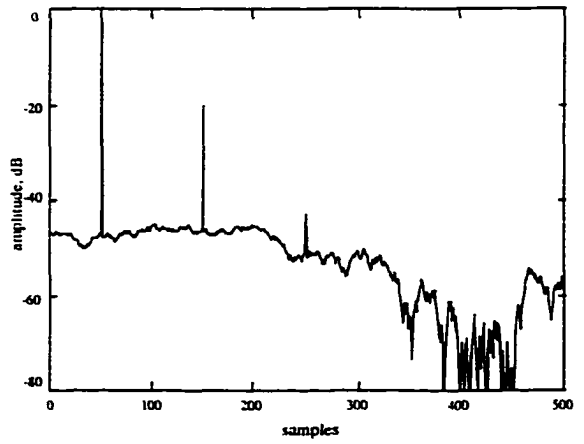
Figure 5.51: SSUE signature-4.
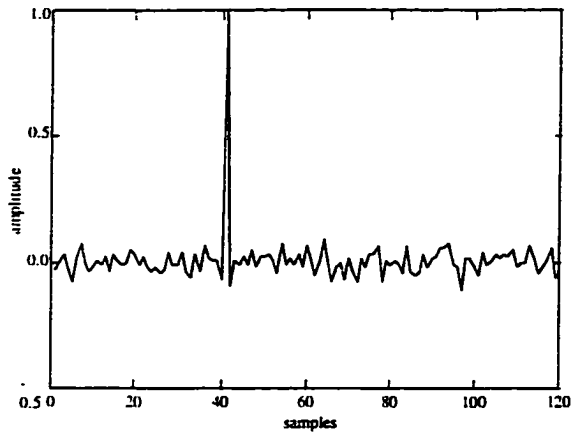
Figure 5.52: Averaged waveform-1.
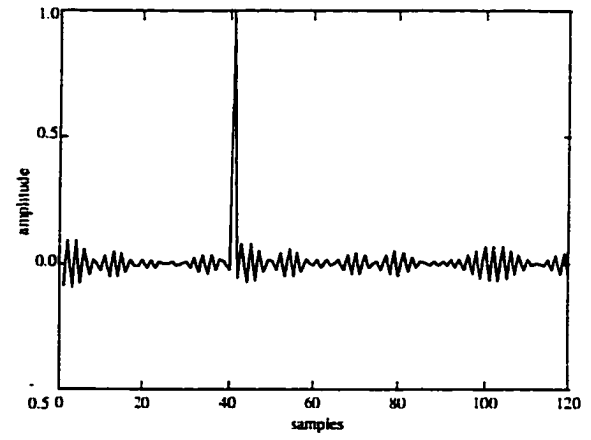
Figure 5.53: Averaged waveform-2.
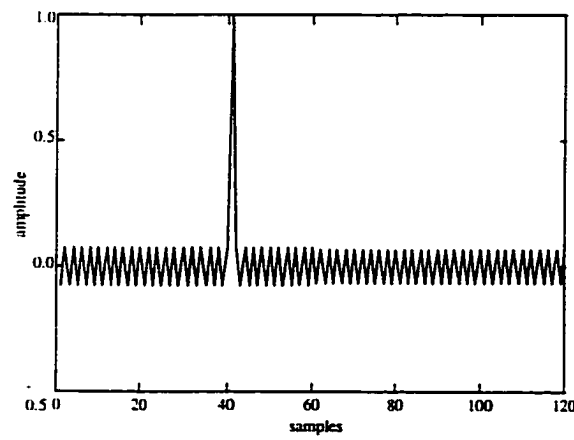
Figure 5.54: Averaged waveform-3.
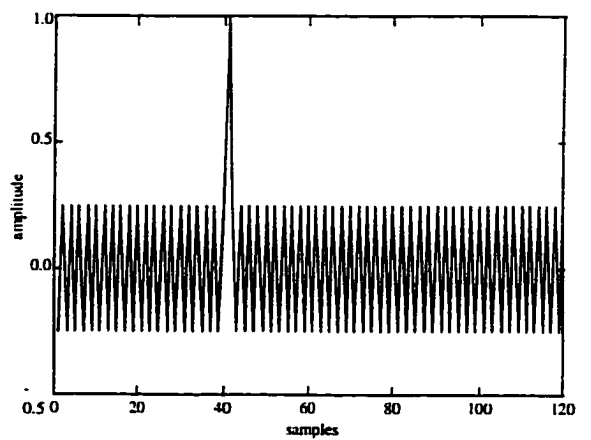
Figure 5.55: Averaged waveform-4.

5.5.4 Discussion/Conclusions:

Comparison of the simulation results of the SSUE technique and the averaging technique verifies the superiority of the SSUE under the conditions of narrowband signal interference. The performance measure was the signal to noise floor level. It has been shown that the performance of the SSUE technique remains fairly constant from the narrowband to wideband case of the interfering noise. For the wideband case, the performance of averaging technique is equivalent to that of the SSUE technique. The performance of averaging technique constantly drops from wideband to narrowband direction. It can be deduced that, in the limiting case of a sinusoidal interfering signal, the averaging technique is no better than the single pulse acquisition technique.

CHAPTER 6   SYSTEM DEVELOPMENT

This chapter discusses the development of an optimized SSUE instrument and analyzes its performance. The effect of various noise sources and other non-ideal factors is studied and the practical limitations of the system are determined. Finally, an efficient design of the correlation filter is developed and its performance compared with the conventional correlator implementations.

6.1 First Generation SSUE Instrument

The first generation SSUE instrument was a fairly straight forward implementation of the basic system block diagram given earlier in Figure 3.6. It used the binary phase shift keying (BPSK) approach for the generation of pseudorandom excitation waveform. Inspite of being less efficient and sub-optimum, it served the following important purposes,

(a) It provided a proof of concept test for the SSUE technique.

(b) It gave a starting point after which further refinements could be made.

(c) It provided insight to certain technological limitations.

Two approaches were pursued in the development of the first generation instrument [62]. First was based on the digital implementation of the transmitter and the receiver (Figure 6.1), while the second was based on the analog implementation of the transmitter and the receiver (Figure 6.2). In case of the digital implementation approach, called maximal-software approach (MSA), the excitation waveform was generated in the computer and downloaded to a waveform generator. On the receiver side, the received signal is captured and digitized through a digitizing oscilloscope and the digitized data transferred to the host computer. The correlator was implemented in the PC software.
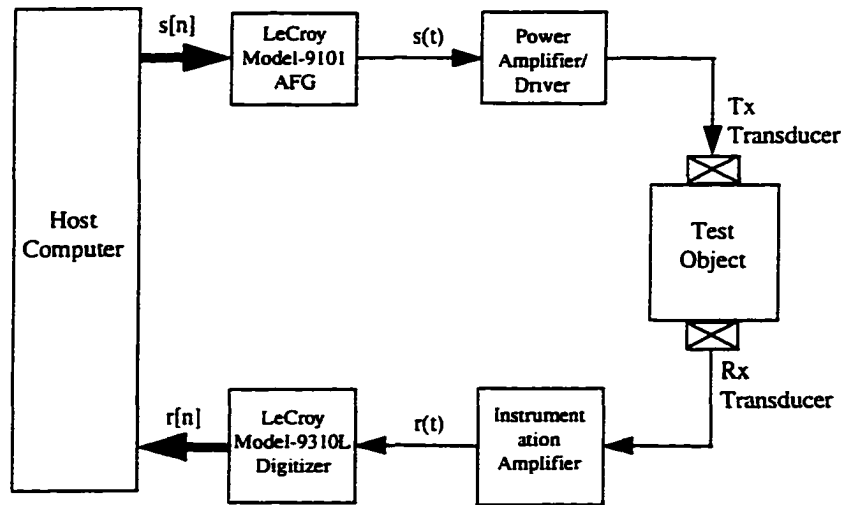
Figure 6.1: First generation SSUE instrument (MSA).
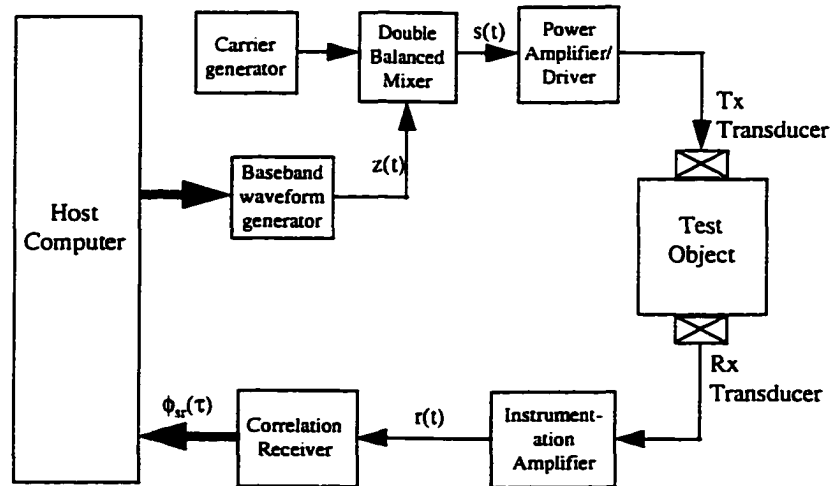
Figure 6.2: First Generation SSUE instrument (MHA).

In case of the analog implementation approach, called maximal-hardware approach (MHA), a baseband pseudorandom waveform was first generated in hardware and then modulated to a carrier signal in the double-balanced mixer, thus producing the bandpass pseudorandom excitation waveform. Also, the correlation receiver was implemented in the hardware. It was realized that, in the current developmental stage of SSUE, the digital implementation approach is better. This is because,

(a)   the digital or software approach is much more flexible,

(b)   the digital correlation receiver had much smaller implementation, losses than the analog one,

(c)   digital signal processing is becoming increasingly faster and cheaper.

6.2 Optimized SSUE Development

The hardware setup of the maximal software approach (MSA) from the first generation SSUE instrument (Figure 6.1) was used as the testing platform for the implementation of various optimized system design approaches developed earlier under Chapter 4 and simulation tested under Chapter 5. The detail of system implementation and the test results are presented in this section.

Five different system design approaches were implemented. These are,

(a)   Binary phase modulation based SSUE system

(b)   Amplitude modulation based SSUE system

(c)   Offset-phase modulation based SSUE system

(d)   Mismatched filter based SSUE system

(e)   On-Off modulation based SSUE system

The binary phase modulation approach (a) was the starting point for the system optimization process. Hence it serves as the reference with which the performance of other approaches are compared. The next two approaches, (b) and (c), are the optimum system design approaches, while the last two, (d) and (e), are the suboptimum approaches. The results presented here correspond to pseudorandom excitation waveforms based upon

a 10th order maximal-length sequence having a sequence length of 1023 symbols. The carrier frequency used for the generation of the waveforms was 5 MHz, and the system bandwidth was 10 MHz.

Two types of tests were performed corresponding to each approach. Test-1 involved bypassing of the ultrasonic transducers and the test object. Hence the transmitted signal is directly fed to the spread-spectrum receiver (Figure 6.3). The idea of test-1 was to eliminate all the random variables associated with the test specimen and the conversion of electrical signal to acoustic signal. Test-2 represented an actual NDE situation and involves the conversion of electrical excitation waveform to ultrasonic excitation signal, propagation of ultrasound through the test material, and finally the
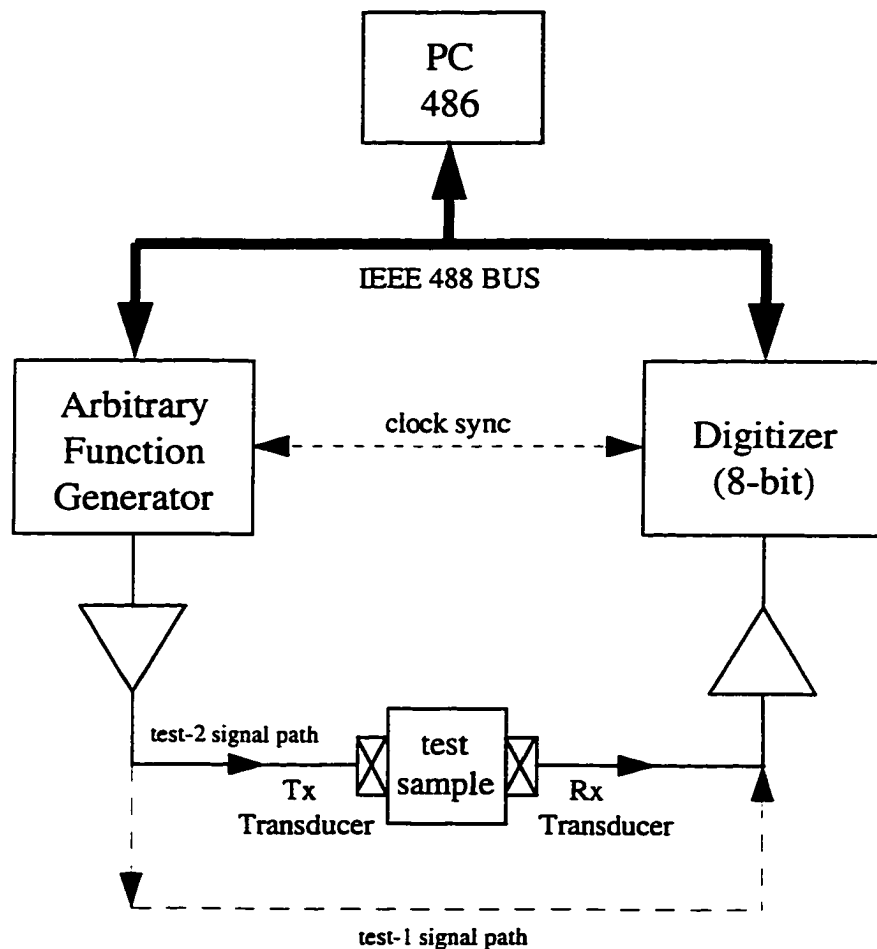
Figure 6.3: Instrument configuration for test-1 and test-2.

reception of acoustic signal by the receive transducer. The test specimen consisted of a plastic (Perspex) disc with .2 inch thickness and a diameter of .7 inches. The transducers used were of 5 MHz center frequency and a diameter of .5 inch. The transmit waveform had an amplitude of 10 volts peak-to-peak.

The following figures (Figures 6.4 through 6.18) present the test results of each approach along with the representation of each excitation waveform. All the waveforms are based on the Blackman pulse function, in order to achieve optimum resolution. It can be observed that, the binary-phase modulated waveform (Figure 6.4) has all signal peaks of constant amplitude, whereas the amplitude modulated waveform (Figure 6.7) has a variation in signal amplitude from one chip to another, even though this variation is very small. The offset-phase modulated waveform (Figure 6.10) has chip-to-chip phase variations of 0° and 179.8°, however, it looks very similar to binary-phase modulation. The mismatch-filter approach uses the binary-phase modulated waveform (Figure 6.13) and the difference comes in the correlation filter. Finally, the on-off modulation
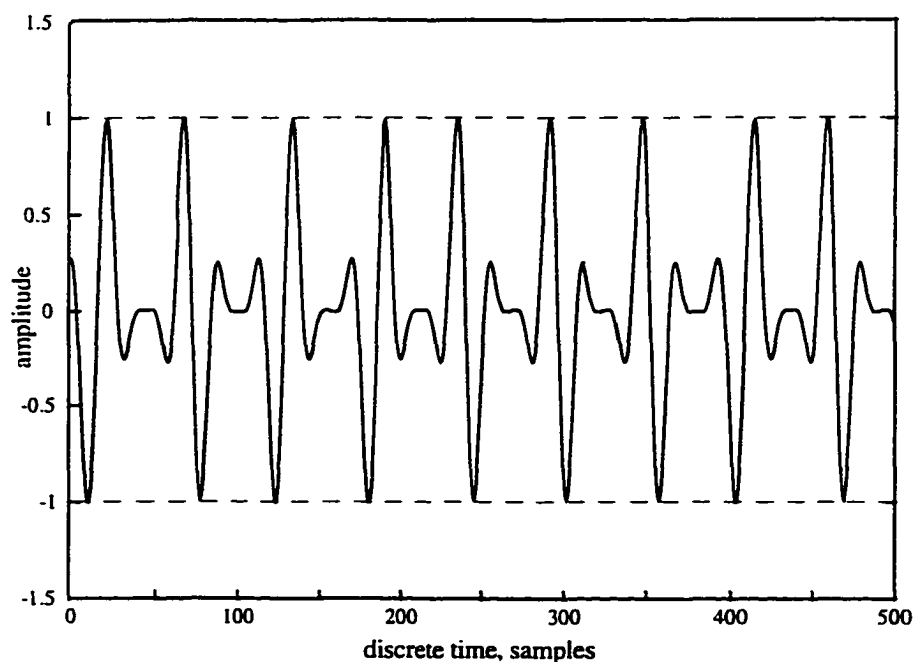
Figure 6.4: Excitation waveform for binary-phase modulation approach.
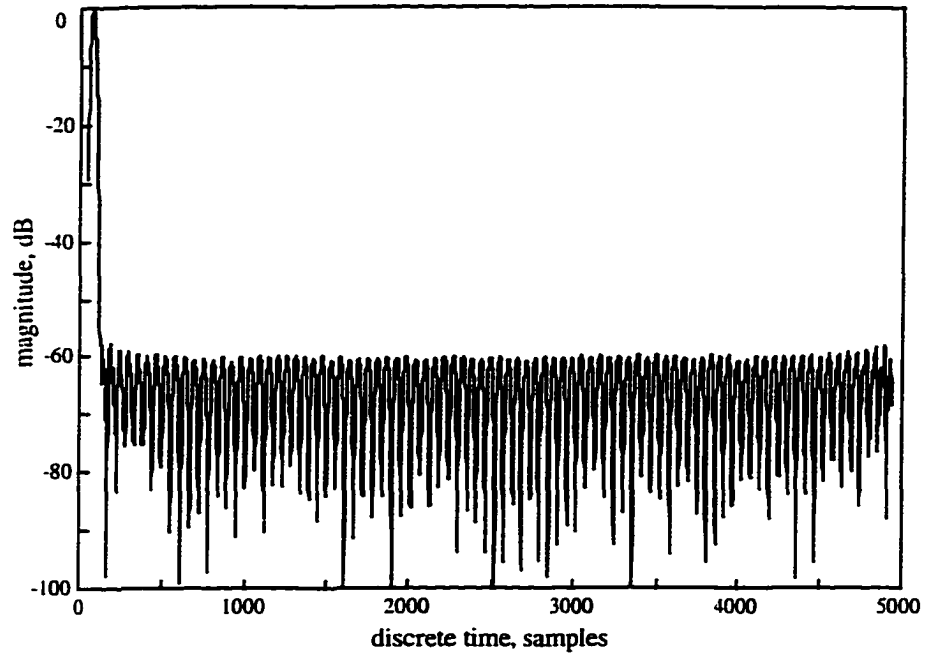
Figure 6.5: Test-1 correlation signature.
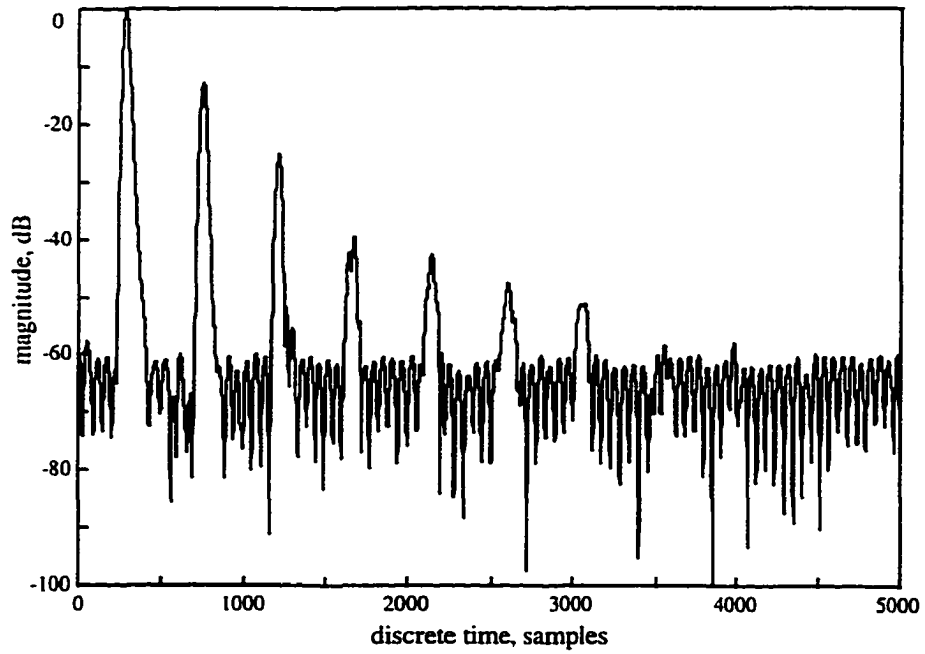
Figure 6.6: Test-2 correlation signature.
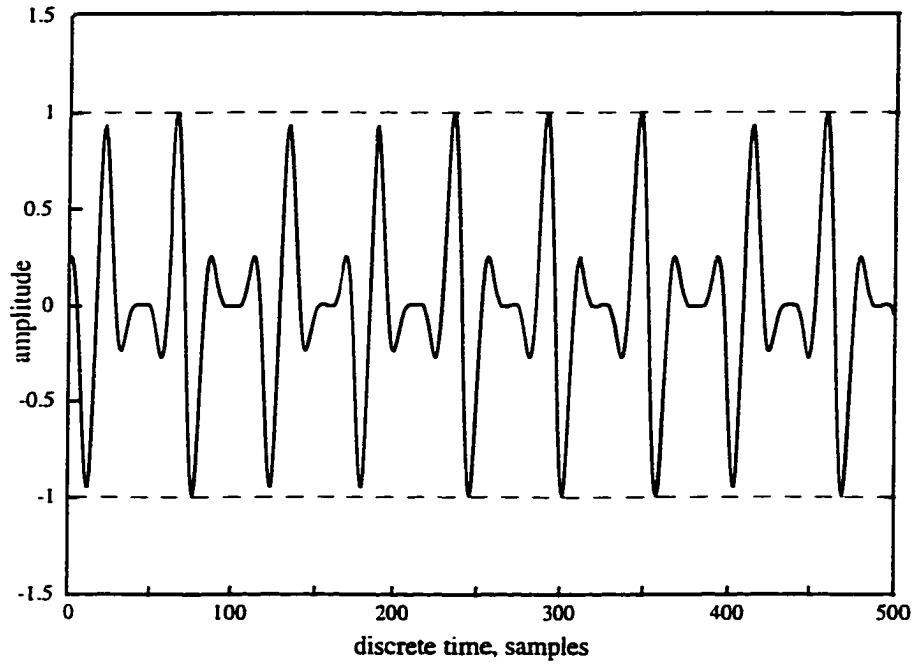
Figure 6.7: Excitation waveform for amplitude modulation approach.
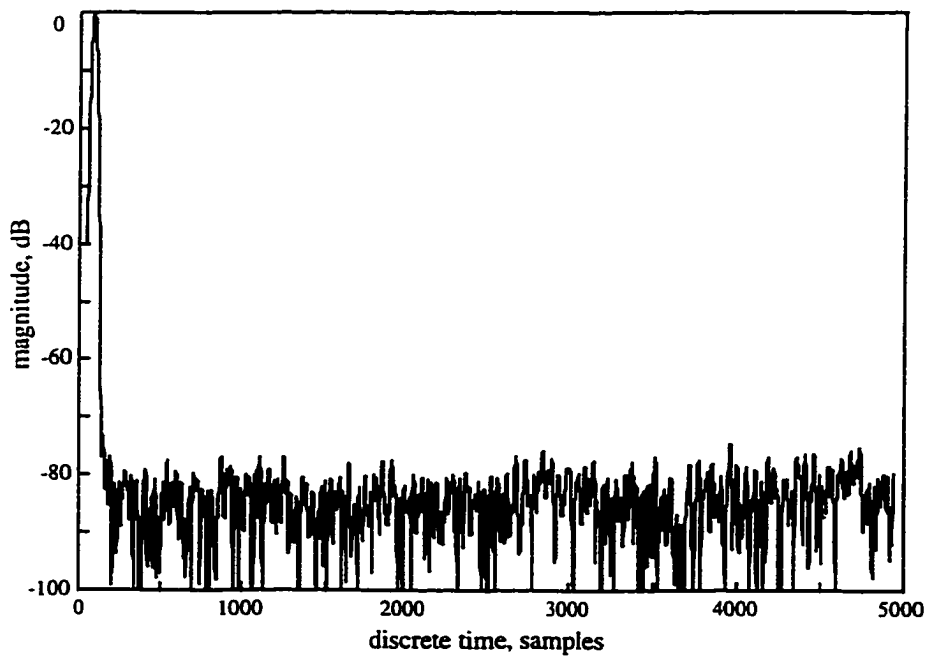
Figure 6.8: Test-1 correlation signature.
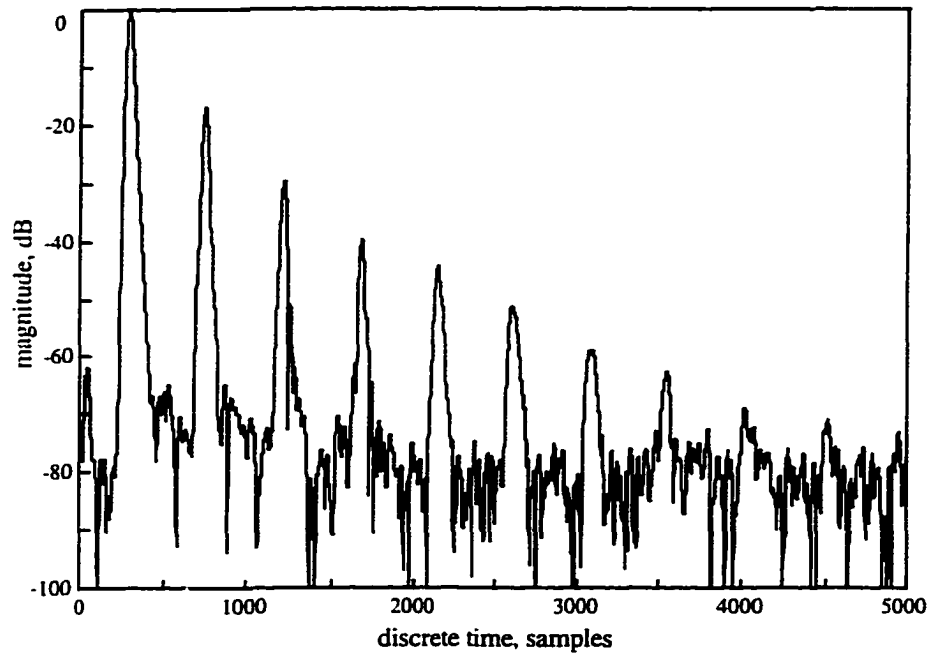
Figure 6.9: Test-2 correlation signature.
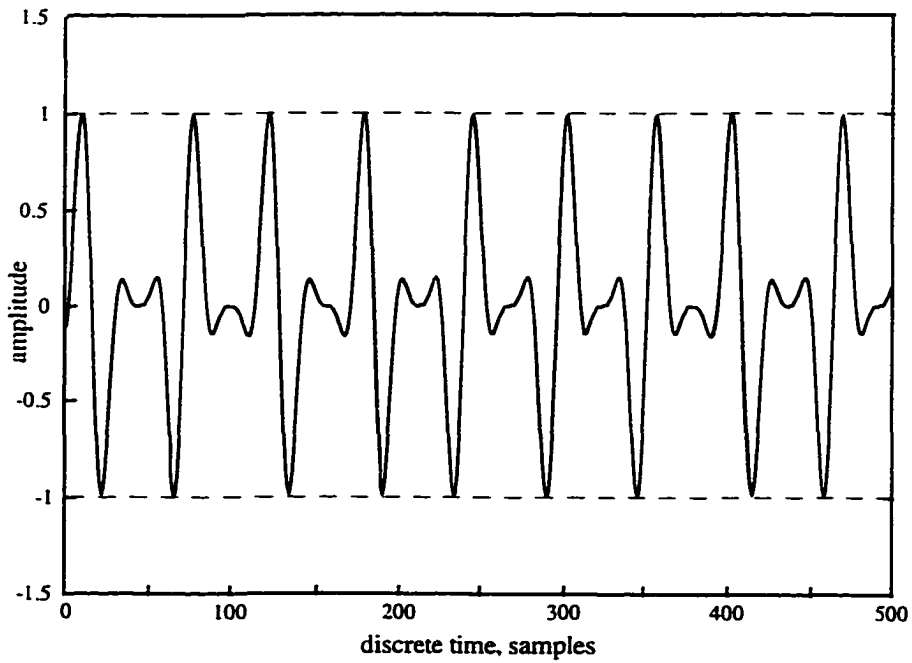
Figure 6.10: Excitation waveform for offset-phase modulation approach.
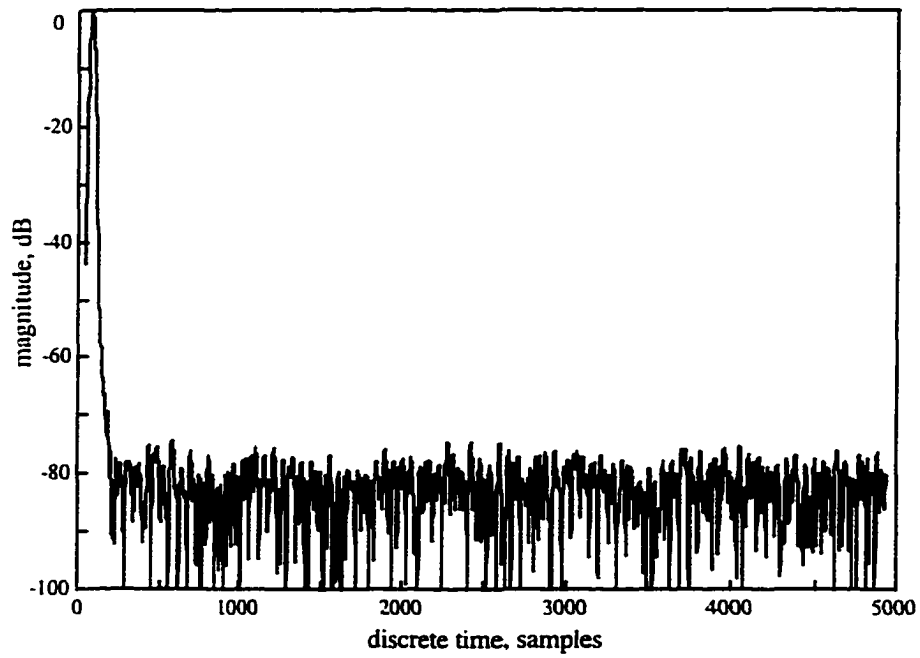
Figure 6.11: Test-1 correlation signature.
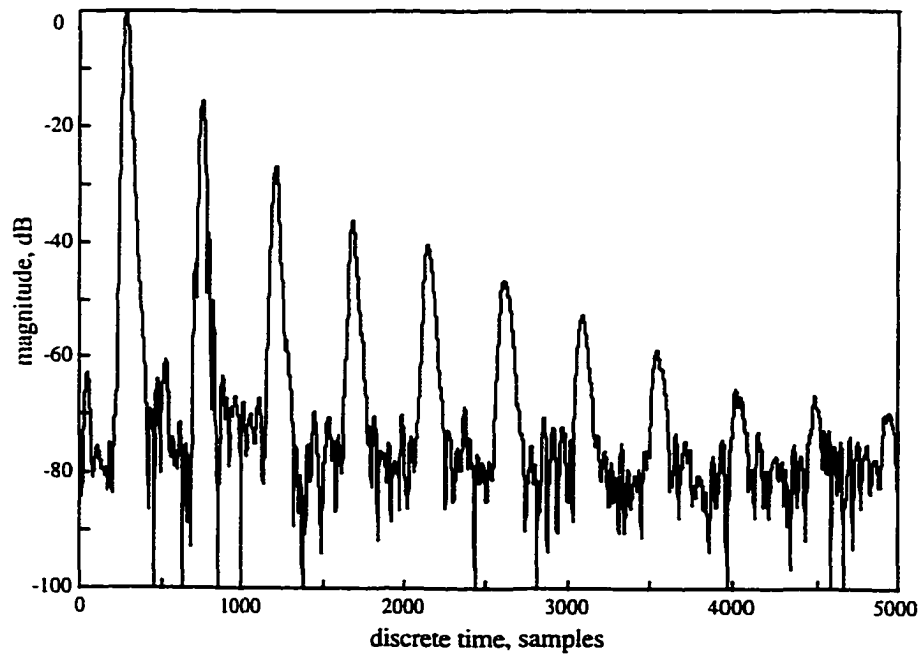
Figure 6.12: Test-2 correlation signature.
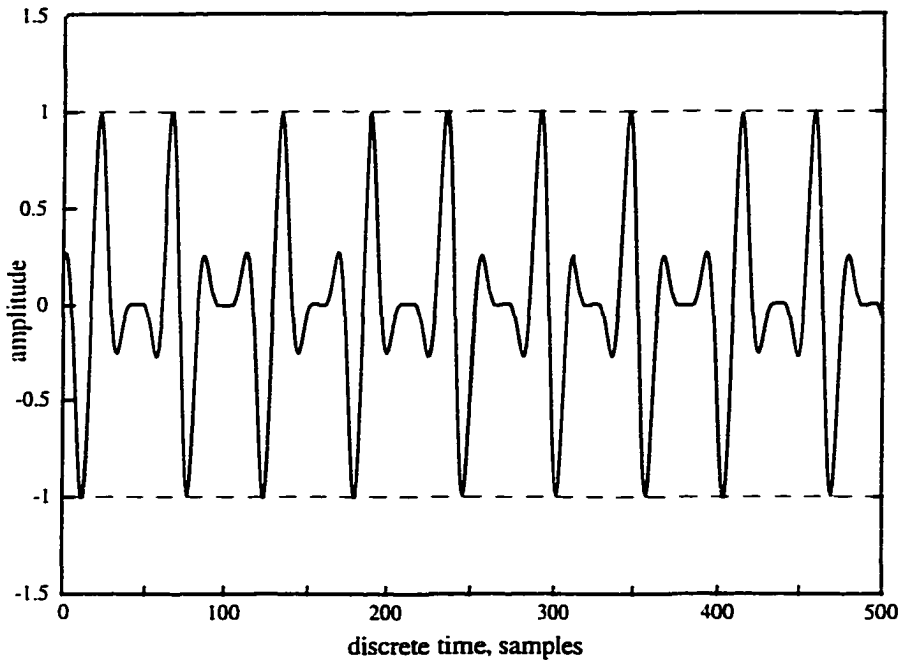
Figure 6.13: Excitation waveform for mismatched correlation filter approach.
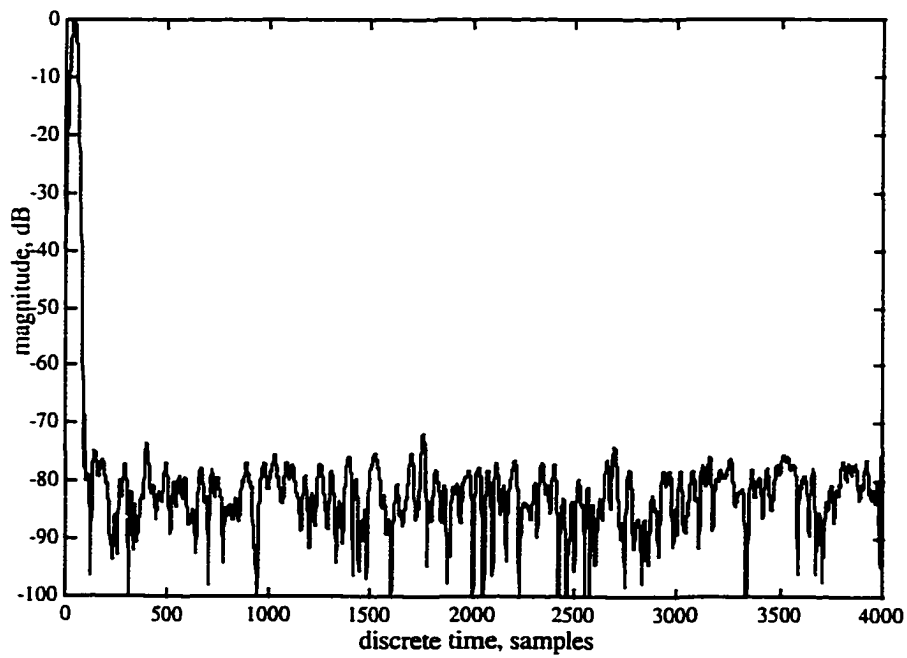
Figure 6.14: Test-1 correlation signature for mismatched filter approach.
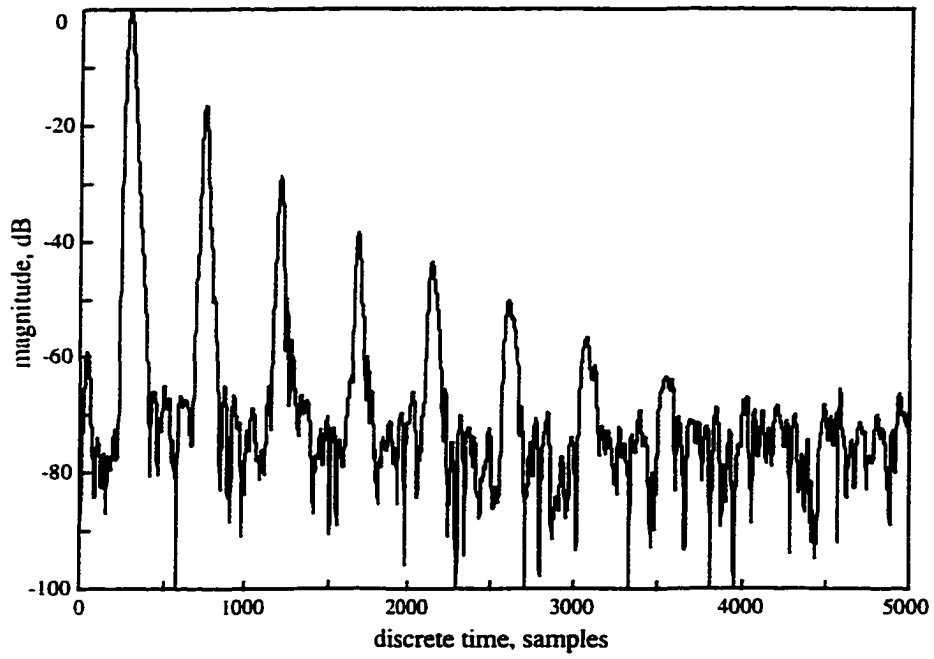
Figure 6.15: Test-2 correlation signature for mismatched filter approach.
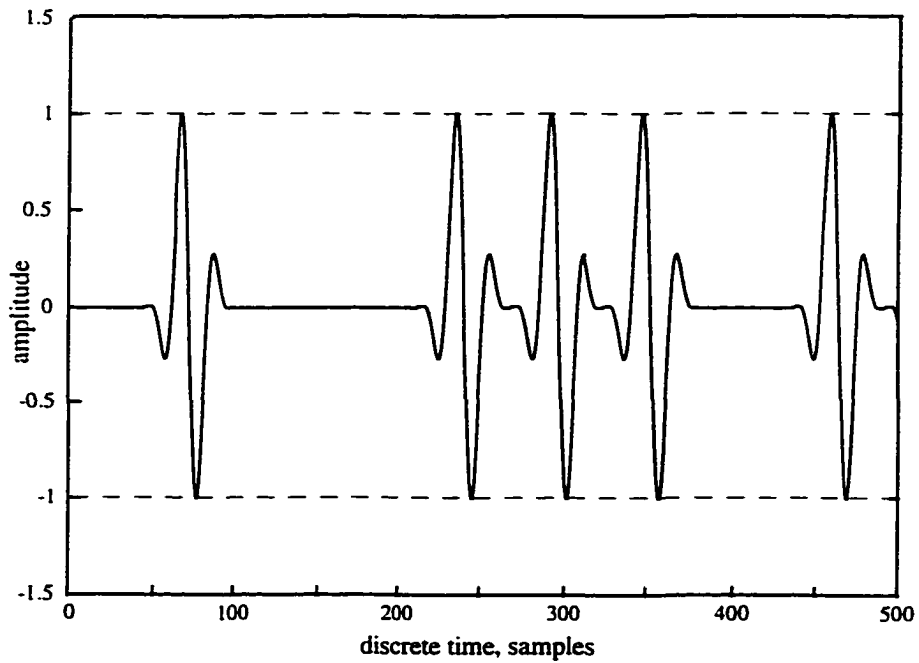
Figure 6.16: Excitation waveform for on-off modulation approach.
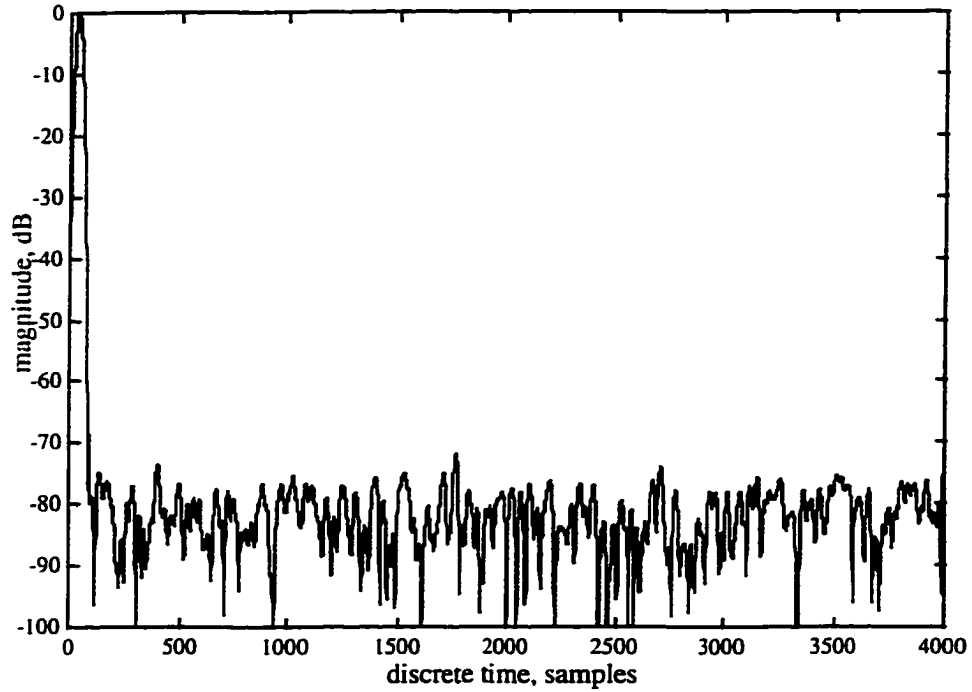
Figure 6.17: Test-1 correlation signature for on-off modulation approach.
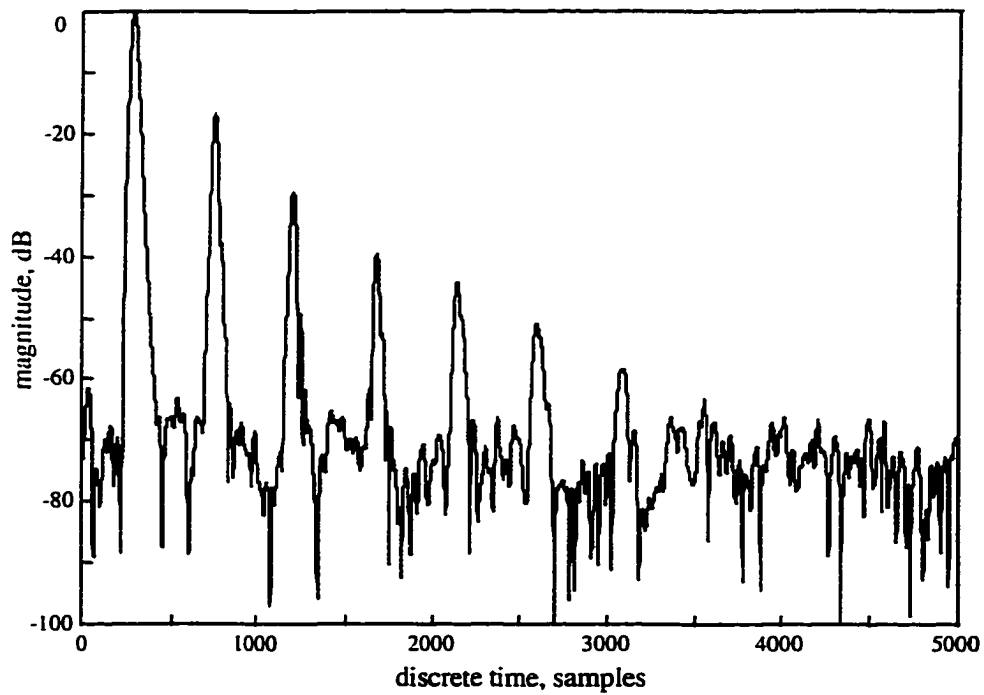
Figure 6.18: Test-2 correlation signature for on-off modulation approach.

approach, as the name implies, uses a waveform (Figure 6.16) that has zero amplitude corresponding to certain chips in the pseudorandom sequence.

6.3 Performance Analysis

The test results of five different approaches to the SSUE system design are presented above. It was observed that in case of the binary phase modulation approach, the dynamic range of the measured ultrasonic correlation signature was limited by the system self-noise level. Hence for a 10th order maximal-length sequence based system the dynamic range is -60 dB (Figure 6.5). As a consequence of self-noise only the first seven reflection components can be clearly detected in the correlation signature of Figure 6.6. In case of the amplitude modulation approach and the offset-phase modulation approach, the test results are very similar. Here, the theoretical and simulation results predict that there is no self-noise and the dynamic range of the correlation signature is determined by the system's random noise level. Thus for a 10th order maximal-length sequence based system, the dynamic range of about -80 dB was achieved (Figures 6.8 & 6.11). This is a 20 dB improvement over the binary phase modulation approach. As a consequence of this 20 dB improvement in the dynamic range, the correlation signatures corresponding to test-2 now clearly show at least ten reflection components (Figures 6.9 & 6.12).

The mismatched filter approach and the on-off keying approach produced almost similar results (Figures 6.14 & 6.17). The dynamic range of the correlation signature was about 6 dB smaller than those of Figures 6.8 & 6.11. This can be attributed to the 6 dB lower SNR gain factor of the mismatched filter. An equivalent effect was observed in the test-2 results (Figures 6.15 & 6.18).

It was, therefore, concluded that the amplitude modulated waveform approach and the offset-phase modulated approach represent the optimum SSUE designs. Even though the theory predicts that the amplitude modulated waveform approach has lower energy transmission efficiency, its effect in a practical system is unobserveable.

6.4 Noise Analysis

The output of the correlator in a SSUE system has been shown to be given by,

$$\phi_{sr}(\tau) = h(\tau) + N_s(\tau) + N_r(\tau) \qquad (6.1)$$

where, $N_s(\tau)$ is the self noise component and $N_r(\tau)$ is the random noise component of the measured correlation signature.

6.4.1 Analysis of Self Noise

Self noise is a result of non-ideal auto-correlation function, $\phi_{ss}(\tau)$, of the pseudorandom excitation signal. It is correlated with the input signal, s(t), and the impulse response, h(t). Magnitude of self noise depends on, (a) the period of the input signal, s(t), and, (b) the nature of h(t). If h(t) contains a strong component like a backwall reflection, the magnitude of $N_s(\tau)$ can be large enough to mask a weaker component of h(t). This fact is evident from the test results presented earlier (Figure 6.2.4). The self-noise is a result of nonideal PACF of the excitation waveform. In general, the self-noise is inversely proportional to the length of the pseudorandom sequence constituting the waveform. The exact level of self-noise depends on the type of sequence involved.

6.4.2 Analysis of Random Noise

Various sources of random noise are, (a) electrical noise, (b) acoustic noise, (c) EMI noise and, (d) quantization noise. All noise components can be assumed to be uncorrelated with each other as well as with h(t) and s(t). If the sum of all the random noise sources is represented by n(t), having a variance of unity, the variance of $N_r(\tau)$ will

be equal to the SNR gain factor and will depend on the period of the input signal, i.e., the extent of pulse compression.

It is interesting to note that the self-noise, $N_s(\tau)$, and the random noise, $N_r(\tau)$, components are uncorrelated to each other and hence the dynamic range of the measured correlation signature will be determined by the dominant component out of the two. Also,

$$N_s(\tau) \propto 1/L \tag{6.2}$$

and

$$N_r(\tau) \propto 1/\sqrt{L} \tag{6.3}$$

where L is the length of the maximal-length sequence. Hence, the self-noise level goes down faster than the random noise level with the increase of sequence (Figure 6.19). This result suggests two things, (a) if in a particular measurement situation, the random noise level is dominant, the basic BPSK system will perform as well as a system employing one
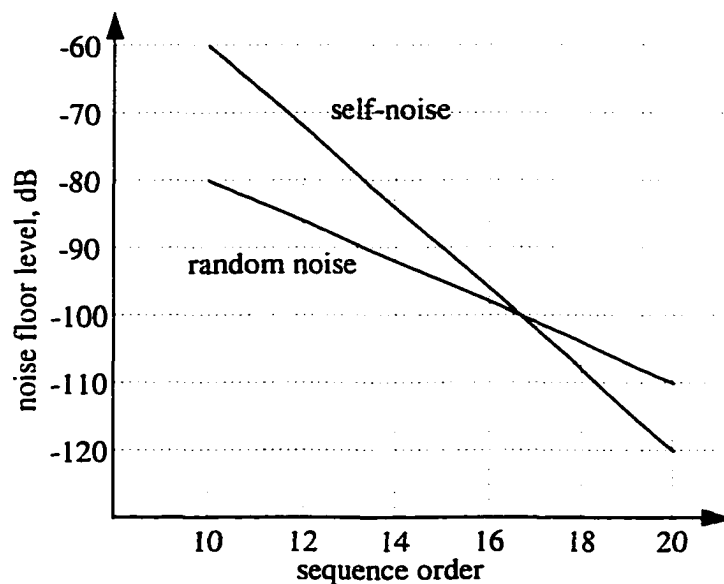
Figure 6.19: Effect of Sequence Length on Self-Noise and Random-Noise.

of the optimized approaches, and (b) one approach to solving the self-noise problem is to employ a longer sequence and thus an excitation waveform with longer period. Of course (b) is not a trivial thing to do as it involves greater system resources of storage capacity and processing power.

6.4.3 Quantization Noise Analysis

Quantization noise is associated with the process of digitizing the received analog signal at the front end of a digital receiver. Since the digitization process involves mapping of the analog amplitudes of a waveform to a certain finite number of discrete levels, it results into truncation or roundoff error. This error in the quantization process can be represented as an additive noise term in the signal expression, i.e.,

$$r[n]=r(t)+n_q(t) \tag{6.4}$$

where r[n] is the digitized representation of the analog received signal r(t) and $n_q(t)$ represents the quantization noise. In most practical situations certain assumptions can be made about the digitization process which make it possible to build a statistical model of the quantization noise. These assumptions are,

(a) quantization noise is uncorrelated with the quantized signal

(b) quantization noise is uncorrelated from one sample to another

The first assumption is always valid for the situations when the input signal to the digitizer has no synchronization with the digitizer clock. In case of SSUE, however, this is not true since the transmitter and the receiver are self synchronized by a common clock. The second condition that makes the assumption (a) valid is when the input signal has a random additive noise component that is uncorrelated with the signal itself. It is this second condition which is valid in case of the SSUE received signal, r(t). The expression for the received signal developed earlier is,

$$r(t)=s(t)*h(t)+n(t) \tag{6.5}$$

Here, n(t) is the additive random noise component that is a result of number of different phenomenon like acoustic noise, electronic noise, electromagnetic interference etc. In a way, n(t) acts like a dither signal that makes the quantization noise uncorrelated with the digitized signal. A natural consequence of the above discussion is the question that what minimum level of n(t) is required to validate the above assumption (a). The answer to this question was not rigorously pursued, however, it was found that as long as the amplitude of n(t) is comparable to the smallest quantization level of digitizer, assumption (a) remains valid. The second assumption (b) implies that the quantization noise is white. This assumption is strictly valid when the digitization is done near the Nicest rate. However, when the signal is greatly oversampled the consecutive samples start becoming correlated.

After establishing the validity of the above assumptions, the quantization noise, $n_q(t)$, can be modeled as a random process with uniform distribution function in the interval $-q/2$ to $+q/2$ [72], where q is the smallest quantization level of digitizer. The variance of $n_q(t)$ is given by,

$$\sigma_q^2 = \frac{q^2}{12} \qquad (6.6)$$

For an eight bit quantizer $q = 1/256$, which gives the variance of -59 dB. If the received BPSK signal is considered to completely fill the digitizer, it represents a signal energy of -6 dB and the signal-to-quantization noise ratio of the digitized received signal, $r[n]$, will then be 53 dB. For the excitation waveform based on a sequence of length L=1023, the SNR gain factor is 30 dB. Hence, the correlation signature will have a SNR_r of 83 dB. In a practical situation, the quantizer can not be completely filled and the digitizer perform slightly below their rated performance and hence a 3 to 6 dB of loss is expected.

Another aspect of change in the statistics of the quantization noise, as it is processed through the correlator is the change in distribution from uniform to an almost Gaussian. This is because the correlator adds multiple samples of an uncorrelated uniformly distributed process and applying the central limit theorem [73], the output of

the correlator can be modeled as a Gaussian random process. This means that the noise floor level in the correlation signature is governed by a $2\delta_q$ confidence interval.

6.4.4 Effect of Master Clock Instability

The correlation processing in SSUE technique is equivalent to the coherent averaging process. Hence the system performance is highly dependent on the stability of its master clock. Conversely, the instability of system clock results into considerable reduction of the effective SNR gain factor. The clock instability can be generally categorized as (a) frequency drift, and (b) clock jitter. The major difference between the two is that the clock jitter is a random uncertainty in the clock transition time which is uncorrelated from one pulse to another, while the frequency drift is the random drift in the clock frequency that results into a gradual change in the clock period.

Effect of Clock Jitter: Clock jitter effects the digitization process in the SSUE receiver. Its effect on the digitized waveform is very similar to the quantization error. We start the analysis by recognizing digitization as a two step process, involving,

(a)   time sampling of analog waveform

(b)   discretization of signal amplitude

The discretization of analog signal amplitude leads to the quantization noise that has been analyzed before. A random timing error (clock jitter) in the sampling of the analog waveform also results into an error term that can be regarded as noise. The random timing error can be modeled as a Gaussian process with sampling time as the random variable. This can be transformed into a random amplitude variable in the digitized waveform assuming a linear transformation (Figure 6.20). Thus the sampling error will result into a Gaussian noise in the digitized received signal and eventually as a Gaussian noise term in the correlation signature. If the jitter noise is smaller than the quantization noise, its effect will be hardly noticeable, however, when jitter noise exceeds the quantization noise, its effect on the correlation signature will be the reduction of effective

quantizer size. Thus the effect of quantizer size and the stability of sampling clock on the correlation signature are inter-related and an increase in quantizer size also requires an improved sampling clock stability.

Effect of Clock Frequency Drift: The clock frequency drift effects the digitization process of the analog received signal, r(t). It is characterized as a random drift in the clock frequency that results into a gradual change in the sampling clock period. The drift is usually so slow that the sampling frequency can be considered constant during one measurement. The effect of frequency drift becomes prominent when two identical
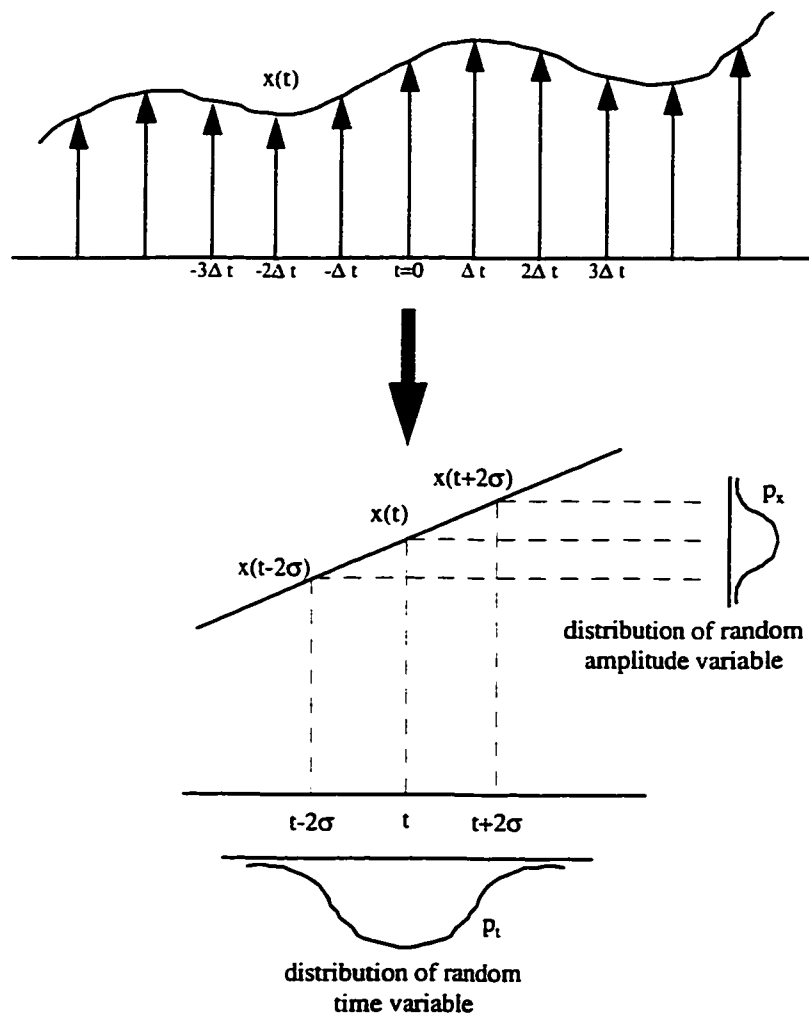
Figure 6.20: Transformation of sampling clock jitter to a random noise component.

measurements are made with a time gap of several hours or a day. Frequency drift can be due to poor temperature compensation, voltage variation, or ageing. Following calculations are based on some typical numbers and provide a rough idea about the extent of clock drift problem in SSUE.

Sampling clock frequency = 100 MHz

Sampling clock period   = 10 ns

Specified clock drift rating = 1 ppm / day

# of samples per period of correlation signature = 100,000

True sampling frequency on day-1 (f_1) = 100,000,000 Hz

True sampling frequency on day-2 (f_2) = 100,000,100 Hz

True length of correlation signature-1 = 100,000 / f_1

True length of correlation signature-2 = 100,000 / f_2

Difference of lengths of two signatures = 1 ns

Percent error in sampling period = 10%

Thus, if we compare two digitized correlation signatures sample by sample, the last few samples will have a sampling error of the order of 1 ns, which is about 10% for the sampling period of 10 ns.

Two things can be deduced out of the above calculations. First, the longer the period of excitation waveform, the larger the effect of frequency drift will be. Second, a direct comparison of the correlation signatures taken at different times is not the best way of detecting an acoustic change in the test sample.

6.5 System Limitations

In theory, SSUE technique is capable of providing arbitrarily high sensitivity of the measured ultrasonic correlation signature and it can be made interference tolerant to any

extant. However, in practice there is a limit beyond which the performance improvement becomes exceedingly difficult. This section discusses the technological limitations of SSUE system.

6.5.1 Separate Transmit and Receive Transducers

While the traditional pulse-echo ultrasonic technique typically uses a single transmitting and receiving transducer by time-sharing the transducer between the transmitter and the receiver, the SSUE technique can not do so. A time or frequency sharing of transducer in case of SSUE is not possible because the transmitter is continuously transmitting a periodic pseudorandom waveform and also the transmit and the receive waveforms occupy the same frequency spectrum. This, however, should not be regarded as a serious limitation of SSUE technique because of two reasons. Firstly, there are many ultrasonic NDE applications that require the transmit and the receive transducers to be separated by some distance or located at some angle with respect to each other, as is the case in pitch-catch measurements. Secondly, in present times the ultrasonic transducer manufacturing technology has significantly developed and it is feasible to manufacture two completely independent transducers in a single casing.

6.5.2 Bandwidth Limitation of Ultrasonic Transducers

The SSUE system features an excitation waveform with large time-bandwidth product. Unfortunately there is not much flexibility in terms of achievable system bandwidth, as that is limited by the bandlimited characteristics of the ultrasonic transducers. Hence, in order to increase the time-bandwidth product, only the time is a controllable variable, which means employing the excitation waveforms with longer period. The bandlimited characteristics of ultrasonic transducers may not be as serious a

limitation as it appears to be. This is because many engineering materials exhibit frequency selective acoustic characteristics and their nondestructive evaluation is often restricted to a certain band of frequencies. Thus it is very important to make an appropriate choice of transducer operating frequencies in order to match them to the characteristics of the test material.

6.5.3 Average Power Limitation of Ultrasonic Transducers

The ultrasonic transducers currently being used with the SSUE system are designed basically for pulsed mode of operation. Their construction is primarily based on the peak power limitation of the piezoelectric crystal. Hence their design is not optimized for the continuous mode of operation which requires heat dissipation considerations. As a result of this, the current operation of SSUE technique can not make full use of the available peak power capacity of the transducers. The transducers currently being used are peak power limited to about 300 volts, while for SSUE application they are only derived at a maximum peak-to-peak signal amplitude of 15 volts because of the average power dissipation considerations.

6.5.4 Impulse Response Fold-over

The governing equations of SSUE technique as developed in chapter 3 are based on the assumption that the system impulse response, $h(t)$, is time limited between ($0 < t < T_o$) and T_o is less than the period of the pseudorandom excitation waveform, T_p. If this condition is violated in a practical application, the phenomenon of impulse response fold-over will occur and there is no easy way to unfold the measured correlation signature to get a true impulse response estimate. Hence, there is a need to exercise extreme care in applying SSUE technique to various test materials. Certain real life materials like aluminum have very small attenuation coefficients and hence their acoustic impulse response can have significantly large time duration before its amplitude drops to an almost

zero level. A particularly unique and interesting material often used for the calibration and testing of ultrasonic NDE instruments is silica (fused quartz). It offers almost negligible attenuation to acoustic signal. When SSUE technique was applied to interrogate a block of silica in the lab, without considering its impulse response duration, the measured correlation signature had multiple fold-overs in it and made no sense at all.

6.5.5 Radiative Coupling Between the Transmitter and Receiver

Ultrasonic transducers can be modeled as a capacitor connected at the end of a coaxial transmission line. Thus at high operating frequencies they act like an antenna. When the two transducers are placed close to one another the signal is radiatively coupled to the receiver. This results into a small signal component at almost zero lag value in the correlation signature. It was found through practical experience that certain types of transducers are better than others in terms of radiative shielding. For the pair of transducers used in the experimental tests of section 6.2, the radiative coupling effect is seen as a signal component close to zero lag with a peak amplitude of about -60 dB. While a small component of radiatively coupled signal is harmless as it can be easily identified due to its near zero lag characteristics, and separated out. It can be a problem when this undesirable signal component grows stronger than the true acoustic signal components, as the digitizer is then filled by the stronger unwanted signal component and the weak desired signal can not be digitized with sufficient resolution. Hence, while selecting a pair of ultrasonic transducers, its radiative shielding characteristics must be kept into consideration.

6.6 Efficient Correlator Design

In the SSUE system, the correlator is the most computation intensive part of the overall system. The maximum size of the pseudorandom sequence that can be practically used is determined by two factors,

(a)   memory size of the waveform generator, digitizer,

and RAM in the PC

(b)   correlation processing speed

The first factor is a hardware limitation and is directly associated with the equipment cost.

However, the second factor is not purely cost dependent. The time required for the

correlation processing depends on, (a) computational load of correlation processing

algorithm, and (b) computer throughput. This means that the implementation of a

correlation filter can be investigated in an attempt to reduce the computational load. This

section presents various algorithms for implementing a periodic correlator and compares

the computational load associated with each of the algorithms along with their limitations.

6.6.1 Digital Correlator Implementation

The earlier correlators were of analog type and their performance was relatively

poor [74]. The present state-of-the-art correlators are DSP-based, with much improved

performance. However, the process is still computation intensive and requires costly

computational resources. Two main techniques exist for the implementation of a digital

correlator. These are:

a)   Time-domain delay-multiply-add correlator (Figure 6.21)

b)   Frequency-domain FFT based correlator (Figure 6.22)

While the time-domain approach is simple and straight forward, it performs poorer

in terms of computational efficiency. However, there is a positive aspect of this approach

also. Sometimes it is only a certain range of lag values for which the correlation results

are of interest. For example, in case of the application of the SSUE technique for flaw

detection, the portion of ultrasonic correlation signature after the first backwall reflection

is not of much interest as a flaw signature is expected to show up before the first

backwall component of the signature. For these kinds of applications, the time-domain

approach of correlator implementation can turn out to be the best choice.
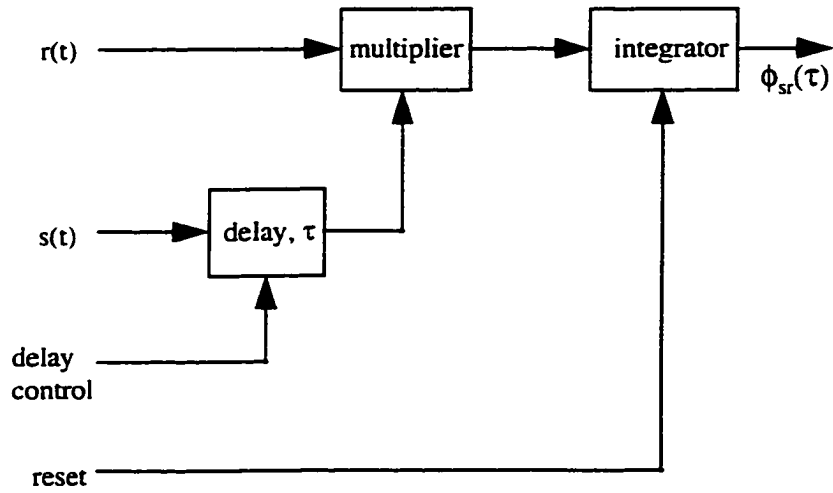
Figure 6.21: Basic correlator block diagram.
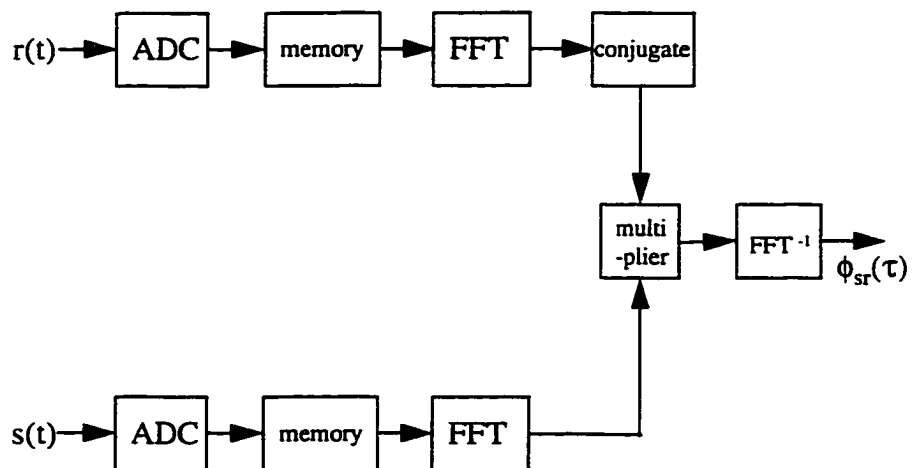
Figure 6.22: FFT-based correlator block diagram.

The frequency-domain approach is comparatively fast and efficient, though perhaps still not the optimum. This approach of correlator implementation is based on the relation between the convolution and the correlation functions, as discussed under section 2.1. In this approach, fast fourier transform (FFT) algorithm is used to determine the frequency spectra of the pseudorandom excitation waveform, $S(f)$, and the received waveform, $R(f)$. The complex multiplication of $R(f)$ with the complex conjugate of $S(f)$, gives the spectrum of periodic crosscorrelation function, $\Phi_{sr}(f)$. An invers fourier transform (IFFT) of $\Phi_{sr}(f)$ gives the desired correlation function, $\phi_{sr}(\tau)$. This approach computes the complete periodic crosscorrelation function all at once and does not provide any control over the partial evaluation of the desired correlation function.

6.6.2 New Computationally Efficient Correlator

A new method of DSP-based correlator implementation was investigated [75]. This method exploits the structural characteristics of a pseudo-random waveform based on the maximal-length sequence. The method can be applied for baseband or bandpass waveforms, and it can handle a wide range of modulation schemes and signalling structures. The new method eliminates various kinds of redundancies in the basic correlation process. The correlation operation is broken into pieces and transformed into a form where the benefits of fast Hadamard transform (FHT) are utilized [76]. The resulting data is regrouped and transformed back to the standard form (Figure 6.23). This method performs most of the mathematical operations in the fixed point arithmetic format, thereby saving lot of storage space and processing time.

6.6.3 Performance Comparison

If L is the length of the maximal-length sequence that constitutes the pseudorandom excitation waveform and there are N samples per symbol, one period of the waveform will consist of NL samples. Hence, the basic time-domain correlator will
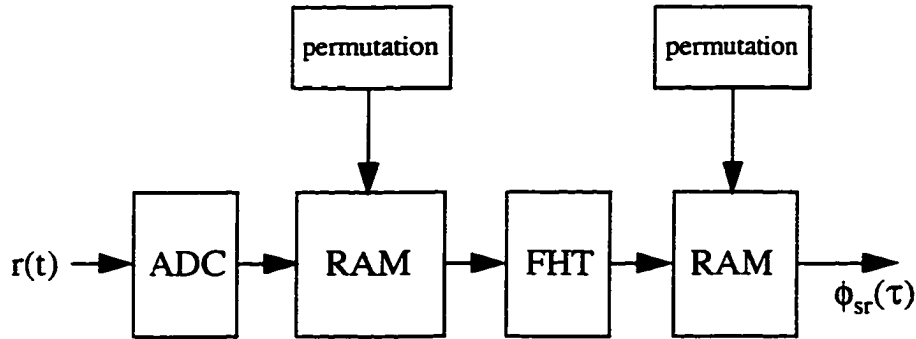
Figure 6.23: Proposed correlator block diagram.

require NL real multiplications and NL real additions, in order to calculate one correlation value. Second is the FFT-based approach, which requires, a) one FFT of length NL, b) one IFFT of length NL, and c) NL complex multiplications. These numbers, however, correspond to all the NL correlation values. Assuming that,

    a)   one FFT requires $NL\ log_2(NL)$ complex multiplications and about the same number of complex additions,

    b)   one IFFT requires $NL\ log_2(NL)$ complex multiplications and about the same number of complex additions,

    c)   one complex multiplication requires four real multiplications and two real additions,

    d)   one complex addition requires two real additions.

This gives us the average of x real multiplications and y real additions for each correlation value.

The proposed approach, on the average requires only N real multiplications and N $log_2(L)$ real additions for each correlation value. In general, L is much larger compared to N and therefore, the new approach is mostly dominated by additions. Table 6.1 compares

the computational requirements of the proposed approach with the existing approaches, taking L=1,000 and N=10.

Table 6.1: Processing requirement per correlation value.

Correlator Type	# of real multiplications	# of real additions
1. Basic time-domain	10,000	10,000
2. FFT-based	110	108
3. Proposed approach	10	100

CHAPTER 7   SIGNATURE PROCESSING TECHNIQUES

This chapter develops various signal processing techniques that can be applied to the ultrasonic correlation signature for the purpose of extracting useful information regarding various structural and material characteristics of the test specimen.

7.1 Deconvolution of Measurement System Effects

In the SSUE the measured ultrasonic correlation signature, $\phi_{sr}(\tau)$, represents an estimate of the composite system impulse response, $h(t)$, which can be represented as the convolution of the test sample impulse response, $h_o(t)$, and the measurement system impulse response, $h_s(t)$, as shown in Figure 7.1. This can be written as,

$$h(t) = h_s(t) * h_o(t) \qquad (7.1)$$

The measurement system impulse response, $h_s(t)$, is the undesirable part of the correlation signature. It contains the effect of various system components like the transmitting and the receiving transducers and the associated electronics. While it is possible to eliminate the adverse effects of electronic circuits by ensuring highly linear amplifiers with wideband response, the ultrasonic transducers represent a "bottleneck". Firstly their response is bandlimited and secondly they show dispersive behavior, both in terms of magnitude and phase.

Ideally, it is desired to have $h_s(t)$ to be a delta function with some deterministic time delay t_s, i.e.,

$$h_s(t) = \delta(t - t_s) \qquad (7.2)$$
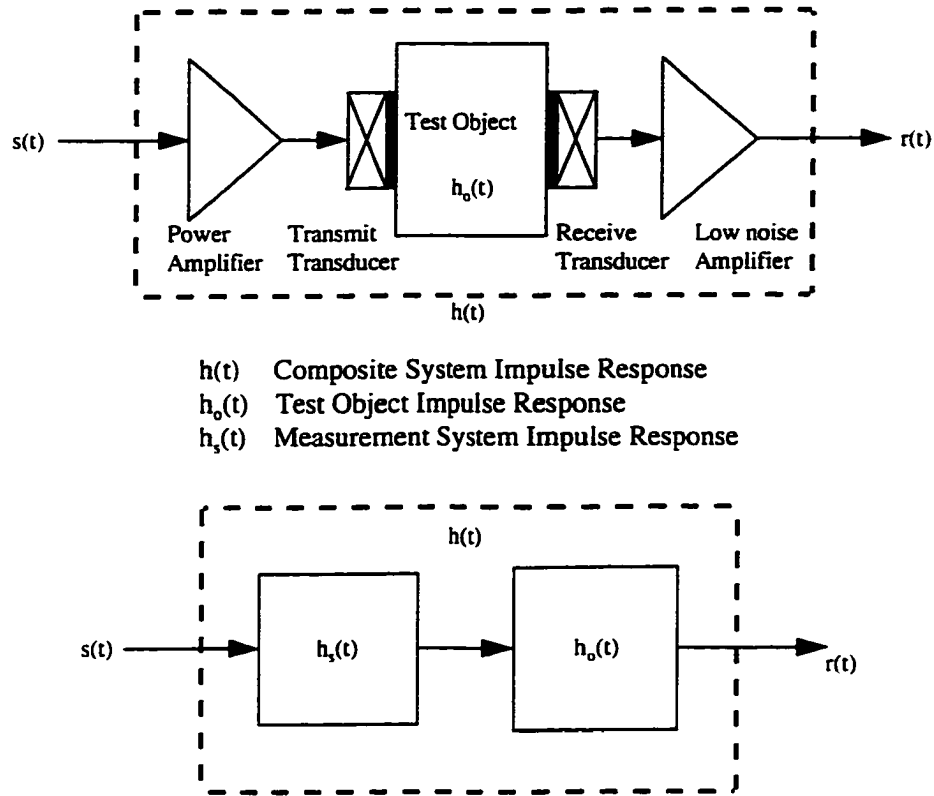
Figure 7.1: Impulse response model of ultrasonic NDE system.

where t_s represents the measurement system propagation delay. In such case, the ultrasonic correlation signature can be written as,

$$\phi_{sr}(\tau) = h_0(\tau - t_s) \qquad (7.3)$$

Since the ultrasonic correlation signature now represents the test object impulse response having a deterministic time shift t_s, all the necessary information is preserved in the signature. In particular, the resolution and the relative positions of various signal

components are preserved. However, in reality, $h_s(t)$ gives both the magnitude and phase distortions. It is therefore important to eliminate the effects of the measuring system response from the ultrasonic correlation signature through a signal processing process generally referred as deconvolution. There are two important factors which indicate the significance of deconvolution processing of the measured ultrasonic correlation signature. These are, (a) resolution enhancement, and (b) system independence.

As a result of magnitude and phase distortions of the transmitting and receiving transducers, the correlation peaks in the ultrasonic correlation signature become broader, thus lowering the resolution. Figure 7.2 compares the loss of resolution in the correlation signature as a result of non-ideal $h_s(t)$. If the ultrasonic correlation signature can be

(a) ideal correlation signature

(b) practical correlation signature
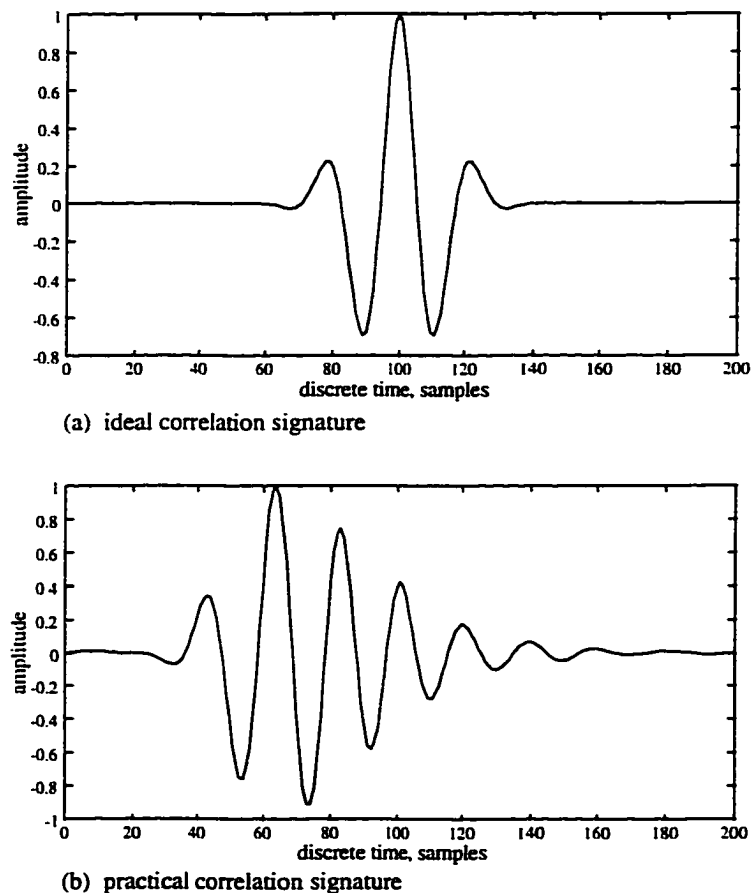
Figure 7.2: Comparison of ideal and practical system correlation signatures.

processed to eliminate the undesired distortion effects, its resolution can be significantly improved.

Since the unprocessed ultrasonic correlation signature includes the effect of the measurement system impulse response, its measurement can produce different results with different instruments and at different time. By applying the deconvolution processing, the ultrasonic correlation signature can become independent of the system characteristics, particularly of transducers. Transducers indicate significant variations from unit-to-unit and also long-term variations due to aging.

7.1.1 Deconvolution Technique

The above mentioned deconvolution problem falls under the general category of deterministic deconvolution, which assumes that a reasonably good estimate of the undesired impulse response component, $h_s(t)$ in this case, is available. Deterministic deconvolution can be considered as a two step process that includes, (a) estimation of $h_s(t)$, and (b) implementation of inverse filter. The estimation of $h_s(t)$ is a crucial step, as if a fairly accurate estimate can be made, the second step of inverse filter implementation becomes relatively simple and straight forward. However, if the estimate is inaccurate or if it has poor SNR, the stability of the inverse filter becomes an important design consideration. Also, in that case, the deconvolution filter, if not well designed can further degrade the quality of measured ultrasonic correlation signature.

Literature survey of a similar type of deconvolution processing for pulsed ultrasonic systems indicate two different methods of estimation of $h_s(t)$ [77, 78]. One method uses the backwall reflection from a block of fused silica as an estimate of $h_s(t)$. Since fused silica is considered nearly ideal propagation medium for ultrasound and the reflection of ultrasound from a smooth, polished parallel surface can be assumed perfect, the backwall reflection serves as a good estimate of $h_s(t)$. The other method is based on the estimation of $h_s(t)$ from a known good sample, or from the known good portion of test sample, in case scanning of large area is involved. In certain applications a well isolated

backwall reflection can also provide a good estimate of $h_s(t)$.

7.1.2 Inverse Filter Implementation

A deconvolution filter can either be implemented as a post-correlation filter (Figure 7.3) or as a pre-distortion filter (Figure 7.4). Each implementation has certain characteristic features. The post-correlation filter implementation is simple in the sense that the ultrasonic excitation waveform and the correlation processing remains unaffected. The drawback, however, is that the input to the deconvolution filter has a noise component, which results into the amplification of certain frequencies of the noise thus degrading the SNR. A pre-distortion filter approach is considered superior as it produces optimum SNR for all frequencies of the deconvolved signal spectrum. Also, the implementation of pre-distortion filter is relatively efficient. A pre-distortion filter can be incorporated as a part of the excitation waveform generation process. Once the pre-distorted waveform has been digitally generated, no additional processing is required during multiple correlation signature acquisitions. In case of post-correlation processing, however, each measured correlation signature has to be independently processed through
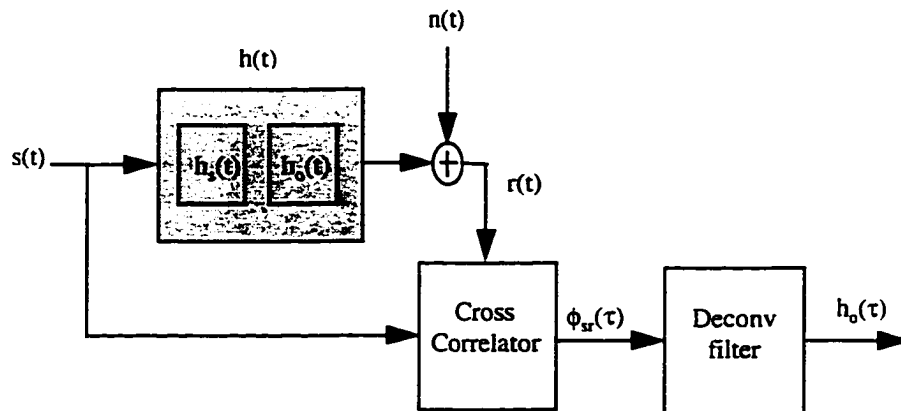
Figure 7.3: Post-correlation filter implementation.
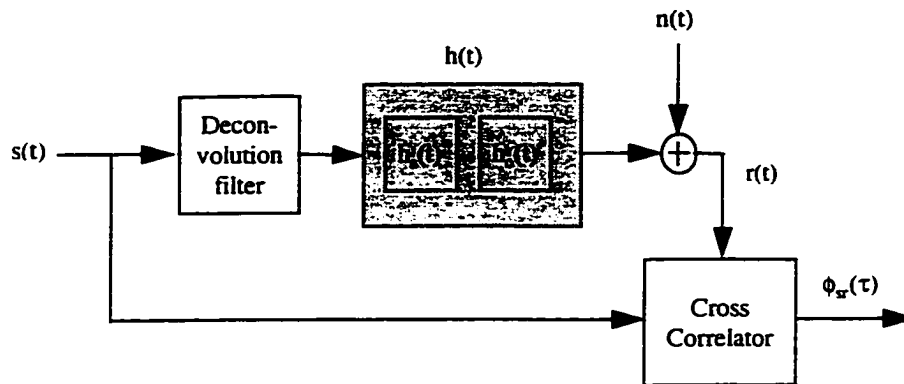
Figure 7.4: Predistortion filter implementation.

the deconvolution filter. Typically, the transducer spectrum is not uniform in the pass-band. Hence, the SNR is not constant over all frequencies. The SNR is relatively poor at the bandedges. A disadvantage of the pre-distortion filter in case of the SSUE system is that it takes away the control over the transmit signal peak amplitude characteristics and the excitation waveform no longer can maintain a constant amplitude thus reducing the transmission efficiency.

7.1.3 Filter Implementation Results

The results of a post-correlation filter implementation are presented. First, the measurement system impulse response, $h_s(t)$, was measured. It is shown in Figure 7.5. The magnitude and phase spectra of this measured impulse response were calculated and is shown in Figures 7.6 and 7.7. It can be seen from these figures that the measurement system exhibits both the magnitude and phase distortions. An inverse filter was developed in frequency domain whose magnitude spectrum is shown in Figure 7.8. Figures 7.9 & 7.10 show a correlation signature measurement with and without the deconvolution filter. The effectiveness of the filter in improving the resolution of the measurement can be
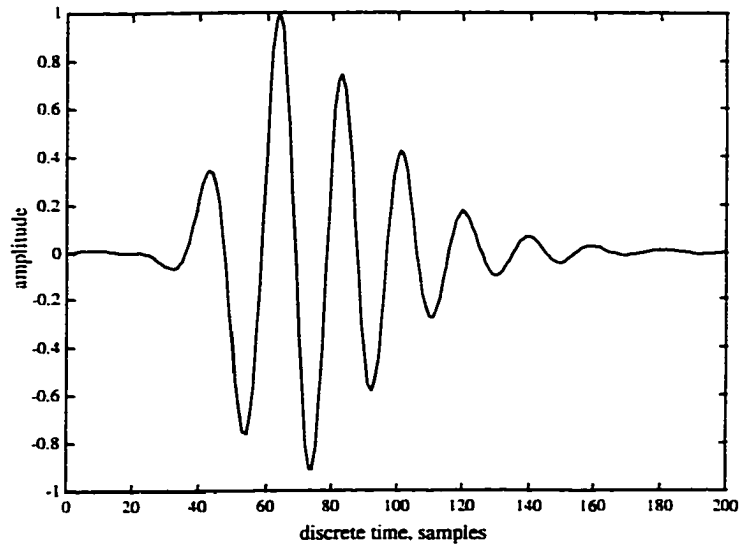
Figure 7.5: Estimated measurement system impulse response.
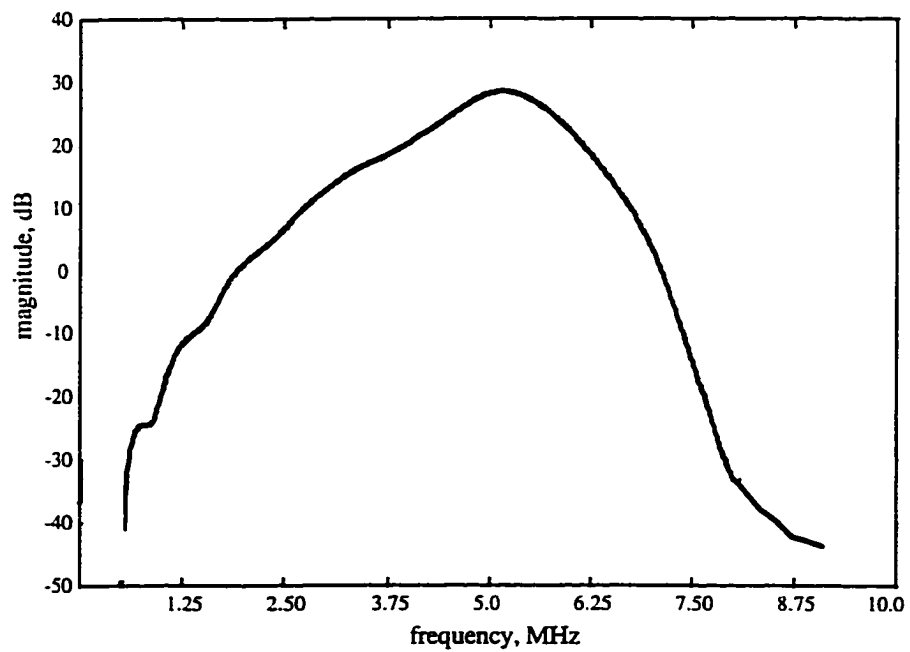
Figure 7.6: Magnitude spectrum of the measured impulse response.
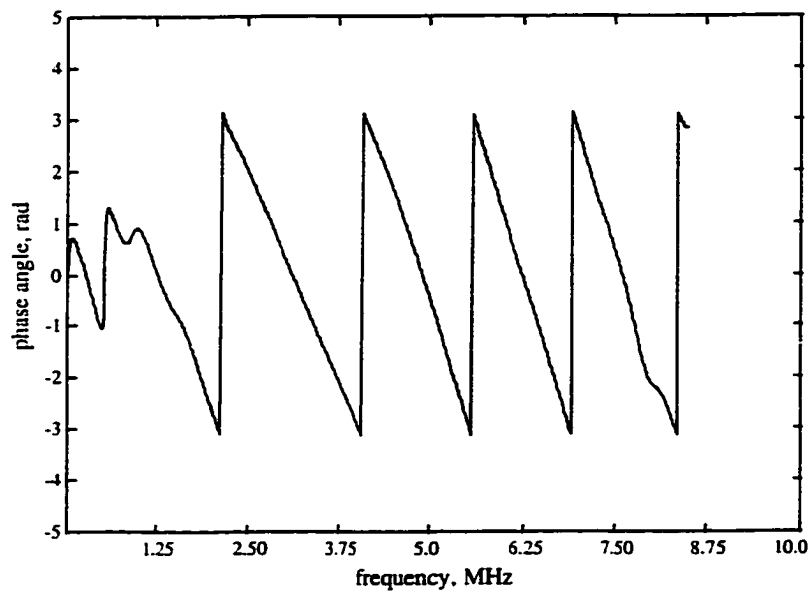
Figure 7.7: Phase spectrum of the measured impulse response.
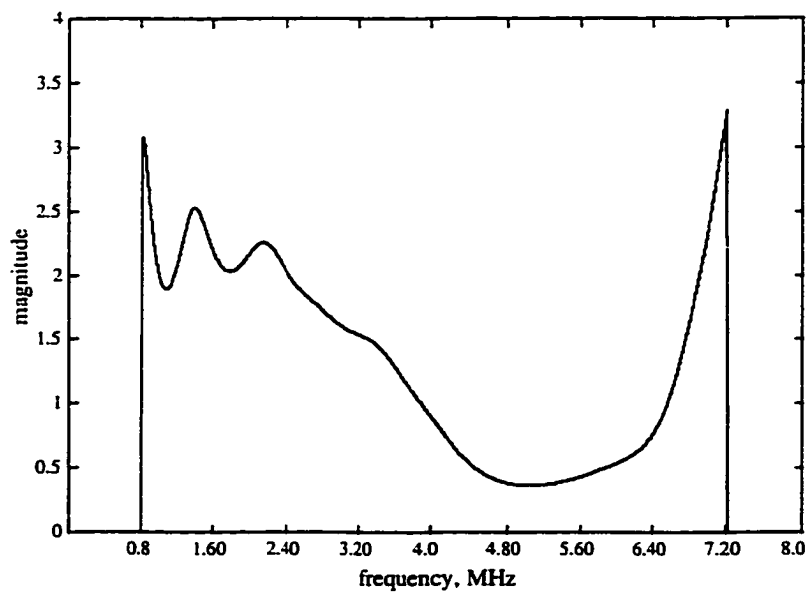
Figure 7.8: Magnitude spectrum of the inverse filter.

159
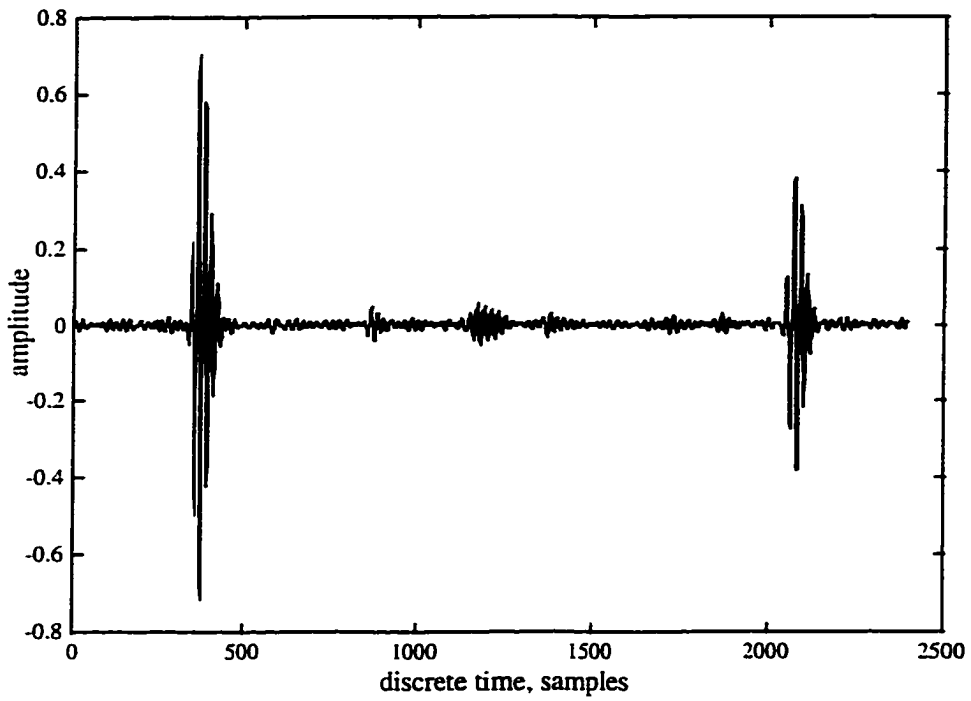
Figure 7.9: Correlation signature without deconvolution filter.
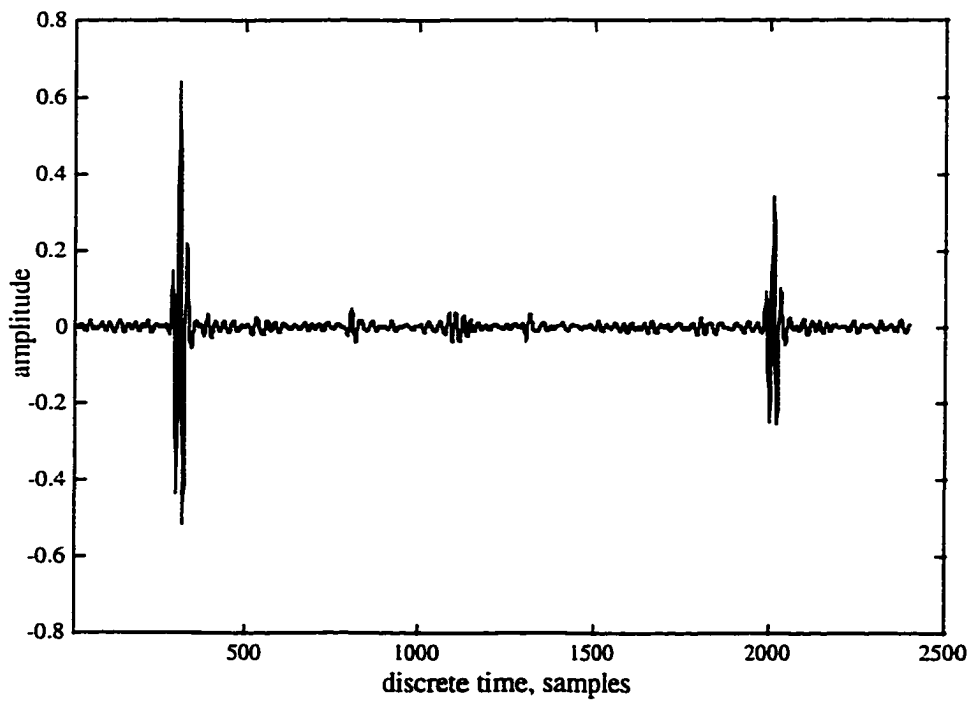
Figure 7.10: Correlation signature with deconvolution filter.

clearly observed by comparing various signature components of the two figures.

7.2   Ultrasonic Parameter Estimation

Ultrasonic nondestructive evaluation of structural and material properties of a test specimen is a three step process (Figure 7.11). First, an appropriate acoustic signature of the test specimen is obtained. Second, various acoustic parameters like, velocity, attenuation, absorption and scattering are determined from the measured acoustic signature. Finally, the measured values of these acoustic parameters are related to the structural and material properties of the test specimen.

This section first presents a brief theoretical treatment of various ultrasonic parameters, and then discusses the extraction of these parameters from the measured ultrasonic correlation signature using SSUE technique.

7.2.1   Ultrasonic Velocity Measurement

Ultrasonic velocity measurements are widely used to determine the properties and states of materials. In the case of engineering solids, measurements of ultrasonic wave

```
┌──────────────┐      ┌──────────────┐      ┌──────────────┐
│   Acoustic   │      │   Acoustic   │      │Characterization│
│  Signature   │ ───▶ │  Parameters  │ ───▶ │ of Test Object│
│ Measurement  │      │  Estimation  │      │(Classification)│
└──────────────┘      └──────────────┘      └──────────────┘
```
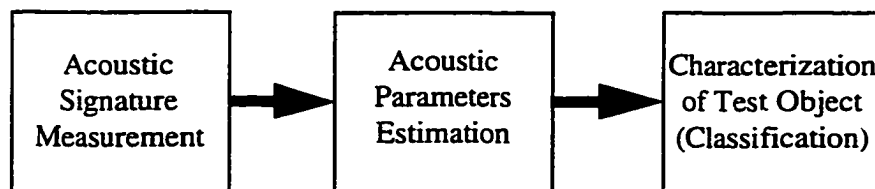
Figure 7.11:   Ultrasonic nondestructive evaluation conceptual model.

propagation velocities are routinely used to determine the elastic constants [79, 80].

Since the SSUE technique employs separate transmitting and receiving transducers, two different instrument configurations are possible for the measurement of correlation signature. Configuration-1 has the advantage that only one surface of the specimen is involved (Figure 7.12). However, it requires the second backwall reflection for velocity measurement, which, in case of attenuative material, might have very poor signal-to-noise ratio. Configuration-2 requires access to both the front and the back surface of the material (Figure 7.13), however, it performs velocity measurement from the through transmission signature component and the first reflection component and hence is superior in terms of accuracy of measurement.

Three methods of measuring the ultrasonic velocity from the correlation signature are considered. These are, (a) echo-overlap method, (b) phase-slope method, and (c) crosscorrelation method.
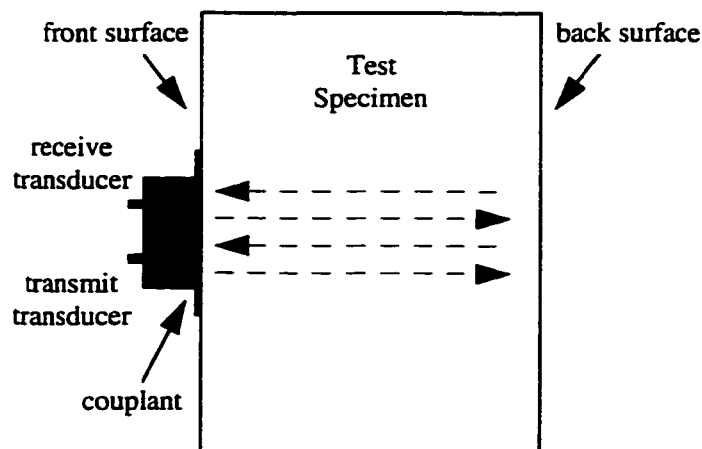
Figure 7.12: Instrument-specimen configuration-1 for velocity measurement.
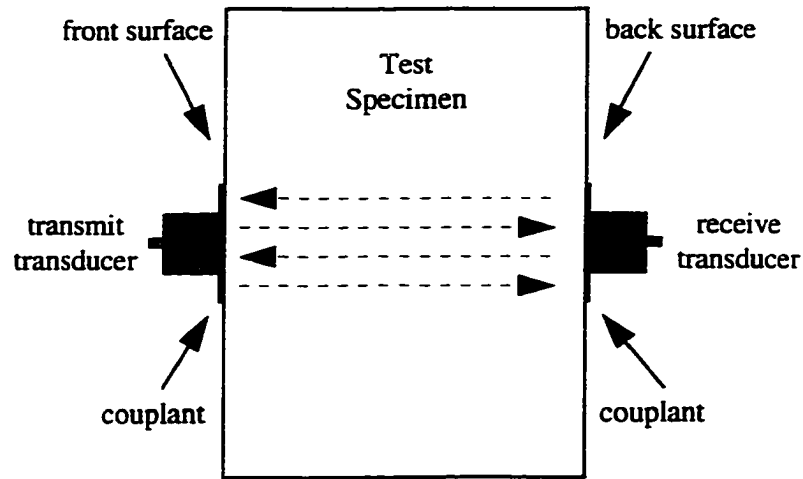
Figure 7.13: Instrument-specimen configuration-2 for velocity measurement.

Echo-overlap Method: This is the simplest of the three methods discussed. It involves the windowing of first signal component, R1, in the correlation signature (Figure 7.14) and sliding it over the second signal component, R2, in order to get an optimum match of the peaks and the zero crossings (Figure 7.15). The amplitude of the two echos will of course be different due to the attenuation effect of ultrasound. Figure 7.15 shows the result of overlapping the echos R1 and R2. The echo-overlap method depends on having a pair of echos, R1 and R2, that exhibit similar waveforms with corresponding features. This method performs poorly when the effects of wave distortions due to noise, dispersion, and other factors that operate on successive echoes are present. Dealing with these distortion effects is facilitated by employing the phase-slope or cross-correlation method.
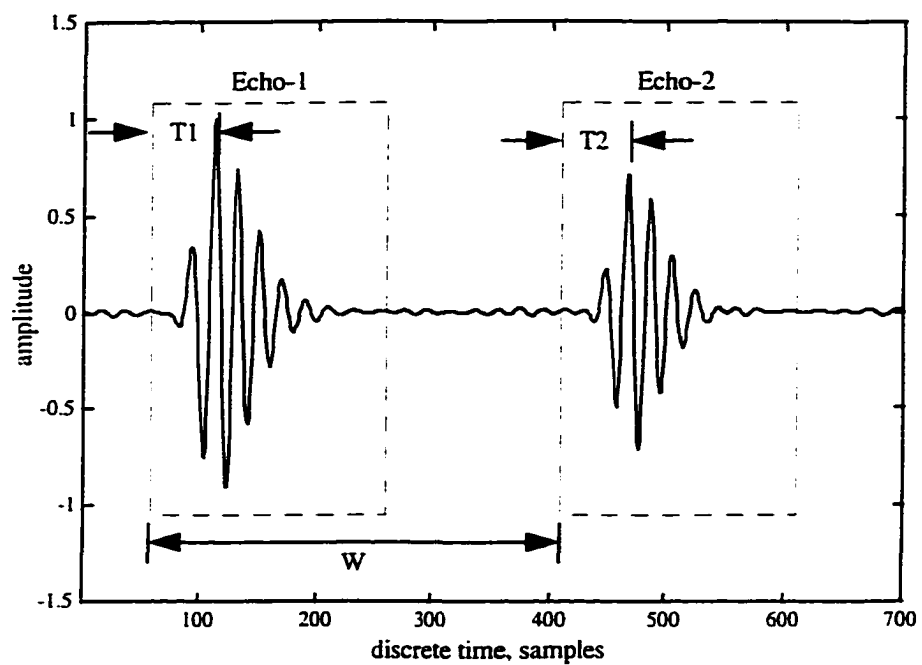
Figure 7.14: Correlation signature containing two successive signal components.
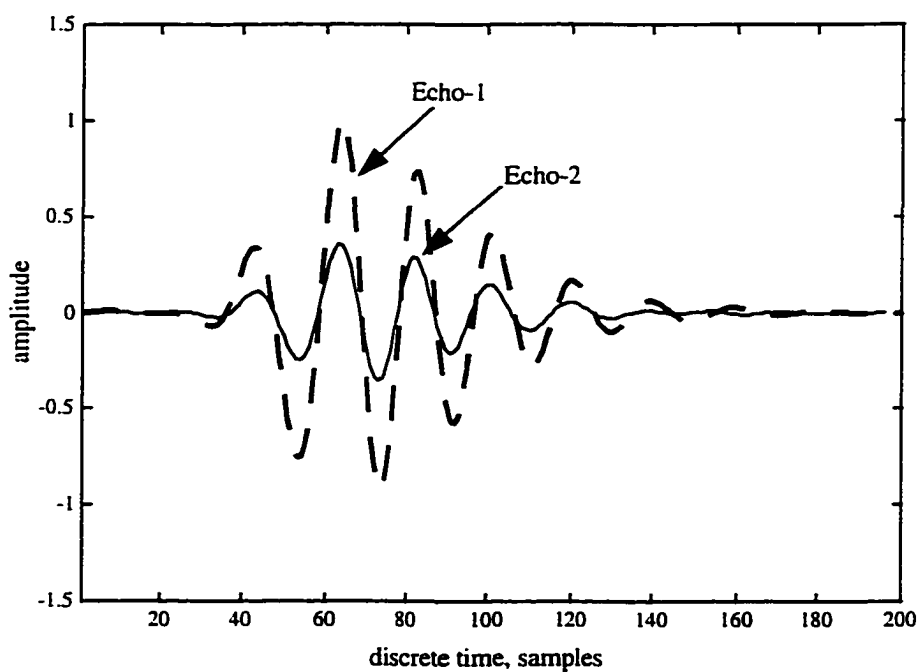
Figure 7.15: Echo overlap method of velocity/thickness measurement.

Phase-slope Method: With the phase-slope method, time between echos is found by the use of phase spectra of echo waveforms. After the echos are digitized, a Fourier transform of each is obtained by a discrete FFT algorithm. The amplitude and continuous phase spectra for a pair of typical echoes are illustrated in Figures 7.16.

After the Fourier transformation, both the amplitude and the phase spectra are used to define a central zone within the frequency domain. For example, this zone may consist of only a narrow range near the center frequency or a frequency range for which the amplitude exceeds some fraction of the peak value, and/or the zone may consist only of the frequency range for which the phase spectrum is linear. These restrictions eliminate the low and high frequency extremes where the signal-to-noise ratio is low.
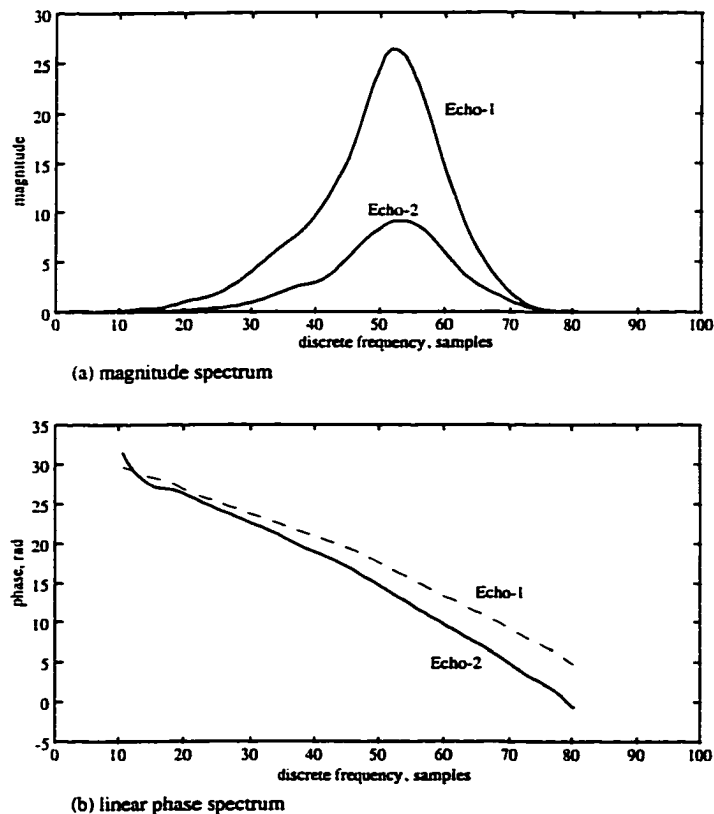
Figure 7.16: Magnitude and phase spectra of two successive echos.

The phase spectra of the two echos can be approximated as linear functions of frequency and the slope of the line is used to determine the time delays T1 and T2. If M1 and M2 represent the slope of the phase spectra of echos R1 and R2 respectively, the corresponding time delays are given as,

$$T1 = \frac{M1}{2\pi} \ , \ T2 = \frac{M2}{2\pi}$$

(7.4)

and the total time delay, T, is given by,

$$T = W + (T_2 - T_1)$$

(7.5)

Crosscorrelation Method: The digital cross-correlation method eliminates the need for somewhat arbitrary criteria (e.g., peak value and zone for phase slope) applied in the two previously described methods. Unlike the echo-overlap or phase-slope method, cross-correlation does not require explicit criteria for accepting or rejecting specific features in echos affected by distortion or low signal-to-noise ratios. The cross-correlation function possesses a maximum in the lag domain (Fgiure 7.17). The displacement of this
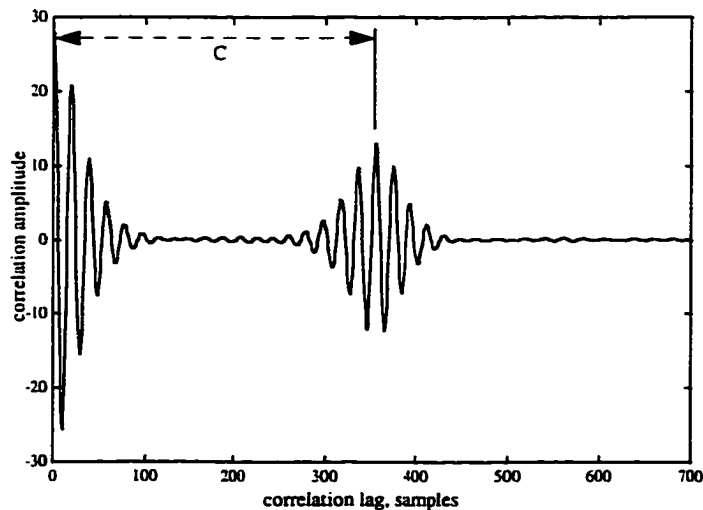
Figure 7.17: Crosscorrelation of two echos.

maximum relative to the zero reference gives the time interval, C, which for ideal case should be equal to T2-T1, as measured by the digital overlap method.

7.2.2 Ultrasonic Attenuation Measurement

Another basic approach to material characterization involves the measurement of energy losses of ultrasonic waves as they interact with the material microstructure. There is a considerable literature based on ultrasonic studies of grain size via attenuation measurements [81, 82, 83, 84]. Strong correlations have been found among ultrasonic wave attenuation and material variations due to hardening, annealing, quenching and cold working.

Given a plane wave of small amplitude, the energy intensity at a distance, x, from the source of ultrasound is given by,

$$I = I_o e^{-\alpha x} \tag{7.6}$$

The total attenuation coefficient, α, combines the absorption coefficient, α_a, and the scattering coefficient, α_s. In general, attenuation coefficient is frequency dependent.

$$\alpha(f) = \alpha_s(f) + \alpha_a(f) \tag{7.7}$$

Attenuation measurements are generally most useful only when made over a wide range of frequencies because the frequency dependence of attenuation is closely tied to the material properties.

Two methods of attenuation measurement are generally used. The first method assumes the attenuation coefficient, α, to be constant over the frequency range of interest. It involves the measurement of multiple reflections from the two parallel surfaces of the test sample (Figure 7.18), and determining the envelope function. The envelope function provides the estimate of attenuation coefficient, α. In order to get more accurate estimate of the attenuation coefficient, α, various corrections for the beam diffraction are carried out. The second method is used for broadband measurement of attenuation coefficient.
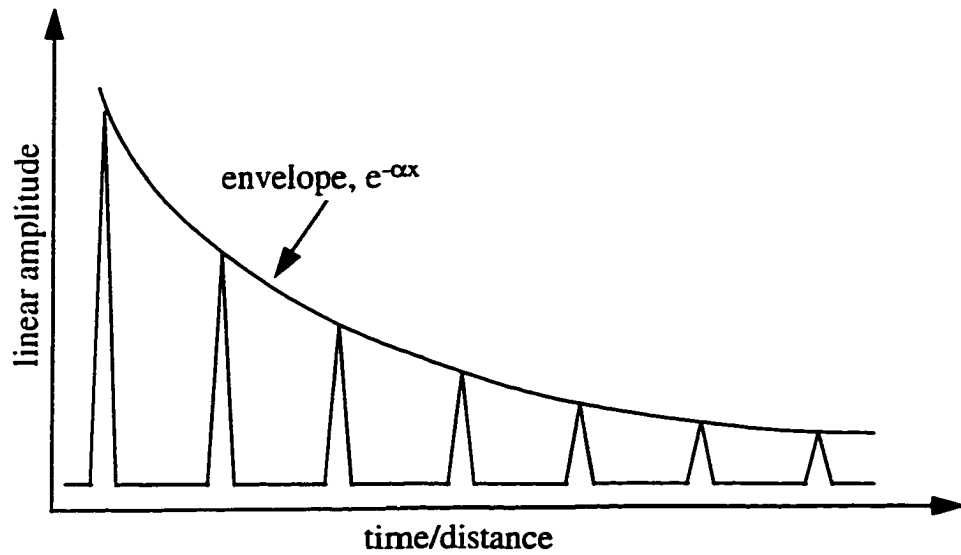
Figure 7.18: Attenuation coefficient measurement method-1.

It measures the frequency dependent attenuation coefficient, $\alpha(f)$, by evaluating the frequency spectrum of each reflection component. If R1(f) represent the amplitude spectrum of the first reflection and R2(f) is the amplitude spectrum of second reflection, the attenuation coefficient, $\alpha(f)$, is given by,

$$\alpha(f) = \frac{R_1(f)}{R_2(f)} \frac{1}{2x}$$

(7.8)

where x is the thickness of the test specimen.

7.3 Signature Discrimination Techniques

In SSUE technique, the measured ultrasonic correlation signature represents the aggregate acoustic characteristics of the test material. Hence a change in any single acoustic parameter of the test material is reflected as some kind of a change in the

measured correlation signature (Figure 7.19). In most practical situations it is only one or a few out of all the parameters that are of interest. In order to detect a change in the acoustic parameter of interest from the measured ultrasonic correlation signature, some kind of discrimination technique is required.

There are two kinds of factors that effect the ultrasonic correlation signature. The uncorrelated measurement system noise (acoustic, electronic, electromagnetic, etc.), and the acoustic parameters of the test object. Since, in addition to the deterministic parameters, there are various random factors affecting the correlation signature, statistical methods have to be applied for the signature discrimination. In general, signature discrimination techniques can be divided into three classes,

Class-I   Controlled experiment

Class-II   Uncontrolled but modelable experiment

Class-III   Uncontrollable and unmodelable experiment
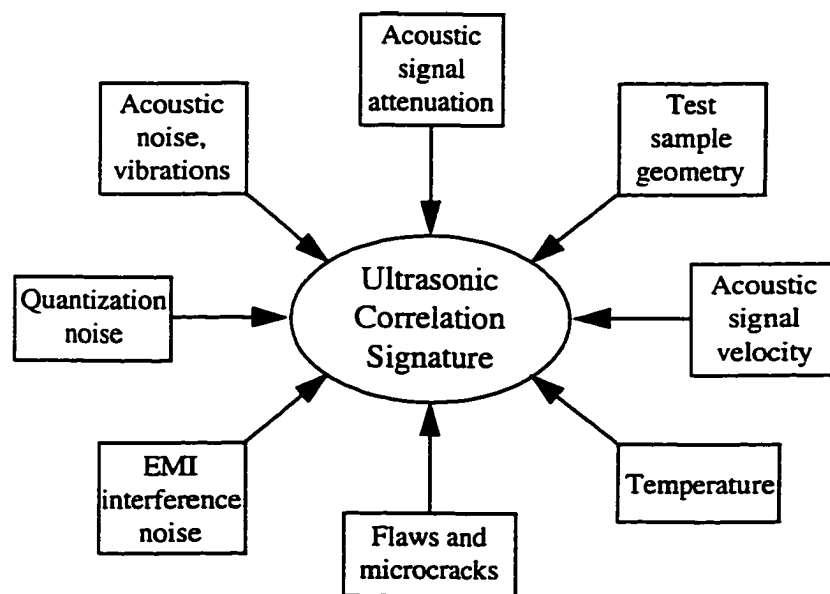
Figure 7.19: Factors affecting the correlation signature in SSUE technique.

In a controlled experiment, except for the parameters of interest all the other deterministic parameters are held constant during the measurement process. Hence, only one deterministic variable is allowed to change the measured correlation signature. Of course all the random factors will still be there, but their statistics can either be modeled or measured, which make it possible to establish the effects of a single parameter of interest on the ultrasonic correlation signature. This class of signature discrimination does not rely on any kind of theoretical modeling of ultrasonic signal propagation and is, therefore, the simplest. However, it puts a lot of restrictions on the experimental setup and may not be practicable in many situations.

The second class of signature discrimination techniques represents the experimental situations where it is not possible to control all the system parameters. However, their values can be independently measured and their effects can be compensated for on the correlation signature. As an example, it may not be possible to control the temperature during an experiment where the attenuation coefficient is the parameter of interest. But if the effect of temperature on the correlation signature is known a priori, the variation of temperature can be compensated. This signature discrimination approach relies heavily on the theoretical modeling of the effects of various deterministic factors on the measured signature. It can work well in moderately complicated experimental situations.

The third class represents the most complex category of signature discrimination techniques. It deals with the experimental situations which are theoretically untractable and hence the theoretical modeling of various aspects of the experiment is very difficult. This class relies heavily on empirical correlation between the acoustic parameters and the correlation signature.

7.3.1 Pattern Classification Approach for Signature Discrimination

In certain NDE situations, the signature discrimination issue can be reduced down to a two class or a multi class pattern classification problem. For example, if the inspection requirement is to check the test specimen for the presence or absence of

internal flaw, then this is a two class identification problem with class-1 representing the presence of flaw and class-2 representing the absence of any flaw. A similar approach can be used for the characterization of multiple flaws, such that,

Class-1   No flaw present

Class-2   Flaw-1 present

Class-3   Flaw-2 present

Without having a theoretical knowledge of how the correlation signature is altered by the presence or absence of a certain type of flaw, a pattern classification approach can be used to discriminate between the three classes of No Flaw, Flaw-1, and Flaw-2.

A pattern classification algorithm typically involves three steps, (a) feature extraction, (b) feature selection (data reduction), and (c) pattern classification [85]. In the following, these three steps of the algorithm are developed for application to ultrasonic correlation signature.

Feature Extraction: An ultrasonic correlation signature represents a data vector to be analyzed by the pattern classification algorithm. As a first step, different features needs to be extracted which eliminate the unnecessary data and are subsequently used for pattern classification. It was decided to analyze the data in frequency domain as it offers three important advantages, which are,

(a)   out of band noise can be eliminated

(b)   data reduction can be achieved without loosing information

(c)   phase error in the data can be accommodated

Hence, the fast Fourier transform (FFT) of the correlation signature is determined and the magnitude of N frequency bins corresponding to the passband spectrum are selected as the feature vector (Figure 7.20).

Feature Selection (Data Reduction): A feature selection criteria is required to rank the feature elements according to their discrimination abiiity and to discard those elements that fall below certain threshold, thus reducing the feature vector length and the vector
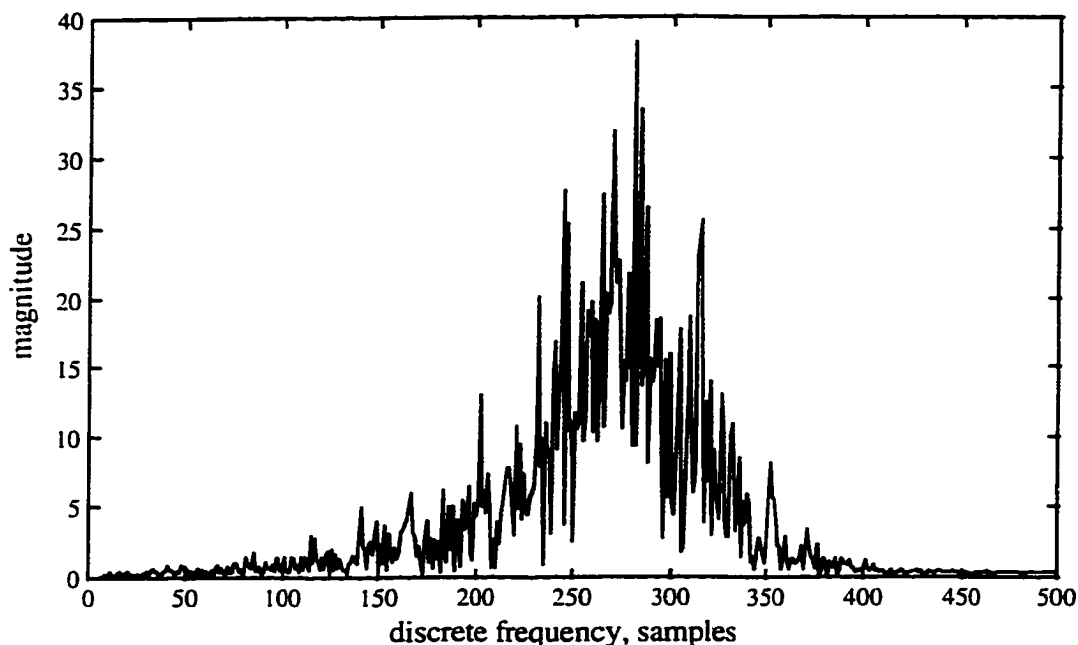
Figure 7.20: FFT magnitude of correlation signature representing the feature vector.

space spanned by it. To do that a set of training data is acquired that is grouped as class 1, class 2 and class 3. Assuming that there are twenty feature vectors in each class, making a total of sixty. A mean feature vector, m_n, and a standard deviation vector, δ_n, for each class is determined, where n = 1, 2, 3 corresponding to the three classes. The mean vector represents the location of a particular class in an N-dimensional vector space, while the standard deviation vector represents the spread of the class in the vector space. In order to rank each element of the feature vector for its discrimination ability, two quantitative measures are defined.

Intra class spread (s_i): This is the average of the ith elements of standard deviation vectors of the three classes.

$$s_i = \frac{1}{3}[\sigma_{1i} + \sigma_{2i} + \sigma_{3i}]$$ (7.9)

Inter class distance (d_i): This is the average difference between the ith element of mean vectors of the three classes.

$$d_i = \frac{1}{3}[(m_{1i} - m_{2i}) + (m_{1i} - m_{3i}) + (m_{3i} - m_{2i})]$$ (7.10)

The ratio of inter class distance to intra class spread (Figure 7.21), called (s_i/d_i) ratio, for each feature element serves as the criteria for ordering the feature elements. Based on an empirically determined threshold, the top M feature elements are selected and the other discarded.

Pattern Classification: With the reduced M-dimensional feature space, the next step is to select a classification criteria and to determine the decision boundaries (Figure 7.22). Mean feature vectors of each of three classes determine the location of each class in the M-dimensional space. A cost function was introduced for decision between flaw and no flaw cases based on the acceptable ratio of "probability of misdetection" to the "probability of false alarm". Since the misclassification between flaw-1 and flaw-2 is
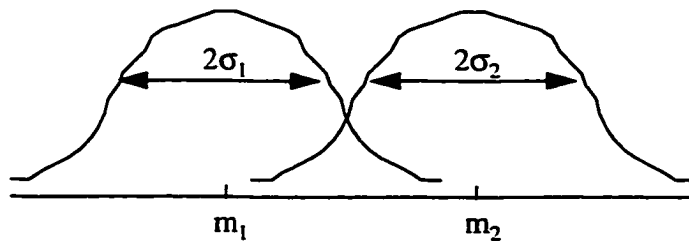
Figure 7.21: Graphical representation of feature selection criteria.
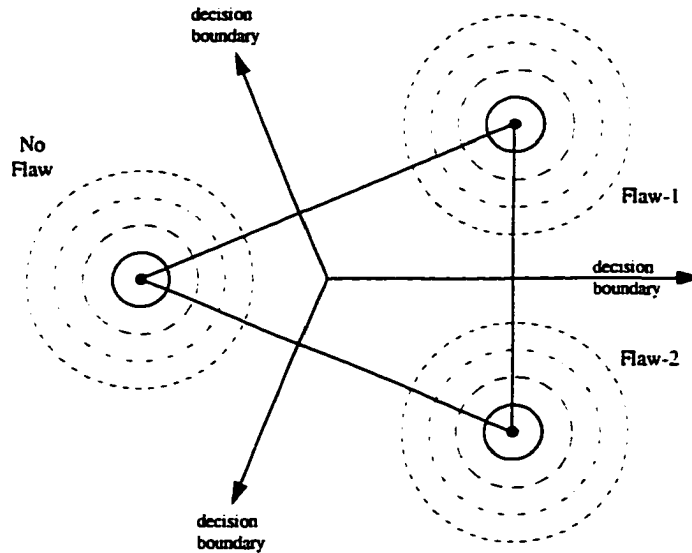
Figure 7.22: Graphical representation of pattern classification algorithm.

considered of equal significance, the decision surface between those two classes is an orthogonal hyperplane bisecting the line joining the vectors m_1 and m_2 (Figure 7.22). With this the vector space is now divided into three regions representing each class. Any unknown data vector is classified by mapping it onto this M-dimensional vector space according to the above algorithm and identifying the region to which it belongs.

7.4 Envelope of Ultrasonic Correlation Signature

In SSUE technique, the measured ultrasonic correlation signature, $\phi_{sr}(\tau)$, represents an estimate of the composite system impulse response function, $h(\tau)$, i.e.,

$$\phi_{sr}(\tau) \approx h(\tau) \qquad (7.11)$$

$\phi_{sr}(\tau)$ is a bandlimited signal having a center frequency, f_0 , and bandwidth, B. In many

practical NDE applications such as, flaw detection and transit time measurement, it is desirable to translate the ultrasonic correlation signature to baseband level. This implies finding a baseband equivalent of $\phi_{sr}(\tau)$, or in other words finding an envelope function of $\phi_{sr}(\tau)$. The ultrasonic correlation signature, $\phi_{sr}(\tau)$, can be written as,

$$\phi_{sr}(\tau) = A(\tau)\cos(\omega_0\tau) - B(\tau)\sin(\omega_0\tau) \tag{7.12}$$

and has a broadband frequency spectrum. A typical ratio of bandwidth, B, to the center frequency, f_0, is around two. Hence, the narrowband signal assumption, $(f_0 >> B)$, can not be applied. This implies that a simple envelope detection of $\phi_{sr}(\tau)$ can not be performed to find its baseband equivalent. The concept of signal preenvelope or analytic signal is therefore applied [61] for this purpose.

In general, the analytic signal or the preenvelope of a real signal, $f(t)$, is the complex-valued function defined as,

$$f_p(t) = f(t) + j f_h(t) \tag{7.13}$$

The real part of the analytic signal is, of course, the real signal, $f(t)$, itself, while the complex part is the Hilbert transform of the real signal, represented as, $f_h(t)$. The envelope of $f(t)$ is the absolute value of its preenvelope $f_p(t)$, given as,

$$\varphi(t) = \sqrt{f(t)^2 + f_h(t)^2} \tag{7.14}$$

Since, by definition, the imaginary part of the analytic signal is the Halbert transform of its real part, the summmation of frequency spectrum of $f(t)$ and $f_h(t)$ results into the cancellation of their imaginary components, while the real part of the spectrum adds up to give twice the magnitude, while the imaginary components cancel each other.

The demonstration of the computation of correlation signature envelope is made in Figures 7.23 through 7.26.
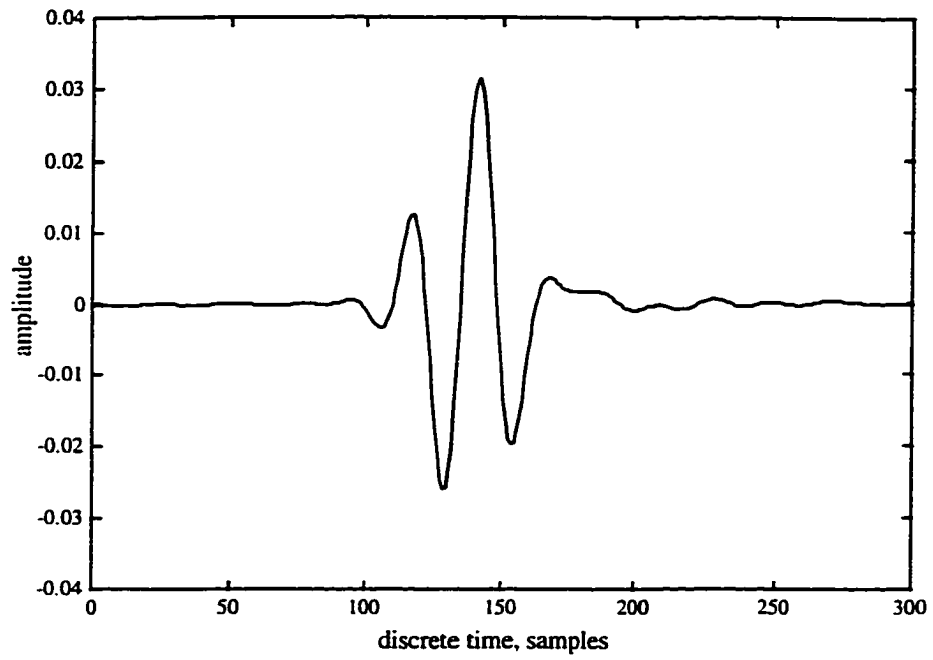
Figure 7.23: Representative correlation signature component
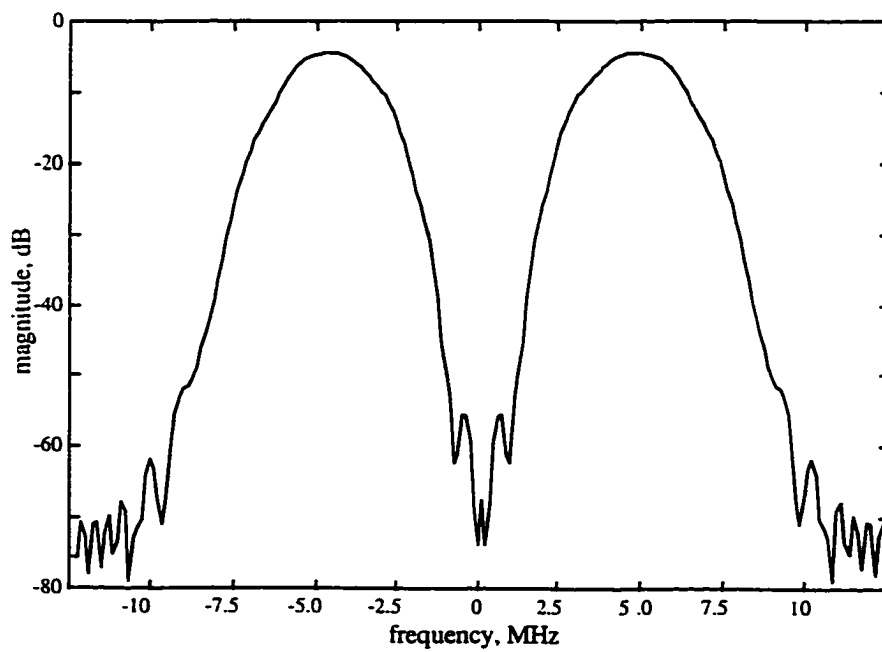
Figure 7.24: Magnitude spectrum of correlation signature.
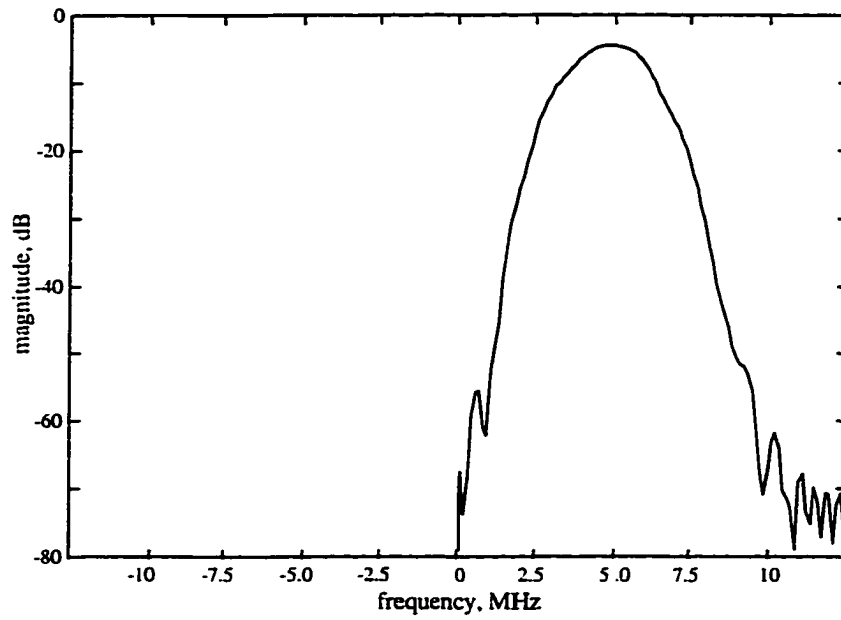
Figure 7.25: Spectrum of the corresponding signal preenvelope.
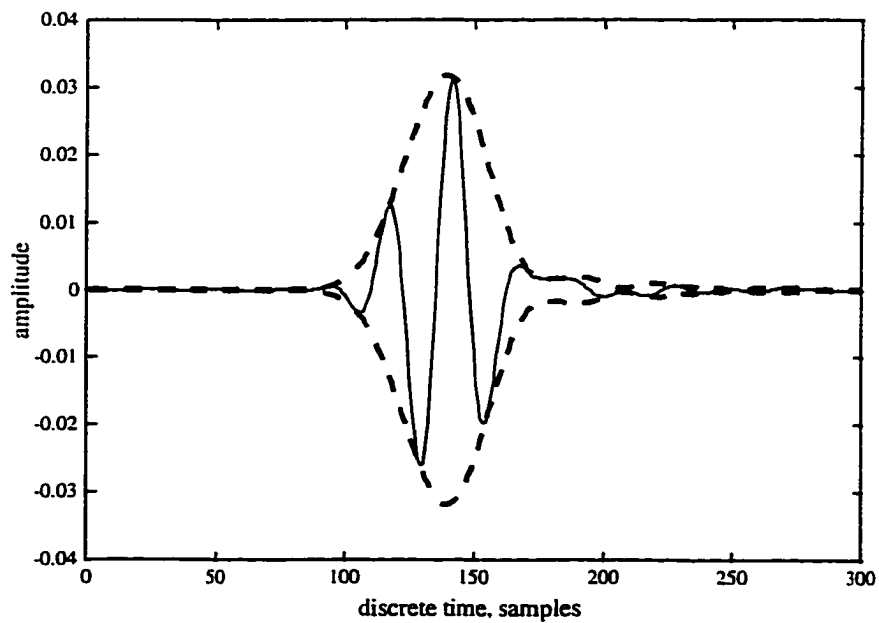
Figure 7.26: Envelope of the correlation signature component.

Hence, the following procedure is adopted for the calculation of the envelope of ultrasonic correlation signature:

(a) compute the Fourier spectrum (FFT) of ultrasonic correlation signature,

(b) set the imaginary part of the computed spectrum to zero,

(c) compute the inverse Fourier transform (IFFT) of the resultant,

(d) take the absolute value of IFFT which is the desired envelope function.

CHAPTER 8   APPLICATIONS OF SSUE

This chapter investigates the application of SSUE technique to various practical NDE problems. It describes a number of different experiments that were conducted in the laboratory environment utilizing the lab-grade prototype instrument. Various signal processing tools discussed in Chapter 7 were applied to the experimental data.

8.1 Flaw Detection in Attenuative Materials

Flaw detection is perhaps the oldest and the most straight forward application of ultrasonic NDE. It presumes that the acoustic signal propagation characteristics of the test material are known. In particular, the mode of propagation of ultrasonic waves and their velocity has to be known. Most flaw detection measurements are performed by employing the longitudinal mode of wave propagation. For the detection of smaller flaws in attenuative materials, high SNR systems are desirable. SSUE technique, by virtue of its inherent noise suppression characteristics is ideally suited for such cases.

8.1.1 Experimentation

The effectiveness of SSUE technique for flaw detection in attenuative materials is demonstrated through the following experiment. The test sample consists of a block of plastic (Perspex) material with two smooth parallel surfaces. A small flaw was simulated by drilling a flat bottom hole of .05 inch diameter and .06 inch depth (Figure 8.1). The transducers were coupled to the parallel surface opposite to flaw and positioned next to each other. This is a typical setup of pulse-echo ultrasonic technique. First, the ultrasonic signature through the standard pulse-echo system was measured and is shown in Figure

8.2. Next, the ultrasonic signature through the SSUE technique was determined and is shown in Figure 8.3. Both the systems used a transducer pair with 5 MHz center frequency and a bandwidth of about 10 MHz. It is obvious that the pulse-echo system could not detect the flaw signal due to poor signal-to-noise ratio, while in case of SSUE measurement, the flaw signal stands out well above the noise floor.

8.1.2 Flaw Characterization

Modern ultrasonic NDE, in addition to flaw detection, also attempts to characterize the nature of flaw. This is partly because the ultrasonic techniques have developed to a level where reliable flaw characterization have become possible, and partly because of the economic reasons of exploiting full potentials of the component's useability. This approach to life prediction of a fatigued component is sometimes referred as a "damage tolerance" approach and is based on fracture mechanics methodology. With this approach, instead of assuming that all flawed components must be taken out of service, the severity of flaw is assessed and a more rational determination of the remaining life of the component is made.

transmit   receive
transducer   transducer

flat bottom
hole
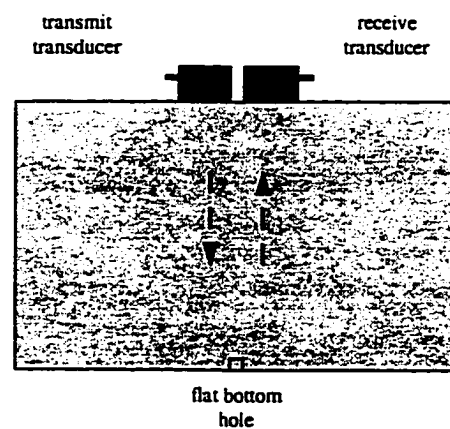
Figure 8.1: Test setup for flaw detection.
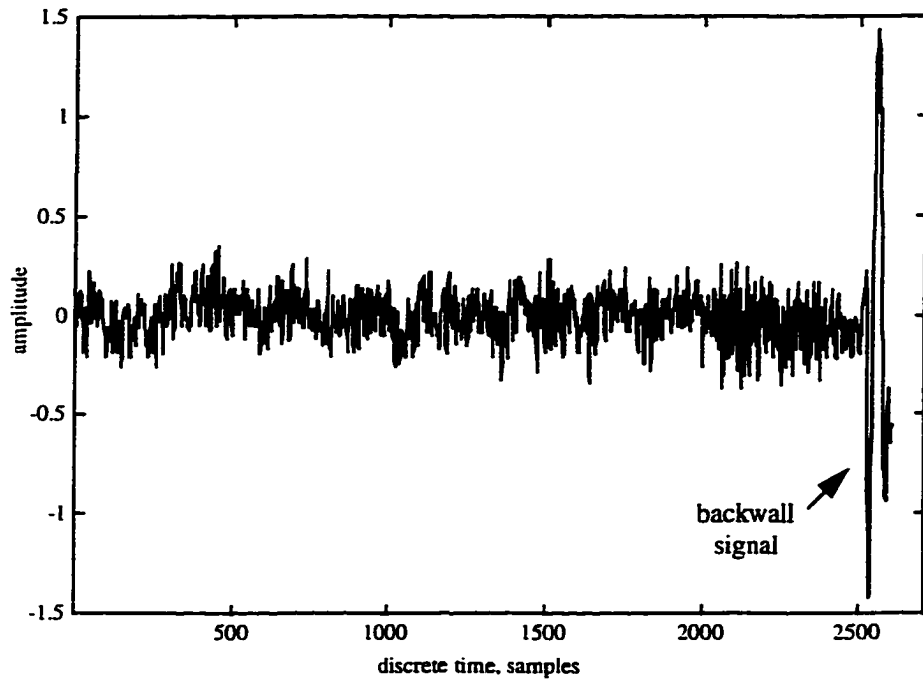
Figure 8.2: Ultrasonic signature measured through a pulse-echo system.
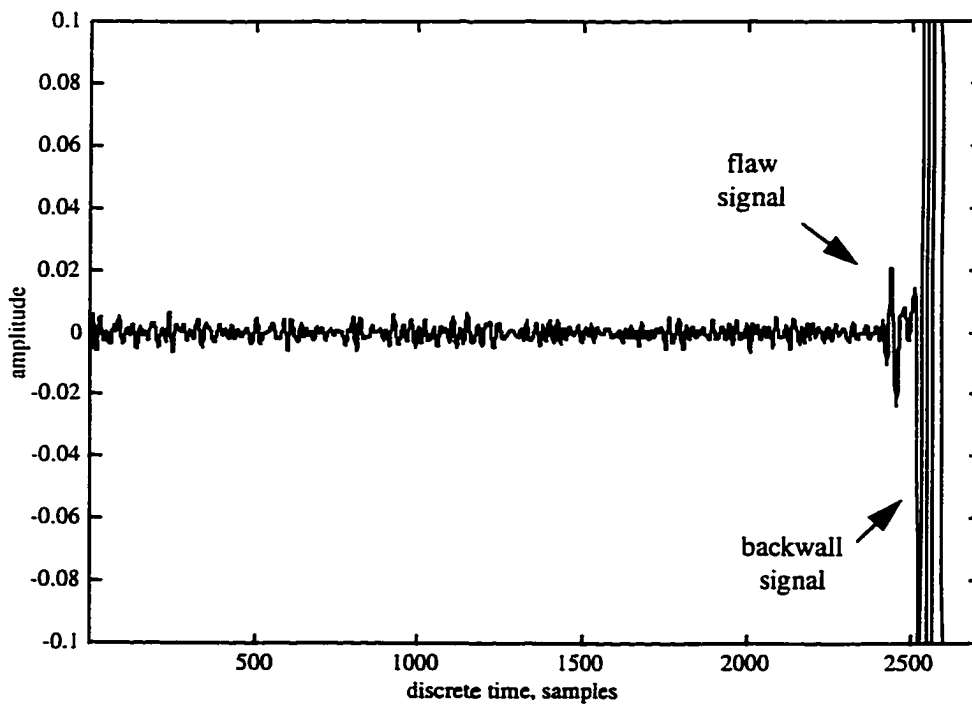
Figure 8.3: Ultrasonic signature measured through the SSUE system.

Various researchers addressed the flaw characterization problem [86, 87, 88]. In most cases, the frequency domain approach was followed. It was verified that various classes of flaws reflect a specific pattern in the magnitude spectrum of the flaw signature. A successful flaw characterization approach requires, as a prerequisite, a very accurate flaw signature. For this, SSUE technique can be applied with considerable success. Although the flaw characterization issue has not been addressed in the current work, there is no doubt that SSUE, owing to its better signature estimation feature, is capable of producing improved results in the characterization of various types of flaws.

8.2 Velocity and Thickness Measurement

The most frequent application of ultrasonics to material property measurement involves the study of elastic constants and related strength properties of test material. According to the physical acoustics theory, the elastic behavior of solids can be determined by the measurement of ultrasonic velocity. Measurement of longitudinal and transverse velocities give the longitudinal and shear moduli, respectively, such that,

$$L = \rho v_L^2 \tag{8.1}$$

$$S = \rho v_S^2 \tag{8.2}$$

where ρ represents the density of the material.

Hence a relatively small change in the ultrasonic velocity can indicate a significant variation of material strength related characteristics. This reflects the significance of making very precise and accurate velocity measurements. The use of SSUE technique for velocity measurements has a three-fold advantage. First, the measured signature has a better SNR, second, it has a higher resolution, and lastly, it can permit the use of multiple echos in order to minimize the measurement error.

8.2.1 Experimentation

The ultrasonic correlation signature was measured and the first and second backwall reflection components were separated. They are shown in Figure 8.4. It can be seen that the echo overlap method (section 7.2.1) of velocity measurement will not work here because the zero crossings of the two echos do not properly match. Hence, the other two methods, which are, phase-slope method and the crosscorrelation method, were used to measure the ultrasound velocity. For the phase-slope method, the two echo components were gated as,

Echo-1   samples (1-200)

Echo-2   samples(401-600)

Hence the sample delay between the two gated echos, represented by W is 400. The continuous phase spectra of the two echos was calculated and is shown in Figure 8.5. The phase spectra were approximated as straight lines and the slope calculated as,

M1=540 rad/hertz,   M2=770 rad/hertz

Hence, in reference to the development of section 7.2.1, the transit time delay between the
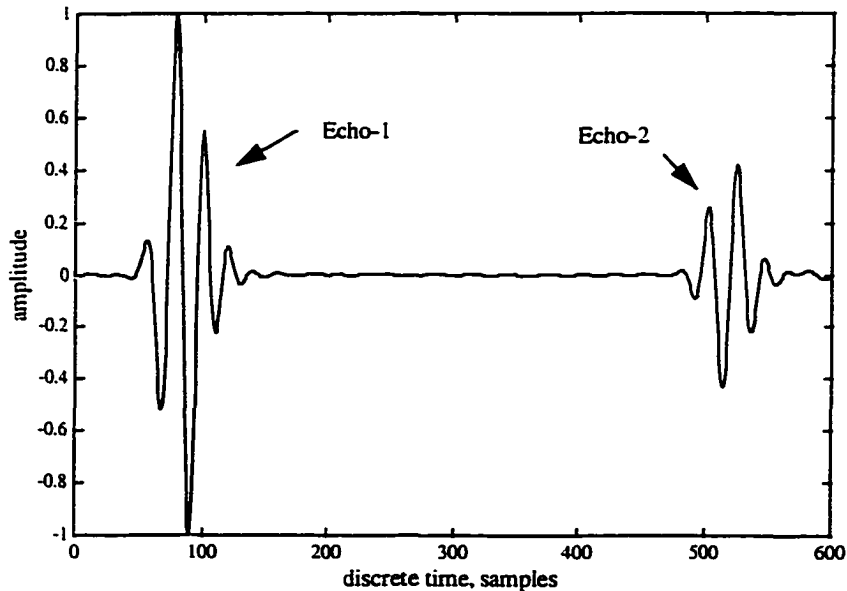
Figure 8.4:   Windowed ultrasonic correlation signature.
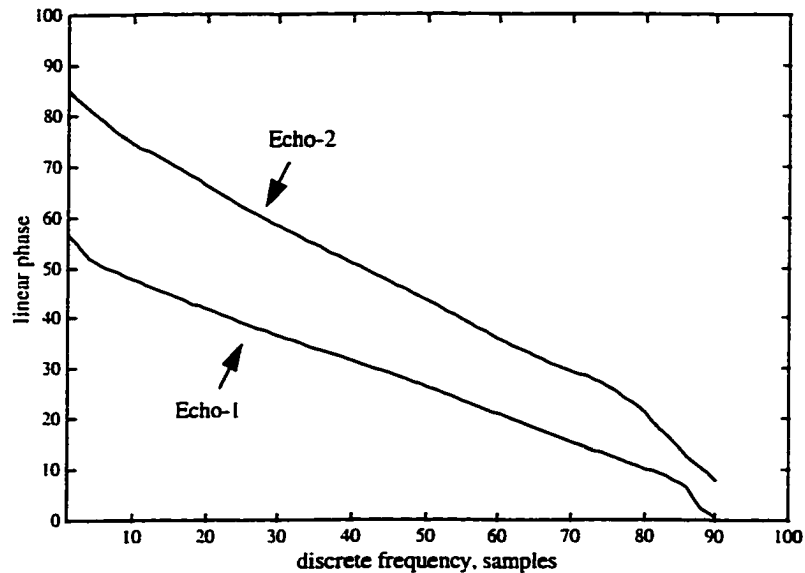
Figure 8.5: Phase spectra of echo-1 and echo-2.

two echos came out as,

$$T=W+(M2-M1)/2\pi=400+36.6 \ samples \tag{8.3}$$

The crosscorrelation method involves calculating the autocorrelation of the correlation signature. This is shown in Figure 8.6, along with the envelope function calculated as per the procedure of section 7.4. The time delay between the first and the second peak of the envelope function gives the transit time delay of the two echos which was measured as 437 samples. This result was in very close agreement with the result from the phase slope method.

8.2.2 Thickness Measurement

Conceptually, thickness measurement is the reciprocal of velocity measurement. When the velocity of ultrasound in the test material is known, a priori, its thickness can
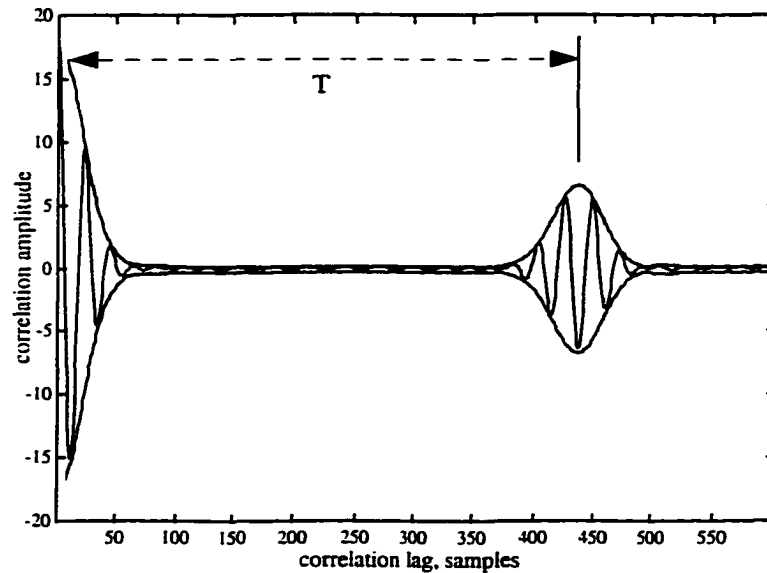
Figure 8.6: Autocorrelation of the ultrasonic correlation signature.

be found by the transit time measurements. However, thickness measurement has a lot of practical significance in real-life ultrasonic NDE applications. In many situations, only one surface of the test material is accessible and it is required to measure its thickness using some ultrasonic NDE technique. One common situation is the measurement of corrosion in a metallic pipeline. Another situation is the measurement of concrete wall thickness. Thus the SSUE technique can be applied for improved thickness measurement in a variety of situations.

8.3 Attenuation Measurement

Ultrasonic attenuation measurement involves the measurement of multiple reflections from the two parallel surfaces of the test specimen. When the test material exhibits highly attenuative characteristics, the measurement of multiple signal reflections with sufficiently high SNR, using conventional pulsed ultrasonic systems becomes

increasingly difficult. Usually, coherent averaging of multiple measurements is done to get a good quality signal for attenuation measurement. SSUE technique can be used for the attenuation measurement as it can provide a good quality acoustic signature of the test specimen thus eliminating the need of coherent averaging.

The frequency dependent ultrasonic attenuation measurement of a test sample using the SSUE technique was performed. The transmitting and the receiving transducer were placed in a through transmission mode (Figure 8.7). The signal processing method explained under section 7.2.2 was used for these measurements.
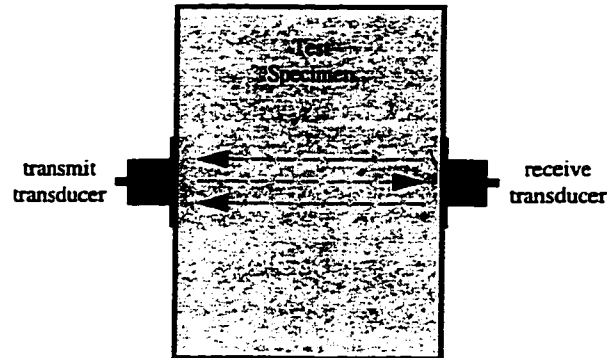
Figure 8.7: Through transmission test setup for attenuation measurement.

The ultrasonic correlation signature is shown in Figure 8.8. Various multiple reflection components can be seen in this figure. The magnitude frequency spectra of the first three reflection components were calculated and are shown in Figure 8.9. Finally, the plot of ultrasonic attenuation versus frequency is shown in Figure 8.10.
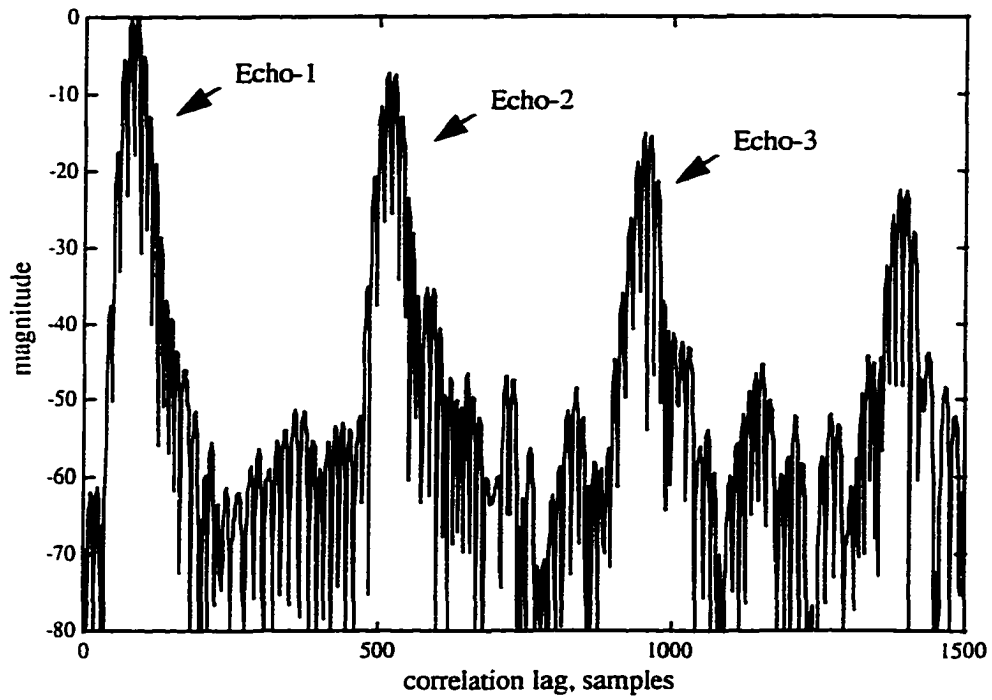
Figure 8.8: Measured ultrasonic correlation signature.
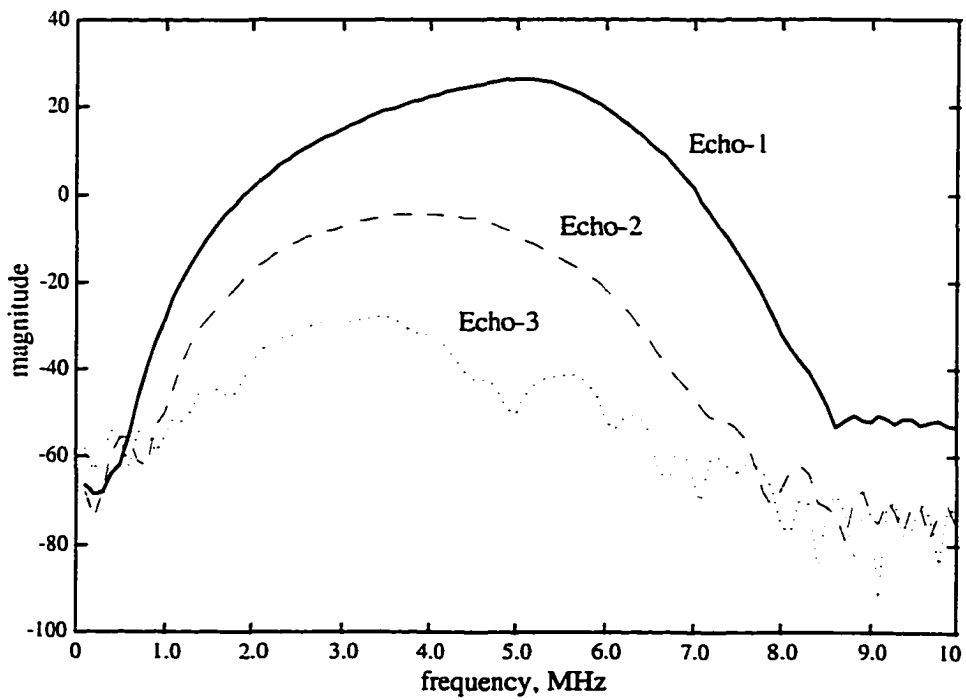
Figure 8.9: Frequency spectra of multiple reflections.
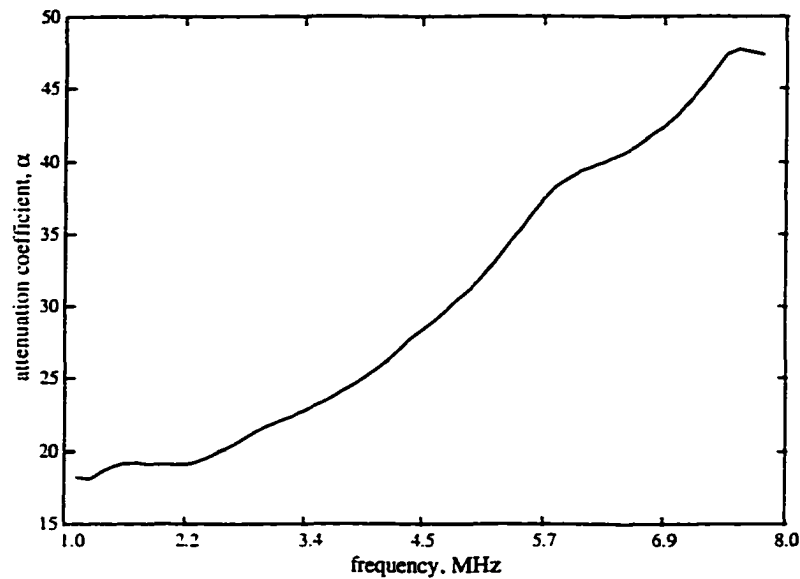
Figure 8.10: Plot of measured attenuation coefficient.

8.4 Global Integrity Assessment of Complex Objects

Global integrity assessment implies the evaluation of integrated effect of distributed damage or property variation within a test specimen. In certain NDE applications, either due to the complex geometry of the test object or the complex nature of the material of the object, it is not possible to identify each isolated critical imperfection. Consequently, the NDE of such objects involve the integrated condition assessment. One practical situation for which the application of SSUE technique is under consideration is the integrity monitoring of security containers carrying nuclear warheads. In this application, it is critical that very low amplitude ultrasonic signals be employed and the technique be very sensitive to monitor all kinds of changes. Incidently, SSUE bears both of these features.

A similar application is the integrity monitoring of pressurized gas cylinders. It was told that the pressurized gas cylinders, during their service life develop small internal

cracks, which propagate and enlarge and, if not detected before a critical limit, can result into a catastrophic explosion. An experiment for the global integrity assessment of these pressurized gas cylinders was carried out and is discussed as follows.

8.4.1 Aluminum Gas Cylinder Experiment

A laboratory experiment was designed to study the sensitivity of SSUE technique in the detection of small notch-like simulated flaws at various regions on the surface of cylinder. The schematic drawing of the cylinder and the position of ultrasonic transducers is shown in Figure 8.11. Various positions for the transmitting and the receiving transducers were tried in an attempt to find the optimum insonification of the entire volume of the cylinder. Finally, the arrangement indicated in the figure was chosen, as it indicates nearly uniform insonification of most of the cylinder volume.

The transducers used for this experiment were of 1 MHz center frequency and therefore the carrier frequency of 1.0 MHz with a chipping rate of 0.5 MHz was used for transmit signal generation. The excitation waveform was based on a 12 th order maximal-length sequence. The digitizer was clocked at 40 samples per chip. Flaws were simulated
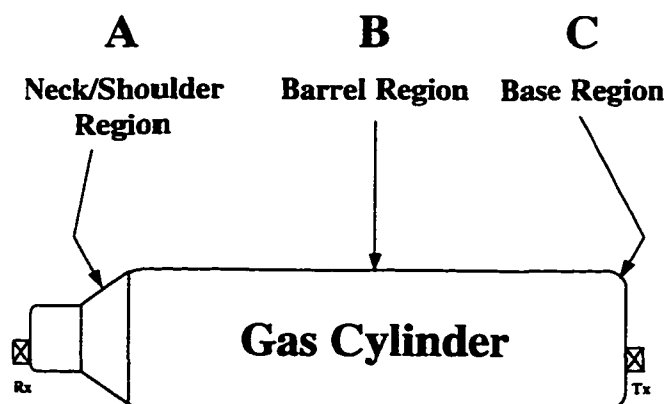
Figure 8.11: Schematic drawing of aluminum cylinder experiment.

at three different regions of the cylinder that were considered critical. The simulated flaws were introduced into the cylinder using a Dremel tool to cut crack-like notches into the neck, barrel and base regions (Figure 8.11). In each region, the flaw size was progressively increased from the smallest to the maximum size. A total of 10 data records were recorded corresponding to each flaw. The data records were grouped into classes where each class represents one physical "state" of the cylinder. The signature discrimination technique discussed in section 7.3 was applied to determine the sensitivity

Table 8.1: Approximate dimensions of different simulated flaws.

Data Set Class	Flaw Type	Dimensions (LxDxW)
Class-1	Baseline for shoulder	
Class-2	Flaw-1 at shoulder	1.5 mm x 5.0 mm x 2.0 mm
Class-3	Flaw-2 at shoulder	1.5 mm x 7.5 mm x 2.0 mm
Class-4	Flaw-3 at shoulder	1.5 mm x 10 mm x 2.0 mm
Class-5	Baseline for barrel region	
Class-6	Flaw-1 at barrel region	1.5 mm x 5.0 mm x 2.0 mm
Class-7	Flaw-2 at barrel region	1.5 mm x 7.5 mm x 2.0 mm
Class-8	Flaw-3 at barrel region	1.5 mm x 10 mm x 2.0 mm
Class-9	Baseline for base region	
Class-10	Flaw-1 at base region	1.5 mm x 5.0 mm x 2.0 mm
Class-11	Flaw-2 at base region	1.5 mm x 7.5 mm x 2.0 mm
Class-12	Flaw-3 at base region	1.5 mm x 10 mm x 2.0 mm

of the SSUE technique to the simulated flaws at various regions of the cylinder.

The flaw classification results are tabulated in Table 8.2. These results indicate that the SSUE correlation signature is sensitive to acoustic changes in all the three critical regions of the cylinder. Also, each incremental flaw was well-discriminated form one another.

Table 8.2: Classification statistics of different simulated flaws.

Data Set Class	Class # i,j	Class Type	Intra-set spread	Inter-class distance D_{ij}
Class-1	1,1	Baseline for shoulder	2.66	0
Class-2	1,2	Flaw-1 at shoulder	1.33	176
Class-3	2,3	Flaw-2 at shoulder	1.49	172
Class-4	3,4	Flaw-3 at shoulder	4.89	247
Class-5	5,5	Baseline for barrel region	12.95	0
Class-6	5,6	Flaw-1 at barrel region	7.66	114
Class-7	6,7	Flaw-2 at barrel region	6.50	104
Class-8	7,8	Flaw-3 at barrel region	5.53	79
Class-9	8,8	Baseline for base region	6.94	0
Class-10	8,9	Flaw-1 at base region	5.44	121
Class-11	9,10	Flaw-2 at base region	5.68	70
Class-12	10,11	Flaw-3 at base region	7.14	89

8.5 Geophysical Exploration

Various seismic methods are utilized for geophysical exploration in order to determine the nature and configuration of rock layers deep in the earth. The traditional method is to generate an acoustic pulse of high intensity through a dynamite and to record the reflections of the incident pulse from various layers of earth, through what is called a geophone. A relatively new technique is called VIBROSEIS. Vibroseis is at present the dominant method of exploring oil on land (Figure 8.12). This method is based on the principle of chirp radar. As discussed earlier under section 2.6.2, a chirp waveform results into correlation sidelobes and even though various techniques exist for the reduction of correlation sidelobes, these can not be completely eliminated and thus restrict the dynamic range of the measurement.

SSUE technique appears to be ideally suited for upgrading the Vibroseis technique of geophysical exploration. In fact, the same equipment with very little modification in transmitter electronics can be used to implement the SSUE technique. As long as the frequency spectrum of the SSUE waveform matches the frequency spectrum of the chirp signal applied in Vibroseis, there is no change required in the vibrator mechanism (Figure

Figure 8.12: Representative Vibroseis system mounted on a truck.

8.13). The only change required is in the waveform generation process and the correlation processing at the receiver, which in present days is almost invariably done in digital domain.
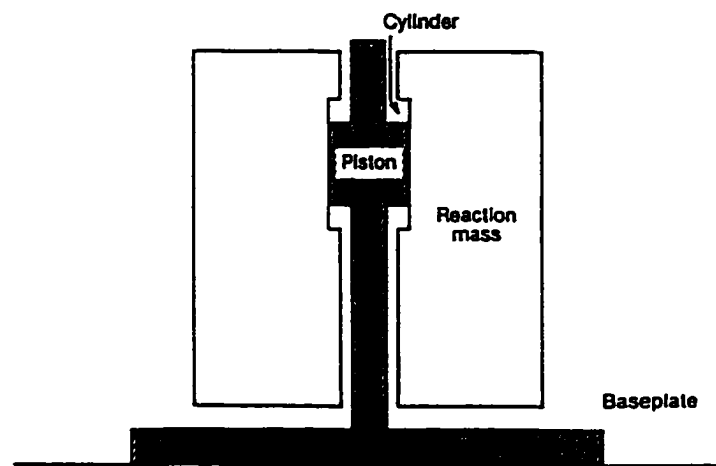
Figure 8.13: Typical vibrator schematic of Vibroseis system.

CHAPTER 9   SUMMARY AND DISCUSSION

This chapter summarizes the research work presented in this dissertation and discusses the strengths and limitations of SSUE technique. Various future application areas of SSUE technique are highlighted, and finally, different possible directions for the future research on the advancement of SSUE technique are presented.

9.1 Summary of Research

A new approach to ultrasonic NDE called spread-spectrum ultrasonic evaluation (SSUE) was investigated. It regards the ultrasonic nondestructive evaluation of a test sample as an acoustic impulse response estimation and characterization problem. This problem has been compared with the analogous problems of radio-detection-and-ranging from communications field and the seismic exploration problem of geophysics. Out of the various options for impulse response estimation, the continuous pseudorandom signal correlation method has been shown to be optimum for peak power limited systems such as the ultrasonic NDE systems. The problem of self-noise associated with the pseudorandom correlation systems and its effect on the system performance are investigated, followed by the development of various optimum and sub-optimum approaches to self-noise elimination.

After verifying the theoretical results through computer simulations, a lab-grade optimized SSUE instrument was developed and analyzed. The application of SSUE technique to various practical NDE situations like, flaw detection, velocity/thickness measurements, attenuation measurement, global integrity assessment, etc., was investigated through various laboratory experiments. It is concluded that the SSUE technique holds great promise for all ultrasonic NDE applications where high signal attenuation results

into the signal-to-noise ratios beyond workable limits.

9.2 Evolution of SSUE Technique

The SSUE technique is based upon the concept of pseudorandom signal correlation. If we view the development of SSUE technique, keeping in perspective the development of various other ultrasonic NDE techniques, we see that the SSUE system can be considered as an advancement of the earlier ultrasonic correlation systems. The evolution of an optimized SSUE system, as described in this dissertation, can be summarized through the following four developmental stages.

      (a)   Conventional Pulsed Systems

      (b)   Pulse-Compression Systems

      (c)   Pseudorandom Correlation System

      (d)   Optimized SSUE System

A common endeavor through this developmental process was to increase the detectability limit of the ultrasonic NDE system by accomplishing better signal-to-noise ratio and improved dynamic range. The conventional pulsed systems had a limitation of peak signal power which led to the application of larger time-bandwidth pulses in pulse-compression systems, the concept borrowed from the radio navigation and ranging systems. The pulse-compression systems solved the peak-power limitation but the system performance is now limited by the system's self-noise. The pseudorandom correlation system was based on the ideas adopted from the spread-spectrum techniques of radio communication. Here, by employing the periodic autocorrelation properties of the continuous excitation waveform, a considerable reduction in the system's self-noise level was achieved. Finally, through what is termed as an optimized SSUE system, the self-noise problem is completely eliminated. The sensitivity of the new system is purely dependent on the signal-to-random-noise ratio, which can be improved to any desired level by employing longer sequences, of course, at the cost of greater system complexity and signal processing.

9.3 Limitations of SSUE System

Like any practical system, SSUE also has a few limitations of its own. In the following, these are categorized as the fundamental limitations and the technological limitations.

9.3.1 Fundamental Limitations

(a) Perfect self-noise suppression is possible only under the continuous or pseudo-continuous transmission of the pseudorandom excitation waveform.

(b) The SSUE technique requires separate transmit and receive transducers.

(c) The measured acoustic impulse response, h(t), will be bandlimited to the transducers' passband.

(d) The period of pseudorandom excitation waveform, T, should be larger than the time span of the system impulse response, h(t).

(e) It is only the uncorrelated noise that is suppressed by the SSUE technique, and the level of suppression is determined by the SNR gain factor.

9.3.2 Technological Limitation

(a) The peak transmit power is limited by the maximum average power handling capacity of the transducers.

(b) The quantization noise level in the received signal is the limiting factor in achieving a large dynamic range.

(c) The maximum useable sequence length is a function of correlation processing speed of the signal processor.

(d) Maximum useable sequence length is limited by the data handling capacities of various system components like the function generator and the digitizer.

9.4 Further Research Areas for SSUE Technique

In order to utilize the full potentials of SSUE technique and to establish its effectiveness in a variety of ultrasonic NDE applications, there are quite a few areas of further research and development. It is likely to take a number of years of dedicated research before SSUE can be accepted as a powerful tool by the NDE community. Here, some of the important areas of further research and development are highlighted.

9.4.1 Customized Transducer Development

The transducers currently available in the market are designed for applications involving pulsed mode operation. Thus their design is optimized to provide maximum peak power capabilities and the average power handling capacity of a transducer has not been the primary design consideration. As a result of this the operating average power levels in SSUE system were limited by the heat dissipation capacity of the existing transducers. This setback to the operation of SSUE system can be avoided if customized transducers can be designed considering the continuous mode of operation. Also, in order to facilitate the pulse-echo equivalence of SSUE technique, for applications like flaw detection, a pair of concentric transducers enclosed in a single casing needs to be developed. Finally the performance of SSUE technique in the estimation of true impulse response of a test specimen is limited by the bandlimited transducer characteristics. Further research into the development of broader operating bandwidth transducers can improve the performance of SSUE technique.

9.4.2 Multiple Transducer System

The linear time-invariant, single-input single-output model of ultrasonic NDE system can be conveniently extended to accommodate multiple-inputs and multiple outputs. In this case the system impulse response is represented by a correlation signature

matrix with each element of the matrix representing a unique input output relationship of the test specimen. This model can be used to develop a multiple input/output SSUE system (Figure 9.1). In case of the NDE of large structures and objects, the single pair transducer SSUE system can prove inadequate in achieving the desired sensitivity of the measured correlation signature. For such applications, a multiple input/output system has to be developed.
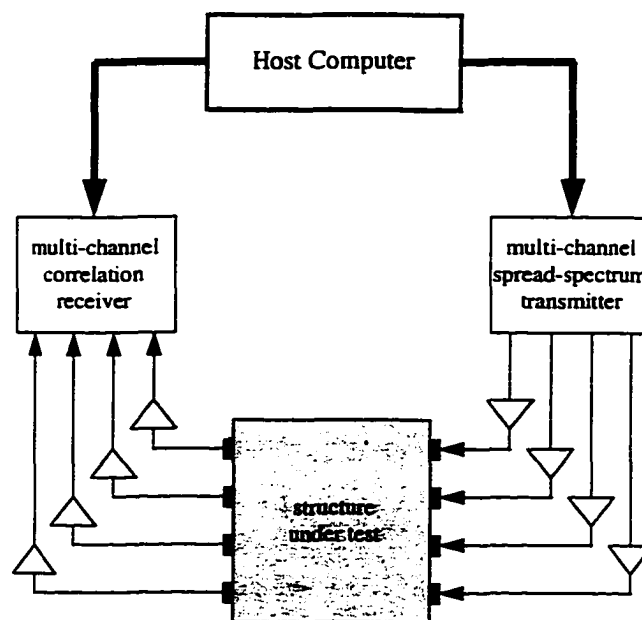
Figure 9.1: Multiple input/output SSUE system.

9.4.3 Expert System Development

In many NDE applications, either due to the complex shape of the test object or the dispersive/anisotropic acoustic properties of the test material, it is very difficult to accurately model the propagation and reception of ultrasonic signal. The measured correlation signature for such cases will consist of multiple overlapping echos. The

development of an expert system that can separate out various components of the measured ultrasonic correlation signature is a research area that has not yet been sufficiently explored. The signature discrimination technique developed as a part of the present research has a very limited scope of application in a real situation. There is a need to develop more robust and powerful techniques that can separate various interacting signature components.

9.5 Future Applications of SSUE

Spread-spectrum ultrasonic evaluation technique opens a new range of possibilities in the effective inspection and characterization of engineering materials. The present results suggest that this technique has potential applications in a wide range of ultrasonic NDE area. Some of the most promising application areas are discussed below.

9.5.1 Testing of Concrete Structures

Concrete is a multiphase composite material consisting primarily of aggregate particles held together by a binding matrix. The binding matrix is a brittle hardened cement paste that demonstrates a viscoelastic nature. Steel reinforced concrete is one of the most widely used building materials in the world. It may be found in the highways, bridges, foundations, and structural members, to name just a few applications. The significance of effective nondestructive evaluation of concrete structures can not be overemphasized. The deteriorating infrastructure of the United States signals the importance of techniques that may quickly and practically assess the condition of large and often complicated structures. The determination of bulk material properties, such as compressive strength, across a large material volume remains a necessary job in the concrete evaluation industry.

Various existing methods for the NDE of concrete are, pulse velocity method, impact echo method, and spectral analysis method. SSUE technique can be used for the

measurement of signal velocity and frequency dependent attenuation in concrete structures. It can also be used for the measurement of acoustic signature variations of a complex structure. By employing an expert system to separate the normal cyclic variations in the correlation signature, it is possible to assess the integrity of the structure.

9.5.2 Grain Size Estimation

The importance of grain size measurement as a means of determining the structural and mechanical properties of materials has long been recognized by the industry. For the same reason significant research has been directed towards the grain size measurement by the NDE community. The literature survey indicates that the ultrasonic evaluation of grain size is the most practical and widely used method. Two major approaches exist for the grain size measurement which are, (a) attenuation measurement, and (b) scattering measurement. Current techniques can only be applied to materials which result in grain boundary echoes that are visible above the received noise level, which implies, (a) large grained samples, and (b) high SNR systems.

Since the SSUE technique is capable of providing very high SNR, it can perform more accurate grain size estimation of typical samples. Also, it can be applied for the grain size estimation of smaller grained materials. A statistical model for the power spectrum of backscattered echos from random grains can be developed and various model parameters can be estimated from the ultrasonic correlation signature measured through the SSUE technique. The estimated parameters provide the grain size information.

9.5.3 Integrity Testing of Composite Materials

Composite materials pose two kinds of challenges to conventional ultrasonic NDE methods. First, they exhibit highly attenuative and anisotropic signal propagation characteristics, and second, they fail in a manner totally different than the common homogeneous engineering materials. Whereas many traditional engineering materials fail

due to the initiation and propagation of a crack, reinforced composite materials degrade and fail in a manner more analogous to the collapse of a structure. Consequently the NDE of such materials involves assessing the combined effect of the material's damaged condition rather than identifying and sizing single critical imperfection. Since the SSUE technique measures the acoustic-impulse-response that represents the aggregate characteristics of the test material, it is possible to get a more accurate assessment of the combined state of a composite material.

9.5.4 NDE of Adhesively Bonded Joints

The application of adhesively bonded joints in structural components made of fiber composites, as replacement for mechanically fastened joints, has increased significantly over the recent years. Bonded joints have the advantages of strength-to-weight ratio, design flexibility, and ease of fabrication. On the other hand, physical discontinuity such as voids and disbonds can easily occur in the bonded joints during the manufacturing process. One of the major limitations on the use of adhesives in structural applications is associated with the difficulty encountered in making an accurate determination of bond quality or its potential performance after the joint has been assembled. In addition, the response behavior of a bonded joint during service could be affected by the environmental conditions. Thus, effective NDE methods for ensuring the quality of bonded joint is a topic of current research. The conventional NDE methods do not prove successful due to the highly attenuative and anisotropic characteristics of the material. A new class of ultrasonic NDE technique called Acousto-Ultrasonic has shown some success. Since acousto-ultrasonic technique has a lot of similarities with the SSUE technique in terms of signature analysis and interpretation, SSUE holds strong potential for future application in this area.

BIBLIOGRAPHY

[1]   R. B. Thompson, and D. O. Thompson,   Ultrasonics in Nondestructive Evaluation,
        Proceedings of IEEE, Vol. 73, No. 12, Page 1716-1755, 1985.

[2]   D. E. Bray, and D. McBride, Nondestructive Testing Techniques, John Wiley and
        Sons Inc., New York, 1992.

[3]   Alex Vary, Analytical Ultrasonics in Materials Research and Testing, NASA
        Conference Publication 2383, Cleveland, Ohio, 1984.

[4]   K. K. Shung, R. A. Sigelmann, and J. M. Reid, "The scattering of ultrasound by
        blood", IEEE Transactions Biomedical Engineering, Vol. BME-23, Page 460, 1976.

[5]   Dale W. Fitting, and Laszlo Adler, Ultrasonic Spectral Analysis for Nondestructive
        Evaluation, Plenum Press, New York, 1981.

[6]   Robert E. Green, Jr., "Ultrasonic Nondestructive Materials Characterization",
        Proceedings of the Conference held at the NASA Lewis Research Center,
        Cleveland, Ohio, Page 1-29, November 13-14, 1984.

[7]   J. C. Duke, Jr., ed., Acousto-Ultrasonics, Theory and Applications, Plenum Press,
        New York, 1988.

[8]   Alex Vary, "Acousto-Ultrasonics: Retrospective Exhortation with Bibliography",
        Materials Evaluation, Page 581-591, May 1991.

[9]   J. Summerscales, ed., Non-Destructive Testing of Fiber-Reinforced Plastics
        Composites, Elsevier Applied Science, New York, 1990.

[10]   Alex Vary, "Acousto-Ultrasonic Materials Characterization", Proceedings of the
        Second International Conference on Acousto-Ultrasonics, Hyatt Regency, Atlanta,
        GA, June 24-25, 1993.

[11]   N. Guo, and P. Cawley, "Lamb wave propagation in composite laminates and its
        relationship with acousto-ultrasonics", NDT&E International, Vol. 26, No. 2, Page
        75-84, 1993.

[12]   S. Tanary, Y. M. Haddad, A. Fahr, and S. Lee, "Nondestructive Evaluation of
        Adhesively Bonded Joints in Graphite/Epoxy Composites using Acousto-
        Ultrasonics", Transactions of the ASME, Vol. 114, Page 344-352, August, 1992.

[13]   P. Karpur, and O. J. Canelones, "Split spectrum processing: a new filtering
        approach for improved signal-to-noise ratio enhancement of ultrasonic signals",
        Ultrasonics, Vol. 30, No. 6, Page 351-357, 1992.

[14]   N. M. Bilgutay, U. Bencharit, R. Murthy, and J. Saniie, "Analysis of non-linear
        frequency diverse clutter suppression algorithm", Ultrasonics, Vol. 28, Page 90-96,
        March 1990.

[15]   J. D. Aussel, "Split-spectrum processing with finite impulse response filters of
        constant frequency-to-bandwidth ratio", Ultrasonics, Vol. 28, Page 229-240, July
        1990.

[16]   V. L. Newhouse, N. M. Bilgutay, and J. Saniie, "Flaw-to-grain echo enhancement
        by split-spectrum processing", Ultrasonics, Vol. 20, Page 59-68, 1982.

[17]   J. L. Rose, P. Karpur, and V. L. Newhouse, "Utility of split-spectrum processing in ultrasonic nondestructive evaluation", Materials Evaluation, Vol 46, Page 114-122, 1988.

[18]   A. S. Birks, and R. E. Green, *Nondestructive Testing Handbook*, 2nd ed., Vol. 7, American Society for Nondestructive Testing, Philadelphia, PA, 1991.

[19]   Eric S. Furgason, Vernon L. Newhouse, Nihat M. Bilgutay and George R. Cooper, "Application of Random Signal Correlation Technique to Ultrasonic Flaw Detection", Ultrasonics, Vol. 13, No. 1, Page 11-17, January 1975.

[20]   D. Kishoni, and B. E. Pietsch, "Ultrasonic Correlator versus Signal Averager as a Signal-to-Noise Enhancement Instrument", Proceedings of the 35th International Instrumentation Symposium, 1989.

[21]   Mohamed A. Benkhelifa, Marcel Gindre, "Echography Using Correlation Techniques, Choice of Coding Signal", IEEE Transactions on UFFC, Vol. 41, No. 5, Page 579-586, September 1994.

[22]   Eric A. Lindgren, M. Rosen, "Ultrasonic Characterization of Attenuative Materials by means of a Correlator System", Nondestructive Characterization of Materials IV, Plenum Press, New York, Page 377-384, 1991.

[23]   Z. X. Ding, P. A. Payne, "A New Golay Code System for Ultrasonic Pulse Echo Measurement", Measurement Science Technology, Vol. 1, Page 158-165, 1990.

[24]   E. A. Robinson, and T. S. Durrani, *Geophysical Signal Processing*, Prentice Hall Int., London, 1986.

[25] Merrill Skolnik, *Radar Handbook*, second edition, McGraw-Hill Int., New York, 1990.

[26] Marvin K. Simon, Jim K. Omura, Robert A. Scholtz, and Barry K. Levitt, *Spread Spectrum Communications Handbook*, McGraw-Hill Int., New York, 1994.

[27] Nigel A. Anstey, *VIBROSEIS*, Prentice Hall, Englewood Cliffs, New Jersey, 1991.

[28] A. J. Viterbi, *CDMA, Principles of Spread-Spectrum Communications*, McGraw-Hill Int., New York, 1995.

[29] S. Haykins, *Communication Systems*, 3rd edition, John Wiley & Sons, New York, 1994.

[30] R. Voles, *Radar, 92*, Proceedings of IEE International Conference, UK, 12-13 October, 1992.

[31] B. L. Lewis, F.F. Kretschmer, and W. W. Shelton, "Aspects of Radar Signal Processing", Artech House, Dedham, MA, 1986.

[32] D. K. Barton (ed.), "Pulse Compression", Radars, Vol. 3, Artech House, Dedham, MA, 1975.

[33] C. E. Cook, and M. Bemfeld, "Radar Signals, An Intriduction to Theory and Application", Academic Press, New York, 1967.

[34] F. E. Nathanson, "Radar Design Principles", Radars, Vol. 3, McGraw Hill, New York, 1969.

[35]   S. W. Golomb, and R. A. Scholtz, "Generalized Barker Sequences", IEEE Transactions on Information Theory, Vol. IT-11, 1965, Page 533-537.

[36]   E. M. Gabidulin, P. Z. Fan, M. Darnell, "Autocorrelation of Golomb Sequences", IEE Proceedings in Communications, Vol. 142, No. 5, October, 1995.

[37]   P. Z. Fan, M. Darnell, "Aperiodic Autocorrelation of Frank Sequences", IEE Proceedings in Communications, Vol. 142, No. 4, August, 1995.

[38]   T. Felhauer, "Design and Analysis of New P(n,k) Polyphase Pulse Compression Codes", IEEE Transactions on Aerospace and Electronic Systems, Vol. 30, No. 3, July, 1994.

[39]   B. L. Lewis, "Range-Time-Sidelobe Reduction Technique for FM-Derived Polyphase PC Codes", IEEE Transactions on Aerospace and Electronic Systems, Vol. 29, No. 3, July, 1993.

[40]   B. L. Lewis, F. F. Kretschmer, "New Polyphase Pulse Compression Wavefroms and Implementation Techniques", Aspects of Radar Signal Processing, 1986.

[41]   F. F. Kretschmer, and F. C. Lin, "Huffman Coded Pulse Compression Waveforms", NRL Report 8894, May 23, 1985.

[42]   M. B. Dobrin, Geophysical Prospecting, McGraw-Hill Int., New York, 1976.

[43]   H. N. Al-Sadi, Seismic Exploration: Technique and Processing, Birkhauser, Boston, 1980.

[44]   H. A. K. Edelmann, H. Werner, The Encoded Sweep Technique for Vibroseis,
       Geophysics, Vol. 47, No. 5, May, 1982.

[45]   T. Bernhardt, and J. H. Peacock, "Encoding technique for Vibrseis system",
       Geophysical Prospecting, Vol. 26, Page 184-192, 1978.

[46]   G. J. Baeten, J. T. Fokkema, and A. M. Ziolkowski, "Seismic Vibrator Modelling",
       Geophysical Prospecting, Vol. 36-1-22, 1988.

[47]   Eric S. Furgason, Vernon L. Newhouse, Nihat M. Bilgutay and George R. Cooper,
       "Application of Random Signal Correlation Technique to Ultrasonic Flaw
       Detection", Ultrasonics, Vol. 13, No. 1, Page 11-17, January 1975.

[48]   Nihat M. Bilgutay, Vernon L. Newhouse, "Evaluation of Random Signal
       Correlation System for Ultrasonic Flaw Detection", IEEE Transactions on Sonics
       and Ultrasonics, Vol. SU-23, Page 329-333, September 1976.

[49]   Charles M. Elias, and T. J. Moran, "A Pseudorandom Binary Noise NDE
       Ultrasonic Correlation System", Proceedings of IEEE Ultrasonics Symposium, Page
       311-315, 1978.

[50]   Charles M. Elias, "An Ultrasonic Pseudorandom Signal-Correlation System", IEEE
       Transactions on Sonics and Ultrasonics, Vol. SU-27, No. 1, Page 1-7, January
       1980.

[51]   B. B. Lee and Eric S. Furgason, "A New Digital Correlation Flaw Detection
       System", Journal of Nondestructive Evaluation, Vol. 2, No. 1, Page 57-63, 1981.

[52] B. B. Lee and Eric S. Furgason, "High Speed Digital Golay Code Flaw Detection System", Ultrasonics, Page 153-161, July 1983.

[53] B. B. Lee and Eric S. Furgason, "High Speed Digital Golay Code Flaw Detection System", IEEE Ultrasonic Symposium, Vol. 2, No. 1, Page 888-891, 1981.

[54] Z. X. Ding, P. A. Payne, "A New Golay Code System for Ultrasonic Pulse Echo Measurement", Measurement Science Technology, Vol. 1, Page 158-165, 1990.

[57] R. C. Cole, "Properties of swept FM waveforms in medical ultrasound imaging", IEEE 1991 Ultrasonics Symposium, Page 1243-1248, 1991.

[58] M. Pollakowski, Pulse Compression in ultrasonic non-destructive testing, Dissertation, Ruhr-Universitat, Bochum, Germany, 1993.

[59] H. Ermert, L. V. Bernus, T. Schmeidl, "The optimum bandwidth of chirp signals in ultrasonic applications", Ultrasonics, , Vol. 31, No. 6, Page 153-161, 1993.

[60] M. O'Donnell, "Coded Excitation System for Improving the Penetration of Real-Time Phased Array Imaging Systems", IEEE Transactions on UFFC, Vol. 39, No. 3, Page 341-351, May 1992.

[61] A. D. Wahlen, Detection of Signals in Noise, Academic Press, New York, 1971.

[62] J. K. Kayani, S. F. Russell, K. F. Hoech, and S. J. Wormley, "Direct-Sequence Spread-Spectrum Ultrasonic Evaluation System Design", Review of Progress in Quantitative Nondestructive Evaluation, Vol. 13A, Page 731-738, 1994.

[63]   J. K. Kayani, S. F. Russell, M. A. K. Afzal, K. F. Hoech, and S. J. Wormley, "Analysis and Design of Two Lab-Grade Prototype Instruments for Direct-Sequence Spread-Spectrum Ultrasonic Evaluation", Review of Progress in Quantitative Nondestructive Evaluation, Vol. 14B, Page 2285-2292, 1995.

[64]   M. A. K. Afzal, S. F. Russell, J. K. Kayani, S. Bae, K. F. Hoech, and S. J. Wormley, "Concept Validation and Accuracy Limitations for Direct-Sequence Spread-Spectrum Ultrasonic Evaluation System", Review of Progress in Quantitative Nondestructive Evaluation, Vol. 14B, Page 2293-2300, 1995.

[65]   M. J. E. Golay, "Complementary series", IRE Transactions, Vol. IT-11, Page 207-214, 1961.

[66]   R. Sivaswamy, "Multiphase complementary codes", IEEE Transactions, Vol. AES-18, Page 163-181, 1982.

[67]   Hermann Rohling, Wilfried Plagge, "Mismatched-Filter Design for Periodical Binary Phased Signals", IEEE Transactions on Aerospace and Electronic Systems, Vol. 25, No. 6, November, 1989.

[68]   V. P. Ipatov and B. V. Fedorov, "Regular Binary Sequences with small losses in supressing sidelobes", Izvestiya VUZ. Radioelektronika, Vol. 27, No. 3, Page 29-34, 1984.

[69]   V. P. Ipatov, "Binary periodic sequences with low sidelobe supression loss", Izvestiya VUZ. Radioelektronika, Vol. 23, No. 1, Page 20-25, 1980.

[70]   V. P. Ipatov, "Choice of Periodic PSK Signal and Filter Combination", Izvestiya VUZ. Radioelektronika, Vol. 21, No. 4, Page 60-67, 1978.

[71]   D. F. Elliott, and K. R. Rao, *Fast Transforms; Algorithms, Analyses, Applications*, Academic Press, New York, 1982.

[72]   B. Sklar, Digital Communications, Fundamentals & Applications, Prentice Hall, Englewood Cliffs, New Jersey, 1988.

[73]   L. J. Bain, and M. Engelhardt, *Introduction to Probability and Mathematical Statistics*, 2nd edition, PWS-Kent Publishing Co., 1992.

[74]   James Jordan, Peter Bishop, Bijan Kiani, "Correlation-Based Measurement Systems", Ellis Horwood Limited, West Sussex, England, 1989.

[75]   J. K. Kayani, S. F. Russell, "A Computationally Efficient Method and Apparatus for DSP-based Correlator", patent filed November, 1995.

[76]   Borish, J. and Angell, J., An efficient algorithm for measuring the impulse response using pseudorandom noise, [1983].

[77]   Jin H. Kim, Bum S. Lee and Song B. Park, Prior Inverse Filtering for the Improvement of Axial Resolution, Ultrasonic Imaging, No. 7, Page 179-190, 1985

[78]   Gordon Hayward and John E. Lewis, A Theoretical Approach for Inverse Filter Design in Ultrasonic Applications, IEEE Transactions on UFFC, Vol. 36, No. 3, Page 356-364, May 1989.

[79]   R. E. Green, *Ultrasonic Investigation of Mechanical Properties*, Academic Press, New York, 1973.

[80]   D. R. Hull, "Measurement of Ultrasonic Velocity using Phase-Slope and Cross-Correlation Methods", Materials Evaluation, Vol. 43, Page 1455, October, 1985.

[81]   J. Saniie, T. Wang, and N. M. Bilgutay, "Statistical evaluation of backscattered ultrasonic grain signals", Journal of Acoustical Society of America, Vol. 84, No. 1, Page 400-408, July, 1988.

[82]   J. Krautkramer, and H. Krautkramer, *Ultrasonic Testing of Materials*, Springer, New York, 1977.

[83]   E. P. Papadakis, "Ultrasonic Attenuation caused by Scattering in Polycrystalline Materials", Journal of Acoustical Society of America, Vol. 37, Page 711, 1965.

[84]   J. Saniie, and N. M. Bilgutay, "Quantitative Grain Size Evaluation using Ultrasonic Backscattered Echoes", Journal of Acoustical Society of America, Vol. 80, No. 6, Page 1816-1824, December, 1986.

[85]   D. J. Hand, *Discrimination and Classification*, John Wiley & Sons, New York, 1981.

[86]   H. L. Whaley, and L. Adler, "Flaw Characterization by Ultrasonic Frequency Analysis", Materials Evaluation, Vol. 29, No. 8, Page 182-188, 1971.

[87]   L. S. Koo, *Ultrasonic Flaw Classification*, Ph. D. Thesis, Iowa State University, 1987.

[88]   A. Rogerson, and R. A. Murgatroyd, "Defect Characterization using Ultrasonic Techniques", Research Techniques in Nondestructive Testing, Vol. 4, Page 451, 1980.

APPENDIX A   CORRELATION AND CONVOLUTION

Correlation and convolution functions are encountered in many scientific and engineering disciplines. These functions take different forms and carry different interpretation under different conditions. The concepts of correlation and convolution are pivotal to the development of the SSUE technique. It is, therefore, important to clearly define these concepts in the framework of present work and develop necessary relations and mathematical notations describing them.

A.1 Correlation of Random and Deterministic Waveforms

One form of correlation function commonly used by statisticians is associated with random processes and waveforms. The correlation function is meant to describe certain characteristics of the waveform generated by a random processe. In particular, the power spectral density and cross-spectral density of a random process are described through their correlation functions. A correlation function is, in general, defined for two random waveforms and it is identified as a crosscorrelation function. In a specific case, when the two random waveforms happen to be the same, it is called the autocorrelation function. Although correlation functions can be defined for non-stationary and non-ergodic processes, our following definitions of correlation functions is restricted to ergodic processes only.

Let x(t) and y(t) be two random waveforms representing independent and jointly ergodic processes. Their crosscorrelation function is defined as,

$$\phi_{xy}(\tau) = \frac{Lim}{T \to \infty} \frac{1}{T} \int_0^T x(t)y^*(t-\tau)dt \qquad (A.1)$$

and the autocorrelation function of the waveform, x(t), is defined as,

$$\phi_{xx}(\tau) = \frac{Lim}{T \to \infty} \frac{1}{T} \int_0^T x(t)x^*(t-\tau)dt \qquad (A.2)$$

As seen by the defining equations of the auto- and crosscorrelation functions, it is not possible to exactly measure these functions as this involves integration over infinite time interval. An estimate of these functions, however, is found by taking T to be finite but sufficiently large.

The definition of correlation functions can be extended to characterize pseudo-random waveforms and processes and eventually to characterize all kinds of deterministic waveforms. To do that, the earlier definitions must be modified to accommodate a variety of situations. A deterministic waveform can either be time-limited or periodic. For time-limited waveforms the correlation function is called linear correlation. Hence the linear autocorrelation function (LACF) of a waveform, x(t), timelimited to ($0 < t < T_o$) is defined as,

$$\phi_{xx}(\tau) = \frac{1}{T_0} \int_\tau^{T_0} x(t)x^*(t-\tau)dt \qquad (A.3)$$

and the linear crosscorrelation function (LCCF) is defined as,

$$\phi_{xy}(\tau) = \frac{1}{T_0} \int_\tau^{T_0} x(t)y^*(t-\tau)dt \qquad (A.4)$$

For periodic waveforms, the correlation function is called periodic or circular correlation. If the two waveforms x(t) and y(t) both have a period T_p, their periodic

correlation functions (PACF & PCCF) are defined as,

$$\phi_{xx}(\tau) = \frac{1}{T_p} \int\limits_{0}^{T_p} x(t)x(t-\tau)dt \qquad \text{(A.5)}$$

$$\phi_{xy}(\tau) = \frac{1}{T_p} \int\limits_{0}^{T_p} y(t)x(t-\tau)dt \qquad \text{(A.6)}$$

Correlation function can also be defined for mathematical sequences of numbers and it can also be either a linear correlation corresponding to the non-repetitive sequences or a periodic correlation corresponding to the repetitive sequences. For two complex sequences $\{x_n\}$ and $\{y_n\}$ each of length L, their linear correlation functions are defined as,

$$P_{xx}(k) = \sum_{n=1}^{L-k} x_n x^*_{n+k} \qquad \text{(A.7)}$$

$$P_{xy}(k) = \sum_{n=1}^{L-k} x_n y^*_{n+k} \qquad \text{(A.8)}$$

where k = 0, 1, 2, . . . , (L-1).

The periodic correlation functions of complex sequences $\{x_n\}$ and $\{y_n\}$, each of period L, are defined as,

$$P_{xx}(k) = \sum_{n=1}^{L} x_n x^*_{n+k} \qquad \text{(A.9)}$$

$$P_{xy}(k) = \sum_{n=1}^{L} x_n y^*_{n+k} \qquad \text{(A.10)}$$

where k = 0, 1, 2, . . . , (L-1), and the sequence is assumed to be periodic with period L.

A.2 Power-Spectral Density and Cross-Spectral Density

The power-spectrum of a random process gives the quantitative description of its frequency components. It is defined in terms of the autocorrelation function of the process as,

$$S_{xx}(\omega) = \int_{-\infty}^{\infty} \phi_{xx}(\tau) e^{-j\omega\tau} d\tau \qquad (A.11)$$

Similarly the cross-spectrum of two random processes gives the quantitative description of the frequency components shared by them. It is defined in terms of their crosscorrelation function as,

$$S_{xy}(\omega) = \int_{-\infty}^{\infty} \phi_{xy}(\tau) e^{-j\omega\tau} d\tau \qquad (A.12)$$

A.3 Convolution of Time-Limited and Periodic Functions

The convolution of two time functions x(t) and y(t) is another function given by,

$$z(t) = \int_{-\infty}^{\infty} x(v) y(t-v) dv \qquad (A.13)$$

and represented by the convolution notation as,

$$z(t) = x(t) * y(t) \qquad (A.14)$$

Another case of interest is when one function, x(t), is time limited to T_0 and the other function, y(t), is periodic with period T_p. The convolution function in such a case will again be periodic with period T_p, and given by,

$$z(t) = \int_0^{T_p} x(v)y(t-v)dv \qquad \text{(A.15)}$$

This result is the corner stone of the pseudorandom signal correlation method of impulse response estimation discussed in section 3.2.

A.4 Relation between Periodic Convolution and Periodic Correlation

Comparison of the expressions of periodic crosscorrelation and periodic convolution reveal that the two can be related by,

$$\phi_{xy}(\tau) = x(\tau) * y(-\tau) \qquad \text{(A.16)}$$

There is a scaling factor of T_p missing in the above equation, but that being a constant is inconsequential for our work and is, therefore, ignored.

APPENDIX B   CONCEPT OF SYSTEM IMPULSE RESPONSE

Impulse response of a system is, by definition, the response of the system when an impulse function is applied to its input. Although, the true impulse response of the system is a non-realizable concept, much like the impulse function (delta function) itself, yet it is a very powerful idea to describe the characteristics of any given system. The concept of system impulse response serves as the basis for developing a mathematical model of a system and analyzing its response to all kinds of inputs (Figure B.1). It provides a common platform to compare various types of physical systems like a mechanical system, an electrical system, and an optical system.

If a system is linear and time-invariant (LTI), its impulse response completely describes the system characteristics. Not only does this means that, given an arbitrary input, the corresponding output can be determined, but a wealth of information regarding the physical nature of the system is also contained in the impulse response. As the input signal (delta function) contains all the frequency components, it excites all the resonance modes of the system and the impulse response acts as the signature function.

input   LTI system   output

$x(t)$ ——▶ $h(t)$ ——▶ $y(t)$
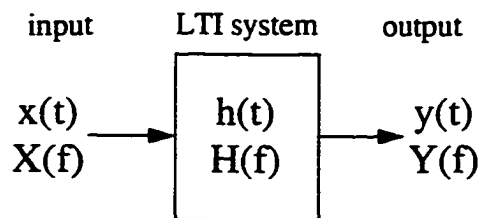$X(f)$ $H(f)$ $Y(f)$

Figure B.1: Impulse response model of an LTI system.

The impulse response of a system is the time-domain equivalent of the transfer function or the frequency response concept in the frequency-domain. The two descriptions of the system response are equivalent and are linked by the relations,

$$h(t) = \frac{1}{2\pi} \int_{-\infty}^{\infty} H(f) e^{j2\pi ft} df \qquad \text{(B.1)}$$

$$H(f) = \int_{-\infty}^{\infty} h(t) e^{-j2\pi ft} dt \qquad \text{(B.2)}$$

where h(t) is the impulse response and H(f) is the frequency response. The responses h(t) and H(f) form a Fourier transform pair.

In an LTI system, the input and the output are related through the well known convolution integral.

$$y(t) = x(t) * h(t) \qquad \text{(B.3)}$$

$$y(t) = \int_{-\infty}^{\infty} h(v) x(t-v) dv \qquad \text{(B.4)}$$

B.1 Impulse Response of a Physically Realizable System

Conceptually, the impulse response can be defined for a non-realizable system and it is a useful tool or concept for certain analysis situations. However, when we restrict our discussion to a physically realizable system, the associated impulse response bears certain unique properties. These are,

(a)   h(t) is a real function

(b)   h(t) is causal

(c)   h(t) is of finite duration

(d)   h(t) has finite energy

When h(t) is a real function of time, the output of the system, y(t), will be real, and hence measurable, for all real inputs, x(t). Causal h(t) implies that the impulse response is zero for t < 0. As a result of this property, the convolution integral in equation (3.21) reduces to a one-sided integral, i.e.,

$$y(t) = \int_0^{\infty} h(v)x(t-v)dv \qquad \text{(B.5)}$$

Also, since h(t) is of finite duration, T_0, the convolution integral now reduces to a finite integral, given by,

$$y(t) = \int_0^{T_0} h(v)x(t-v)dv \qquad \text{(B.6)}$$

APPENDIX C   IMPULSE RESPONSE ESTIMATION METHODS

The impulse response of a linear-time-invariant system is physically non-realizable, which means that we cannot measure the true impulse response of a given physical system. However, it is possible to make a reasonable estimate of the true impulse response, and there exists more than one method of doing so, each with its own merits and demerits. These methods are,

(a)   applying an impulsive signal as the input,

(b)   applying a single frequency tone and sweeping the frequency,

(c)   applying an expanded-pulse and performing pulse compression,

(d)   applying a purely random signal and performing crosscorrelation,

(e)   applying a pseudo-random signal and performing crosscorrelation,

(f)   applying a pseudo-continuous pseudo-random signal and doing crosscorrelation.

C.1 Impulsive Excitation Method

In measuring the impulse response of an LTI system, the most direct approach is to apply an impulsive excitation to the system and observe the response. Owing to the simplicity of the approach and the instrumentation involved, this method finds its application in many areas like radars, pulse-echo ultrasonics, seismic analysis. There are two basic difficulties with this approach. The first is generating the impulsive excitation, and the second is obtaining adequate dynamic range. Because the duration of the impulse is, by definition, very short, it is difficult to deliver enough energy to the system to overcome the ever present noise. The amplitude of the impulsive excitation is limited by the range of linearity of the system and its duration by the system bandwidth. The

convolution integral relating the output, y(t), with the input, x(t), is given as,

$$y(t) = \int_0^\infty h(v)x(t-v)dv \qquad (C.1)$$

When $x(t) = \delta(t)$, the convolution integral simplifies to yield,

$$y(t) = h(t) \qquad (C.2)$$

The impulsive excitation method is the simplest, fastest and least expensive. Hence, it is the most commonly used method for all ordinary measurement situations. When the impulse response to be measured has signal components with very wide dynamic range (> 60 dB), or the measurement system has a poor signal-to-noise ratio, this method does not perform very well and is, therefore, not the best choice.

C.2 Single Frequency Excitation Method

The continuous wave excitation method has the advantage that monochrome signals can be generated reliably and repeatably, and system interrogation can be limited to the frequencies of interest. However, a series of separate measurements must be made. The cw source permits the use of low power, since coherent time integration can be used. A major limitation, however, is that the system must remain acceptably stationary over a sufficiently long measurement period. The frequency domain equivalent of the input/output convolutional relation of equation (C.1) is,

$$Y(f) = H(f)X(f) \qquad (C.3)$$

Hence, for an input signal at frequency f_n, the magnitude of the corresponding output is given as,

$$|Y(f_n)| = |H(f_n)| \, |X(f_n)|$$
<div align="right">(C.4)</div>

and the phase as,

$$\theta_Y(f_n) = \theta_H(f_n) + \theta_X(f_n)$$
<div align="right">(C.5)</div>

The single-tone excitation method is, on one hand, very slow, since the tone frequency has to be sweeped over the entire bandwidth of interest. Secondly, the generation of very narrow frequency tunable waveform is not a very simple task. It requires very complicated and expensive equipment.

C.3 Pulse Compression Method

This method is an improvement to the impulsive excitation method of section C.1. It is based on the use of a pulse compression waveform, which is an expanded pulse with large time-bandwidth product. Various kinds of expanded-pulse waveforms, having large time-bandwidth product are possible. Two major classes are FM Chirp waveforms and Coded waveforms. Such types of waveforms are used in order to achieve greater pulse energy and large pulse bandwidth, and consequently high accuracy, without sacrificing range resolution in a peak-power limited system. At the receiver, the received signal is passed through a filter matched to the transmitted expanded pulse that compresses the received signal energy into a short pulse (Figure C.1).

This method of impulse response estimation is used in most modern pulse radars, certain seismic exploration systems, and conventional ultrasonic correlation systems. While this method provides greater signal-to-noise ratio by increasing the transmit signal energy, it suffers from the problem of self-noise. Self-noise is a result of incomplete pulse compression in the receiver which in turn is a consequence of the non-ideal linear autocorrelation function (LACF) of the expanded-pulse excitation waveform.
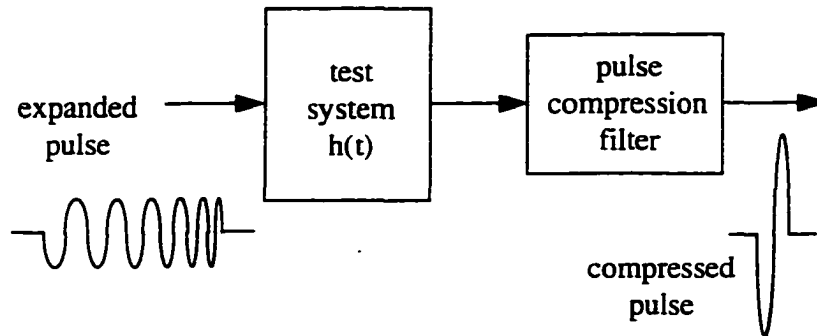
Figure C.1: Pseudorandom signal correlation method.

C.5 Continuous Random Signal Correlation Method

A different approach to impulse response estimation is to excite the system with continuous, random noise. Because the excitation is applied continuously, more energy is delivered to the system for a given amplitude of signal, circumventing the peak-power limitation problem. Further, it is easier to assure the uniformity of the energy distribution over the frequency range of interest. The response of the system is the convolution of the excitation signal with the system's impulse response (Figure C.2). The impulse response can be extracted from the measurement by cross-correlating the noise input with the output .

Let u(t) be the input to the system and v(t) be the system output. Then, u(t) being a white noise signal, has an autocorrelation function, $\phi_{uu}(\tau)$, given by,

$$\phi_{uu}(\tau) = \frac{Lim}{T \to \infty} \frac{1}{T} \int_0^T u(t)u(t-\tau)dt = \delta(\tau)$$

(C.6)

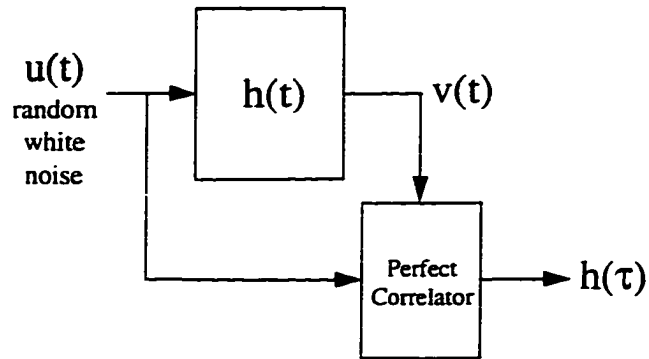The cross-correlation function, $\phi_{uv}(\tau)$, is given as,

Figure C.2: Random signal correlation method.

$$\phi_{uv}(\tau) = \frac{Lim}{T \to \infty} \quad \frac{1}{T} \int_0^T v(t)u(t-\tau)dt \tag{C.7}$$

The convolution integral relating the output, v(t), with the input, u(t), is given as,

$$v(t) = \int_0^{T_0} h(v)u(t-v)dv \tag{C.8}$$

Substituting equation (C.8) in equation (C.7) gives,

$$\phi_{uv}(\tau) = \frac{Lim}{T \to \infty} \quad \frac{1}{T} \int_0^T \int_0^{T_0} h(v)u(t-v)u(t-\tau)dvdt \tag{C.9}$$

$$\phi_{uv}(\tau) = \int_0^{T_0} h(v) \quad Lim[T \to \infty]\frac{1}{T}\int_0^T u(t-v)u(t-\tau)dtdv \tag{C.10}$$

$$\phi_{uv}(\tau) = \int_{-\infty}^{\infty} h(v)\phi_{uu}(v-\tau)dv \qquad\qquad (C.11)$$

From equations (C.6) and (C.11), we get the final result as,

$$\phi_{uv}(\tau) = \int_{-\infty}^{\infty} h(v)\delta(v-\tau)dv = h(\tau) \qquad\qquad (C.12)$$

There are three practical problems associated with this approach of impulse response estimation,

(a) generation of a truly random signal

(b) variable delay generation for correlation

(c) realization of correlation filter with infinitely large integration time

A truly random signal is more of a concept than a physical reality. It is, by definition, non-periodic and non-reproducible. In a practical system, however, it is required that various delayed versions of the input signal be accessible for correlation purposes. A practical correlator has to have a finite integration time. Hence, a lot of memory space is required for the correlator and the variable delay generation. This results into an inefficient system with very slow operation.

C.6 Pseudorandom Signal Correlation Method

This method of impulse response estimation is, in theory, very similar to the one described under section C.5. However, it is much more convenient for practical implementation. It takes advantage of the fact that the impulse response of a physical system , h(t), is of finite duration, T_0. The basic approach is to apply a periodic pseudo-random waveform as the input to the system and perform a periodic crosscorrelation at the output (Figure C.3).

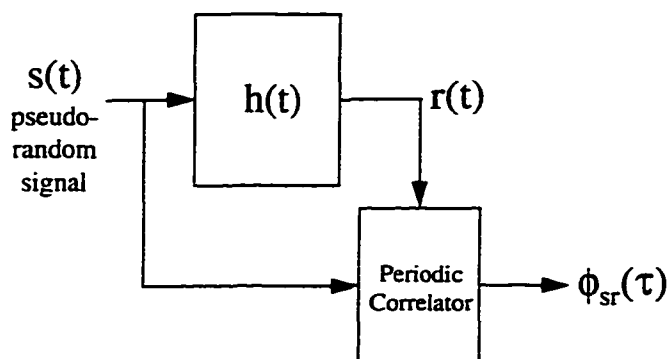If we let the input to the system be a pseudo-random waveform, s(t), having a

Figure C.3: Pseudorandom signal correlation method.

period, T_s , such that, $T_s > T_o$, and the periodic autocorrelation function given by,

$$\phi_{ss}(\tau) = \delta(\tau - nT_s) \tag{C.13}$$

where n is an integer. Following the mathematical analysis of section C.5, the output of the correlator can be written as,

$$\phi_{sr}(\tau) = \int_0^{T_0} h(v)\phi_{ss}(v-\tau)dv = h(\tau)\delta(\tau - nT_s) \tag{C.14}$$

Following deductions can be made from the above results,

(a)   The correlator output represents the system impulse response repeated after every T_s. As long as ($T_s > T_o$), the system impulse response can be unambiguously extracted from the correlator output. When ($T_s < T_o$), the foldover of the impulse response occurs and it is no longer possible to unambiguously extract h(t).

(b)   It is only the autocorrelation characteristics of the input signal which is critical when extracting the impulse response from the correlator output,

otherwise true randomness of the excitation waveform is not a must. Since auto-correlation is not a unique function, any waveform deterministic or pseudo-random can be used equally successfully as long as its PACF is of the form of equation (C.13).

C.7 Pseudo-Periodic Pseudo-Random Signal Correlation Method

This method is a simplification of the pseudo-random signal correlation method described under section C.6. The calculation of PCCF of two periodic waveforms, requires only one period each of the two waveforms. Thus, if we transmit s(t) only for the time duration until all the transients in the receive signal die down and one period of the stabilized received signal can be acquired, it is sufficient for the off-line evaluation of the impulse response function (Figure C.4).

The time interval required for the stabilization of the received signal is equal to the length of the impulse response function, T_o. Also, since $T_s > T_o$, a time interval equal to one period of the excitation waveform, T_s, is sufficient for the stabilization of the received signal and another one period is required to be able to capture one period of the received
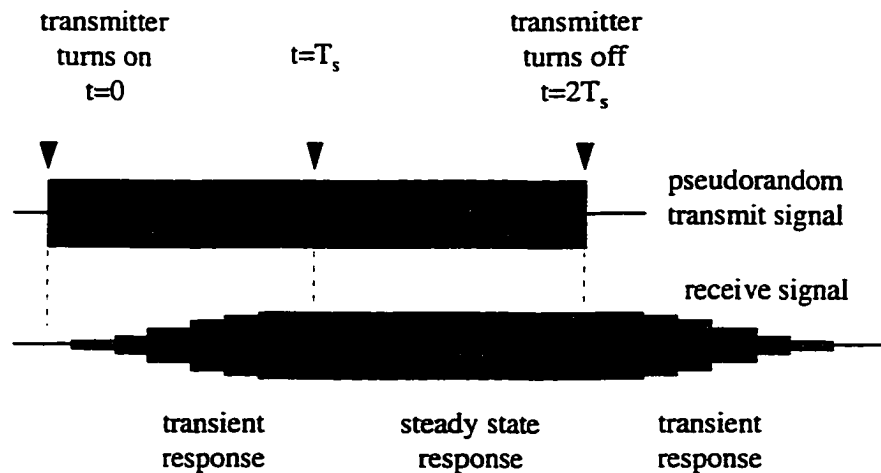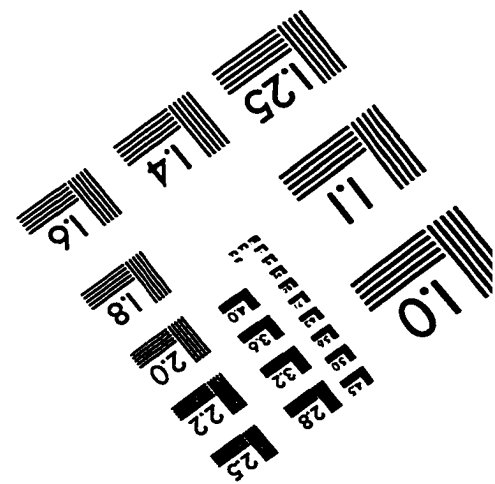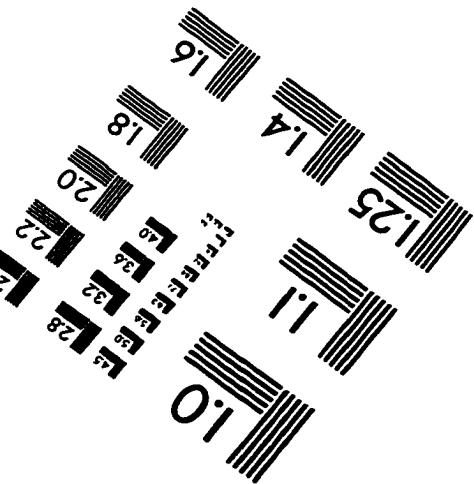
transmitter
turns on $t=T_s$
t=0

transmitter
turns off
$t=2T_s$

▼   ▼   ▼

pseudorandom
transmit signal

receive signal

transient
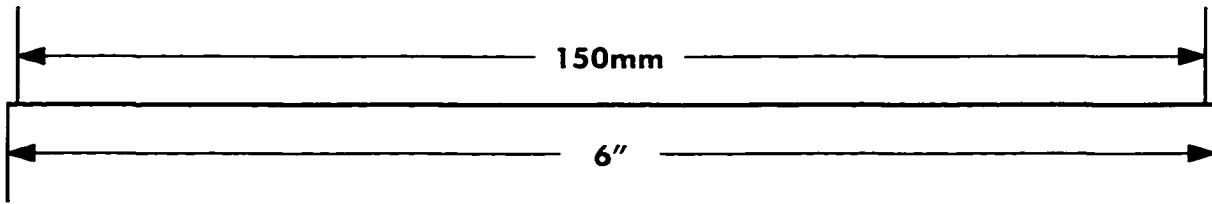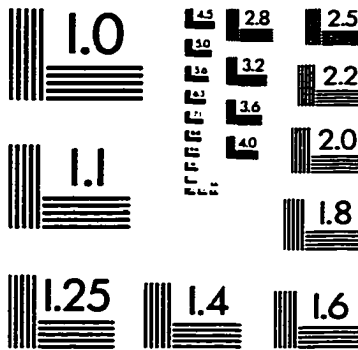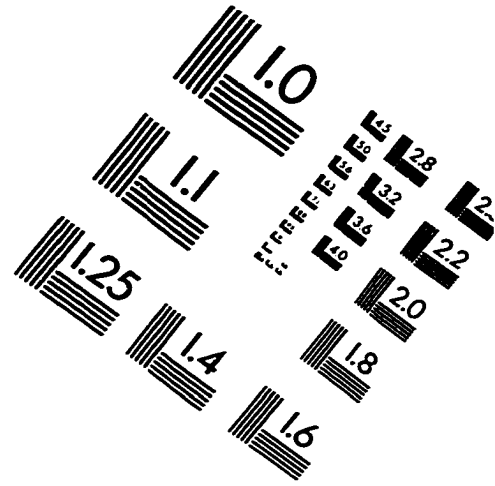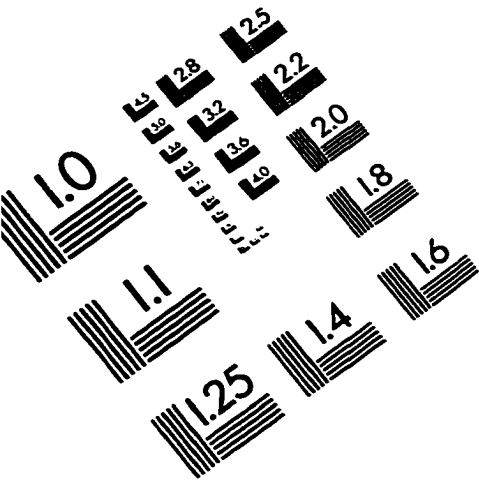response

steady state
response

transient
response

Figure C.4: Schematic representation of transmit and receive signal waveforms.

signal. Hence, it is not really necessary to transmit a continuous, periodic waveform to take the benefit of periodic correlation function. Instead, if a waveform consisting of only two concatenated periods are transmitted and a specific portion of the received waveform is selected to perform the periodic crosscorrelation, it results into an equivalent performance.

IMAGE EVALUATION
TEST TARGET (QA-3)

150mm

6"